Novel insights into Mediterranean forest structure using high-resolution remote sensing

Harry Jon Foord Owen

Submitted for the degree of Doctor of Philosophy

Supervised by:

Dr. Emily Lines,

Prof. Lisa Belyea & Dr. Stuart Grieve

Department of Geography

Queen Mary

University of London

June 2021

I, Harry Jon Foord Owen, confirm that the work presented in this thesis is my own. Where information has been derived from other sources, I confirm that this has been indicated in the thesis.

…….

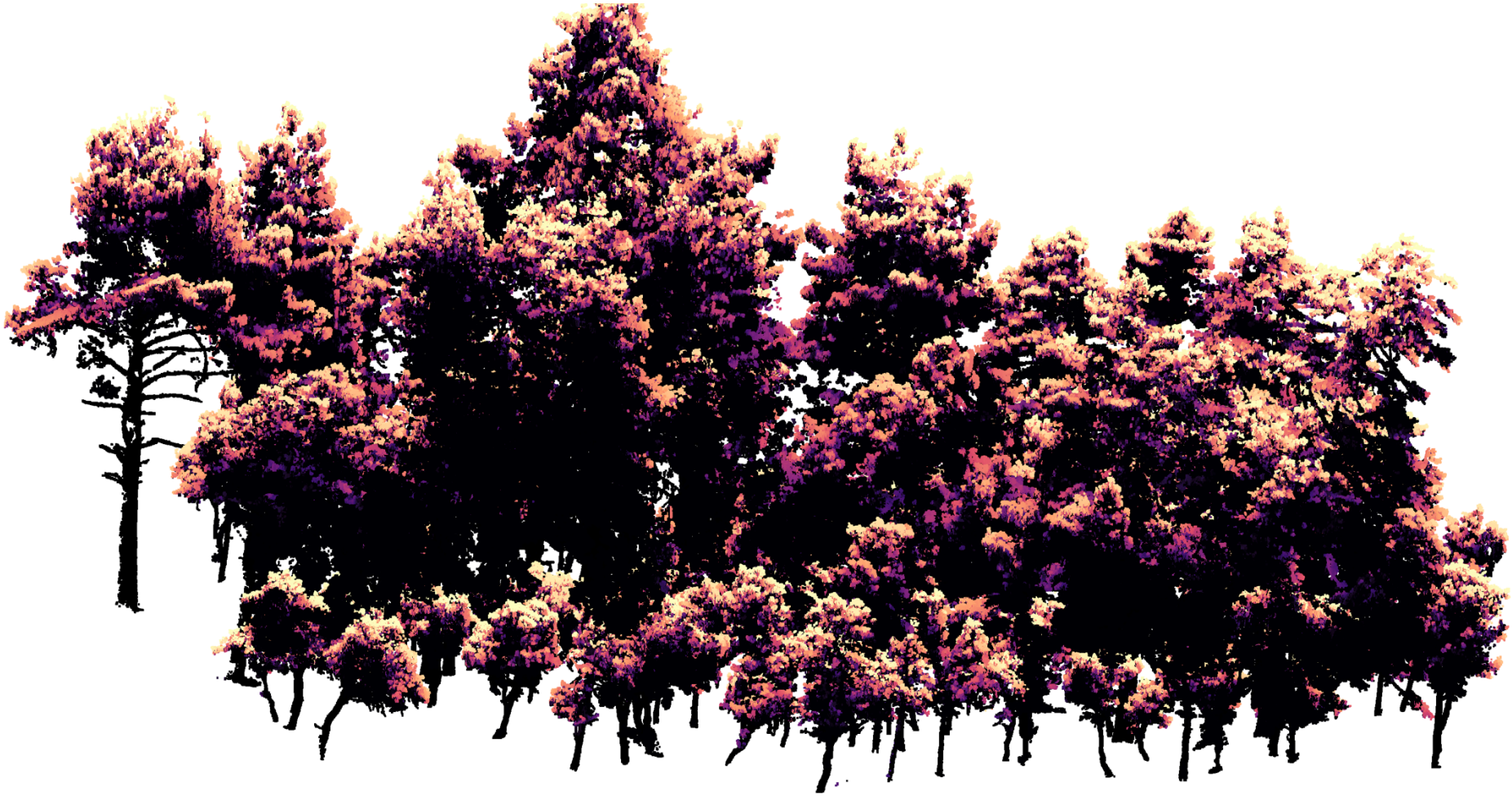

Three-dimensional light capture for a mixed pine-oak forest plot in Alto Tajo national park, Spain

Abstract

Tree crown morphology and arrangement in three-dimensional space is a key driver of forest dynamics, determining not only the competitiveness of an individual but also the competitive effect exerted on neighbouring trees. Many theoretical frameworks aim to predict crown morphology from first principles and assumptions of Euclidean form and ultimately infer whole forest stand structure and dynamics but paucity in data has limited vigorous testing. Tree crowns are also not rigid in form and due to their sessile nature, must morphologically adapt to immediate abiotic and biotic surroundings to enhance survival.

The characterisation of tree structure has been limited by the simplicity and associated error of traditional crown measurements. This project uses Terrestrial Laser Scanning data collected from a water limited Mediterranean forest community in Spain to highlight methodological opportunities presented by TLS in understanding forest structure and also the various developments required to extract ecologically meaningful metrics from these data. It then applies these novel metrics to answer questions about how tree crowns scale with size, the effects of competition and how plasticity in shape and arrangement interacts with light capture at the individual and plot scales.

Modification to existing code as well as bespoke development were required to segment and calculate individual metrics from trees in this forest type. Accurate measures of crown morphology highlighted allometric scaling deviations from theoretical predictions and intra-specific differences in response to competition, calculated using more representative neighbourhood metrics. Inter-specific differences in crown plasticity and significant effects of size (height) were also evident, along with trade-offs between morphological plasticity and crown size. Light capture was positively affected by plasticity with inter-specific differences highlighting various biomass allocations strategies species undertake to acquire light. At the plot scale, mixed-genus plots intercepted less direct light and were structurally more complex rather than more volume filling.

Acknowledgements

I would firstly like to thank my supervisors Stuart Grieve and Lisa Belyea, and in particular, my primary supervisor Emily Lines for their endless support and sharing of knowledge throughout the entirety of this PhD. Thank you Will Flynn and Julen Astigarraga for vital assistance in data collection and Fernando Valladares, Paloma Ruiz-Benito, Jaime Madrigal-González and Laura Marqués López for your invaluable knowledge and assistance towards the organisation of field work. Thank you James brasington for emparting your knowledge on TLS systems.

I am also indebted to my very supportive and loving family that not only encouraged me thoughout my academic endevours but also provided a reassuring presence throughout. Thank you mum (Stephanie), dad (Marcus) and my two sisters, Ashleigh and Amelia. I would also like to share my deep appreciation of the unconditional support from my partner, Adele Tuttlebee, throughout the entirty of this project, which was crucial in making the duration of the PhD both enjoyable and successful.

Finally, to all those friends that I have not explicitly mentioned, you know who you are, thank you for you ongoing support and invaluable company over the years.

This project was funded by the Natural Environment Research Council [NE/L002485/1].

Contents

Chapter 1

Introduction

1.1 Forest function

A forest canopy is the functional interface between 90% of Earth's terrestrial biomass and the atmosphere (Ozanne et al., 2003). The spatial arrangement, variety in sizes and flexibility in crown shape are fundamental factors in determining the overall structure at this interface (Purves et al., 2008), and subsequent productivity (Williams et al., 2017). The overall structure of a forest is therefore a net result of all individual tree crown optimisations in positioning, nutrient content and leaf angles (Coomes et al., 2012) and the mixture of species with different resource acquisition strategies (Sapijanskas et al., 2014). The increasing variety in optimisation strategies within a forest leads to higher structural complexity, which itself is tightly linked to forest productivity (Gough et al., 2019; Stark et al., 2012) due to structural complexity metrics incorporating factors that affect growth, such as crown packing (Juchheim et al., 2017; Jucker et al., 2015), connectedness between tree crowns (Davies and Asner, 2014) and differences in shade tolerance (Toïgo et al., 2018), leading to higher light absorption (Atkins et al., 2018; Sapijanskas et al., 2014). Many suggest that tree species diversity alone promotes higher structural complexity (Fotis et al., 2018; Juchheim et al., 2017), and higher light interception (Duarte et al., 2021), for example through interspecific variation in light transmission (Yi et al., 2020) and high variability in mechanical capacity to laterally extend to acquiring light (Loehle, 2016). Recent high-resolution 3D analyses have revealed high predictability of species richness from structural complexity (Walter et al., 2021) suggesting that the two go hand in hand. However, functional diversity may be key; Toïgo et al., (2018), point to differences in shade tolerance as the key driver of positive diversity-productivity relationships, with phylogenetic distance between species an irrelevant proxy for species functional dissimilarity. Modelling analyses using 300,000 forest stands found forest structure, not species richness, as the key variable determining forest productivity (Bohn and Huth, 2017), while (Gough et al., 2020) found maximum height a stronger predictor of complementarity than leaf area or diversity, signifying the availability of space within the canopy volume as a primary constraint on development of structural complexity.

Although, biodiversity-productivity relationships are crucial and key to nature-based climate solutions due to tight links between species richness and carbon drawdown from the atmosphere (Mori et al., 2021), the relative contribution of belowground competition in water and nutrient limited environments is poorly understood (Craine and Dybzinski, 2013). In some cases, positive relationships between species above ground completely reversed when belowground resource availability dwindled with species better equipped to extract water prevailing (Jucker et al., 2014). In such scenarios, the identity of neighbouring trees matters to the survival of an individual through drought (Grossiord, 2019). Although modelling techniques often treat all trees equally in striving for enhanced light capture (Fisher et al., 2018), shading by neighbours can ameliorate drought stress (Domingo et al., 2020) and be of benefit to an individual but can be dependent on focal tree shade tolerance (Kothari et al., 2021)

1.2 Threats to forest structure

Although many factors are contributing to the demise of the worlds' old-growth forests, deforestation is the major contributor (Hansen et al., 2013), and removes not only habitat for vast biodiversity but also to key ecosystems services used by humanity, with intact forests thought to provision approximately $16.2 trillion in services a year (Costanza et al., 2014). In ecosystems such as the Spanish Mediterranean, land that was once used for agriculture has since been abandoned, and these systems are experiencing afforestation following land abandonment and lower demand for wood (Khoury and Coomes, 2020). There are approximately three trillion trees on earth (Crowther et al., 2015) and the array of species within them enhance the variety of ecosystems function (Gamfeldt et al., 2013) and its resistance to climate extremes (Isbell et al., 2015). The benefits of high forest species diversity is not limited to tropical regions, with European forests also highlighted as having unrealised potential to increase multi-functionality through restored diversity in forests (van der Plas et al., 2018). Large swaths of boreal forest store vast amounts of carbon but are also under threat (Gauthier et al., 2015), in particular to changing disturbance regimes (Seidl et al., 2017). Many forests are experiencing large scale crown dieback due to fungal disease (McMullan et al., 2018), hydraulic failure due to drought (Nolan et al., 2021) with direct consequences to food webs and the life sustained within them

(Carnicer et al., 2011). Tree crowns and their deterioration are often early warning signs of declining forest function, and as such their monitoring is fundamental in understanding threats such as species-specific vulnerabilities to drought induced mortality (Camarero et al., 2015). Fortunately, tree canopies can be readily monitored at large scales using remote sensing techniques onboard satellites (Khoury and Coomes, 2020) but delineation at the individual scale still a complex undertaking, even with higher resolution airborne sensors (Duncanson and Dubayah, 2018).

Forests, alongside ocean phytoplankton, are responsible for the majority of Earths' primary production, releasing oxygen into the atmosphere as a by-product (Field et al., 1998) but are under threat from drought induced dieback (McDowell and Allen, 2015), insect invasion and disease (Fei et al., 2019) and of course, deforestation for land conversion and timber production (Curtis et al., 2018). Unfortunately, whilst the significance of old growth forests is well understood (Luyssaert et al., 2008), so is the fact that larger trees are more predisposed to drought (Stovall et al., 2019); an alarming fact given that many forests are predicted to get drier with climate change (Dai, 2013). High susceptibility of trees and the carbon stored within their long-lived and slow growth woody tissues to rapid shifts in climate are likely given the sessile nature of trees and inflexible damage thresholds (Brodribb et al., 2020). Drought has considerable negative impacts on terrestrial primary production (Zhao and Running, 2010), with shifting precipitation regimes likely to have profound effects on future climate-carbon feedback cycles (Carvalhais et al., 2014). Forest dynamics, the processes of recruitment, growth, mortality and species turnover are changing globally, with shifts towards younger and faster turnover forests at the expense of old-growth forests (McDowell et al., 2020). In addition, widespread decline in crown condition across southern Europe through altered leaf structures and higher defoliation in response to water deficit have been observed (Carnicer et al., 2011). There is a global concern around forest health and its resilience to global change (Trumbore et al., 2015) and therefore effective monitoring of tree crown health at scale is an important endeavour (Jump et al., 2017; Camarero et al., 2015).

1.3 The importance of individual tree architecture

Interest in tree architecture dates back to Leonardi da Vinci, who observed that branching networking within a tree follows self-similarity, where the cross-sectional area of branches is conserved along branching orders (Minamino and Tateno, 2014; Richter, 1970), i.e., the sum of the cross-sectional area of the daughter branches is equal to the parent branch. Later, Thompson, (1917) introduced architecture and its biological relevance, and subsequent work by Halle et al., (1978) advanced the concept of architecture, leading pioneering work on understanding the organisational principles of a whole plant across space (e.g. branching) and through time (ontogeny), proposing 23 distinct descriptions of tree form.

A tree's overall structural form is a product of its inherent genetic development programme and its adaptive response through semi-autonomous allocations to growth to its immediate surroundings (Valladares and Niinemets, 2007). Recent work has shed new light on climatic and developmental constraints on architecture, highlighting how simple architectures enable frequent transitions to new forms in high disturbance and stressful conditions while complex structures emerge under stable climates but have less evolvability (Anest et al., 2021). The resulting structural form of individual trees has implications of the fluxes of energy, water and carbon from the individual leaf through to an entire forest ecosystem (Enquist et al., 2009). Many analyses linking tree form and function have used scaling relationships that simply characterise how one body part (e.g., tree height) scales to another, which conventionally represents body size, for example a trees diameter at breast height (DBH). These vary from interpretations within the context of hydraulics such as the pipe model theory (Shinozaki et al., 1964), mechanical constraints apposed on height and branch extension (McMahon and Kronauer, 1976), structure-function relationships representing trees as a network of elementary units (Sievänen et al., 2014), frameworks predicting metabolism from principles of efficient resource transportation (Enquist et al., 2009; Price et al., 2012; West et al., 1997) and integration of thermodynamics (Bejan et al., 2008). The difficulty in such deriving principles and mechanisms behind structure-function relationships is that trees often have to do many things well in response to their surroundings (Niklas, 1994), leading to deviations from optimisation principles and trade-offs between allometric relationships of various components' of tree structure (Pretzsch and Dieler, 2012).

Of all these theories on the relationship between form and function on trees, none have sparked as much interest and debate as did the emergence of metabolic scaling theory (MST), mostly because it states clear hypotheses that both explain and predict allometry. MST makes scaling predictions of height and diameter from mass, which itself is derived from assumptions of fractal volumetric filling and elastic similarity in mechanical stress, with vascular tapering ensuring constant resistance independent of hydraulic path length (West et al., 1999). Essentially, MST is grounded on the basis of evolutionary forces maximining transport efficiency along its vascular network to its photosynthetic parts. An array of empirical tests have been conducted on MST predictions of allometry (Lines et al. 2012), growth (Coomes and Allen, 2009), mortality (Muller-Landau et al., 2006), and stem densities (Lin et al., 2013). Other work has proposed extensions or adaptations of MST, through the addition of more realistic ecological detail in how trees compete for light (Coomes et al., 2012), and more representative depictions of the hydraulic transport system (Savage et al., 2010). Theoretical frameworks such as MST therefore offer an excellent platform to assess tree structure, tree space filling and the scaling of organisation principles from leaf to forest (West et al., 2009). Explicit tests of branching rules within MST are limited, mostly because of the highly laborious nature in measuring individual branches manually (Bentley et al., 2013) but new detailed 3D remote sensing measurements may open up new avenues to testing (Disney, 2019, Owen et al. 2021).

A fundamental critique of MST is in its marginalisation of competition for light (Coomes, 2006), but forest ecologists have long interpreted tree structure in respect to light capture, understanding form as a means for trees to respond to shade or sun-lit conditions and leading ‘mono-layered’ and ‘multi-layered’ depictions of crown form (e.g. Givnish, 1988; Horn, 1971). While the principle reason to grow a trunk is to overtop neighbouring trees and escape low light (Henry and Aarssen, 1999), a tree’s crown shape, arrangement and size is the result of growth patterns to maximise light capture (Valladares and Niinemets, 2007) across a gradient of light availability (Martin-Ducup et al., 2020). Plasticity in structure can occur as soon as any form of lateral shading occurs (Harja et al., 2012), with partial shading thought produce a stronger response than full shade (Schoonmaker et al., 2014). Given the exponential decrease in light availability with each additional layer of foliage, there is a premium placed on deploying leaves above others to not only maximise

photosynthetic rates (Craine and Dybzinski, 2013) but also though competitive benefits to shade neighbouring leaves and slow growth and other resource use (Falster and Westoby, 2003). To avoid excessive and inefficient respiratory and maintenance costs for a given set of light conditions, leaves are optimised to economically coordinate acquisition with availability that matches a species' life history (Wright et al., 2004), and this can also vary within a single tree crown (Williams et al., 2020). Theories such as MST assume homogenous photosynthetic rates across an individual's tree crown (West et al., 1999). However, shade cast by neighbours and self-shading through, for example, increasing crown depth, can invalidate such assumptions (Duursma et al., 2010) while water limitation can result in trees expressing different traits on shaded compared to sunlit parts of a crown (Mediavilla et al., 2019). Within ecosystems where water is limiting and excessive radiation can create stress, trees can express an architecture whereby the upper most leaves at as a protective barrier to productive foliage below (Miller et al., 2021; Pearcy et al., 2005), demonstrating the potential ecological benefits of shade in drier ecosystems (Valladares et al., 2016). Within ecosystems with multiple stressors, as are found in the Mediterranean, plasticity in structure can be constrained, for example, stem extension to avoid shade is also associated with increased risk of mortality during cold snaps in winter (Valladares et al., 2005). Similarly, favourable conditions at one time can lead to structural overshoot and therefore higher risk of mortality when conditions rapidly change (Jump et al., 2017), and which are predicted to increase under a rapidly changing climate. A more holistic assessment is need in such environments that consider a multitude of stresses from shade (Valladares and Niinemets, 2007), drought (Lines et al., 2012) and wind exposure (Brüchert and Gardiner, 2006).

A tree's overall structure is therefore a result of trade-offs between extension in width and height to acquire more light within the constraints of minimising hydraulic and mechanical risk (Verbeeck et al., 2019). Hydraulic path length, i.e., the length of conduits from the tree base to leaves, poses strong constraints on maximum tree height and branch extension (Olson et al., 2018), and conduits widen from tip to base according following scaling rules that enable constant stress along a hydraulic pathway irrespective of its length (Olson et al., 2021; West et al., 1997). Without tapering, tree height would be capped at limits below those we see today, but its presence leads to the assumption that trees of various sizes transport water and nutrients at the

same rate (Enquist et al., 2009). It also leads to the conclusion that a trees response to drought is through path length shortening (reduce tree hight) rather than changes to conduit diameter at the base (Fajardo et al., 2020, 2019). This neatly coincides with observations that branch dieback often occurs along the longest hydraulic pathways (Rood et al., 2000), leading to narrower crown widths in dry environments (Lines et al., 2012) with implications for understanding tree structural response to drought (McDowell et al., 2008). Measuring branch lengths from base to tip is necessary to improve our understanding of tree structure and the interplay between hydraulics (Olson et al., 2021) and light acquisition (Smith et al., 2014) but existing techniques are incredibly laborious, meaning small sample sizes are prevalent in studies.

Trees are constrained by gravity and mechanical limits to prevent them from buckling under their own weight (McMahon and Kronauer, 1976), leading to structural response to ensure mechanical safety (Groover, 2016) and a balance between light acquisition and resisting the forces of gravity (Duchemin et al., 2018). Creative approaches have been applied to independently analyse the effect of wind loading on tree structure, Nicoll et al., (2019) used guy lines to provide support and stability for a subset of trees, while Hale et al., (2012) monitored wind speed and tree stem response and experimental set-ups have been formulated that directly control for other factors such as drought (Niez et al., 2019). Recent 3D simulation modelling using real-life trees capture by terrestrial laser scanning (TLS) has highlighted the significance of architecture over material properties in determining wind induced mortality (Jackson et al., 2020), with large and dense crowns more predisposed to wind throw risk (Huang et al., 2020). Irrespective of water and light limitation, trees have been found to invest biomass into radial growth that increases stability (Bonnesoeur et al., 2016; Niez et al., 2019) at the expense of primary growth (Coutand et al., 2008), highlighting the importance of mechanical safety against abiotic stressors. Wind exposure can limit lateral crown expansion (Loehle, 2016), tree height (Coomes et al., 2018), root growth patterns (Tamasi et al., 2005), and the capacity to lean stems and branches towards light (Alméras and Fournier, 2009). However, lower windspeeds can be beneficial for light capture by enabling light to penetrate deeper into the crown (Way and Pearcy, 2012), increasing total carbon gain (Uemura et al., 2006).

Although it is clear that trees must respond to an array of biotic and abiotic stresses, the relative contribution and prioritisation of traits to responses is less understood, partly because of paucity in data, which leads to difficulties in accounting for a multitude of environmental factors that affect tree growth and allocation of biomass. Under a given set of environmental conditions, plasticity in one structural trait may pose an advantage under one extreme abiotic factor but also maladaptive to extreme values of another abiotic factor. For example, seedlings responding to limited light by stem elongation suffered most during a cold-snap (Valladares et al., 2007). Plasticity to simultaneous extreme values can be difficult, for example, under a deep shaded but dry understorey frequently found in Mediterranean forests (Niinemets and Valladares, 2006), leading to only few species able to survive there (Valladares and Pearcy, 2002). Plasticity can therefore be constrained when multi stresses are prevalent leading to narrow, more co-ordinated expressions of plasticity (Benavides et al., 2021), and trees that are vulnerable to rapid abiotic change (Valladares et al., 2007). Mediterranean forests make for an excellent study system to understand how a multitude of stressors affect tree structure, due to its high seasonality, mountainous terrain, and high biodiversity, as well as changing climate to hotter and drier conditions (Guiot and Cramer, 2016).

1.4 Mediterranean forests

Globally, Mediterranean ecosystems are considered biodiversity hotspots (Myers et al., 2000) and countries such as Spain that straddle this climatic belt are host to a considerable amount of forests. Unfortunately, these ecosystems are also under considerable threat from climate change creating hotter and drier conditions, with increasing mortality rates (Bravo-Oviedo et al., 2006; Ogaya and Peñuelas, 2007), pervasive shifts towards ecosystem dominance by more drought tolerant species (Ogaya and Peñuelas, 2021), and concerns over negative effects on ecosystems services. Some studies have even documented trees shifting from carbon sinks to sources due to increasing temperature and aridity (Reichstein et al., 2002). Within the Spanish Mediterranean, there is considerable interest in studying the dynamics of common pine -oak ecosystems, these species' coexistence and how this might vary with water limitation (Gea-Izquierdo et al., 2020).

In Mediterranean mountains, the climate fluctuates between two extremes, with frequent hot dry summers and cold winters (Moreno and Oechel, 2012), the former expected to become more extreme with climate change

(Christidis et al., 2015), with likely ramifications for species composition, structure and carbon dynamics (Ogaya and Peñuelas, 2021; Ruiz-Benito et al., 2014). Changes in tree growth and structure depend on water availability in Mediterranean forests, affecting their capacity to accumulate carbon in the future (Ruiz-Benito et al., 2014) with individual species' variability in response to water availability affecting forest composition (Galiano et al., 2012). It is becoming increasingly apparent that globally water may have a more profound effect on vegetation than direct effects of temperature (Franklin et al., 2015). Within a topographically complex and heterogenous environments where the climate is highly varying, strongly heterogenous environmental conditions and accompanying biotic responses can develop over relatively short distances. For example, sap flow measurements looking at drought response found significant differences between trees within plots only a few hundred meters apart (Forner et al., 2014). Topography can govern fire dynamics with topographic positioning on slope, ridges and valleys affecting fire severity (Kane et al., 2015), and interact with drought by constraining roots to only certain depths (Fan et al., 2017; Zhang et al., 2020). But recent work has found hydraulically vulnerable trees need to compensate for water-stress related mortality through accessing deeper water reserves, with important implications to our understanding of forest dynamics under future climate change (Chitra-Tarak et al., 2021). This shows the importance of groundwater and its recharge to plant transpiration in water-limited forests (Barbeta and Peñuelas, 2017) to lessen drought impacts (Carrière et al., 2020; David et al., 2007), but the current state and future stability of groundwater at the global scale is largely unknown (Taylor et al., 2013). In the Spanish Mediterranean extreme drought events along with persistent drier conditions are expected to deplete deep water reserves, with likely determinantal consequences to forests (Barbeta and Peñuelas, 2017). Water availability and its interaction with tree rooting is therefore a crucial research area in arid and semi-arid ecosystems, but is mostly unaccounted for in simulation models, causing uncertainty in the effects of aridity on productivity and carbon dynamics (Nadal-Sala et al., 2021).

In Mediterranean forests, fire disturbance can maintain forest structural complexity and have lasting impacts on tree crown morphology. Mediterranean forests are shaped by tightly coupled and co-evolving human and fire processes, and recent trends in land use change are interacting with a changing climate to drive changes in the fire regime (Viedma et al., 2015), necessitating different management protocols (Molina and Galiana-

Martín, 2016). It's for these reasons that Spain is one of the few countries in Europe showing an upward trend in fire occurrence (Turco et al., 2016). A mixture of severity in fire disturbance can foster forest structural complexity (Meigs et al., 2017), with suppression of fire altogether thought to homogeneous structure (Fry et al., 2014). At the individual scale, tree crown allometric scaling can reflect fire disturbance frequency with crowns shortening crown depth faster with height to avoid the risk of crown ignition (Panzou et al., 2021; Tredennick et al., 2013) but physiological damage to hydraulic transport tissues can leave a tree more predisposed to drought impacts (Bär et al., 2019)

1.5 Measurements of forest structure from the ground to satellites

Forest structure is traditionally characterised by ground-based metrics such as stem density counts, stem diameter and height size distributions, basal area and crown shape. Forest inventories collect data in a systematic manners, and often measure tree height and dimeter, which together enable the direct calculation of plot-scale tree density, basal area and indirectly, estimates of biomass and volume through species allometric equations (Annighöfer et al., 2016; Zianis et al., 2005). If stem locations are measured, distance-dependent competition indices can be calculated enabling a more comprehensive assessment of tree-tree interactions (Kunstler et al., 2016) but forest inventory plots tend to be small, exacerbating edge effects (Hynynen and Ojansuu, 2011).

The information content in ground-based metrics does not always enable accurate quantification of properties of interest, leading to research into new ways to understand forest structure. Tree height and crown diameter are two metrics that may be obtained from airborne laser scanning (ALS), and recent tropical biomass work has found that the inclusion of crown diameter results in substantial improvements to estimates of biomass (Jucker et al., 2017). Tree height can be extracted from ALS data with higher accuracy than in the field (Zolkos et al., 2013), and ALS can provide sub-metre accuracy of surface heights (Lee et al., 2010; Lefsky et al., 2005). However, retrieval accuracy can be affected by canopy height and distribution (Hopkinson and Chasmer, 2009), slope of the terrain (Breidenbach et al., 2008) and the number of returns per m^2 (Hyyppä et al., 2000). Nonetheless, dependable retrievals of stem density, vertical foliage profile (Coops et al., 2007) and basal areas

(Lee and Lucas, 2007) and above ground biomass measurements (Mascaro et al., 2011; Simonson et al., 2016) have been made using low density ALS data (e.g. less than 10 points/m2). Although relatively less common, repeat ALS has been shown to be able to provide insights into structural dynamics (Simonson et al., 2016) and growth (Yu et al., 2004), whilst large surveys can determine successional stage (Falkowski et al., 2009) and tree-health (Shendryk et al., 2016).

At national to global scales, measurements of forest structure have mostly been of biomass or wood volume (and therefore aboveground carbon storage) extracted from satellite data, including from passive microwave (Liu et al., 2015), optical (Gómez et al., 2014) and C-band (Santoro et al., 2010) and L-band Synthetic Aperture Radar (SAR; Mitchard et al., 2011). For hereon, I will mostly focus on SAR based platforms due to them providing a more direct measure of structure relative to optical instruments. Measurements of structure collected at scale, for example onboard satellites, often require calibration using ground-based estimates (Rodríguez-Veiga et al., 2017), which are usually calculated using allometric equations that are heavily biased towards smaller trees (Disney et al., 2018). Typically, SAR biomass estimates are calculated by correlating backscatter coefficients related to volume and/or allometry, whereas polarimetric interferometry (PolInSAR) provides an estimate of height (Le Toan et al., 2011; Mette et al., 2004). The upcoming European Space Agency BIOMASS mission is the first mission to focus on biomass retrieval and as such, has been engineered to include two approaches to estimating biomass; SAR backscattering and PolInSAR to enhance accurate retrieval (Le Toan et al., 2011). Space-borne LIDAR such as ICESat GLAS and the recently launched GEDI (Duncanson et al., 2020) have been used to quantify biomass at the global scale (Simard et al., 2011), showing close agreement to airborne measurements (Popescu et al., 2011), while its integration with long-term satellite has effectively retrieved forest height at the global scale (Potapov et al., 2021)

Satellite monitoring of crown and canopy properties is largely of leaf area index (LAI), which is the projected leaf area relative to ground area (m^2 m^{-2}), and interpreted as a good proxy of ecosystem productivity and health, including plant responses to water availability (Jump et al., 2017). Leaf area index is a key input and parameter within global dynamic vegetation models, as it forms the interface between vegetation and the atmosphere (Fang et al., 2019). GEDI is providing LiDAR estimates of LAI at global scale (Dubayah et al.,

2020), while older ICESat GLAS data (Cui et al., 2020) has been used to estimate both LAI and vertical foliage profiles (Cui et al., 2020), though accurate retrieval with spaceborne LiDAR platforms is thought to be considerably affected by topography (Wang and Fang, 2020). ALS retrieval is less affected by terrain but even with its relatively higher resolution and coverage, retrieval here can be limited by the selection of height thresholds, types of return (discrete vs full-waveform) and point density (Wang and Fang, 2020). Still, ALS may be used to derive LAI based on metrics of canopy structure and percentage hits (Riaño et al., 2004), and the use of radiative transfer models (Tang et al., 2012) - the latter of avoiding saturation issues inherent in passive optical estimates (Peduzzi et al., 2012).

The patchiness of current and future space-borne platforms means spatial interpolation is often necessary to develop products with spatial and temporal consistency (Potapov et al., 2021; Silva et al., 2021), a concern particularly in the context of driving and constraining long-term simulation models. Alternatively, long-term SAR-sensors with high temporal resolution and global spatial coverage, such as Sentinel-1, can quantify habitat structure and vertical heterogeneity directly (Bruggisser et al., 2021), with strong correlations with species composition also evident (Bae et al., 2019). However, various forest and topographical factors affect SAR backscatter coefficients, requiring further work to establish exactly the forest attributes that are attainable with SAR (Woodhouse et al., 2012). This is particularly important with short-wavelength C-band, where the scattering signal primarily originates within the tree crown (Pitts et al., 1987). Tools such as TLS could shed new light on these exact mechanisms (Joshi et al., 2017), with its enhanced capacity to characterise branch topology (Martin-Ducup et al., 2020) and foliage arrangement (Béland and Baldocchi, 2020), beyond single and vertical stratified height profiles (Bae et al., 2019). Indeed, TLS may be able to show which features are detectable with C-band RADAR that complement longer wavelength L- and S-band sensors, where scattering is understood to be within the main woody parts of a tree (Huang et al., 2018; Mitchard et al., 2012).

Although very high resolution satellite data has shown potential in locating tree crowns in arid landscapes (Brandt et al., 2020), these approaches to date cannot function in more complex, multi-layered canopies, where individual tree delineation becomes difficult (Aubry-Kientz et al., 2019), and suitable data are often available

only upon payment. Aerial approaches are therefore likely to continue to be used, and crown metrics can be estimated from high point density discrete ALS platforms (~ 8- 20 points m^2; Wu et al., 2016), including crown volume (Korhonen et al., 2013), depth (Lee et al., 2010), diameter (Jucker et al., 2017; Morsdorf et al., 2004), cover (Lee and Lucas, 2007) and complexity (Murray et al., 2018). Full waveform datasets can go a step further by describing vertical structural complexity (Nie et al., 2017), including understorey characterisation (Hancock et al., 2017) and crown morphology (Lindberg et al., 2012). However, inaccuracies persist; for example Hastings et al., (2020) show that species traits can determine the success of LiDAR based crown mapping in mixed temperate forests, affecting its applicability in drawing widespread ecological conclusions. ALS's main strengths are in its ability to collect data across vast areas (Stovall et al., 2019) but it fails to capture smaller trees occluded in the understorey (Donager et al., 2021), leading to some integrating to integrate TLS with ALS data to better monitor understorey volume (Liu et al., 2017) and improve biomass calculations (Stovall and Shugart, 2018). Given the steady increase in occlusion with depth with ALS (Morsdorf et al., 2018), along with its inability to capture small-scale tree crown topology, TLS is paving the way towards analysing tree structure from a three-dimensional perspective never before possible (Malhi et al., 2018).

1.6 Opportunities for structural insights from Mediterranean forests using terrestrial laser scanning

TLS provides a complete, quantitative and repeatable means to measure tree form and in doing so, creates a wholly new perspective on the rules that govern tree form and its variability across space (Martin-Ducup et al., 2020) and time (Yrttimaa et al., 2020). Trees are under a multitude of biotic and abiotic stresses in Mediterranean forests and given their sessile nature must balance growth that maximises light interception and carbon gain with mechanical and hydraulic safety to ensure survival under current and highly variable conditions. Theory postulates trees as structured as highly optimised transport networks but within this is only likely hold true under benign conditions, while the scaling from branch through to crown and up to the forest scale rely upon coarse simplifications of crown shape, size, and plastic arrangement in space. The primary objective of this thesis is to demonstrate the potential of TLS data to derive new ecological meaningful metrics from three-dimensional point clouds and use these to answer ecological questions from a new perspective. I

undertook this work in Mediterranean forests in Spain where the altitude means very cold winters are combined with hot dry summers which interact with a highly complex mountainous terrain, resulting in a highly heterogenous environment and an ideal environment to explore tree architecture and its key drivers.

1.7 Thesis outline

The primary objective of the thesis is:

To demonstrate how individual tree crown allometry, plasticity and light capture can be quantified using new 3D measurements, and to use new metrics to provide novel insights into how trees and different species grow, fill space, express plasticity in structure, and how structural plasticity interacts with light capture.

The layout of the thesis is as follows:

Chapter 2 highlights not only the exciting opportunities presented by TLS in developing a more comprehensive understanding of tree structure but also the complexities that arose in applying existing methods to a water limited forest ecosystem. Modifications to existing code, bespoke algorithm development and the construction of efficient processing pipelines were essential in extracting the necessary ecological metrics for the proceeding chapters (chapters 2 and 3). Adaptations to an open-source tree segmentation algorithm involved accounting for leaning trees, enhancing cylinder fitting procedures that improved the search of tree stems and the extraction of diameter at breast height. In addition, a new approach to identifying and extracting diameter measurements from multi-stem trees is also presented. Comparisons between TLS and estimates from inventory type data demonstrated not only substantial variability in discrepancies between shapes but also consistent overestimations of crown volume. Finally, this chapter presents the exciting new prospects that can emerge in deriving spatially explicit metrics of three-dimensional light capture.

Chapter 3 demonstrates how these TLS-derived crown morphology metrics provide robust means to test longstanding ecological theory and gives novel insights into tree-tree interactions through the quantification of novel neighbourhood competition metrics. Symmetric and asymmetric competition was quantified and used to test the importance of neighbourhood genus diversity on crown morphology. Competition negatively affected all crown metrics except crown depth, and asymmetric competition was the strongest driver of pine

crown morphology, but oaks were more sensitive to symmetric competition. Most species and crown dimensions had height-crown scaling exponents below those predicted by MST, which may be due to water-limitation effects. Pines and oaks showed large differences in crown depth to height scaling, with the former shallower and the latter deeper, in contrast to theoretical predictions.

Chapter 4 provides novel insights into tree structural plasticity and trade-offs, the interaction between individual structural plasticity and light interception indices, and plot scale crown packing and light capture. Tree structural plasticity metrics were derived including stem elongation, stem and crown displacement, crown foliage distribution and crown filling and complexity. Trees exhibited various forms of plasticity with inter-specific differences in plasticity evident across all species. Crown foliage distribution variation led to increases in light capture across all species, and elongation was evident under lower light irrespective of shade tolerance. Plot scale analysis found that more diverse plots are more structurally complex but do not occupy canopy volume, in contrast to findings reliant on ground-based measurements.

Chapter 5 presents an overview of the key findings of the thesis and discusses future opportunities and necessary steps required for TLS to be adopted not only across the wider forest ecology community but also to forest inventory. Methodological development that functions across both different instrumentation and ecosystem type is especially important if TLS is to be integrated into forest inventory protocols where replicability, repeatability, and scalability are priorities. The forest ecology community also needs to find consensus on calculating metrics from TLS that have independent ecologically meaning whilst ensuring inter-study interpretability and back compatibility to historical inventory data. The impact of three-dimensional light capture metrics is discussed in both the context of improving our understanding of belowground competition and in developing deeper insights into light-structure relationships. Finally, future analyses should look to quantify and include topographical variables readily available from both ALS and TLS to provide a more comprehensive understanding of tree form and function, its relationship along abiotic gradients and the interplay between these gradients and tree-tree competition for resources.

Note that some of the contents of this thesis have been published in the peer-reviewed literature, specifically:

Parts of section 1.5 of Chapter 1 have been published in Ruiz-Benito, P., Vacchiano, G., Lines, E. R., Reyer, C. P., Ratcliffe, S., Morin, X., ... Owen, H.J.F & Zavala, M. A. (2020). Available and missing data to model impact of climate change on European forests. *Ecological Modelling*, 416, 108870.

Chapter 3 has been published as: Owen, H.J., Flynn, W.R. and Lines, E.R., 2021. Competitive drivers of interspecific deviations of crown morphology from theoretical predictions measured with Terrestrial Laser Scanning. *Journal of Ecology*.

Chapter 2

Terrestrial Laser Scanning for Mediterranean Forest Ecology: Methodological Developments

Abstract

The automation in processing of TLS from data collection through to the quantification of tree structural metrics is fundamental to its widespread adoption across forest ecology but to date, most development has been within simple structure plantations or tropical forests. This chapter briefly outlines the emergence of TLS in forest ecology, highlighting its journey from simple replications of forest inventory to what is now fully three-dimensional characterisation of branch topology and foliage and proceeds in to highlighting the complexities encountered in applying this tool to a water-limited Mediterranean forest ecosystem.

In segmented individual trees various methodological hurdles were encountered that necessitated algorithm modification, refinement and in some cases new development to extract trees and stem metrics (DBH) as best possible from a phase-shift instrument. Once segmented, further algorithms are essential to extract structural measures from these highly detailed point clouds that translate into ecological meaning within subsequent chapters. Here, I outlined various bespoke algorithm development together with existing tools that were deployed to derive, one through to, three dimensional measures of tree structure and its morphological plasticity in three-dimensional space. Where TLS measures are comparable to ground-based alternatives, comparative analysis were conducted to assess the degree in discrepancy between 'old' and 'new' means in deriving these measures and discuss where conceptual development is also necessary to move forward.

This chapter finishes by outlining an exciting opportunity in TLS quantifying individual tree light capture in a spatially explicit manner by applying a new ray-tracing algorithm and showcases two-new metrics that were developed to condense this vast information into holistic measures of light interception.

2.1 Introduction

2.1.1 Emergence of TLS in forest ecology

Historically, insights into tree architecture have come from tape-measurements, hand sketches, photography and manual digitisations (Preuksakarn, 2012). Computer-generated visually realistic depictions of trees have been produced using 'rules' for structure, including stochastic growth, assumptions of fractality, and growth grammars such as the Lindenmayer system (Honda, 1971; Prince et al., 2014) but now the advent of three-dimensional data means a complete description of a trees topology can be extracted. The advent of ground-based light detection and radar (LiDAR) laser scanning technologies has made direct measurement of fine-scale tree structure possible, opening new opportunities to infer detailed structural insights from three-dimensional data. Mounted to an aircraft, airborne laser scanning (ALS) can cover large areas and reach those that are difficult to access, but its view from above means trees below the upper canopy as well as branching structures are often occluded and therefore not measured (Morsdorf et al., 2018). In contrast, terrestrial laser scanning (TLS), with comparatively much higher point density and a viewpoint from below, creates a rich and highly detailed three dimensional image of branch and crown structure (Morsdorf et al., 2018). TLS is now being used to provide new insights into tree mass, including deriving better allometric relationships for larger trees (Disney et al., 2020, 2018), as well as opening new and exciting opportunities in forest ecology (Calders et al., 2020; Malhi et al., 2018), where theoretical understands of tree structure can now be vigorously examined with data.

Much of the earliest work with TLS in forests were attempts to quantify measures of forest structure that were taken using ground based approaches in forest inventory (Liang et al., 2012; Maas et al., 2008; Thies and Spiecker, 2004; Watt and Donoghue, 2005), or replace passive instruments to derive attributes such as gap fraction (Danson et al., 2007). Later developments enhanced measures that were difficult to measure on the ground without making geometrical assumptions, including crown volume (Moskal and Zheng, 2012) and morphology (Kunz et al., 2019), above ground biomass (Calders et al., 2015) and its temporal dynamics (Kaasalainen et al., 2014). Now, the integration of TLS into long-term monitoring projects is growing (Orwig et al., 2018), and the fusion of satellite data with TLS (Kaasalainen et al., 2015) and other forms of remote

sensing (i.e. UAVs) offers the opportunity to revolutionise the way we assess forest structure across scales (Morsdorf et al., 2018). However, caution is needed when adopting any new technology, and for TLS this is particularly important because of the wide range of instruments, suitable for different needs, with ramifications for the scale and detail at which a trees structure can be analysed.

2.1.2 Instrumentation

Terrestrial Laser Scanners are active ground-based remote sensing instruments that construct three-dimensional point clouds of an environment by emitting laser pulses and recording the returning signal. For example, in time-of-flight systems the distance between the scanner and target is measured by calculating the time between the fired pulse and its return at the scanner (Jupp et al., 2007), and located using angular information to create a 3D point cloud. TLS instruments may also record intensity information and the full waveform response of each pulse. The basic premise for TLS 3D collection data is similar across instruments, but there are two distinct platforms with contrasting ranging methods: phase-shift (PS) and time-of-flight (TOF). These have their distinct advantages and differ primarily in cost and signal-to-noise ratio (Dassot et al., 2011). Phase-shift instruments determine distance by analysing the phase shift between a laser beam that is continuously emitted and received with only a single return recorded for each azimuth and zenith direction, whereas TOF measures the time taken for a beam to return from an object, which is then divided by two (Dassot et al., 2011). In general, TOF instruments are slower in acquisition and lower resolution, but have a longer range and better signal-to-noise ratio, whereas PS sensors can scan in near full 360 in one acquisition, are quick in acquisition, but have higher signal-to-noise ratio. There is some consensus seems that TOF sensors are better suited to forests, where structure is complex and partial hits abundant due to leaves that are dealt with waveform filtering, and TOF ranges are better suited to high canopies (Calders et al., 2020; Dassot et al., 2011; Jupp et al., 2007). To date, TOF sensors have been thought of as the ‘gold standard’ for TLS acquisition across a variety of forest types (Newnham et al., 2012), however substantial success has been had with PS systems (Walter et al., 2021), where data limitations can be overcome in medium-height canopies using a dense sampling strategy to produce high fidelity data. Not least, PS systems can be smaller and much less expensive than TOF systems. PS systems can also be much more mobile, with no tripod needed, scanning

much larger areas efficiently (Bienert et al., 2018). In this thesis I use a phase-shift system – the Leica HDS6200 – and discuss the associated methodological issues in this chapter.

2.1.3 TLS for Forest Ecology

Historically, the accurate measurement of tree structure has been hampered by the size and complexity of trees themselves, making detailed direct measurements time consuming and usually limited to a handful of simple metrics, primarily of the trunk. If we take biomass as one example, direct measurements can only be derived from destructively harvested trees, so these have historically been used to estimate a coefficient for allometric equations (Disney et al., 2018). However, use of allometric equations derived from destructive sampling has meant many widely used equations are derived from very small sample sizes with considerable size bias, with very few very large trees, and most samples from commercial plantations. The accurate estimation of biomass is crucial for understanding the terrestrial carbon cycle (Houghton et al., 2009) so better approaches were needed. The biomass of a tree may be estimated as the volume of wood multiplied by the wood density, and TLS offers the opportunity to estimate volume with very high accuracy - Quantitative Structure Models (QSMs) of TLS point clouds have been shown to be able to derive accurate estimates of tree volume, overestimating biomass by 9.68% with destructively harvested Eucalyptus trees, compared to a 36.57-29.85% underestimation through the use of allometric equations (Calders et al., 2015). More recently, TLS-derived biomass estimates have shown that traditional allometry methods have underestimated the biomass of some of the largest trees on earth by up to 30% (Disney et al., 2020).

Use of TLS for biomass is one example of substantial improvement in estimation of an important property that cannot practically be measured by other methods. However, TLS has further promise for the more precise estimation of metrics that may be estimated using traditional forest inventory methods. For example, crown depth, radius and volume are key drivers of demographic processes in many forest modelling frameworks. How one part of tree crown scales with another (usually size) is a simple means to model how crowns grow, fill space and compete with other trees for space (West et al., 2009), and models are usually parameterised using crown allometric relationships reliant on readily available size-based measurement such as DBH and height. However, crowns are complex and tessellating in form, making measurement from the ground using

tape measures and range finders difficult and time-consuming. The inclusion of TLS is therefore an exciting prospect for future inventory collection (Bauwens et al., 2016).

The most exciting contribution of TLS to forest ecology may yet come from novel insights into crown structure of properties only quantifiable with high-resolution remote sensing. Examples include branch lengths and order (Lau et al., 2018), foliage and stem arrangement in space (Béland and Baldocchi, 2020; Eichhorn et al., 2017), leaf angle distribution (Vicari et al., 2019; Xu et al., 2019), path length of branching network (Chapter 4), and characterisation of crown interactions (Chapter 3; Owen et al., 2021). For such metrics consideration of data acquisition techniques is required, and a multiple scanning strategy is absolutely necessary to minimise occlusion effects and capture the full crown (Yun et al., 2019). The availability of TLS presents an exciting opportunity for the field of ecology with researchers no longer forced into formulating coarse abstractions of tree structure from limiting two-dimensional data. However, there remain methodological complexities that hinder its widespread uptake across the research community. Despite huge efforts to develop open-source tools (e.g. Burt et al., 2019; Hackenberg et al., 2015; Vicari et al., 2019), data consistency is still an issue as many algorithms are reliant on expensive, high-fidelity full-waveform TOF scanning systems (e.g., Riegl VZ400; Calders et al., 2016). The majority of algorithm development for TLS data processing has focused on data collected from either the tropics or conifer type plantations of commercial value, driven by interest in biomass and woody stock volume, which are very difficult to measure on the ground but of great importance to carbon accounting and commercial valuations. Many exciting developments have been made within this context, including automated tree segmentation (Burt et al., 2019), leaf/wood separation (Vicari et al., 2019) and quantitative structure modelling (QSM; Hackenberg et al., 2015; Raumonen et al., 2013). However, in order for TLS to be used to its full potential for ecology, TLS processing needs to be developed beyond biomass, to extract metrics that are relevant to forest ecologists, and to open opportunities to explore complex individual tree structure from a dimensional perspective never before possible (Malhi et al., 2018).

In this chapter, I describe the development of a processing pipeline for data collected across 34 30 x 30m plots in protected, unmanaged mixed Mediterranean forests in central Spain. Here, I describe existing TLS processing approaches, the issues faced when applying them to how these to the Mediterranean context, and

how these were overcome. I also present the derivation of new, ecologically focussed metrics that demonstrate the full potential of these data for forest ecology. The forests in my dataset include two oak species (*Quercus faginea* and *Q. ilex*) and two pines (*Pinus sylvestris* and *P. nigra*), situated within a landscape that is highly variable topographically, features that are fully described in Chapter 3. Collectively, the abiotic environment combined with the intra and inter-specific adaptions of the species that live there, mean structure is highly variable and distinct to purely light limited forest types, and shows substantial contrast to the kinds of forests in which TLS processing algorithms have been developed. Here, stems are highly irregular; canopy trees bifurcate very low to the ground along with a significant shrub layer; and multi-stem trees are widespread due to past management history (pollarding and coppicing) and as a natural response post-disturbance (e.g., fire). For this project, many modifications to existing openly available code as well as bespoke algorithm development was necessary to transform 3D point clouds into ecologically meaningful data. Much of the work utilised the C++ point cloud library (PCL) toolset and packages within R (R Core Team, 2021) together with shell scripts for data management and pipeline construction. In the next few sections, I give an overview of the TLS processing pipeline for forest data, describe the main developments I have introduced within each step, and discuss future directions.

2.2 Overview of TLS processing steps

2.2.1 Workflow Schematic

There are many processing steps that are necessary to progress from TLS data collection in the field to finally producing ecological metrics for statistical analyses. In Figure 2.1, I outline the various steps that were taken in chronological order starting from the top (step 1), progressing through TLS data processing within proprietary software, and ending with metrics of crown morphology (chapter 3), tree structural plasticity and light capture indices (chapter 4). Across the pipeline, I highlight the various software and coding languages that were employed by displaying their respective symbols and cite these when required within the text. The orange text highlights the more bespoke algorithm developments while black text only necessitated minor changes and/or running existing functions. Once data were collected (step 1) they were imported into cyclone where targets were identified (step 2; section 2.2.2), merged and exported to an open file format (section 2.2.3).

The raw plot point cloud was then clipped (step 5) to 37.5 x 37.5 m, denoised and downsampled (steps 6-7) for individual tree segmentation (step 9.1-9.4) where the output trees were manually refined and tagged with species IDs (step 9.5; section 2.4.5). All individual trees had leaves separated from wood (step 10; section 2.5.1) and a path length attributed to each point (step 11; section 2.5.5). The leaf/wood separated clouds then proceeded onto sections of ecological metric extraction. Across steps 12.1-12.10, both the leaf and wood components were used to extract DBH and classify stems as single or multiitem (section 2.3.5) and calculate crown morphological metrics and neighbourhood competition indices (step 12.10) used in chapter 3 (section 2.4). Again, the leaf/wood clouds were used in steps 13-13.6 to derive measures of tree plasticity and crown filling (section 2.5), and together with a new light capture software (steps 14.1-14.6; section 2.6.5) and metrics (steps 14.7-14.9; section 2.6.5-2.6.6), provided new insights into light-structure relationships in chapter 4.

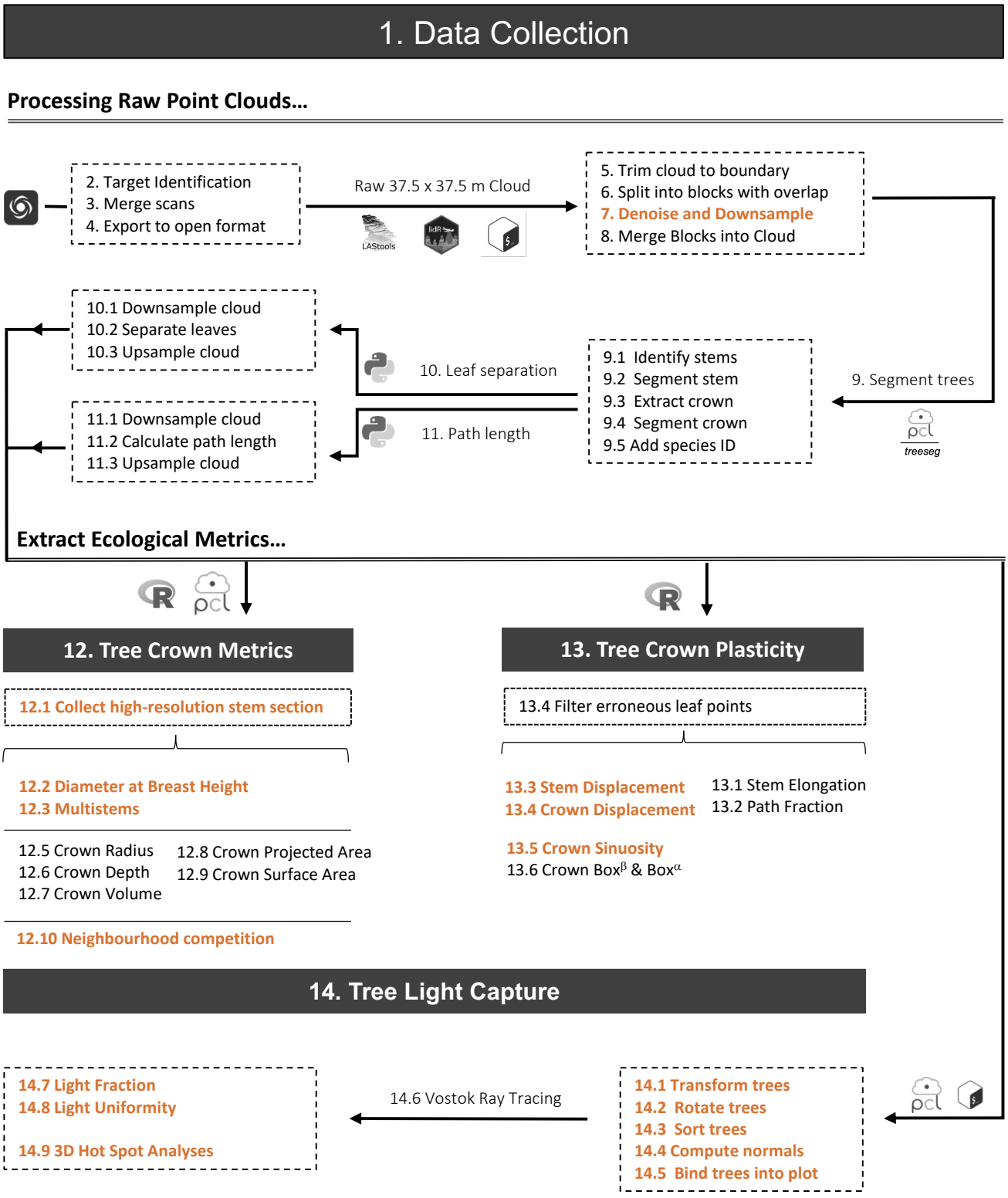

Figure 2.1 Workflow of all processing steps undertaken for this project. This figure shows the steps necessary to extract ecological metrics from Terrestrial Laser Scanning data with orange highlighting aspects of the work which involved bespoke development.

2.2.2 TLS Data Collection

We scanned plots using a Leica HDS6200 scanner (Figure 2.1 step 1), using a square grid system of 16 scans spaced at 10 m, (Wilkes et al., 2017) within 34 plots across two sites in Spain, Alto Tajo and Cuellar (Figure 2.2). We used a scanner resolution set to 3.1 mm and spherical targets (see Figure 2.3) to enable scans to be combined to create whole plot point clouds (Figure 2.1 steps 2-3).

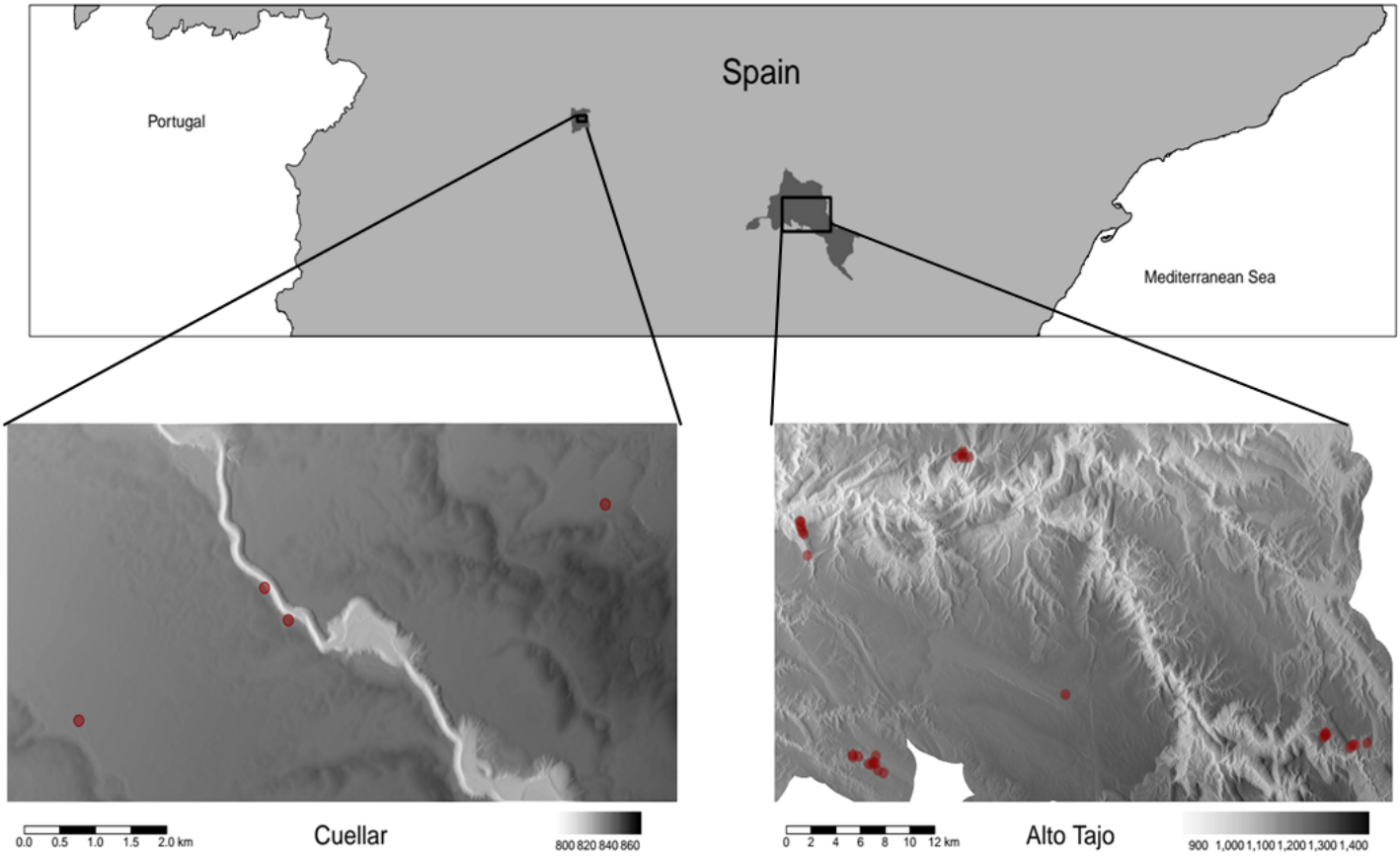

Figure 2.2 Map displaying the locations of the plots within the two field sites in central Spain. Red points show plot locations, with high-resolution digital terrain models enhanced with hill shading shown in greyscale (m asl; sourced from the Spanish National Orthophoto Program). On the left, Cuellar is situated on flat terrain and contains four plots, two of which are located within the riparian zone. To the right, Alto Tajo is an area of high relief with the 34 plots arranged in five zones varying in exposure.

I made the targets to be lightweight, cheap and functional as replacement for Leica's own £500 alternative that are precise, but heavy and less practical, limited to being mounted on tripods (Figure 2.3). Twelve targets were needed in total in sight of each scan with 8 the minimum necessary to stitch two scans together, and four extras for precaution, as on occasion, targets can move or be poorly scanned and therefore of no use for co-registration.

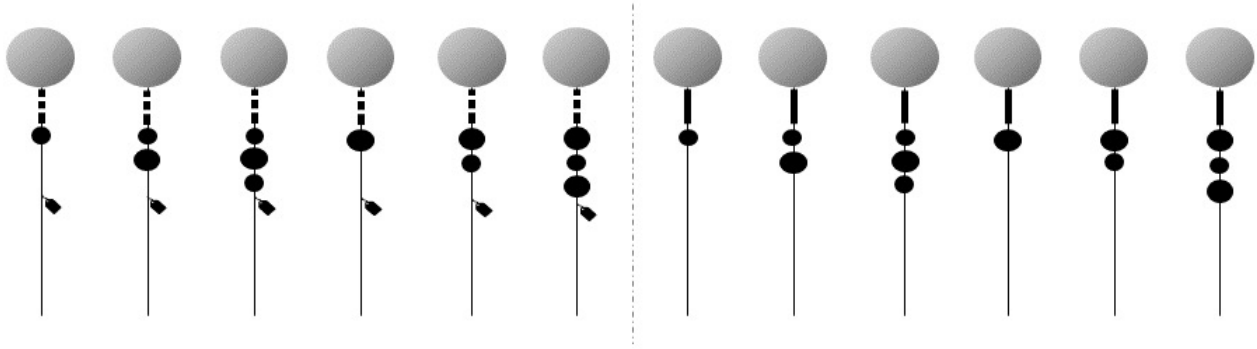

Figure 2.3 A depiction of the DIY targets that were made to enable my gridded scanning strategy. Associated unique patterns and markings that distinguish two groups (dashed line) and made each target identifiable across scans are shown. Target spheres were hard plastic cistern balls purchased from a DIY shop and were 150 mm in diameter. Spheres were mounted on garden stakes, with wooden mounting. Tape on the wooden mounting and foam spheres of varying sizes attached to the stakes were used to form distinct patterns identifiable in the TLS point cloud.

The scanning strategy operates in a chain-like manner along a predefined grid where each scan must contain six targets from the scan before and another six in front, visible from the next scan location (Wilkes et al., 2017), requiring two distinct groups of targets. At each scan location, the appropriate group of targets are lifted and placed in front of the scan location, and this process is repeated until the last scan. To ensure no errors in the field, targets need to be clearly grouped, and to enable post-process target matching, all targets needed to be visually identifiable within each scan. I therefore created a unique labelling scheme for all targets (Figure 2.3). Under the sphere of each target, I attached a wooden mounting rod, upon which stripes of tape were added with a label attached to each stake so that two groups of targets were established. Within each sub-group, individual targets were identified using a combination of large and small spheres that were

specifically arranged, creating a bespoke identification scheme. This scheme was identical between both groups of targets, differentiated by the stripes of tape. Altogether, a target would be labelled either “A” or “B” depending on its group (striped and labelled vs. no-stripe and no-label) and an integer (one to six) determined using the pattern along the stake.

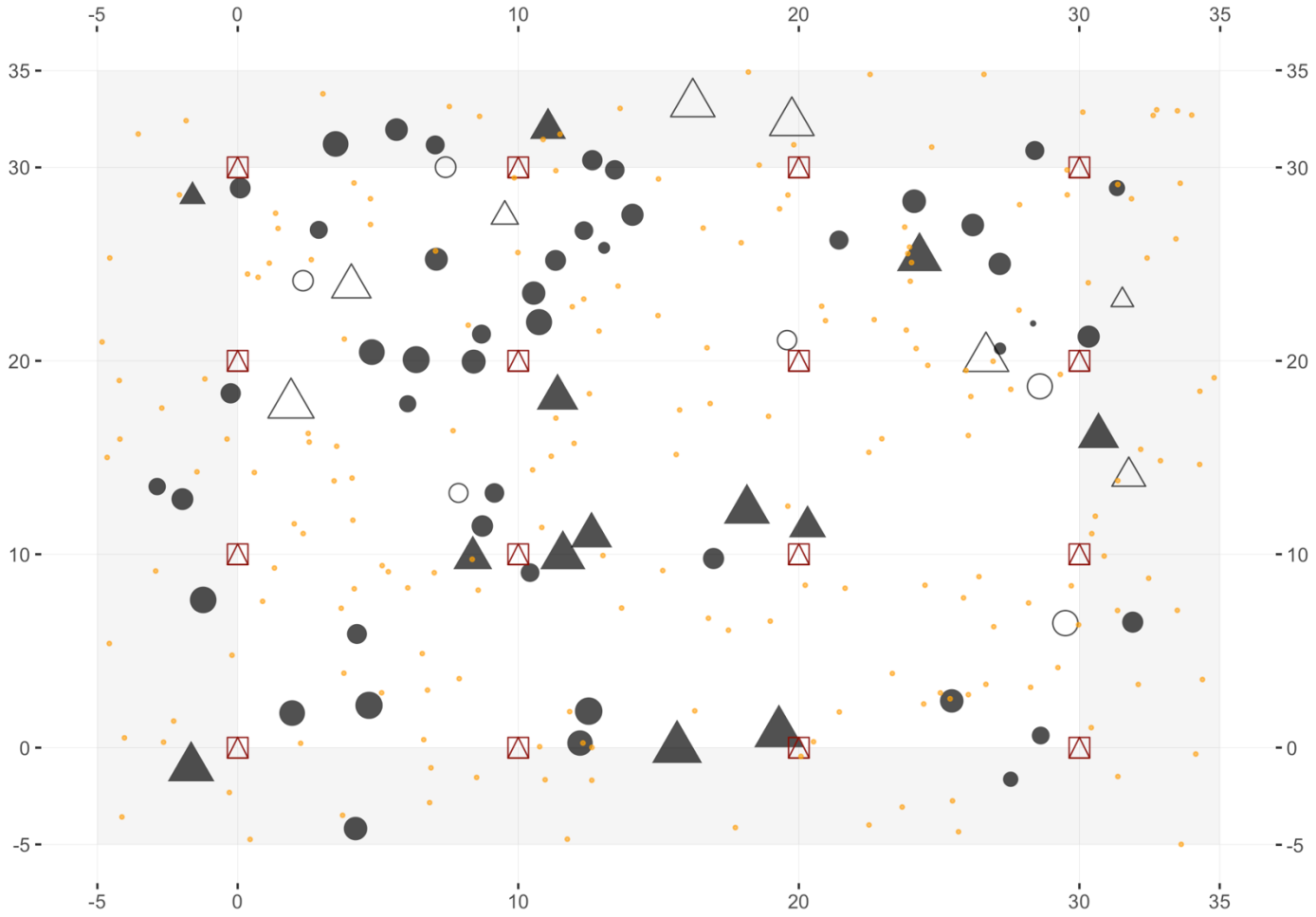

Figure 2.4 A stem map for a mixed pine and oak plot where scan locations are shown as red squares containing triangles, targets are shown in as orange dots, and individual trees are black and outline circles and triangles. Closed circles are *Quercus. faginea*, open circles *Q. ilex*, closed triangles *Pinus. sylvestris* and open triangles *P. nigra*. The plot outer buffer zone is grey. Scans started in the (bottom left) corner and proceeded along a (vertical) chain through the plot.

2.2.3 Data Preparation and Management

Within the early stages of processing the TLS data (Figure 2.1 steps 2 - 8), challenges related to file formats and data storage arose, and in the end in excess of 3 Terabytes was necessary to hold all data from all 34 plots. Files from LEICA HDS6200 scanners are compressed and closed within a proprietary file format (.ZFS) making them only accessible within the proprietary Cyclone software. Individual scans in this study were approximately 700 mb in ZSF format but expand to around 3 GB when exported in open formats such as a XYZ text files.

For each plot, all scans were loaded into Cyclone and all 194 targets were manually identified and tagged (Figure 2.1 step 2) following the formula described in section 2.2.2. This was a highly laborious process, taking between one and two days depending on the plot. Unfortunately, this manual identification was necessary because automatic identification only works in Cyclone with Leica proprietary targets, which were unworkable for our environment. Once targets were identified, individual scans could be co-registered and combined (Figure 2.1 step 3). Each plot was then exported as an open format .PTS file format (X, Y, Z, Intensity) at full resolution, with each plot around 50 GBs in size (Figure 2.1 step 4). Files were named with the site prefix (‘alt[plot number]_’ for Alto Tajo and ‘cue[plot number]_’ for Cuellar) and this naming convention was held throughout the processing chain, with individual tree files numerically labelled (i.e. alt[plot number]_[tree number]), for both .txt and .pcd file formats. As a long-term storage solution, each raw plot cloud was converted into .LAZ files - a highly compressed file format widely used within the ALS community - reducing whole-plot file sizes from ~ 50 GB to ~ 2.5GB (https://rapidlasso.com/laszip/). At this stage, the LAS2LAS function of LASTools was used to crop the cloud to within 7.5 m of the plot boundary and reduce precision to 3 decimal places (Figure 2.1 step 5). In order to parallelise both the downsampling and denoising steps (Figure 2.1 step 7), each plot had to be split into small blocks (Figure 2.1 step 6), using the lidR package in R (Roussel et al., 2020). A 0.25 m buffer was applied to each section of cloud to avoid edge effects from both downsampling and denoising procedures and converted to PCD using (https://github.com/murtiad/las2pcd), ready for import into PCL. Each block was denoised and downsampled (Figure 2.1 step 7), with the buffer removed within the downsampling step. Finally, all de-noised and

downsampled blocks were re-merged back into one 0.025 m resolution point cloud (Figure 2.1 step 8). Details of these steps, and adjustments made to standard methods to account for the Mediterranean context, are discussed in Sections 2.3.2 - 2.3.5 below.

2.2.4 Segmentation of individual trees from whole-plot point clouds

Extracting individual trees from point clouds of large areas is one of the most crucial methodological components in the application of TLS at spatial scales beyond that of an individual tree. Approaches range between full manual segmentation (e.g. Hess et al., 2018) and semi-automatic (Burt et al., 2019), although this requires checks and refinements after application (Calders et al., 2016). Automatic methodologies include stratified approaches whereby trees are 'built' from the bottom up (e.g. treeseg; Burt et al., 2019), and deep learning techniques that require no user input (Xi et al., 2018). The latter are starting to demonstrate capacity for extracting detailed branch structure (Halupka et al., 2019), but openly available packages are few and computational demands very high. Stem detection from TLS is a well-studied topic (Liang et al., 2018), so many methods of tree segmentation that are openly available follow a bottom-up approach - first identifying the locations of all stems within a plot and subsequently 'growing' these stems into a tree by iteratively adding and removing clusters of points at each stage of building (i.e. from stem to branches, and eventually whole crown; Burt et al., 2019; Heinzel and Huber, 2018; Raumonen et al., 2015; Tao et al., 2015). Others have manually tagged stems in the field with objects that are identifiable in scans, which together with k-nearest neighbour algorithms, are used to segment trees (e.g. Barbeito et al., 2017), but this kind of approach is fairly labour intensive when applied at scale. A cluster-based approach is taken by the package 3Dforest (Liang et al., 2018), which doesn't rely upon stem identification explicitly but instead slices the cloud along the vertical axis, and then divides each slice further into point clusters based upon a point-point distance threshold parameter set by the user. Each cluster is assumed to be a tree and is merged vertically to other clusters within the next slice based on distance and angle characteristics (Trochta et al., 2017). This kind of approach works well for sparse forest plots where crown interactions are minimal but is limited otherwise due to difficulty in disentangling crowns using only distance-based parameters.

One of the most widely adopted tree segmentation packages is the open-source treeseg (Burt et al., 2019), which has been formulated to deal explicitly with issues of crown segmentation. Rather than treating all point clusters as a possible tree (as in 3Dforest) treeseg instead locates tree stems within a defined horizontal slice, and fits cylinders to definitively distinguish stems from other spurious clusters (e.g., within the shrub layer). Here, thresholds to cylinder length, diameter, and angle, as well as tolerances in cylindrical fitting variability, can be defined by the user to suit the specific ecosystem and instrument. Once identified, a tree is extracted based on each stem (seed point) using conventional point cloud processing algorithms which include Euclidean clustering, region growing segmentation, principal component analysis, Random Sample Consensus (RANSAC) shape fitting and connectivity tests. Such tools analyse the distance connectivity between points, their curvature, direction and geometric similarity to build a tree from its seed point and differentiate whether points and clusters are connected to the current ('target') tree or not. One issue with this approach is that at the crown building stage, predefined limits determine the geographical extent to search for connectivity, and with overlap between trees inevitable this can lead to the assignment of points to more than one individual. The entire framework also relies upon a vertically homogenous distance between points, which with occlusion usually means downsampling is necessary (Morsdorf et al., 2018). Manual refinement and quality assurance is still a necessary step with these algorithms (e.g., Calders et al., 2016), particularly where occlusion causes topological breaks within a crown. This can lead to information loss or crown overlap and spatial connectivity between trees, causing the false incorporation of neighbouring tree branches. The latter issue may be lessened by using theoretical limits (e.g. MST; Tao et al., 2015) or ecological context (neighbourhood structure) to constrain horizontal search. In general, manual intervention in the semi-automatic process is highest in highly layered and structurally complex forests, and in those containing short trees with dense and homogenous outer foliage that reduces the number of returns from inner woody crown structure. Where such trees are present, especially within Mediterranean forests, a hybrid approach might be more suitable, using a larger cluster type approach such as 3D forest in sparse and short forest plots, and the more complex bottom-up approach of treeseg in taller, more complex plots.

A central issue to selecting between segmentation algorithms is that the majority are evaluated based on stem locations with only one study, Heinzel and Huber (2018) comparing crown volumes between automated and manually extracted trees. However, given the high variability in maximum tree height, horizonal structure and species compositions across my plot network, I determined that 3D forest was less suitable than treeseg due to its reliance and sensitivity on one single distance parameter, and because its implementation within a Graphical User Interface was less flexible to adjustments, and the high-performance parallel computing needed for data at this scale. Therefore, I used the segmentation method treeseg for these analyses (Figure 2.1 step 9). Applying the package in an off-the-shelf approach extracted approximately 50% of trees accurately, with stem identification stronger in taller and crown segmentation in more sparse oak plots, which needed substantial manual segmentation (see example of range of structures in plots; Figure 2.5). I tailored aspects of treeseg to better suit the Mediterranean forest system and describe these in section 2.3 below.

Figure 2.5 Example segmentations resulting from the semi-automatic algorithm treeseg followed by manual refinement. The top is a short *Q.* ilex-dominated plot and the bottom a tall *P. sylvestris*-dominated plot.

2.3 Adaptation of existing TLS approaches to Mediterranean Forests

2.3.1 Point Cloud Resolution

An integral component of treeseg is the definition of the neighbouring point-to-point distance, hereon termed *NN*, as it forms an integral part in connectivity testing (Burt et al., 2019). In an ideal scenario, the *NN* value would simply be the resolution of the instrument, but beam divergence is an inherit feature of all scanning instruments and must be accounted for when defining point spacing resolution. An optimal solution is to downsample point clouds to the expected minimum spacing between points (resolution) at the furthest beam returns within a forest plot, i.e., what's the minimum possible distance between points, given the constraints of the instrument and distance from the scanner. This ensures consistency in point spacing along the vertical column of the point cloud and can be estimated from knowledge of tree height alongside the chosen sampling strategy and scanner resolution settings. Using the scanning strategy outlined in section 2.2.2, along with 3.2 mm resolution (at 10 m) settings (with 0.22° mrad beam divergence) and a 25-metre maximum tree height, the theoretical maximum point spacing would be 8 mm at the furthest point from each scan.

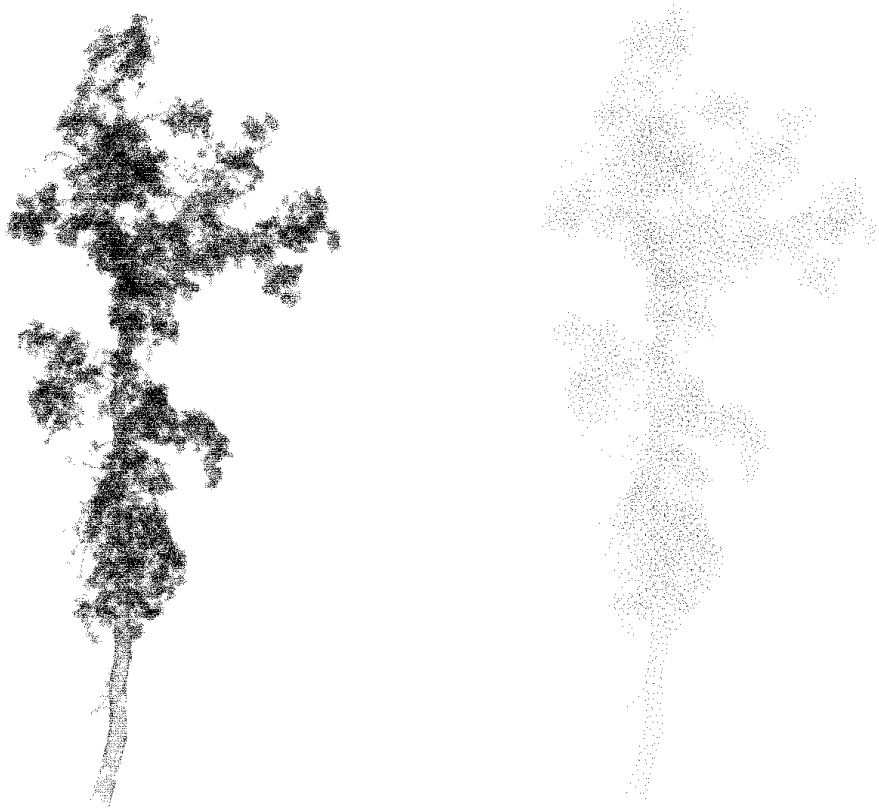

Figure 2.6 Two *Q. faginea* trees at two different resolutions (point spacing). Left is a tree at 0.025 m and right 0.05 m.

Given the likely presence of occlusion even with a 10 m scanning strategy (Morsdorf et al., 2018), along with computational constraints, a more practical resolution was chosen that aligned with each chapter's objectives. For example, Chapter 3 focused on overall crown size and shape and as such there is little need to work at resolutions finer than 0.05 m but Chapter 4 incorporated branching, foliage filling and shading metrics that benefit from finer scale analyses. In this project, 0.025 m was deemed the highest possible resolution that balanced both occlusion and computational constraints and used in Chapter 4, whereas 0.05 m trees were used in Chapter 3 (see Figure 2.6). All trees were initially downsampled to 0.05 m (Figure 2.1 step 7) for tree segmentation and then subsequently upsampled to 0.025.

2.3.2 Denoising Point Clouds

Denoising and downsampling are critical steps, to both remove erroneous points often associated with PS scanners, and to improve computational performance by reducing data size whilst retaining important information. A drawback with PS systems is the poorer signal-to-noise ratio, leading to spurious ghost points within a point cloud (Dassot et al., 2011) that must be dealt with prior to stem segmentation, making denoising a necessary processing step with these systems (whilst e.g. Riegl time-of-flight systems with full waveform information can filter out ghost or partial returns within their proprietary software). Conventional denoising methods include radius and statistical filtering, that determine whether a point should be removed using spatial and statistical relationships between points. Radius filtering has two parameters, *R* (radius of sphere in meters) and *K* (threshold number of points) and filters out points with fewer than *K* neighbours within a spherical neighbourhood of the set radius. Statistical denoising functions similarly but rather than *K,* a standard deviation (*SD*) threshold is assigned by the user and any point that falls beyond this threshold is removed. Considering point spacing and occlusion risk increases with height, parameterising a denoising filter with one fixed set of values for the entire point cloud is problematic, risking either leaving in erroneous points or filtering too heavily and losing information. For example, where point density is highest near the stems a more aggressive approach is helpful to isolate low branches and automatically identify stems in treeseg. However, at the top of the canopy the opposite is needed, and a softer filter ensures that sparse points needed for accurate height and crown shape estimation are retained, whilst still removing ghost points.

Using PCL, I developed a statistical denoising algorithm (Figure 2.1 step 7) that steadily eased the denoising tolerance parameter (multiple of standard deviation that defines the neighbourhood of a given point) as height increased, in order to retain information at the top of the canopy whilst efficiently removing it lower down. Statistical rather than radius filtering was chosen as the main filter, but a first pass on the entire cloud was conducted using the radius filter with *NN* set to 0.10 m and *K* to 10 to remove very distant points before slicing. The algorithm followed these steps:

Vertically stratified denoising:

Set minimum and maximum for multiples of standard deviation (SD) x within statistical denoising (x_{min}=1 and x_{max}=3). Then, for each raw point cloud dataset pc^{raw}:

1. Apply initial radius filter on cloud pc^{raw} ($K=10$ and R = 0.10 m)

2. Segment the cloud pc^{raw} along the vertical axis into a series of n 0.25 m tall raw slices $(slice^{raw}{}_1 \ldots slice^{raw}{}_n)$ from lowest point

3. a. Set $x_{slice1} = x_{min}$,

b. For each additional slice ($i = 2 \ldots n$) set $x_{slicei} = x_{slicei-1} + (x_{max} - x_{min})/n$

4. For each raw $slice^{raw}$ ($i = 1 \ldots N$)

a. Apply statistical denoising filter with $K=10$ and x_{slicei} as parameters and $slice^{raw}{}_i$ and $slice^{Out}{}_i$ as input and output

b. Push $slice_i^{Out}$ into $pc^{Filtered}$

5. Return $pc^{Filtered}$ as the vertically stratified denoised point cloud.

I used a defined slice height rather than number of bins, which means clouds with small maximum height and therefore higher point density are filtered with the same intensity to a cloud with greater maximum height, reflecting the role of actual, rather than relative, physical distance in determining point density. Applying this vertically stratified algorithm resulted in stems being more automatically identifiable within the initial steps of treeseg (Figure 2.1 steps 9.1 – 9.2), whilst overall crown morphology was retained in tall, complex and/or noisier point clouds (Figure 2.1 step 9.4). A comparison, of unfiltered, homogeneously filtered, and vertical stratified filtered point clouds is show in Figure 2.7.

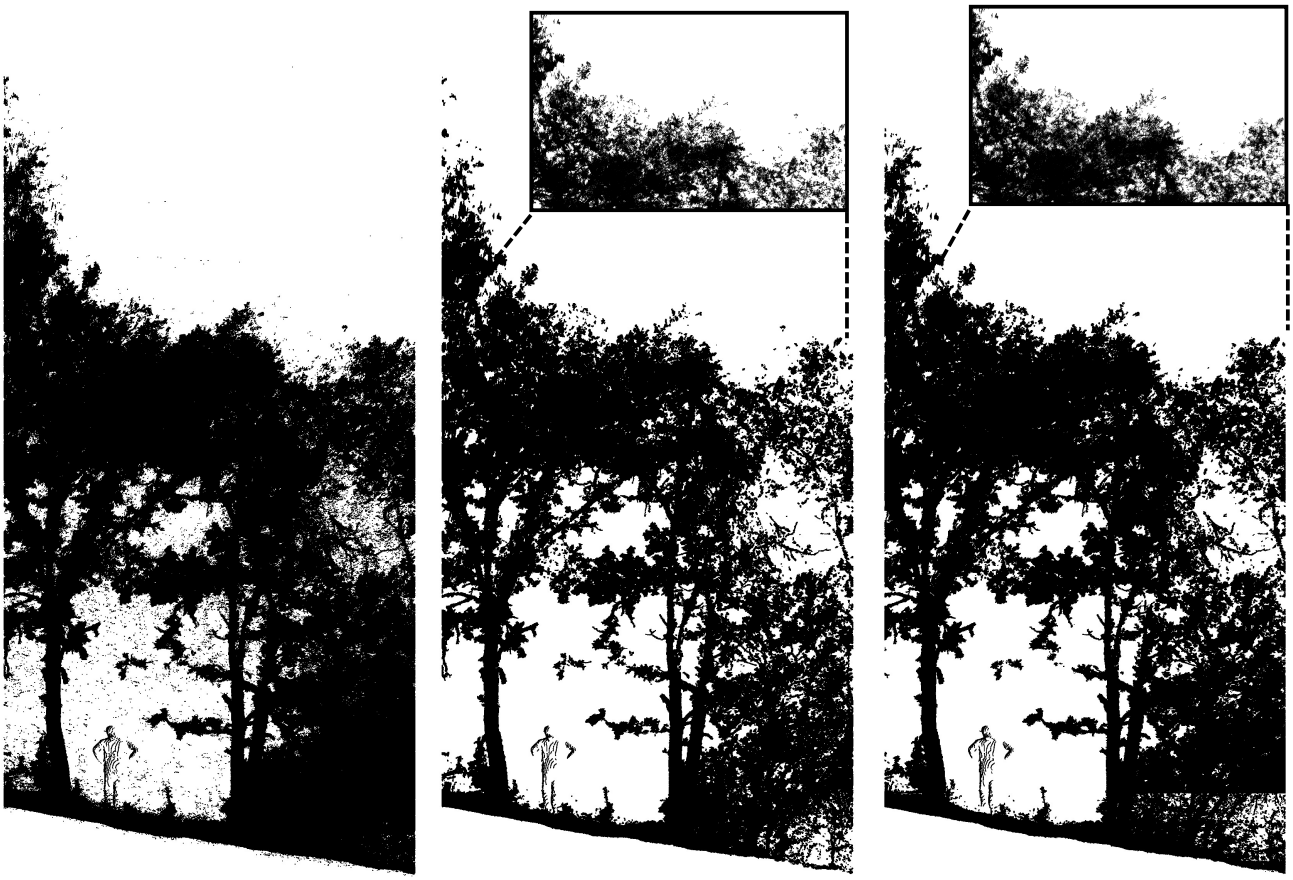

Figure 2.7 This image shows the difference between no point cloud denoising (left), a vertically homogenous filter with equal parameters across the vertical axis (middle) and a vertically stratified approach where parameters are eased along with height to reduce over filtering of the upper parts of a tree crown (right). With the denoised images, smaller zoomed in images are also displayed.

2.3.3 Tree stem location

Cylinder fitting techniques to locate stems are reliant on a search algorithm that can locate a clearly cylindrical-like object within the point cloud. Larger trees with longer sections of trunks without branching are more likely to be identified with this approach. Treeseg was developed within a tropical context, and coded so that should a cylinder not be found at the standard height (above any buttress on the tree), treeseg's cylinder-fitting algorithm will simply search up the stem until the correct computational conditions are met. The structure of the forests for which it was developed, with reliably tall trees with long straight trunks, makes the process of finding cylindrical stability relatively straightforward. However, as discussed in Section 2.2.4 above, in my

study sites, and indeed in many Mediterranean ecosystems, short trees, with crowns low to the ground, that bifurcate close to the ground, and resprout into multi-stem individuals, are common. Therefore, a different approach to finding and identifying stems, and calculating DBH, was needed.

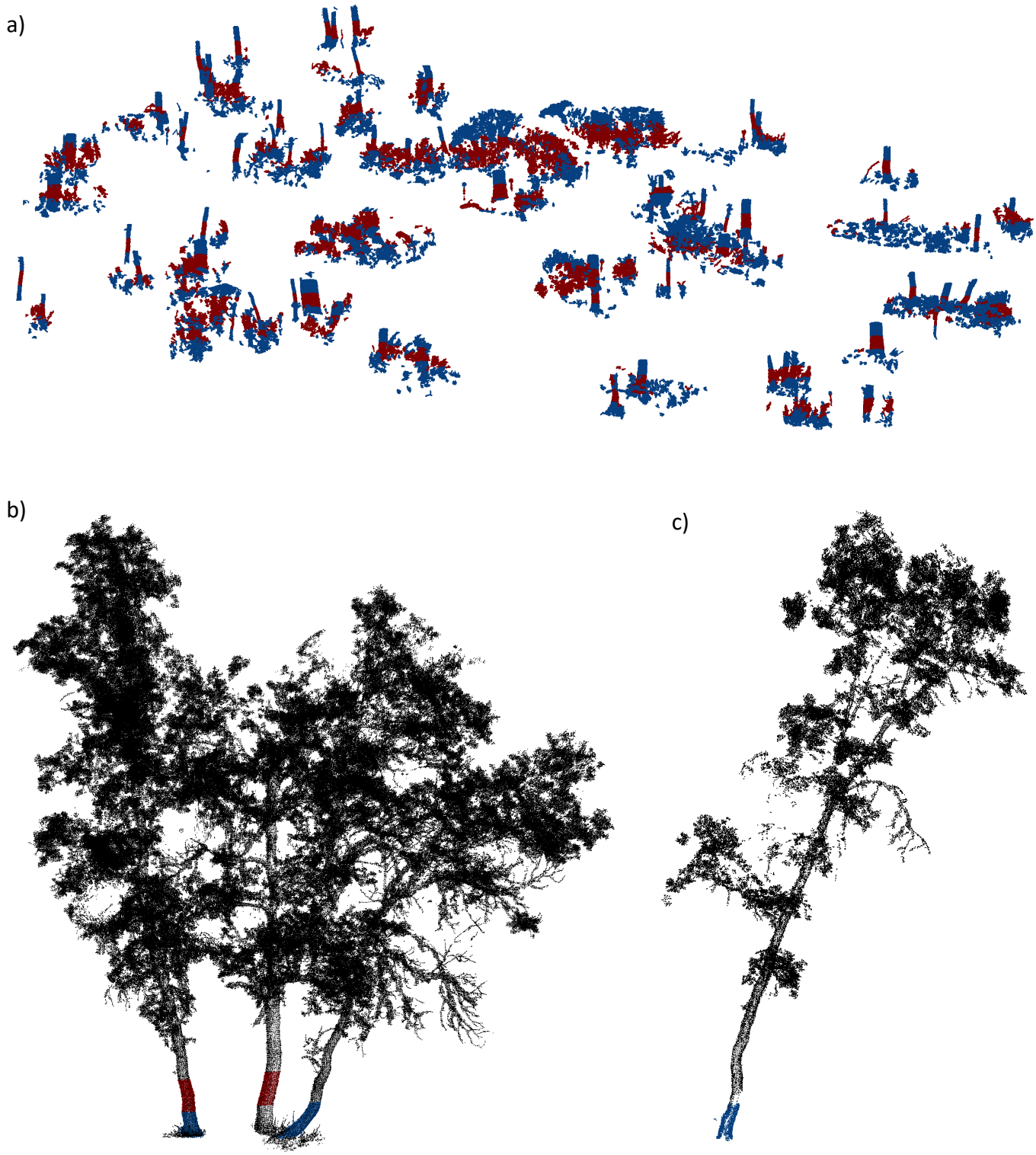

Figure 2.8 This figure shows a) the slicing procedure undertaken to help find cylindrical sections along a tree's trunk for both stem identification and DBH calculation b) a multi-stem tree (right) neighbouring a single stem c) a single stem demonstrating how at times tortuosity meant cylinders had to be fit much lower. Both a) and b) show alternating blue and red colours that illustrate which slices were stable enough to fit cylinders

To locate stems, treeseg extracts a slice from the point cloud, which as standard is set as between 3-6 metres above the tree base and depends upon this length to run diagnostic cylinder procedures that ensure a stem is indeed cylindrical and likely part of a tree. To do this, cylinders are fit above and below the middle of the slice and if these are also cylindrical in shape, determined through criteria set by the user, the stem proceeds to the next stage of segmentation (Burt et al., 2019). This makes complete sense in tropical systems where trees are very large and with an extensive surface available to fit cylinders. For many trees within my data, crowns were developed within 3-6 metres of the ground, and as such, I set treeseg to extract a slice much closer to the ground (0.5 m to 2.5 m). This slice was then stratified into three additional cross sections that essentially splits a tree's trunk into three vertical components – this helped increase the chances of finding stability, as irregularity in shape isn't always constant along a stem's entire length. For example, the tree in Figure 2.8.c has a stem that is misshaped from ~ 1 m and up, but a stable cylindrical shape was found near the base of the tree, facilitated through slicing. The stem on the furthest right in Figure 2.8 b) shows another example where a cylinder fitting procedure is destined to fail if the entire length of the stem (here 1.83 meters) is used to fit a cylinder, but where some smaller and more geometrically stable sections of the stem area available, and a cylinder may be found (highlighted in blue and red). Examples in Figure 2.8, though by no means the extreme, are highly representative of both *Q. faginea* and *Q. ilex* stem topology throughout the dataset.

My modifications to this approach worked as follows. Firstly, a 2 m slice is taken from the plot point cloud from height 0.5 to 2.5 meters. Next, the slice is segmented into clusters based on Euclidean distance and then each cluster is sliced again vertically into three sections, so tripling the number of clusters (see Figure 2.8.a). Slices were created with small vertical overlap so that clusters belonging to the same stem could later be removed. Any clusters that do not span at least 66% of the vertical range of the slice (1.33 m of the 2 m) were removed, leaving only elongated clusters. Each cluster passes through a final region-based-segmentation stage that separates clusters according to neighbourhood smoothness, curvature and minimum size (points = 100) criteria, aiding the separation of more planar point arrangements to those more randomly distributed (i.e., shrubs; foliage and noise). Finally, region-based clusters pass through cylinder fitting procedures, where each "cylinder" must be within the plot boundary, a certain length and diameter threshold, and meet cylindrical

stability criteria (Burt et al., 2019). Overlap is checked across all clusters to remove cylinders that are part of the same tree, in order to avoid duplicate tree building later on. The coded procedure for this stage was as follows:

Modifications to treeseg to improve stem identification:

For each plot point cloud:

1. Cut a slice along the vertical axis from 0.5 to 2.5 m using the lowest point within a grid as the ground.

2. Segment the slice into clusters using Euclidean distance and region segmentation into n clusters $cluster_1, \ldots, cluster_n$

3. For each $cluster_i$ $(i = 1 \ldots n)$

a. Cut $cluster_i$ into 3 vertical slices with small vertical overlap (to enable matching later)

b. Remove any slice whose points do not span at least 66% of slice height along the z-axis

c. Push remaining slices into $cluster^{Filtered}_i$

3. For each $cluster^{Filtered}_i$ $(i=1 \ldots m, \text{ where } m \leq n)$

Check cylindrical stability using procedure outlined in (Burt et al., 2019).

a. IF classified cylindrical and within plot boundary,

b. Push $cluster^{Filtered}_i$ into $clusters^{cylinders}_i$

4. For each $cluster^{cylinders}_i$ $(i=1 \ldots p, \text{ where } p \leq m)$

a. Check location of $cluster^{cylinders}_i$ against location of $cluster^{cylinders}_j$ $(i \neq j)$ and remove if location overlaps.

b. Return $cluster^{cylinders}_i$ as a seed point location for a tree in the plot.

My modifications to the existing treeseg procedure improved the capacity to automatically identify stems across the plot network and were particularly effective in exposed plots containing *Q. ilex* and *Q. faginea* trees of short stature where ~ 25% improvement was reached, but manual refinement was still necessary where stems of short trees were highly occluded by shrubs. Therefore, within the treeseg shell script, a pause was added after the stem identification process had finalised to enable a manual evaluation of the output. If stems were missing, they were manually segmented using CloudCompare (*Cloud Compare*, 2021) and added into the relevant folder before the next stage of segmentation (Figure 2.1 steps 9.2 - 9.4) and any false positives (visually identified) deleted. There is a trade-off when setting segmentation parameters (e.g., cylinder shape criteria), where stricter criteria will lessen false positives but increase stems missed. Stricter criteria are more

appropriate when only large canopy trees are of interest (e.g., for biomass monitoring), and more tolerant criteria when identifying the full spectrum of size classes is a priority, for example when addressing questions with a stronger ecological focus.

2.3.4 Crown segmentation in leaning trees

In my study system, and especially in pine stands where competition for light is intense (Pretzsch, 2019), tree lean and stem displacement is commonplace, in particular in the understorey, presumably to intercept more light (e.g. see understorey in Figure 2.5). Before crown segmentation occurs within treeseg (Figure 2.1 step 9.4), a cube of the point cloud is segmented from the plot point cloud above each tree stem seed point (Figure 2.1 step 9.3) and the crown associated with each stem is segmented only from this cube. General allometric principles using diameter breast height to predict height and crown radius, and therefore the limits of each block, are used. Because the cube is centred directly above the top of the stem, when a tree is leaning this process is likely to miss crown points (see example, Figures 2.5 and 2.9).

To address this issue, I made use of cylinder fitting and segmentation procedures already constructed for the earlier stem identification procedure within treeseg to segment potential crown points using a leaning cylinder rather than a fixed cuboid. Note that although this was necessary for these data, cuboid extraction is computationally faster so should be retained if the data allow. To implement this modification, rather than segmenting the point cloud based on predefined three-dimensional limits determined by allometry, a cylinder was fit to the top of the stem, with width determined using the treeseg crown radius calculation. I used the 'spatial3DCylinderFilter' function within treeseg (Burt et al., 2019) that utilises RANSAC cylinder fitting procedures within PCL, and includes detail on cylinder orientation such as angle. The modification expanded a cylinder form the stem top outwards to a predefined radius determined through an allometric relationship, incorporating all points along a leaning tree (see red colour in Figure 2.9 a and b). The computational cost is high compared to the default treeseg cuboid crown extraction. Although I implemented cylinder segmentation for all trees, this could be improved upon by an initial step to test tree lean, so that non-leaning trees (likely the majority of a dataset), are extracted more efficiently. Furthermore, the approach is sensitive to the location

in which the cylinder angle is extracted with calculations nearer the top of the stem most suitable but occlusion often more of an issue here due to the presence of branches and foliage. This modification was most impactful in the understorey of highly competitive pine stands (e.g., Figure 2.5) where shade intolerant species (Niinemets and Valladares, 2006) are leaning extensively to increase light capture

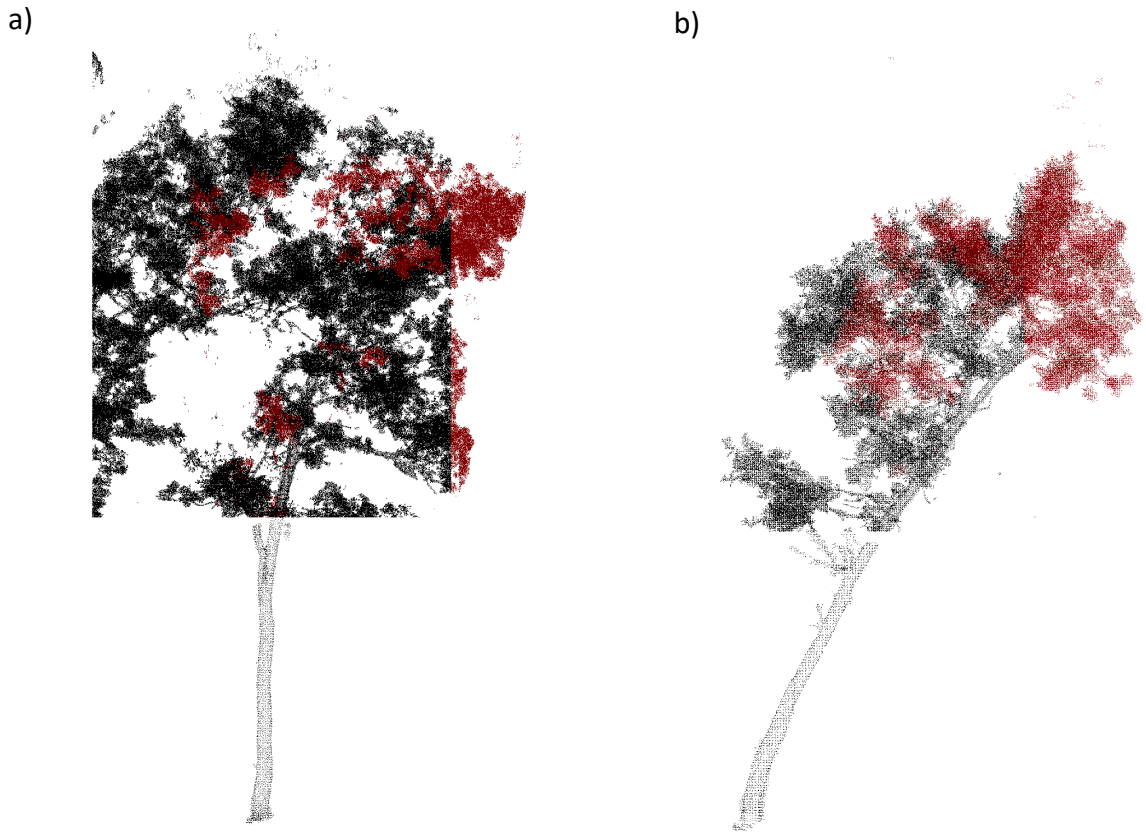

Figure 2.9 Figure showing how extracting a crown volume in treeseg that accounts for stem lean is more effective in capturing the entire tree crown. Red represents additional points captures through cylinder extraction and black those collected using a cuboid. Both a) and b) are *Q. faginea* trees.

Once the cylindrical point clouds identifying the potential volume for each crown were identified, crowns progressed to the next stage in treeseg where crowns are segmented using the 'buildtree' function. Here, the potential volume from the previous step is split into clusters using both Euclidean clustering and region-based segmentation. Beginning with the tree stem (Figure 2.1 step 9.2), these clusters are iteratively added or discarded to the stem, steadily building a tree in the process. To determine whether a cluster is part of a tree, its distance and angular relationship to nearby clusters that have been added in previous steps is assessed, this

ensures that clusters that quickly descend in angle or are suddenly further away in relation to those nearby are likely part of a neighbouring tree crown.

2.3.5 DBH calculation and multi-stem identification

Modifications to stem identification (section 2.3.3; Figure 2.8) improved its scope of identification but manual intervention was still necessary to ensure all stems were extracted. Visual checking of stem locations is relatively straightforward, however manual intervention when calculating metrics such as DBH is not appropriate, and further complicated by the presence of multi-stemmed trees within this dataset (for which treeseg is not configured). A new approach was therefore necessary. I built upon the framework within the stem identification script (section 2.3.3) to formulate a processing chain that both identified whether a tree was a single stem or part of a multi-stem group, and calculated DBH values for all stems (Figure 2.1 steps 12.1 - 12.3).

In this ecosystem, high resolution data low to the ground is important, as many trees have low crowns and branches (see section 2.1.3), leaving less physical space for cylinder fitting to measure DBH. The search for cylinders must therefore operate within much finer margins than the default approach in treeseg, as there is much less scope to simply look higher up the stem for stable trunk sections. Although the higher resolution of PS scanners doesn't necessarily translate into data with higher information content (as, for example, reducing occlusion is likely a better means to improve scan quality), resolution does affect the smallest resolvable scale (i.e., smallest detectable branch or tree stem). In order to successfully fit cylinders to smaller sections of point cloud, the higher resolution is advantageous in providing more samples to the PCL RANSAC procedure. Bespoke code was needed to both extract DBH and to identify and group multi-stems (according to their stem number). To do this I implemented the following:

Extracting Stem^{DBH} and Stem^{N}:

For each *tree* (i=1…N) in a given plot

1. Slice $tree_i$ from the base to 2.0 m above the ground
2. Calculate bb_i (bounding box) of $slice_i$
3. Load high resolution point cloud ($pc^{1\ cm}$) and extract points within bb_i
4. Calculate *NN* of $pc_i^{1\ cm}$ (see Burt et al., 2019)
5. Filter ground points by fitting a plane across the base of $pc_i^{1\ cm}$, retaining only outliers
6. Slice $pc_i^{1\ cm}$ into three vertical sections $slice_{1...n}^{1\ cm}$
7. For each *slice* (i=1…m)
   - **a.** Segment $Slice_i^{1cm}$ into clusters using Euclidean clustering and region segmentation (section 2.3.3)
   - **b.** Check cylindrical stability as per (Burt et al., 2019) but with 50% overlap between clusters ($clusters_{1...n}$) to account for smaller stem lengths
8. Filter $clusters^{cylinders}{}_{1...n}$ that are leaning more than 30 degrees, are within a certain size (*radius*) and length
9. For each $clusters^{cylinders}$ ($i=1...p$, *where* $p \leq m$)
   - **a.** Check location of $cluster^{cylinders}{}_i$ against location of $cluster^{cylinders}{}_j$ ($i \neq j$) and remove if location overlaps
10. Calculate number of cylinders (Stem^{N}) and DBH (Stem^{DBH} or Stem^{Dia})
    - **a.** Find the height x at which the max number of cylinders are located
    - **b.** IF number of cylinders = 1, extract DBH using cylinder located at x = 1.3 (Stem^{DBH}) but if no cylinder found at this height, drop down to cylinder at lower height and extract stem diameter (Stem^{Dia})

      Stem^{N} = 1
    - **c.** IF number of cylinders > 1, extract diameter from cylinders located at height where most cylinders found and sum all cylinder diameters Stem^{Dia}

      Stem^{N} = $\sum(clusters^{cylinders}{}_{1, ..., } clusters^{cylinders})$ at height x
11. Return $Stem_i^{DBH}$, $Stem_i^{Dia}$ and $Stem_i^{N}$

The first step was to determine the location and bounding box of each tree stem up to 2 meters high and use this bounding box to collect a higher resolution equivalent from the raw 0.01 m plot cloud. Next, for each tree, load the high-resolution (1 cm point cloud) bounding box and run both Euclidean clustering and region segmentation to isolate stems (point clusters), then retain only stem clusters that align with the original tree stem in 3D space. Following the same approach as in section 2.3.3, I sliced the stem or stems in each location

into three slices along the vertical axis, (Figure 2.8.a) with a small 0.05 m vertical overlap. I then fit cylinders according to default treeseg settings (Burt et al., 2019) where stability criteria must be met. Any cylinders with overlapping locations were tagged as duplicates and removed. For all cylinders that remained, the number of cylinders within each slice height was determined, and the one with the highest number of cylinders (stems) was used to calculate stem characteristics. Where multiple cylinders were present, as is the case for multi-stem trees, stem diameter (DBH) was calculated as the sum of all cylinder diameters and the number of stems recorded as the total number of cylinders. For single stems, stem diameter extraction was prioritised in descending height order, where calculation is first attempted at 1.3 m, and subsequently lowered until the last slice containing cylinders was reached. All stems where diameters were extracted at 1.3 m, and therefore at the standardised inventory height (DBH) were marked to ensure consistency in subsequent analyses.

2.4 Extracting Traditional Metrics

2.4.1 Crown radius

Crown radius, along with tree height and DBH, is a core metric for many forest inventory protocols, providing an essential measure of a tree's lateral extension and the baseline for calculating crown area and volume. It has also been used to formulate geometrical approximations within modelling frameworks that aim to incorporate crown plasticity (Purves et al., 2007) and at the centre of crown scaling theory (e.g. West et al., 2009). The emergence of ALS has meant crown radius has become of increasing importance for quantifying carbon stocks in forests, with its integration into allometric equations outperforming height alone (Jucker et al., 2017). Crown radius is it increasingly more difficult to measure accurately from the ground as tree height increases; using ALS the opposite is true, with understorey trees mostly unobserved (Morsdorf et al., 2018). Regardless of measurement method, crown radius can be captured in several different ways, including: the maximum (Rautiainen and Stenberg, 2005); the average of the maximum and its perpendicular radius (Blanchard et al., 2016; Harja et al., 2012; Popescu et al., 2003); or the average of several measures at different angles across the tree crown (Fleck et al., 2011; Popescu et al., 2003; Ritter and Nothdurft, 2018). The third approach is thought to be more accurate, and also provide better crown projected area estimates (Ritter and Nothdurft, 2018), whilst maximum estimates are likely to overstate crown cover (Gill et al., 2000). The richness of dense ALS and TLS data means a more refined approach can be undertaken to calculate crown radius. For the trees in my dataset, I calculated maximum radius and its perpendicular, and also averaged measurements spanning the entire perimeter of a tree crown (Figure 2.1 step 12.5). To calculated maximum/perpendicular and mean crown radius I used 2D concave hulls (see section 2.4.2 below, describing how these are used for direct calculations of crown area). For each hull the centroid was located and the maximum distance between this centroid and the edge was found, and subsequently, a 90-degree angle was computed to find its perpendicular. A similar procedure was used to calculate mean crown radius, where from the same centroid, a clockwise iteration extracted a vector of distances around the entire tree crown hull perimeter, which was then averaged. I used the average crown radius in Chapter 3 and the maximum and perpendicular measurements were used below in sections 2.4.2 and 2.4.4 to make comparisons to measurements that aim to incorporate crown plasticity in computing crown area and volume, for example,

through the assumption of an ellipse rather than a circle (Purves et al., 2007) and an ellipsoid than a sphere (Jucker et al., 2014).

2.4.2 Direct measurements of crown projected area

Crown area is important to for a crowns growth efficiency in lateral space (Pretzsch and Schütze, 2005), shading of neighbouring trees (Zambrano et al., 2020), and is used in modelling to determining forest stand dynamics (Purves et al., 2008). Different protocols for determining crown radius (section 2.4.1), used to estimate crown area means comparisons between field sites are difficult (Blanchard et al., 2016); the advent of LiDAR technology has meant that this important structural attribute can be measured in a direct and consistent manner. Comparisons between TLS and traditional approaches have found crown complexity to be a fundamental factor leading to inter-observer biases in its estimation – but TLS provides a robust and accurate means retrieve it accurately (Ritter and Nothdurft, 2018). I calculated crown projected area using only the leaf point of each tree point cloud, which was collapsed into two-dimensional space by removing the z-axis (Figure 2.1 step 12.8; see the following section 2.5.1 in this chapter for leaf separation details). Calculations were conducted using the concaveman package in R (Gombin et al., 2020) that efficiently fits concave hulls to all points with the alpha parameter (determining the 'tightness of fit'; here set to 2, see Chapter 3). An alpha value that is too low will not only take longer to compute but can also incorporate too much complexity that has minimal impact on area estimates.

In order to assess the gained accuracy of TLS based crown area compared to traditional measurements, I simulated conventional ground-based measurements using the crown radius measurements discussed above (section 2.4.1) and fit a regression line between these and my TLS crown area. I simulated both a circle and ellipse, with the latter using the average of all crown radii and the former using the maximum and perpendicular distances as input. The relationship between the ground-based crown area of both circle and ellipse, and TLS crown area was statistically significant ($P < 0.01$), but simulated ellipse ground-based measurements overestimated crown area compared to TLS by more than 2.5 times the TLS amount for both oaks and pines (Figure 2.10 a - b). This shows the importance of taking multiple crown diameter measurements for crown area estimation if only ground-based methods are available. It is however important to note that the

simulated circle was created using the best possible mean radius data, as it incorporated an averaged value that included radii measurements from the centre to every vertex of the TLS concave hull, which in the field, measurements that accounted for the entire crowns undulating perimeter would be time-consuming to achieve. Nonetheless an optimal number can be found; with some evidence that 8 measurements is a good a compromise between accuracy and time (Fleck et al., 2011; Grote, 2003; Ritter and Nothdurft, 2018). The effect of having a large number of radii samples, capturing full crown complexity, was beneficial to accurate estimation when compared with the maximum and perpendicular values. Although an ellipse is used as an effective means to incorporate flexibility in shape (differences in width and length), it leads to much higher overestimations of crown area than circles using averaged radii (compare Figure 2.10 a-b).

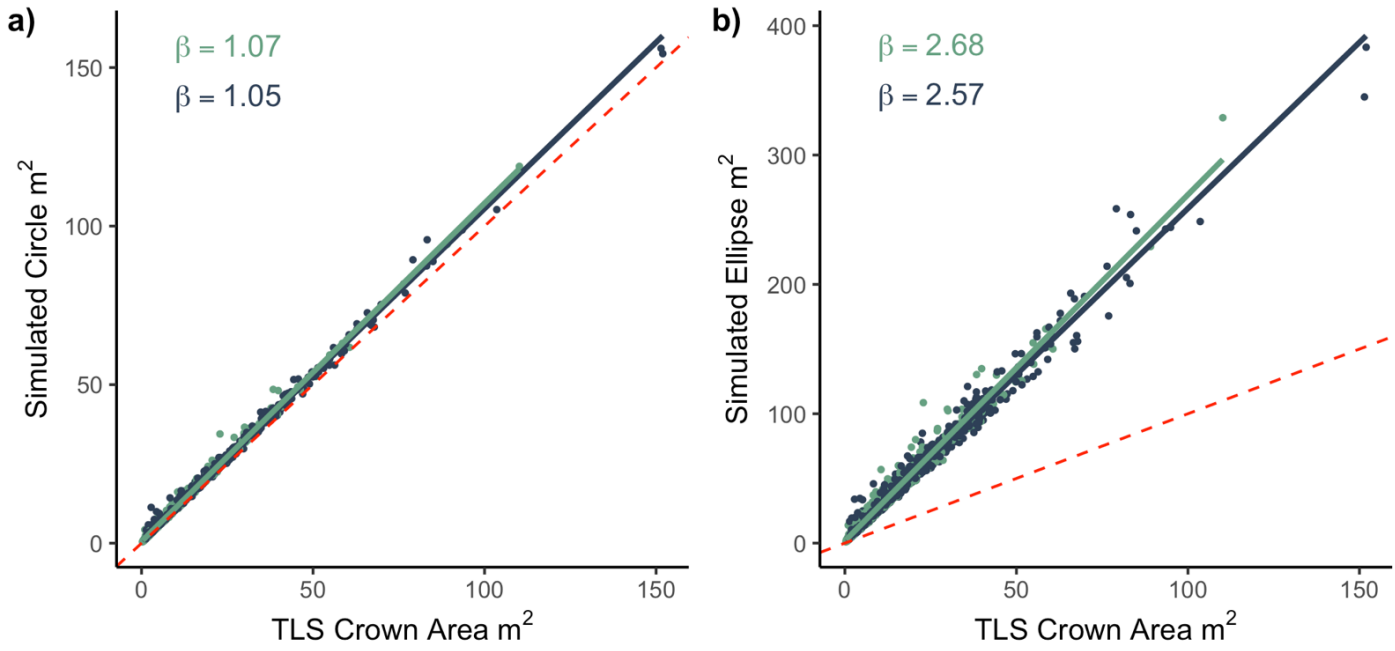

Figure 2.10 Shows linear relationships between TLS crown area and a) simulated circle area that was computed using the average crown radius derived from TLS and b) simulated ellipse area that was calculated using the maximum diameter and its perpendicular. 1:1 relationship is displayed in red and β values (slope) shown for both pines (blue) and oaks (green).

2.4.3 Crown depth

Like crown radius, crown depth is a well-studied measurement that captures three-dimensional properties in a one-dimensional measurement. It has ecological importance, and is used to characterise self-shading (Poorter et al., 2003; Sterck et al., 2001) and general light capture strategies (Aiba and Nakashizuka, 2009). A common difficulty in its measurement that spans both traditional methods and newer LiDAR technologies is in objectively defining a trees' crown base. Field techniques often identify the lowest branch with a 'substantial' amount of foliage that is not some spurious resprout as the crown base (Shenkin et al., 2020), but the advent of TLS necessitates automatic procedures that do not rely on subjective decisions. Crown depth from TLS is still determined manually through visual assessment in some work (Martin-Ducup et al., 2020), but this is impractical when analysing thousands of trees (as is the case here). If constructing quantitative structure models (Raumonen et al., 2013), the lowest branching point may be used as an estimate of crown base - but this doesn't account for slumped branches, and therefore could lead to erroneous estimates, particularly when estimating light interception and shading of neighbouring trees. Here, when applying default settings in treeseg, many exported trees had missing lower sections of tree crowns due to branches that were heavily slumped. A more defensible method is to replicate the spirit of field approaches by identifying the first significant bundle of foliage, representing the beginning of the major photosynthetic component of the tree; this was the approach I chose to undertake (Figure 2.1 step 12.6). Here, new TLS leaf separation algorithms such as leafsep (Vicari et al., 2019) and LeWos (Wang et al., 2020) provide the necessary means to quantify crown depth using the foliage component alone, through advanced wood/leaf separation algorithms (see section 2.5.1 below). Given both erroneous classifications and the presence of spurious sprouted foliage, crown depth needed to be quantified using a percentile along the z-axis that effectively ignored these points but also had minimal impact on crown depth estimation. To test this, I conducted a sensitivity analysis where threshold percentiles ranging from 0 through to 0.15 were used to calculated depth and plotted against percent change in crown depth (Figure 2.11).

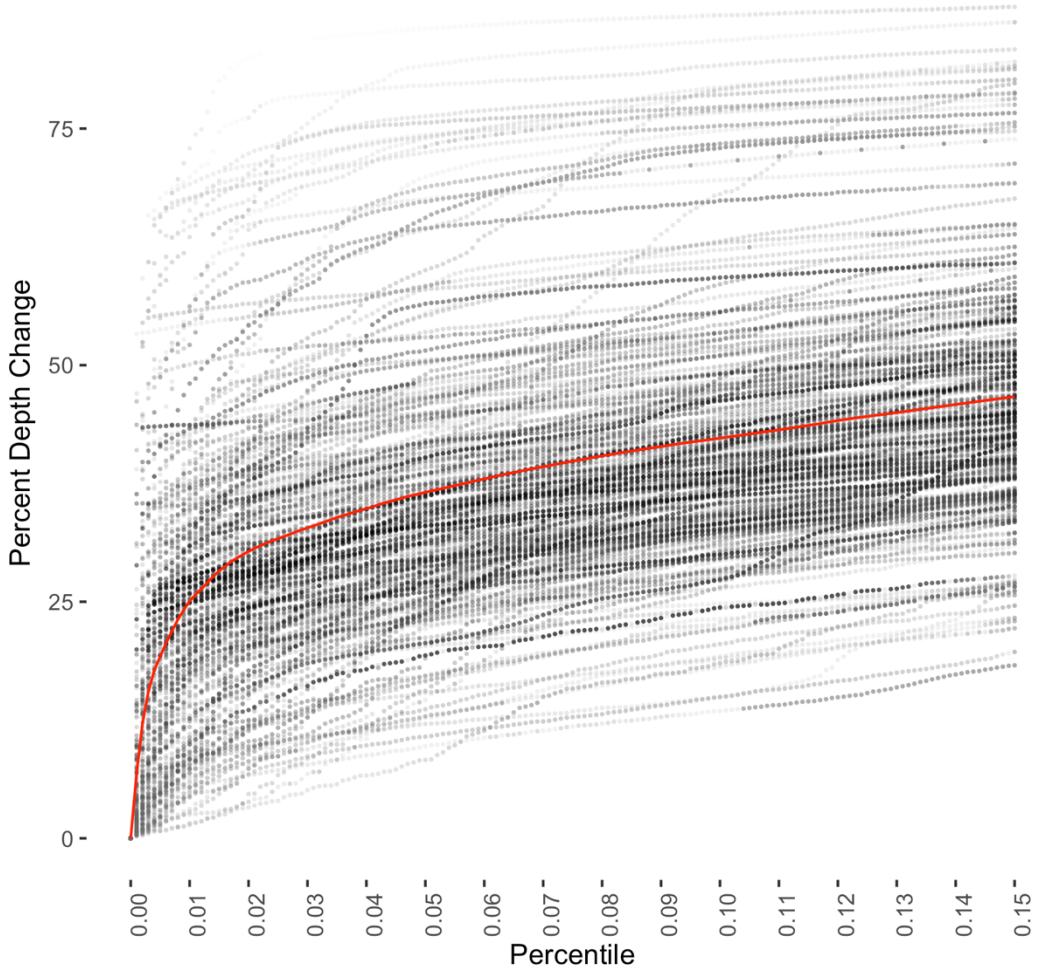

Figure 2.11 Showing the percentage change in individual tree crown depth as the percentile cut-off is increased. The red line is a polynomial fit used to visually identify the asymptote.

The large variation in the intercept across trees was driven by small erroneous leaf points near the base of a tree, which upon removal (by increasing the threshold percentile) lead to large differences in crown depth. At around 0.03 the rate of change of depth became approximately constant, so this was identified as the optimal threshold for cutting the lowest leaf point cloud points to accurately capture crown depth.

2.4.4 Crown volume

Tree crown volume is a measurement of great interest to forest managers, who wish to identify the most vital and productive trees (Zarnoch et al., 2011). It also plays an important role within theoretical frameworks as a metric of how trees compete for space (Taubert et al., 2015; West et al., 2009), and has been empirically

interpreted in the context of tree adaption to varying biotic (Jucker et al., 2015) and abiotic conditions (Barbeito et al., 2017; Jacobs et al., 2021). However, a universal definition of crown volume has eluded ecologists and forest managers, prompting entire reviews discussing its measurement and assessment (e.g. Zhu et al., 2021). One widely accepted definition describes a tree crown as the upper section of a tree that includes living branches and foliage (Gschwantner et al., 2009). Others offer a more nuanced perspective, for example describing a tree crown within a fractal framework, as neither a 3D solid or 2D photosynthetic plane but a collection of holes and cavities where light and gases exchange (Zeide, 1998). Essentially, crown volume encapsulates the three-dimensional space occupancy of the photosynthetic components of a tree, but even within national forest inventories, directions and means to measure crown volume are offered but without clarification on its definition (Gschwantner et al., 2009). Using traditional techniques, measurements are confined to two-dimensional space with an assumption of geometric shape necessary to estimate 3D volume, leading to the inclusion of empty space created by irregular and complex branching patterns. LiDAR technology offers the means to measure volume directly using hull algorithms that envelope all points, and voxels that cover all points with cubes with their sum equating to volume. However, hull algorithms do necessitate the setting of an alpha parameter that defines the 'tightness' of fit, and voxelisation incorporates internal crown structure, which again, requires clarity on what exactly constitutes crown volume.

In this project, I used the hull approach rather than voxels to calculate crown volume (Figure 2.1 step 12.7) as it better aligns with existing ecological concepts of what constitutes volume, and is more consistent with existing data including those generated from ALS platforms (Jung et al., 2011). Voxel approaches have been found to be better suited to space filling characteristics such as foliage density (Lecigne et al., 2018; Olivier et al., 2016), and fractal dimension analysis (Seidel et al., 2018). I fit hulls to the foliage component of the tree only, capitalising on new algorithm developments that separate leaves from wood (see section 2.5.1 below), focussing on the amount and spatial occupation of foliage, more recently defined as 'green crown volume' (Zhu et al., 2021). Figure 2.12 shows the same tree wrapped in two hulls with contrasting alpha values where 2.12 (a) had a tighter fit ($\alpha = 0.3$) and 2.12 (b) a looser convex fit ($\alpha = 10$), the latter incorporating more empty crown space. All volumes in this project were quantified using the lower alpha value (Figure 2.12a), closely

matching existing literature (Cattaneo et al., 2020; Olivier et al., 2016) that aim to envelope a crown as closely as possible without incorporating large holes in the hull.

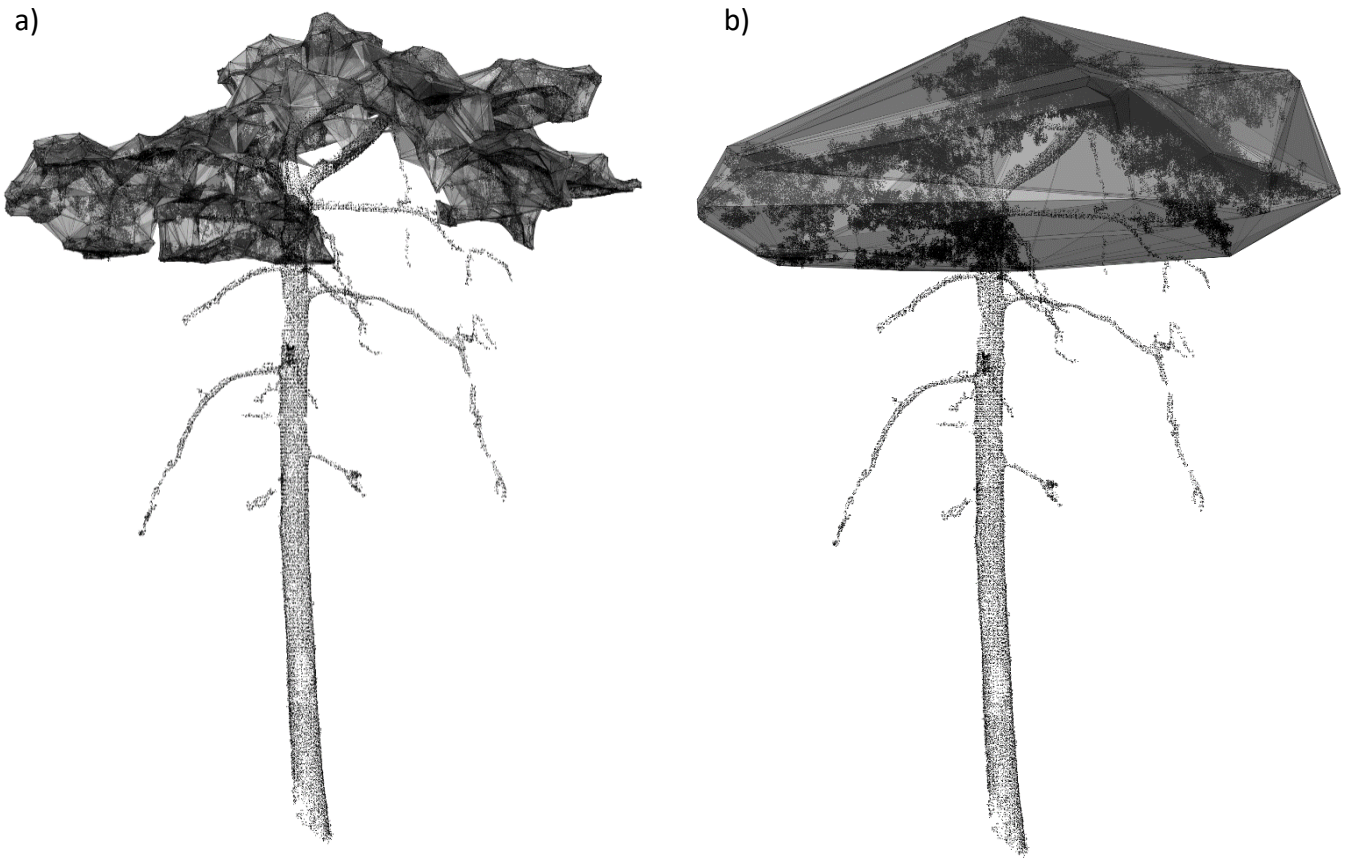

Figure 2.12 Showing the same *P. sylvestris* but wrapped by a) a tight-fitting concave hull, and b) a loose convex hull, showing how the alpha parameter controls in the inclusion of empty space when convex hulls are used.

An array of geometrical primitives have been applied to traditional ground measurements to derive crown volume including; spheres (Estornell et al., 2018), ellipses (Jucker et al., 2014; Korhonen et al., 2013), cylinders (Hecht et al., 2008) and cones (Estornell et al., 2018; Meng et al., 2007), with different shapes sometimes applied to different tree functional types, for example broadleaf and conifer (Jucker et al., 2015). With all these shapes, there is minimal evidence behind choices and to my knowledge, no comprehensive analyses have been undertaken to assess the impacts of assuming varying shapes on volume. Therefore, I simulated these four widely used shapes, with TLS-derived mean crown radius and crown depth as input and plotted them against my TLS derived crown volume using convex hulls. Across all shapes there were

substantial overestimations between assumed shapes and TLS volume were variable, though no apparent bias between the two genera in my dataset (Figure 2.13). Cylinders overestimated volume the most, while cones had slope values much that were closest to the 1:1 line (red dashed lines in Figure 2.13) and both spheres and ellipsoid had similar slope values. The absolute differences were large, cylinders overestimating relative to TLS by more than 400%, spheres and ellipsoids by around 250%, and cones much less, between 73% and 85%.

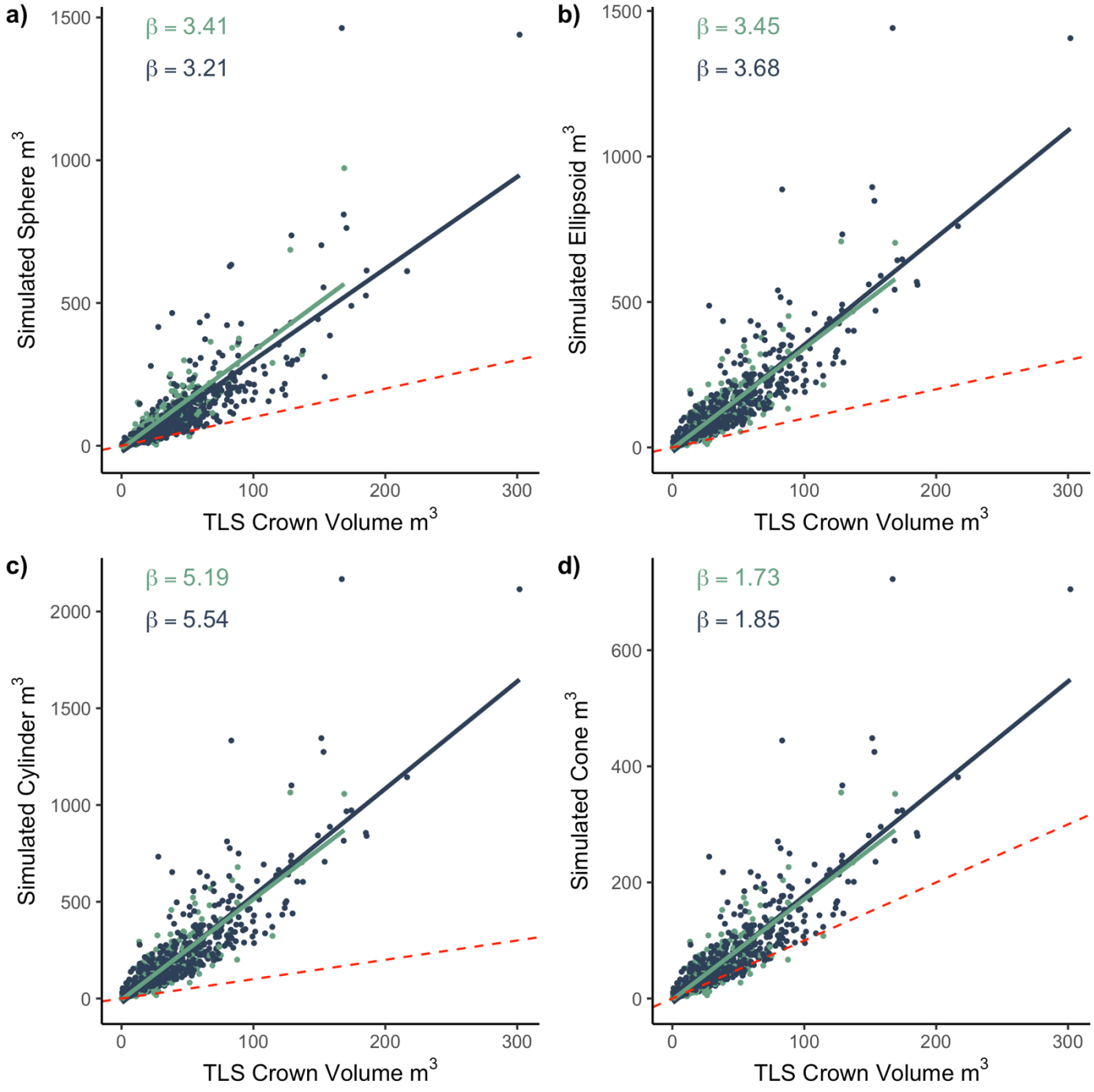

Figure 2.13 Shows linear relationships between TLS crown volume computed using a concave hull and simulated a) spheres b) ellipsoid c) cylinders and d) cones. 1:1 relationship is displayed in red and β values (slope) shown for both pines (blue) and oaks (green).

It is clear that ground-based measurements overstate crown volume, with likely ramifications when scaling from individual to community interactions and competition for space, but for the full-potential in TLS to be realised there needs to be consensus on what exactly is crown volume and then develop standardised approaches in its calculation. An important element within this newly realised framework will be to both retain interpretability with historic inventory data whilst also complimenting newer metrics of crown space filling that include fractal analysis (Seidel et al., 2019a) and foliage density and distribution (Martin-Ducup et al., 2018).

2.4.5 Co-locating TLS and field data to tag species

In order for TLS to have realise its full potential within forest ecology, it is crucial that individual trees can easily be tagged with species ID, and many are now attempting to automatically identify species based on structural and topological characteristics combined with classification techniques (AAkerblom et al., 2017; Terryn et al., 2020; Xi et al., 2020). For the work of this thesis, hand drawn stems maps were created in the field that were than cross-matched to TLS stem maps (Figure 2.14) after all tree segmentation procedures. Maps were drawn after laying out a 10 m grid within plots to reduce human error. One issue that in plots with denser understorey was the challenge of laying out straight and correctly orientated tape measures. Alignment between the two stem maps didn't pose big problems for this project - not only because there were only four species but also due to a large proportion of the plots containing either one species or a mix of one pine and one oak, simplifying identification even when reliant on TLS data only, but in highly diverse tropical forest accurate species recording is likely to be a major concern. An alternative to automatic classification is new barcode systems, using tags that are visible within TLS scans and automatically identifiable, with unique identifiers tied to a species ID (see https://github.com/philwilkes/qrdar). This means the placement of small labels on each tree within a plot, increasing fieldwork, but as an approach shows promise for robust and accurate records with minimal manual-post processing.

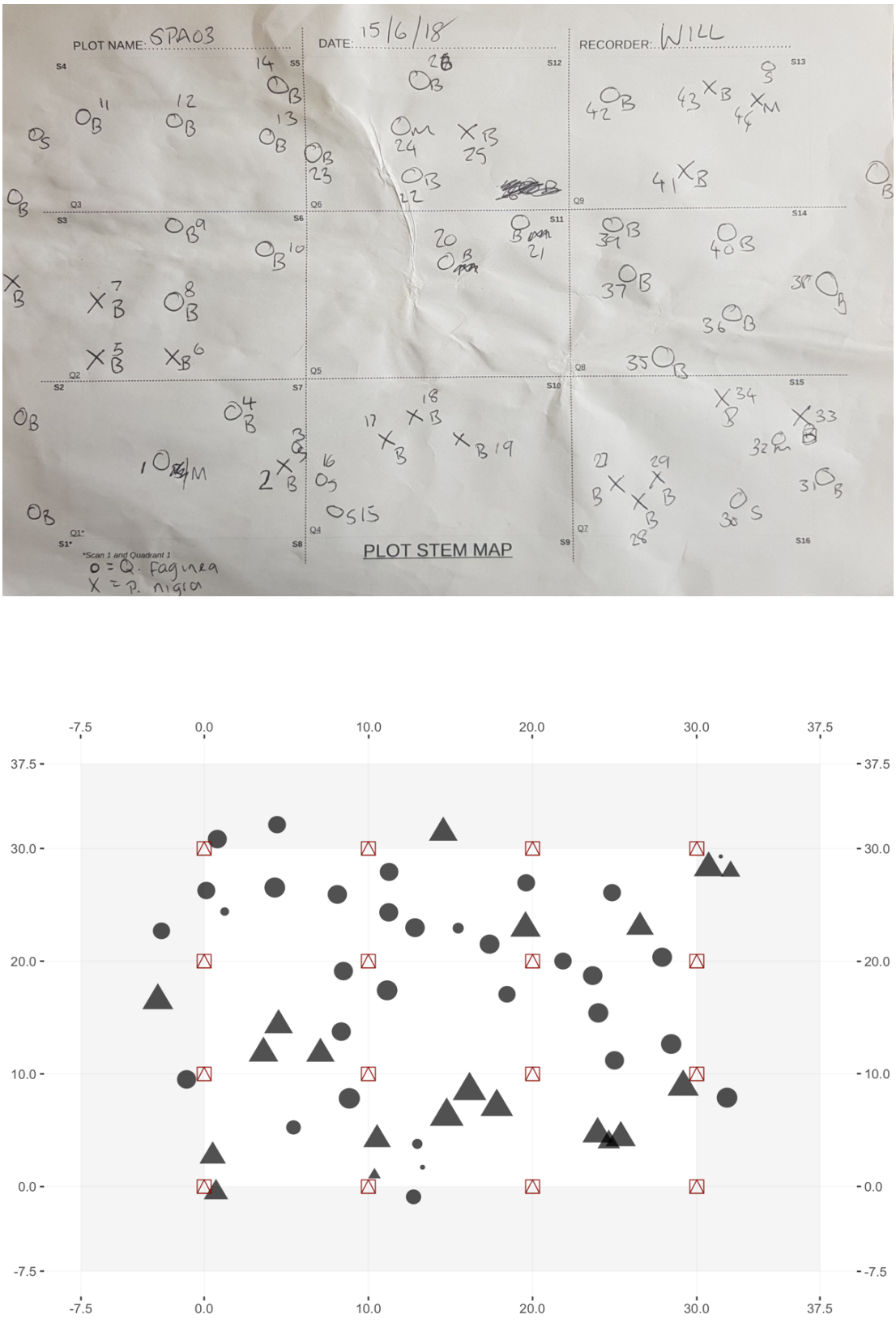

Figure 2.14 An example of a hand drawn stem map produced in the field to aid species tagging later on in the TLS data (top) and bottom the corresponding TLS-generated stem map (scan locations in red, closed triangles are *P. nigra* and closed circles are *Q. ilex*).

2.5 New insights into crown displacement and plasticity

2.5.1 Separation of leaf and wood in point clouds

The initial need for and applications of leaf separation procedures arose from the need to supply wood-only point cloud returns for cylinder fitting procedures to calculate volume, mass and carbon storage (Burt et al., 2020; Disney et al., 2018). Other applications include accounting for the varying contributions of each material when computing variables such as leaf area index (LAI) using indirect approaches (Woodgate et al., 2016), vertical leaf distribution (Martin-Ducup et al., 2018) and to derive leaf angle distributions (Vicari et al., 2019). Previously, as with tree segmentation, most resort to manually separation of leaves from wood (e.g., Martin-Ducup et al., 2020) within visual software such as cloud compare (*Cloud Compare*, 2021), but recent open source development has produced an automated approaches with promising results (see Figure 2.15) using only XYZ point information (Vicari et al., 2019; Wang et al., 2020). Although a lot of focus has been on isolating the woody element, there is huge potential to analyse the foliage component, including analyses on clumping and light-mediated spatial arrangement (e.g., Béland and Baldocchi, 2020 and Schraik et al., 2021) to test our theoretical understanding of how trees construct an efficient canopy, and how these change with environmental conditions (Valladares et al., 2002).

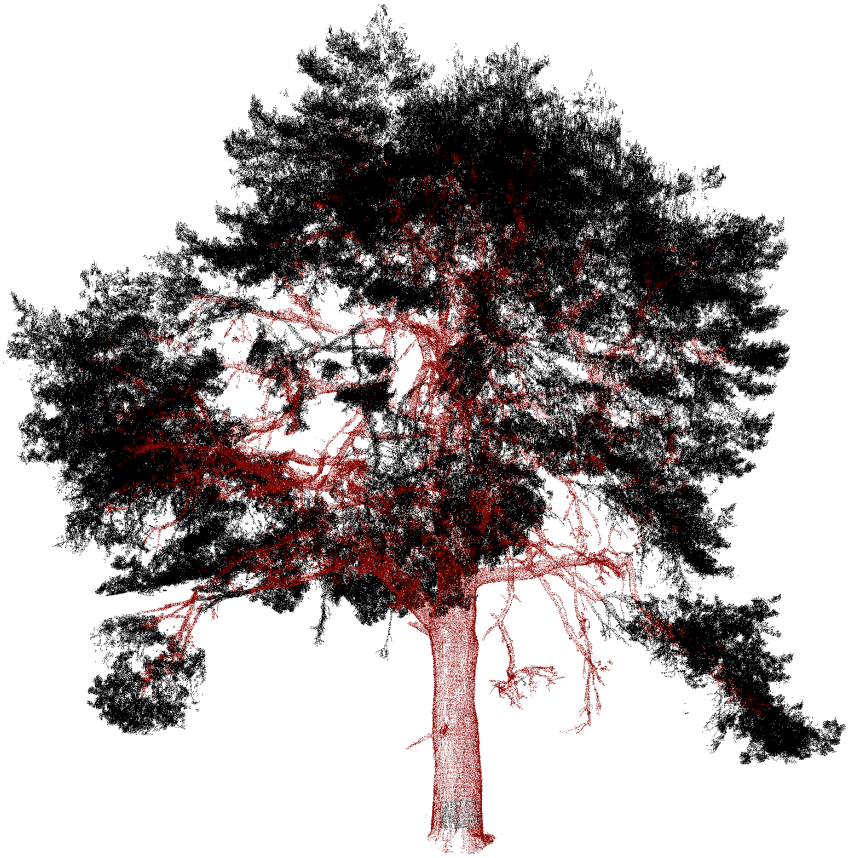

Figure 2.15 An example output from leaf/wood separation using TLSeparation (Vicari et al., 2019) with wood points in red and leaves in black. This *P.* sylvestris tree is one of the largest in this dataset, with a DBH of 1.01 m.

In this work I applied the python TLSeparation package (Vicari et al., 2019) to separate leaves from wood for all trees (Figure 2.1 steps 10.1-10.3). The process is memory intensive and required the use of high-performance computing alongside downsampling procedures. For smaller trees higher resolution 0.025 m point cloud was used, but to manage computation time, for large trees (those above 10 mb in file size) the 0.05 m point cloud was used for separation, and then subsequently upsampled using the 0.025 m point cloud. This optimised total computation time and memory use by only applying high resolution where needed. During the separation step, the XYZ file for each tree had an additional binary column added containing the classification, to allow for easy sub-setting within all subsequent processes and metric calculations, including morphological (Chapter 3), plasticity (Chapter 4) and light interception indices (Chapter 4).

2.5.2 Displacement

A tree crown's placement in three-dimensional space is a result of a trees structural response and biomass investment patterns to avoid shading by neighbouring trees and improve its own light capture (Novoplansky, 2009). This simple mode of plasticity helps trees to optimally fill canopy space and is a central component for two-dimensional forest dynamic models (Purves et al., 2008). Displacement of a tree crown is often not included within forest ground surveys due to the difficulty in determining a tree crowns' centre of mass from below, but this is rather straightforward with TLS after point clouds are wood/leaf separated. To do this, I defined two metrics of displacement within R (Figure 2.1 steps 13.3 – 13.4); stem displacement, calculated as the angular displacement of the crown base relative to the stem base, and crown displacement, calculated as the angular displacement of the centroid of the foliage component, relative to the base of the crown. These metrics capture two independent means of displacement as shown in Figure 2.16 below, where a) a *Q. ilex* tree shows strong stem displacement and b) a *P. sylvestris* tree shows crown displacement only.

Figure 2.16 Showing differences in displacement between two trees where a) is a *Q. ilex* tree showing high stem but minimal crown displacement and b) a *P. sylvestris* tree showing the direct opposite.

The most challenging step in the calculation of these metrics is the extraction of the stem top/crown base. I used both leaf and wood clouds as well as including some stability checks to ensure that the stem top centroid was predominantly determined by the points on the stem bole (rather than any lateral branching at the same level). To do this, the lowest height of foliage was extracted which was then used to extracted three 0.25 m slices from the wood cloud that were centred around this height. The slice with the lowest standard deviation on both X and Y axes then averaged, resulting in a stem top coordinate.

Locating Stem-Top Centroids:

For each *tree* (i=1…N)

1. Locate the base of the foliage component using the 0.03 percentile of the z-axis

2. Extract three 0.25 m slices vertically from the wood cloud centred at the height of the base of the foliage

3. For each *slice* (i=1…*3*))

a. Calculate the standard deviation of both the X and Y axes of $slice_i$, and store in a vector $slice_i^{SD}$

b. Select the slice with the lowest mean values in $slice_i^{SD}$

c. Calculate the mean of XYZ coordinates from the selected slice, and return as stem top centroid

---

2.5.3 Sinuosity

Crown and stem displacement are metrics that represent a trees quest to intercept light, but they don't measure the capacity of a tree to twist, turn and morphological flex along its vertical axis. This form of morphology is often termed sinuosity or tortuosity, but I will stick to the former term here. Attempts have been made to calculate sinuosity from TLS data (Guillemot et al., 2020; Olivier et al., 2016) but mostly within the context of vertical displacement of material (Bohlman and Pacala, 2012), characterising how foliage is displaced to varying degrees along the Z axis. However, this metric only accounts for displacement of foliage as distance with no consideration of direction, so predominantly characterises a tree crown's variability in horizontal displacement rather than the 'twisting' and 'bending' that define sinuosity. I constructed my own sinuosity algorithm in R (Figure 2.1 step 13.5) that characterises angular changes in foliage arrangement along the stem axis, weighted by distance, i.e., when all slices are analysed as a whole, the slices further away from the axis contribute more to the overall measure of angular standard deviation than closer ones. This can be seen conceptually in Figure 2.17, where the lower crown is growing in an opposing direction to both the overall stem axis and foliage in the upper crown, leading to high angular dispersion and therefore, high sinuosity.

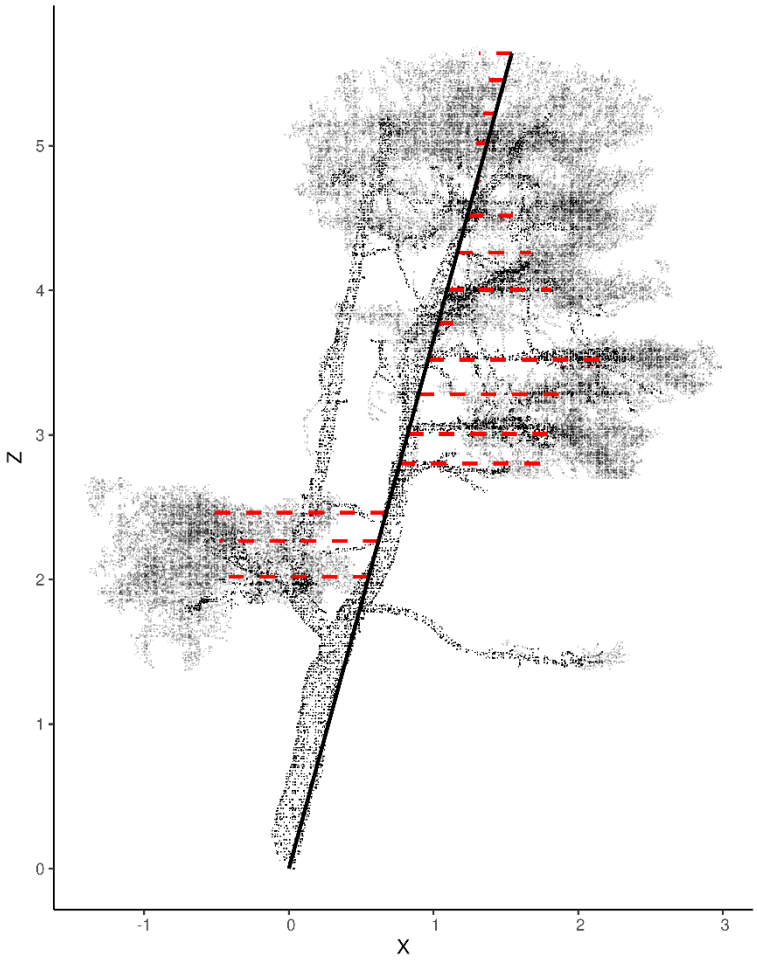

Figure 2.17 Crown sinuosity with dashed lines representing displacement from the modelled plane (overall lean of the tree; black solid line) of a *Q. faginea* tree. Side-on two-dimensional view along x and z-axes.

2.5.4 Crown arrangement and filling

Trees can spatially arrange foliage to either enhance light capture, as for example, to increase light interception in low light environments (Givnish, 1988) or alternatively in water limited environments, formulate a protective barrier that reduces the exposure of the more productive shaded leaves to excess raidation (Pearcy et al., 2005). The majority of historical work on foliage arrangement has been through modelling (Pearcy et al., 2005) or calculation of indices such as gap faction and LAI (Li et al., 2017), but comprehensive, detailed analyses at the whole crown scale have mostly been confined to smaller plants (e.g. Bell and Galloway, 2007). In this study, I apply fractal analyses of TLS data (Figure 2.1 step 13.6), to all tree crowns in my dataset to

derive a crown filling metric – box dimension - that reflects both complexity and spatial filling of material (Seidel, 2018). The box dimension was calculated to extract the fractal dimension using the R package 'rTLS' (Guzmán et al., 2020). Box dimension is calculated by essentially covering a tree with progressively smaller boxes, counting the number of boxes needed to cover all points at each incremental step in resolution (see Figure 2.18), and fitting a linear relationship between box size and number of boxes required. The slope of the relationship (the alpha-parameter Box^{α}) between the number of boxes and resolution is the box dimension itself, with steeper values representing higher complexity where many more boxes are needed as the resolution gets finer. The intercept of this relationship is also extracted (the beta-parameter Box^{β}) and is an indicator of overall size (Mandelbrot, 1977). The availability of three-dimensional data has meant this metric has seen a recent rapid increase in use, with it being linked to growth (Seidel et al., 2019a), competition (Dorji et al., 2019) and overall tree stand metrics (Guzmán et al., 2020). Its applicability is likely driven by its effectiveness in representing structural complexity in its entirety, reflecting vertical, horizontal and internal characteristics (Seidel et al., 2019b), but further work is needed to understand its drivers (Saarinen et al., 2021). At its core though, the fractal dimension provides a holistic measure of filling and complexity (Mandelbrot, 1977), and with fractal dimension a central component to metabolic scaling theory in ecology (West et al., 1999) it is this interpretation that is used within this work.

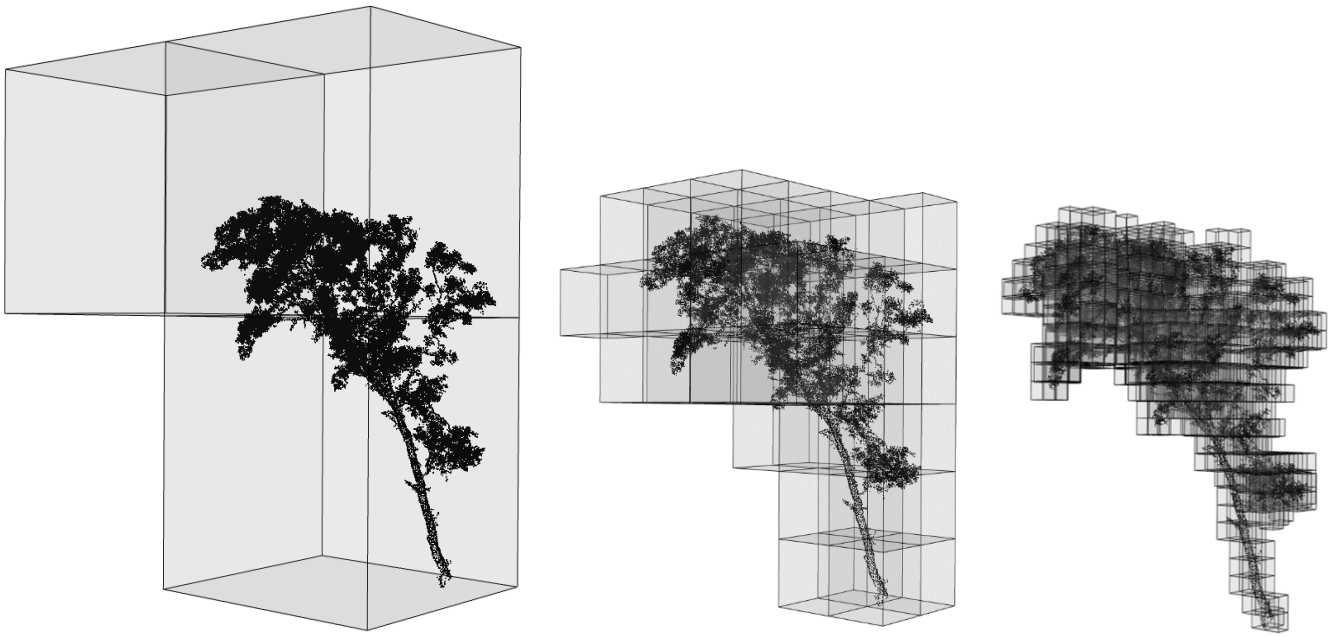

Figure 2.18 A visual demonstrating showcasing the voxelisation process in calculating the box dimension (Seidel et al., 2019a) where from the left towards the right a tree is covered with increasing voxel resolution (4 m, 1m and 0.25 m).

Exciting future directions for work on crown arrangement metrics with TLS is likely to include explicitly quantifying foliage clumping, a variable that has large ramifications for light penetration through the canopy (Duursma and Makela, 2007). Clumping of leaves is a key variable within radiative transfer models (Braghiere et al., 2021), as well as foliar arrangement in 3D space relative to incoming light but is notoriously difficult to quantify on the ground. Progress here using TLS will provide a much needed deeper empirical understanding of structure-light relationships across various ecosystem types (Niinemets, 2010).

2.5.5 Network analysis of branching and foliage arrangement

The majority of analyses of tree architectural hydraulic efficiency have studied it through lateral extension (crown expansion), primarily because of constraints associated with traditional measurements (Lines et al., 2012). However, a tree's true hydraulic vulnerability is related to path lengths throughout its branch network (Koçillari et al., 2021), which can now be captured fully with TLS. A tree's structure is a result of multiple trade-offs (Verbeeck et al., 2019) and within water-limited ecosystems, a significant trade-off exists between

extending to acquire light and retaining hydraulic safety, for both height and crown expansion. Aspect ratios - width divided by crown height (Lindh et al., 2018) - have been applied using TLS (Olivier et al., 2016) as a potential means to reflect such trade-offs (Verbeeck et al., 2019) , but as when considering traditional crown measurements, irregularity in crown structure can lead to values that don't accurately capture a crown's branching patterns. Furthermore, these surface-level characteristics fail to account for photosynthetically active material that is within the outer crown boundary, so reduce a complex three-dimensional arrangement of foliage into a simple measure of width and height. However, the three-dimensional nature of TLS data means a network can be extracted from the point cloud from the stem base, along branches to the leaf tip. Interpreting a tree's structure as a network has the potential to provide greater insight into analysis conducted at the branch scale, such as shedding due to drought and spread of crown dieback (Rood et al., 2000), as it characterises tree structure in a way that reflects the manner in which trees transport resources to all its parts through its vessels (Savage et al., 2017).

A major advantage of network analyses is that, compared to cylinder fitting approaches, it is less dependent on data resolution and coverage (although high occlusion will lead to errors in path length estimation). For this work, I quantified path length using the python library "pc2graph" (https://github.com/mattbv/pc2graph), using downsampled clouds to 0.05 m to facilitate computation and memory use (Figure 2.1 steps 11.1-11.3). This approach was used to quantify the path fraction for every tree (Figure 2.19), calculated as is the mean path length to all leaves divided by the maximum possible path length for that tree, and a is holistic measure of a trees hydraulic and light capture efficiency (Smith et al., 2014). Values close to zero represent cylindrical like trees – which have conservatively arranged foliage, whereas values those closer to one represent more 'umbrella' shaped trees - where both hydraulic and light capture efficiency is maximised. Path fraction has been found to be ecological meaningful to represent strategic resource acquisition (Malhi et al., 2018), and is a valuable inclusion to analyses in ecosystems where both water and light limitation are present, such as Mediterranean forests.

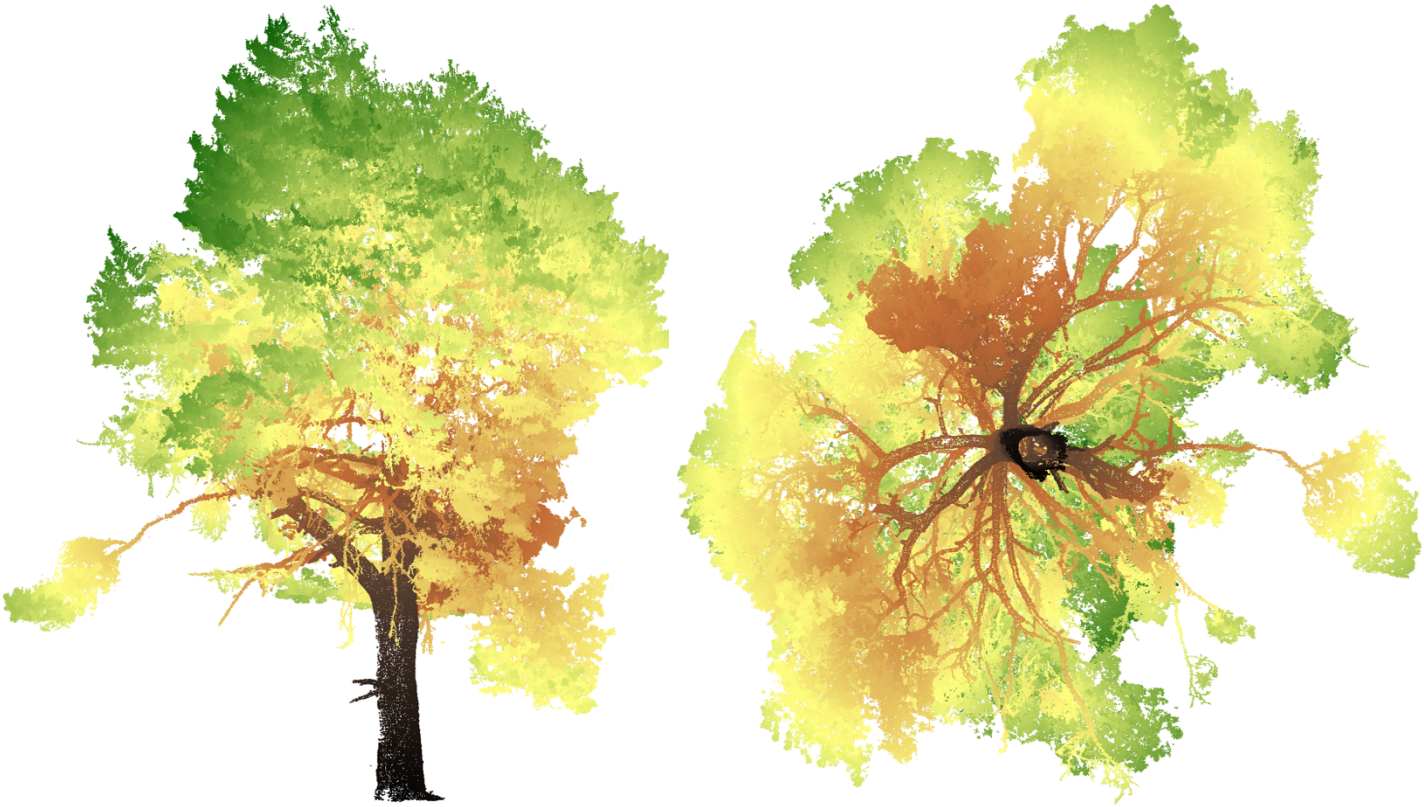

Figure 2.19 A *P. sylvestris* tree where the colour of each point represents the distance to the stem base (following the shortest path along the branches). Low values are black/brown, and longer path lengths shown in green.

2.6 New insights into tree-tree interactions

2.6.1 Neighbourhood competition

Understanding how trees compete with one another for space and resources is fundamental to understanding growth, mortality and metabolism, and the study of neighbourhoods is an established field that spans over one hundred years (Keddy, 2017). The majority of traditional approaches have involved easy to measure tree attributes such as DBH as a measure of size and distances between stems used to determine neighbourhood effects, perhaps including a distance decay effect for strength of effect of neighbouring trees. Although interactions have been studied at the neighbourhood scale for some time (Stoll and Weiner, 2000), many studies quantify competition using plot scale statistics providing very coarse representations of competition, such as plot-averaged basal or crown area (Lines et al., 2012). A commonly accepted theory within tree-tree interactions is that resource uptake is proportional to size, so creating asymmetric competition where larger trees negatively affect smaller ones (Weiner, 1990). The effect of asymmetric shading makes conceptual sense

above ground where trees tower above others and intercept proportionally more light and shade smaller surrounding trees, creating a steep light extinction gradient (Freckleton and Watkinson, 2001). In drier sites, competition is often stronger belowground (Pretzsch and Biber, 2010), but it effects may be symmetric rather than asymmetric (Weiner et al., 1997); making symmetric competition an important and necessary component of tree-tree interactions in many ecosystems (Coates et al., 2009).

2.6.2 Arbitrary neighbourhood distance thresholds

Irrespective of asymmetric and symmetric effects, when quantifying competition at the neighbourhood scale, a distance must be predefined that dictates the distance at which competition is believed to influence a focal tree. However, there is no consensus on what that distance should be. For instance, both 5 m (Grossiord et al., 2014) and 10 m (Gómez-Aparicio et al., 2011) neighbourhoods have been used in Mediterranean forests of Spain, 10 m in temperate forests of British Columbia, Canada (Thorpe et al., 2010), 15 m radius in the French Alps (Kunstler et al., 2012), 25 m in the Southeastern USA (Zhao et al., 2006), and 30 m in tropical rainforests of on Barro Colorado Island, Panama (Chen et al., 2016). An alternative approach, taken in this work, is to set neighbourhood size to vary according to the dimensions of the focal tree crown (Lorimer, 1983; Pretzsch and Biber, 2010). The inconsistency in determining a zone of influence makes inter-study comparison difficult, initiating discussions on potentially new ways to quantify competition that is easily interpretable and transferable, such as crown overlap (Zambrano et al., 2020). In fact, Biging and Dobbertin, (1992) used crown overlap as a means to separate aboveground (asymmetric) and belowground (symmetric) competition, the latter quantified using neighbourhood basal area. However, crown overlap estimations have historically relied on ground-measures of crown radius and assumptions of geometric shape, leading to similar issues to those discussed in section 2.4.2 (Figure 2.20). Although crown overlap shows promise, it has previously only been demonstrated using inventory data in a tropical system, where competition for light is fierce (Zambrano et al., 2020). Moreover, crown overlap implicitly assumes that overlap from the vertical only is important. Given that light availability of an individual is a result of complex interactions between surrounding structure and diurnally changing sun angles, a metric of overlap from a purely zenith angle is unlikely to capture the full complexity.

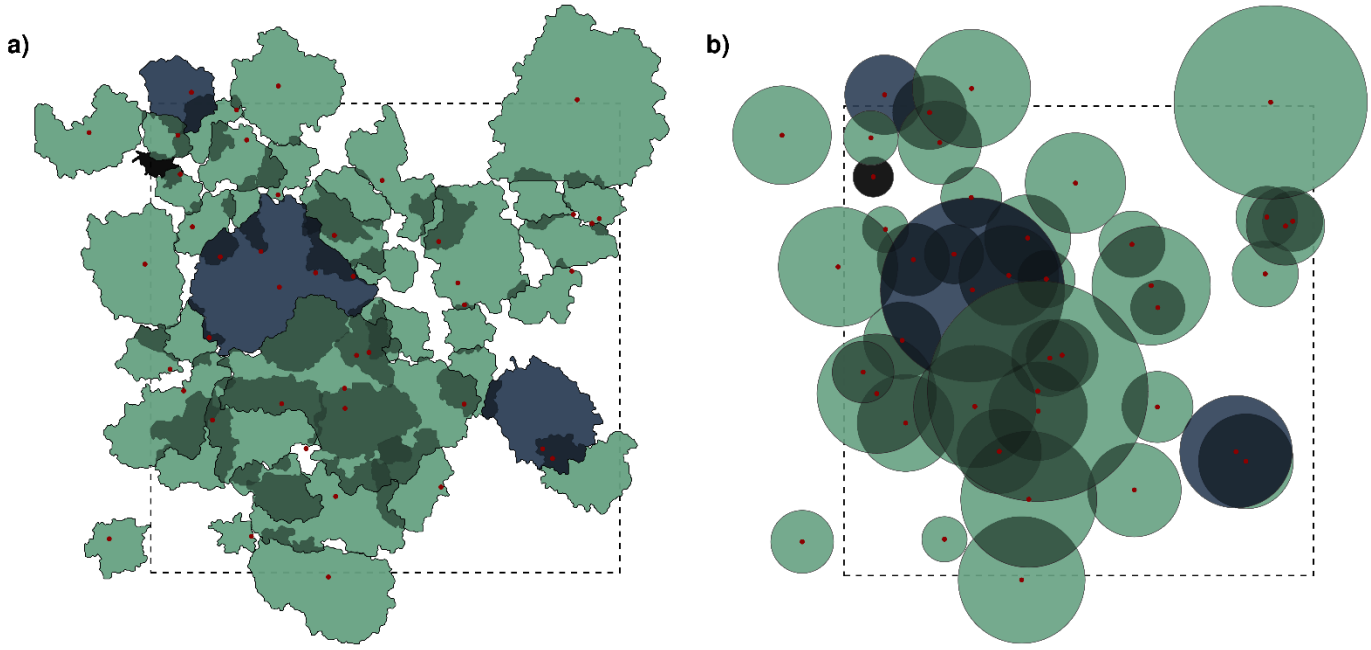

Figure 2.20 Top-down views of one plot canopy with a) constructed from TLS with red dots representing crown position and b) using average of max and perpendicular crown axes to model circles which are located above stem base coordinates in red. Oaks are coloured green and pines blue.

2.6.3 Quantifying Neighbourhood Competition

To characterise competition and attempt to tease-apart the separate effects of asymmetric and symmetric competition on individual trees, I computed a metric that builds upon existing crown competition concepts (Figure 2.1 step 12.10), but that capitalises on the spatial accuracy and arrangement of trees crowns available from TLS (see Figure 2.20.a). I applied a variable buffer dependent on focal tree crown size, defining a tree's neighbourhood diameter as double its crown diameter, with a minimum neighbourhood of 5 m (the smallest I found in the literature). I applied this to all trees, but when the neighbourhood area intersected the plot boundary (dashed line in Figure 2.20) the tree was removed from this analysis. To separate asymmetric and symmetric effects, overlap from trees that were at or above 90% of focal tree's height were included as causing asymmetric competition, whereas all trees were included when calculating symmetric competition. Each competition metric was the proportion of crown projected area within the focal trees' neighbourhood covered by tree crowns, with separate competition calculated for separately for each genus, computed as follows:

Neighbourhood Competition:

For each $tree_i$ (i=1…N)

1. Load the leaf point cloud pc_i

2. Collapse pc_i into two dimensional space (x,y)

3. Compute a concave hull using concaveman in R

4. Calculate the crown radius as the average of radii across the concave hull

5. Create a polygon with a radius twice that of the focal tree crown radius

IF polygon intersects plot boundary, stop analyses on tree i; restart step 1 on $tree_{i+1}$

6. Find all tree's whose crowns that intersect the circular neighbourhood, compute their crown hulls

7. Clip all neighbour tree's hulls to neighbourhood extent, and attach tree genus ID to each polygon

8. Sum the crown projected area of each genus within the circular neighbourhood

9. Return area of each genus as symmetric metrics

10. Subset only polygons from trees at or above 90% of focal tree height, and return area each genus as asymmetric metrics

---

2.6.4 Disentangling above and belowground competition

In order to understand the full spectrum of tree-tree interactions, the disentanglement of above ground competition for light and belowground competition for water and nutrients is crucial (Coates et al., 2009). Competition for light is one of key resources for productivity, often posing limits on tree growth in closed forest stands (Pacala et al., 1996) but its characterisation is difficult within the limits of traditional ground measurement, with shading presumed to be a simple product of being surrounded by larger individuals. Both water (Grossiord, 2019) and nutrients (Coomes and Allen, 2007) effect tree growth and survival but the scale at which they influence is difficult to ascertain given the difficultly in measurement. Early attempts to disentangle these affects involves simple differentiations in competitive metrics such as using basal area within a set distance from tree base and crown overlap as belowground and aboveground competition respectively (Biging and Dobbertin, 1992). More sophisticated modelling techniques arose that aimed to characterise light interception as best as possible using mathematical models and assumptions of crown shape with residual crowding effects assumed to be belowground (Canham et al., 2004; Coates et al., 2009). However these early ray tracing models still depended on geometrical assumptions in shape that don't reflect a trees true complexity

and placement in space (Sapijanskas et al., 2014) and therefore cant explicitly characterise competition for light.

2.6.5 Novel measurement of light capture

TLS has begun to show huge promise in modelling how light interactions with vegetation (Calders et al., 2016) and differences in light transmission between different forest types (Kükenbrink et al., 2021) but spatially explicit quantification of an individual trees light environment has not been attempted until now. Fully quantifying individual light capture has high potential for impact in forest ecology, not only to fully disentangle above- and below- ground competition (building on earlier works, e.g. Canham et al., 2004), but also to understand how a tree's structure, plasticity and size create its light capture and productivity (see Chapter 4). For this project, I demonstrate how the application of exciting new ray tracing algorithm can quantify a trees light environment (Figure 2.1 steps 14.1 -14.6, Figure 2.21), and here discuss the data pipeline I constructed to produce ecologically interpretable light indices (Figure 2.1 steps 14.7 – 14.9).

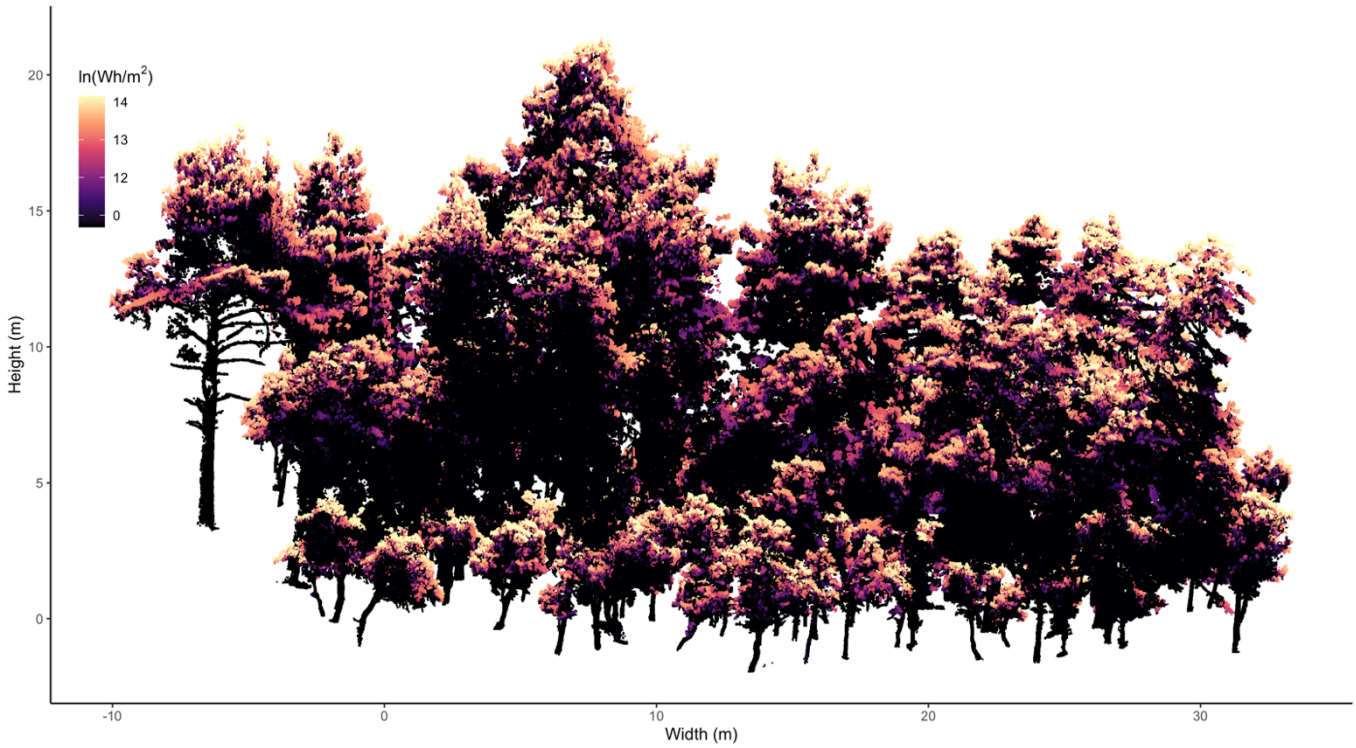

Figure 2.21 Example output from the Vostok ray tracing algorithm of an example plot containing *P. sylvestris*, *P. nigra*, *Q. faginea* and *Q. ilex* in Alto Tajo National Park, Spain. Points are coloured according to irradiance (black to yellow) on a log scale with 0 meaning completely shaded. Black points are the wood cloud.

I characterised the irradiance received for each tree crown using the openly available C++ library ray tracing algorithm 'vostok' (Bechtold & Höfle, 2020; available at - https://github.com/GIScience/vostok). This algorithm simulates the diurnal movement of the sun across the sky, firing rays into a three-dimensional point cloud which are either intercepted by a point, miss all points or are shaded by a neighbouring point. A necessary prerequisite step is to ensure all plot point clouds are orientated correctly so that as the sun is simulated across the sky, its relative position to all trees reflects reality. I rotated all point clouds using PCL and used the plot cardinal direction data collected in the field. In order to use the vostok approach to determine whether a point will intercept a ray of light at a given point in time, surface normals are required (Figure 2.22a) that define the orientation of a point relative to a flat surface (plane), which itself is modelled from neighbouring points (see Figure 2.22b). Any normals that were negative, i.e., pointing downwards and facing towards the ground or crown were flipped 180 degrees (see Figure 2.22c). Choosing the number of points neighbouring a focal point to model a plane is important because, as explained above, these serve as the reference point to which the point itself facing (see Figure 2.22b). I decided to define this parameter by calculating the number of points that are expected to be contained within a cube of side 0.25 m, given a specific point spacing, defined here as the nearest neighbour distance (*NN*). I decided on 0.25 m as I wanted the normals to be computed on a scale comparable to a 'cluster' of leaves, balancing inclusion of enough points to represent the crown surface well with avoiding 'over-smoothing' and losing detail of a crown's undulating surface.

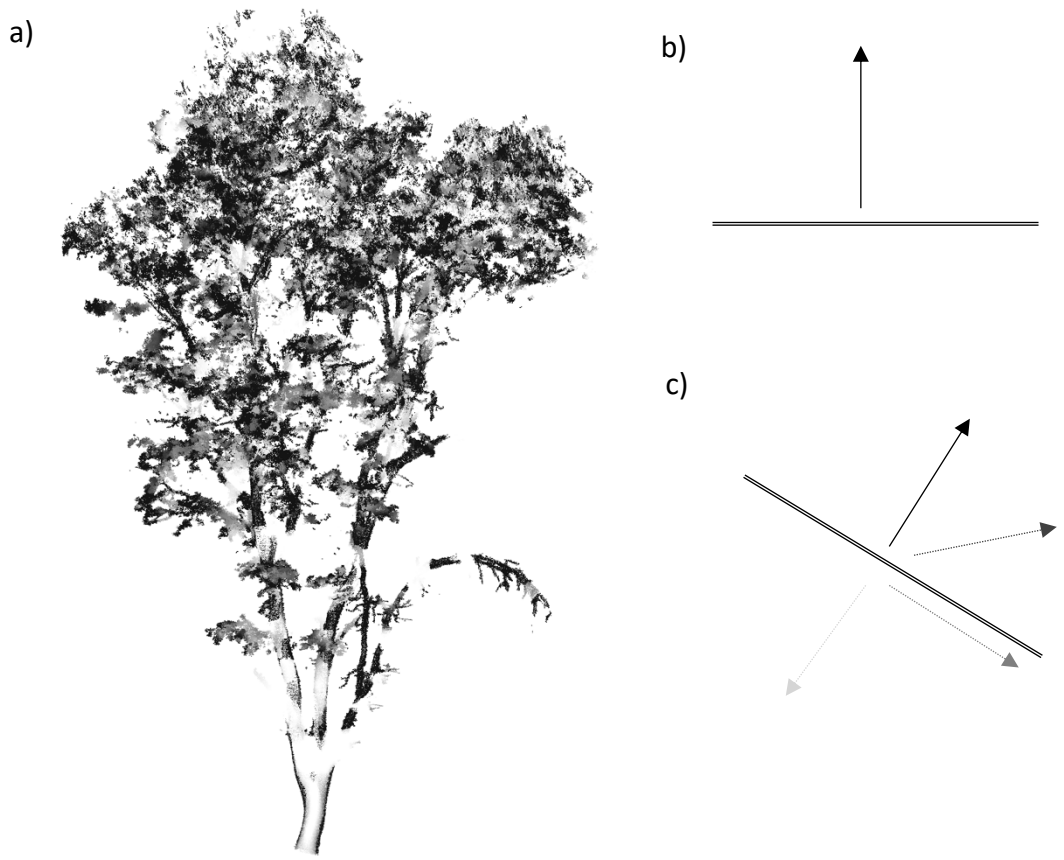

Figure 2.22 a) An example of a tree with surface normals visualised where, increasingly bright (white) values indicate the normal facing towards this viewpoint and darker away b) A surface normal perpendicular to a surface demonstrating how a surface normal is calculated and c) a visual depiction of how normals facing inwards or downwards were flipped 180 degrees.

I applied the vostok algorithm to the re-combined plot point cloud, combining all individual tree point clouds in their original locations, but including ID tags within the filenames prior to the irradiance calculation step. I then applied the vostok algorithm to calculate irradiance for the summer of 2018 (April to October) at 30-minute increments within a single day and at monthly increments (i.e., one day for each month). This temporal resolution accounted for diurnal and monthly variability in sun angles with greater emphasis on diurnal (every 30 minutes), using a spatial resolution for the plot point cloud (0.025 m) that was computationally pragmatic. Parameters used to derive sun angle were automatically extracted from a database (http://rredc.nrel.gov/solar/codesandalgorithms/solpos/). The output for each point within each plot was the summed irradiance intercepted (watt hours per m^2, see Figure 2.21) and individual trees were then re-separated using the ID column that was affixed to the input point cloud. I calculated individual light capture as follows:

Individual Tree Light Capture:

For each *plot* (i=1…M)

---

1. For each *tree* in $plot_i$ (ii=1…n)

a. Load and downsample *point clouds* (including leaf/wood classification and pathlength columns for subsequent analyses)

b. Calculate point normals for $tree_{ii}^{xyz}$ using $k^{neighbours}$ points, where:

$k^{neighbours}$ = ceiling($(0.25/NN)^3$) where: NN is the nearest neighbour distance between points

2. Combine all trees including point normal information into one cloud, retaining tree ID for each point

3. Create the shadow point cloud ($plot^{xyz}$) extracting X, Y, Z columns from $plot^{xyz,normals,id}$

4. Create the vostok parameters file with the following important parameters (Bechtold & Höfle, 2020):

lat, long = {40.70, 2.05}	time zone = GMT+1	DOY = {121,…,304}
year = 2018	daily Iteration = 28	time iteration = 15 mins

5. Run *vostok* algorithm with both $plot^{xyz,normals,id}$ and $plot^{xyz}$ clouds set to 0.025 m resolution

6. Combine *Vostok* output with tree attribute data

a. Drop plot normals ($plot^{xyz,id,irradiance}$)

b. Bind $tree_{ii}^{leafsep}$ and $tree_{ii}^{pathlength}$ attribute columns to the plot *PC* ($plot^{xyz\ ,id,irradiance,leafsep,pathlength}$)

c. Separate $plot^{xyz\ ,id,irradiance,leafsep,pathlength}$ into individual trees and reurn indiivudal tree point clouds

$tree_{1,\ldots,n}^{xyz,irradiance,leafsep,pathlength}$

The next important step was to condense this highly detailed three-dimensional representation of received irradiance into ecologically meaningful holistic measures of light capture (Figure 2.1 steps 14.7-14.9). To reflect overall tree crown light capture, I adopted an approach similar to Kothari et al., (2021), who used ceptometers to measure incoming light, and derived ratios of light received at the top of a tree to that available in open canopy space. I calculated the mean of irradiance across the entire tree crown and divided this by the maximum light available within the plot for each individual tree, a metric I termed *light fraction*. This metric is highlights the relative availability of light to each tree, a value that usually should have a strong correlation with the percentage of light accessible by an individual tree over much longer time-scales (Parent and Messier, 1996).

To complement this light fraction metric (which characterises overall light capture), I formulated another that defines the degree to which a tree crown intercepts light vertically through the crown. A tree's response to light is complex with partial shading thought to significantly effect crown growth (Schoonmaker et al., 2014), along with trees expressing different foliage traits dependent on the direction of growth (and therefore varying heat and water stress; Mediavilla et al., 2019). In order to determine the vertical heterogeneity of light capture for each tree, I sliced every individual crown into 10 bins along the vertical axis and determined whether each slice was in direct light or not by calculating the 75th percentile of irradiance and if above the minimum value of the entire crowns, was assigned a value of 1. The metric, which I termed Crown^{LiUni}, is then simply proportion of slices in direct light. Both of these metrics were used in Chapter 4 to characterise individual tree light capture, with light fraction also used to assess whole plot light capture.

2.6.6 New insights and opportunities

The availability of spatially explicit information on tree light capture has the potential to open up new avenues of research and eliminate some of the technical and methodological barriers that have to date constrained the testing of theory on light mediated tree structure to small plants within experimental set ups. These experiments have revealed interesting insights into how plants respond to both mechanical stimuli and light (Nagashima and Hikosaka, 2012), respond to competition in different ways depending on the structure of

neighbouring plants (Gruntman et al., 2017) and possibly how plants can sense and respond to competing plants growing from below (Zhang et al., 2021). In the field, light environments have traditionally been quantified using hemispherical photos (Fotis and Curtis, 2017) and light meters (Kothari et al., 2021), with 3D quantification of irradiance confined to modelling techniques that involve abstraction using geometrical primitives (Pearcy et al., 2005; Sapijanskas et al., 2014; Valladares et al., 2002). Even when light gradients are comprehensively considered, subjects are usually of small stature such as saplings (Escudero et al., 2017; Valladares et al., 2012), small herbaceous species (Gruntman et al., 2017), or confined to small sample sizes due to the laborious nature of the data collection (Mediavilla et al., 2019). There is an exciting opportunity to not only analyse tree structure in the context of its light capture as a whole but also to supplement field campaigns looking at foliar traits (e.g., Mediavilla et al., 2019; Williams et al., 2020) by predetermining individual canopy sampling strategies through 3D irradiance mapping using TLS data. To finalise this chapter, I present one final metric that quantifies how light capture varies across a tree crown. This is a novel metric, the calculation of which I programmed in C++, using PCL functions, and drawing upon methodological approaches used in 2D (Figure 2.1 step 14.9). The *getis-ord* statistic (Getis and Ord, 1991) derives statistical "hot" and "cold spots" based on Euclidean distance and attribute values (Peeters et al., 2015). The term 'hot spot' has been applied across disciplines as a means to describe how a value or cluster of values that is higher relative to its surroundings (Harris et al., 2017). Using inferential statistics, it is possible to define hot spots as locations where attribute values are not a result of a random process and therefore represent a form of underlying process that has led to the observed emergent pattern (Getis and Ord, 2010). To calculate the statistic in 3D, I used efficient search algorithms provided by KD-trees in PCL (*Point Cloud Library*, 2021) to calculate summary statistics of each points neighbourhood attribute values. The term 'attribute' hereon refers to irradiance values for each point but could be any continuous variable of interest. Here statistical measures of intensity in clustering of high or low values of a points attribute relative to its neighbouring points are determined, that are weighted according to the distance away from the focal point. The algorithm then compares the local pattern of values (point attribute and attribute values of its neighbours) to the overall pattern, i.e., the attribute value of the entire tree crown to determine whether values are significantly cold (lower than expected) or significantly 'hot' (higher than expected). The algorithm returns Z-scores that

correspond to standard deviations, where 1.96 was used as a cut-off ($P < 0.05$; $Z\text{-score} > 1.96$ or $Z\text{-score} < -1.96$). I also made full use of the wood/leaf separation data by only applying Getis-Ord to the foliage point cloud, assigning 0s to all the wood points on export.

I adapted the 2D implementation to calculate Getis-Ord in 3D as follows:

3D Getis-Ord:

For each *tree* (i=1…m)

---

1. Split point cloud into wood and leaf point clouds using binary leaf separation column
2. Push attribute data (irradiance) for each point $pc_{1,\ldots,n}^{attribute}$ into the vector $attribute_{1,\ldots,n}$
3. Extract maximum $attribute^{max}$
4. Calculate nearest neighbour distance NN (see Burt et al., 2019)
5. Calculate whole crown irradiance statistics;

    a. $\text{crown}_{\text{attribute}}^{\text{sum}} = \sum\{\text{attribute}_{1}, \ldots, \text{attribute}_{n}\}$

    b. $\text{crown}_{\text{attribute}}^{\text{sum2}} = \sum\{\text{attribute}_{1}, \ldots, \text{attribute}_{n}\}^2$

    c. $\text{crown}_{\text{attribute}}^{\text{mean}} = \sum\{\text{attribute}_{1}, \ldots, attribute_{n}\} / attribute_{n}$,

    d. $\text{crown}_{\text{attribute}}^{\text{variance}} = \sqrt{(\sum\{\text{attribute}_{1}, \ldots, \text{attribute}_{n}\} / \text{attribute}_{n}) - \sum\{\text{attribute}_{1}, \ldots, \text{attribute}_{n}\}^2}$

6. Determine number of neighbouring points to use;

    a. $K^{neighbours} = \text{ceiling}((0.25/NN)^3)$

For each *point* (ii=1…N)

7. Locate all neighbouring points to $point_{ii}$ using KD-tree search in PCL and $K^{neighbours}$ (*Point Cloud Library*, 2021)
8. Push $\text{neighbours}_{1,\ldots,n}^{\text{attribute}}$ into vector $\text{attribute}_{1,\ldots,n}$
9. Calculate weights and apply to attribute;

    a. $\text{weight}_{1,\ldots,n} = \text{distance}_{1,\ldots,n} / NN$

    b. $\text{weight}_{1,\ldots,n}^2 = \text{weight}_{1,\ldots,n}^2$

    c. $\text{attribute}_{1,\ldots,n}^{\text{weighted}} = \text{weight}_{1,\ldots,n} * \text{attribute}_{1,\ldots,n}$

10. Sum neighbour weights and attributes

    a. $\text{attribute}_{\text{sum}}^{\text{weighted}} = \sum\text{attribute}_{1,\ldots,n}^{\text{weighted}}$

    b. $\text{weights}_{\text{sum}} = \sum\text{weight}_{1,\ldots,n}$

    c. $\text{weights}_{\text{sum}}^2 = \sum\{\text{weight}_{1,\ldots,n}\}^2$

11. Compute the Getis-Ord statistic for the point;

$$point_{ii}^{GetisOrd} = (attribute_{sum}^{weighted} - (crown_{attribute}^{mean} * weights_{sum})) / (crown_{attribute}^{variance} * (\sqrt{(((\sum_{1,\ldots,n} * weights_{sum}^{2}) - weights_{sum}^{2}) / \sum_{1,\ldots,n} - 1)}))$$

12. Save $point_{ii}^{GetisOrd}$ within the tree point cloud, and return $tree^{xyz,Irradiance,GetisOrd}$

Example outputs can be seen in Figure 2.23, where a) and c) show in colour only foliage that is significantly cold (*Z-score < -1.96; P < 0.05*) whereas b) and d) show in colour foliage that is significantly hot (*Z-score > 1.96; P < 0.05*). It is important to note that the vostok approach doesn't account for transmission, scattering of radiation or indirect light (Bechtold and Höfle, 2020). The precision to which it assigns a point as sun-lit or shaded heavily depends on the resolution of the voxelised shading input within the irradiance processing steps (Figure 2.1 step 14.6) and as such self-shading within an individual (cold spots) may be overstated. Nevertheless, this is a promising approach to analyse light mediated tree structural patterns between trees and within individual crowns.

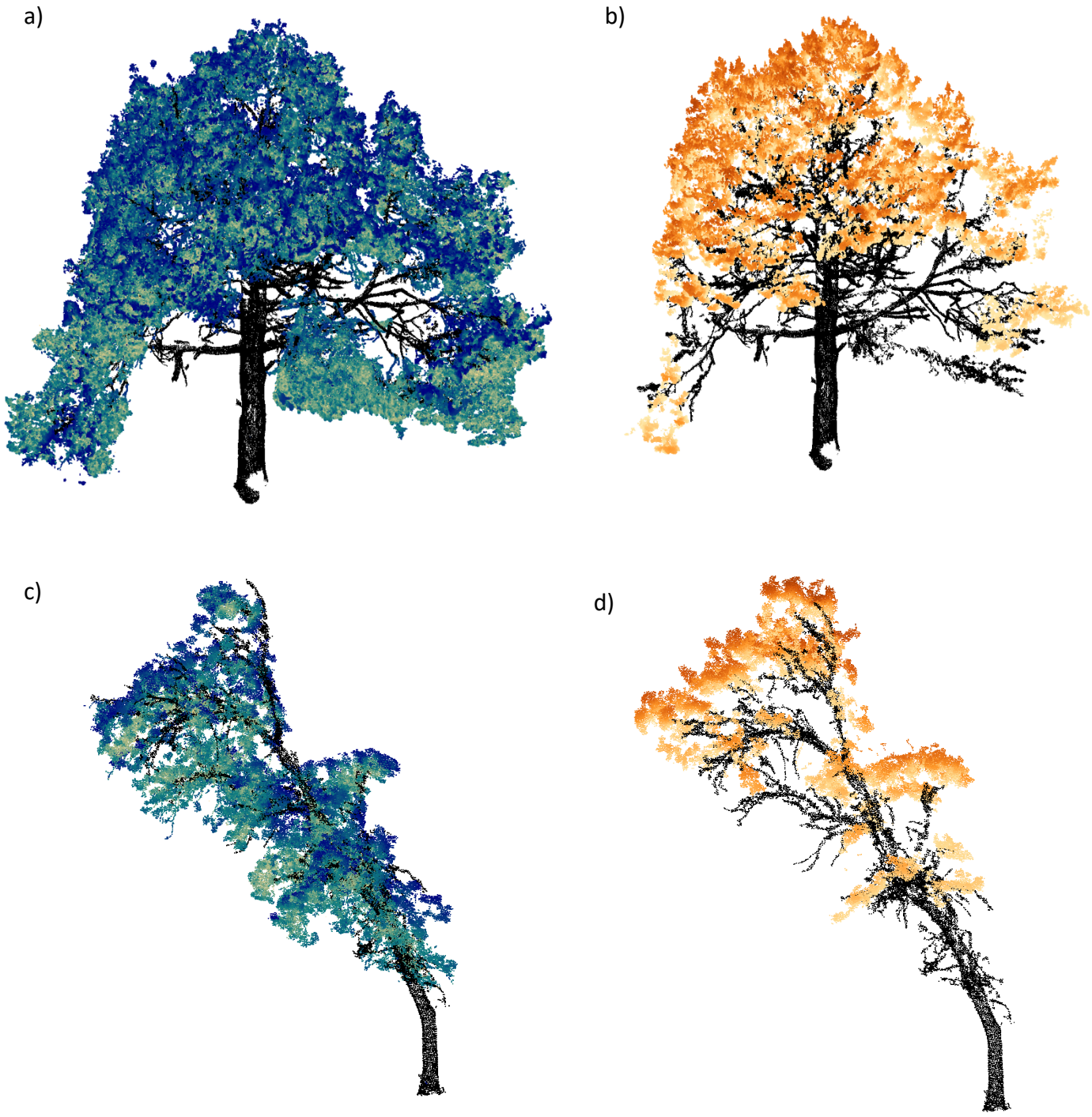

Figure 2.23 A visual demonstration of statistically significant cold spots (left) and hot spots (right) for two different trees (top and bottom) quantified using the 3D Getis-Ord code I developed. a) and b) is a *P. sylvestris* and c) and d) Q. *faginea*. Significant cold spots are shown in a) and c) for both species, where the significance cut-off was set at $P < 0.05$ and colours from yellow to blue indicate increased statistical significance. The same statistical cut-off was used to show hot spots ($P < 0.05$) in b) and d) with increasing statistical significance from yellow to red.

2.7 Conclusion

Terrestrial Laser Scanning has already made a large impact in forest monitoring, but its full potential is yet to be realised for forest ecology. Many methodological hurdles are yet to be overcome before its widely adopted as a replacement, or even enhancement, of conventional measurements. In this chapter, I have shown how, despite automated tree segmentation being an important component to TLS, its applicability to different instruments and ecosystem types needs further refinement and that although open-source tools such as treeseg are paving the way here, context-specific refinements are necessary. It is also evident TLS can be used to test the validity of ground-based approaches – for example my analyses show that ground-based measurements of volume, irrespective of the geometric primitive used, likely considerably overstate crown volume, but that crown radii calculated from an average of a range of TLS-derived samples may be an accurate method to derive crown projected area. For some metrics including crown depth and volume, an array of tools and approaches exist but a consensus on definitions is lacking. High-resolution TLS data lays bare these discrepancies, necessitating collective thinking to both retain interpretability with older measurements and also look forward to offering a wider range of TLS-based measures of crown structure.

Crown plasticity metrics such as displacement, sinuosity and space-filling are only available through TLS and provide new insights into how trees compete for space and morphological adapt to their surrounding environment. My neighbourhood metric demonstrates how accurate positioning of trees relative to one another can enhance current measure of tree competition, but new light interception approaches can take this even further by providing, for the first time, spatially explicit measure of individual tree light capture at scale and accounting for neighbours. This is an exciting time in forest ecology, and whilst many are developing metrics and tools to best extract measures of interest from point clouds, what is needed now is a strong ecological focus to refine metrics and ensure applicability across scales, instrumentation, and ecosystem type.

Chapter 3

Competitive drivers of inter-specific deviations of crown morphology from theoretical predictions measured with Terrestrial Laser Scanning

Abstract

Tree crown morphology is a key driver of forest dynamics, determining not only the competitiveness of an individual but also the competitive effect exerted on neighbouring trees. Multiple ecological theories, including Metabolic Scaling Theory (MST), predict crown morphology from first principles, but typically lack consideration of competition. The accurate quantification of crown morphology to test theoretical predictions, and the canopy interactions that could alter them, has historically been limited by the simplicity and associated error of traditional crown measurements.

In this study, we calculate high resolution two and three-dimensional crown metrics from Terrestrial Laser Scanning data for 1441 *Pinus. sylvestris*, *P. nigra*, *Quercus. faginea* and *Q. ilex* trees from a water-limited forest community in central Spain and test height-crown metric scaling relationships. We demonstrate new TLS methods to define symmetric and asymmetric neighbourhood metrics based on tree height, crown size and neighbour projected crown area, and test the importance of neighbourhood genus diversity on crown morphology by separating competition from congeneric and heterogeneric neighbours.

Competition negatively impacted all crown metrics except crown depth where only *P. nigra* showed sensitivity. Asymmetric competition was the strongest driver of pine crown morphology, but oaks were more sensitive to symmetric competition, in line with shade tolerance expectations. Congeneric competition reduced *Q. faginea* crown size and changed its shape, but we found no significant effects of heterogeneric neighbours. Most species and crown dimensions had height-crown scaling exponents below those predicted by MST, which may be due to water-limitation effects. Pines and oaks showed large differences in crown depth to height scaling, with the former shallower and the latter deeper, in contrast to theoretical predictions.

3.1 Introduction

The size and shape of tree crowns are first-order determinants of the light and microclimatic environment experienced by individuals, which drive growth, mortality and fecundity rates, and therefore whole-forest dynamics (Kobe et al., 1995; Pacala et al., 1996; Purves & Pacala, 2008). Accurate representation of tree allometry (how the dimensions of a tree change with size), is therefore an important consideration for predictive modelling frameworks (Fischer et al., 2019). Theories about the morphology of crowns, such as Metabolic Scaling Theory (MST, West et al., 2009), provide an attractive approach to generalising allometric scaling, but testing their accuracy is challenging with traditional ground measured data, which typically require assumptions of uniformity of crown morphology to estimate properties such as area and volume (Liang et al., 2016; Ritter & Nothdurft, 2018). Terrestrial lasers scanning (TLS) offers a novel method of quantifying tree morphology in high-resolution 3D detail (Disney, 2019), permitting testing of theoretical allometric relationships in detail never before possible.

Tree crown morphology is subject to multiple trade-offs, including lateral extension for light capture, maintenance of mechanical stability and hydraulic safety, and slow versus fast growth strategies (Verbeeck et al., 2019). MST, the most widely debated ecological scaling theory, does not directly consider these factors in crown allometry predictions, instead these play an ancillary role within the normalising constant. Others make simplified assumptions of crown morphology without accounting for evolutionary and environmental factors (such as sphere packing; Taubert et al., 2015). Similarly, competitive convergence points to community-wide shared architectural responses to physiological and environmental constraints (e.g. Iida et al., 2011; MacFarlane & Kane, 2017) as opposed to an ecological perspective where species, spatial and temporal niche and life-history are favoured (e.g. Sapijanskas et al., 2014). MST infers allometric scaling from evolutionary optimisation principles (Enquist, 2002) and makes predictions of crown scaling through assumptions of elastic similarity (McMahon & Kronauer, 1976) and Euclidean-uniform crown shape (West et al., 2009). MST proposes that a tree is optimised for space filling, hydraulics efficiency, and mechanical stability to reduce buckling risk. Some tests of MST using large datasets have found evidence against its generality, including its omission of competition for light (Coomes, 2006), and lack of consideration of abiotic effects including

drought and cold (Lines et al., 2012; Olson et al., 2018) and ontogeny (Poorter et al., 2015). However, others have found supporting evidence (Enquist et al., 2009) and one recent tropical TLS study found branching exponents near MST but only for trees that were not water limited and were under direct light (Martin-Ducup et al., 2020). Traditional crown measurements taken with tape-measures or rangefinders can only be used to estimate crown properties if assumptions about overall shape (e.g. that crowns are spherical, ellipsoidal or cylindrical) are made, limiting the extent to which scaling theories can be tested using such data.

The difficulty in accurately characterising tree crown morphology means that competition between trees is often quantified in similarly simplified ways, or even abstracted to the plot level using properties such as stem counts or basal area. Competition is often characterised as either asymmetric competition as competition for light and resources from larger individuals, or symmetric competition as competition from all surrounding individuals, including below ground factors (Potvin & Dutilleul, 2009; Pretzsch & Biber, 2010). Competition is known to influence tree shape, for example, asymmetric competition for light drives trees to extend vertically (Henry & Aarssen, 1999; Harja et al., 2012; Lines et al., 2012), often at the expense of crown expansion (Forrester et al., 2017). These allometric shifts have been found to align with species' shade tolerances, with less shade tolerant species responding more to shade cast by taller neighbours than to overall crowding (Coates et al., 2009, but see Bourdier et al., 2016). Neighbourhood diversity has been shown to have a positive effect on crown volume (Kunz et al., 2019), potentially driven by enhanced aboveground light capture due to structural and physiological differences (Jucker et al., 2015). For example, due to temporal differences in light capture (Jucker, Bouriaud, Avacaritei, Dănilă, et al., 2014), or differing internal crown structure and arrangement leading to some crowns casting less shade than others (Ameztegui et al., 2012; Messier et al., 1998). Lack of diversity and associated similarity in function and niche occupation can lead to simpler homogenous canopies where mechanical canopy abrasion is high (Putz et al., 1984; Pretzsch, 2014). Within water limited systems, tree-tree competition is further complicated by complex interactions belowground between species with different rooting structures and acquisitive strategies (Grossiord et al., 2015; Grossiord, 2019). Under low soil water availability more drought tolerant species become more competitive, which can lead to reduced diversity effects (Jucker et al., 2014; Grossiord et al., 2014).

With both water limitation and competition for light present, Mediterranean forests represent an exciting environment to test theoretical allometric predictions and the competing trade-offs between crown expansion for light capture and the need to minimise hydraulic risk from embolism in long branches (Smith et al., 2014; Verbeeck et al., 2019), as well as interacting asymmetric and symmetric competitive effects (Coates et al., 2009). Within these environments, shade can exert positive effects (Valladares et al., 2016), for example self-shading through adaptive crown shape and arrangement (Pearcy et al., 2005; Domingo et al., 2019) and shade cast by neighbours (Kothari et al., 2021) can reduce abiotic stresses. Horn (1971) hypothesises that crown depth is driven by both drought tolerance, increasing with aridity, and shade tolerance, with conservative species minimising self-shading by reducing crown depth. Others argue that only shade tolerant species can maintain a positive carbon balance within lower self-shaded leaves (Poorter et al., 2012), leading to conflicting hypotheses when shade and drought tolerance rankings align. The significance of water-limitation on tree allometry has been demonstrated in Iberian forests using simple ground-based measurements, with trees shorter and narrower in width under more severe drought (Lines et al., 2012). Now, new TLS methods allow us to analyse complex three-dimensional crown morphology within these ecosystems.

The ability of TLS to produce highly accurate measurements of a range of tree properties has been extensively demonstrated for tree mass (Calders et al., 2015), crown morphology (Kunz et al., 2019), leaf area (Calders et al., 2018), branching topology (Martin-Ducup et al., 2020), height (Liu et al., 2018) and stem diameter (Heinzel & Huber, 2018). In this study we present the first test of MST predictions of crown morphology scaling using Terrestrial Laser Scanning (existing studies have tested branching topology in the tropics: Lau et al., 2019; Martin-Ducup et al., 2020). We used 1422 focal trees measured in central Spain to generate new neighbourhood competition indices and compared models of drivers of variation in crown morphology using a stepwise model comparison approach. Specifically, we tested four hypotheses: (**H1**) We hypothesise that there will be strong inter-specific variation in height-crown scaling exponents and that these will fall below MST predictions, which may be due to water limitation in this system. Specifically, we expect crowns to be smaller in volume and narrower in lateral extent for a given height than predicted by MST, to reduce hydraulic

path length (Ryan & Yoder, 1997; Olson et al., 2018) and total evaporative demand (Dawson, 1996) to minimise risk of embolism. (**H2**) We test whether crown depth varies with species' tolerance to abiotic stressors according to theoretical predictions, namely; whether drought intolerant species have deeper crowns to reduce direct exposure to radiation, and whether shade tolerant species have shallow crowns reflecting their conservative resource-use strategies (as hypothesised by Horn, 1971). (**H3**) We hypothesise that observed differences in scaling exponents between species will be explained by shade tolerance, and that asymmetric competition will drive crown morphology in less shade tolerant species, and with symmetric competition important for shade tolerant species. (**H4**) We hypothesise that congeneric-dominated neighbourhoods will have a negative impact on crown size and drive changes in crown shape through reduced complementarity in light use strategies (Fridley et al., 2012; Williams et al., 2017) and increased crown abrasion (Pretszch, 2019).

3.2 Materials and methods

3.2.1 Field site and study design

We sampled 38 Mediterranean pine/oak 30 x 30 m forest plots in two areas of central Spain in July 2018 (Figure 2.2): 34 in Alto Tajo Natural Park, in Guadalajara province (40.9°N, 1.9°W), and four in Cuellar in Segovia province (41°N, 4°W). Plots in Alto Tajo (Jucker et al., 2014) form part of the wider FUNDIV project network, are situated at 960-1400 m a.s.l and dominated by two pine (*Pinus sylvestris* and *Pinus nigra*) and two oak (*Quercus faginea* and *Quercus ilex*) species. *P. sylvestris* is the most shade intolerant species, followed by *P. nigra, Q. faginea* and finally *Q. ilex*. Drought tolerance follows the same ranking (Niinemets and Valladares, 2006; Puglielli et al., 2021). In total, there were 172 *P. sylvestris,* 338 *P. nigra,* 579 (132 multi stem) *Q. faginea* and 173 (47 multi stem) *Q. ilex* focal trees. The area is characterised by rugged topography and Mediterranean climate (mean annual temperature = 10.2°; mean annual precipitation = 499 mm $year^{-1}$). Plots in Cuellar (Madrigal-González et al., 2017) are situated at 841 m a.s.l. and is dominated by *P. pinaster,* with *P. sylvestris* in riparian zones. The terrain is flat and climate Mediterranean (mean annual temperature = 11.9°; mean annual precipitation = 430 mm $year^{-1}$).

3.2.2 TLS data collection and initial processing

We scanned plots using a Leica HDS6200 scanner, using a square grid system of 16 scans spaced at 10 m, (Wilkes et al., 2017). We used a scanner resolution set to 3.1 mm and spherical targets to enable scans to be combined to create whole-plot point clouds. Scans were co-registered using Leica's propriety Cyclone software, and xyz coordinate data were exported. Using tools from the Point Cloud Library (PCL), we cut plot clouds with a 7.5m horizontal buffer to the plot boundary, filtered using height-dependent statistical filtering to minimise information loss in the upper areas of the canopy where returns were less dense, and downsampled to 5 cm to reduce computational time. Trees were automatically identified and segmented from the whole-plot cloud using the treeseg package (Burt et al., 2019), followed by manual refinement to ensure all canopy trees were identified and represented correctly (Calders et al., 2020). Individual tree point clouds were processed to separate leaf and wood material using the TLSeparation python library (Vicari et al., 2019). Stem maps recorded in the field, created using a 10 m grid within our plot, were used to determine species of each tree in each point cloud. Multi-stem trees were identified automatically as stems that bifurcated below 1.3 m, and results were visually verified and corrected where necessary.

3.2.3 Characterisation of tree crown morphology from TLS data

We computed crown metrics for each target tree using the leaf cloud, with the lowest (by vertical height) 3% of points removed to avoid errors due to inaccurate classification, returns from re-sprouts or otherwise spurious foliage. This approach avoided using the common first primary branch as a determinant of crown depth, which can lead to inter-specific biases in estimation due to pines often having multiple dead lower branches (Schoonmaker et al., 2014). We characterised crown morphology using a concave hull approach in both 2D and 3D (Figure 3.1) and used this to calculate our six crown metrics: radius, projected area, depth, surface area, volume and crown depth-to-diameter ratio (hereafter termed "relative depth"). For multi-stemmed individuals we fit hulls to all stems' crowns together and treated these individuals separately within statistical analyses. All metrics were calculated using the Point Cloud Library (PCL) and R (R core development Team). Crown volume and surface area were calculated using a 3D concave hull fit as opposed to convex (Figure 2.12), to the leaf point cloud using the alphashape3D package in R (Lafarge & Pateiro-Lopez, 2017) with

alpha (tightness of fit parameter) set to 0.3 (Figure 3.1a). Crown radius and 2D projected area were calculated using the concaveman package in R (Gombin et al., 2020) with alpha set to 2 (Figure 3.1b), which is higher to reduce computational time and deemed appropriate visually. The mean distance of all hull vertices (points on the edge of the hull) to the centroid was used to calculate crown radius. To derive crown depth, we subtracted the minimum of the leaf cloud Z axis from height. We calculated tree height using the extent of the whole tree cloud along the z-axis, and relative depth was calculated as crown width (radius multiplied by 2) divided by crown depth. Given the low stem bifurcation point, irregularity in shape and occlusion near the stem base due to shrubs, reliable DBH estimates are hard to extract for all trees in this system. We adapted the approach within treeseg (Burt et al., 2019) to extract sections of the trunk at a higher resolution (1 cm) from the original point cloud to provide more space to fit cylinders. Each section was sliced three ways and cylinders detected within each slice. This not only helped locate sections of cylindrical shape along sinuous stems but also provided an automated means to detect multi-stems. Only stems with high stability had DBH values (N=972; 77% of total single stems). Distributions of all crown metrics can be found in the appendix (Figure A3.1).

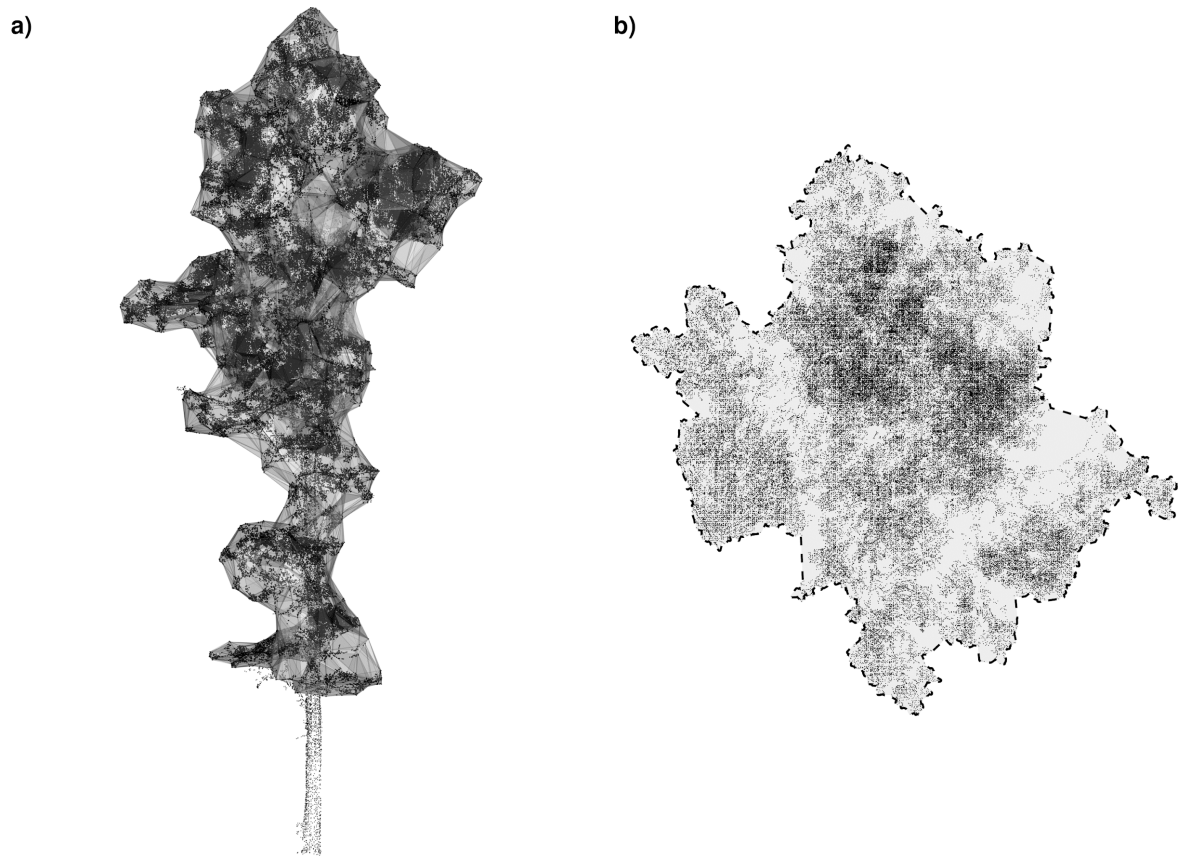

Figure 3.1 Example of TLS data processing and crown metric calculation. a) TLS point cloud of a *Q. faginea* in Alto Tajo, showing the leaf point cloud wrapped in a 3D concave hull. b) Top-down view of the same tree (leaf cloud only), showing crown projected area calculation using a 2D concave hull. 2D and 3D hulls were used to calculate metrics of crown radius (mean), diameter, projected area, depth, surface area, volume and relative depth. Whole-tree point clouds were used to calculate tree height.

3.2.4 MST predictions

MST crown predictions assume elastic similarity scaling (with exponent = 2/3) of tree height with stem diameter (McMahon & Kronauer, 1976) and isometric (i.e., linear) scaling (exponent = 1) between tree height and crown radius and depth. We tested exponents for height-crown rather than diameter at breast height (DBH)-crown scaling due to the below canopy complexity within our study system (e.g. multi stemmed trees and occlusion) which affected accurate DBH retrieval. Both height and DBH are predicted directly from mass in MST (West et al., 1999), with convention choosing DBH due to ease of measurement in the field but in the future height is most likely to become more relevant with the emerge of remote sensing technologies. Our use

of height instead does not affect our ability to test the predictions of MST crown scaling, but we do present height-diameter exponents in Figure A3.2 for a subset of the data where DBH was extractable and robust. MST predicted exponents for height-crown scaling are: 3 for crown volume, 2 for crown surface area and projected area, 1 for crown radius and depth and 0 (no relationship) for crown relative depth (the ratio of crown depth to crown width (West et al., 2009).

3.2.5 TLS-derived competitive neighbourhood metrics

We used the TLS point clouds to define measures of neighbourhood interaction based on nearby trees' crown area. We define a target tree's competitive neighbourhood as a circular neighbourhood centred on the centroid of the target tree's crown and with diameter twice the maximum crown diameter of the target tree (Figure 3.2), with a minimum neighbourhood of 5 m diameter (due to possible poor performance at smaller diameters, Fraver et al., 2014). Our neighbourhood distance criteria is towards the smaller end of the range within the literature (Lorimer, 1983; Pretzsch and Biber, 2010; Bella, 1971; Berger and Hildenbrandt, 2003; Grote et al., 2020; Fraver et al., 2014), but was chosen to avoid known steep declines of competition with distance (Thorpe et al., 2010). We define competition for a focal tree as the canopy cover within the neighbourhood from other trees (crown area index, allowing values greater than 1; Figure 3.2). Focal trees with a neighbourhood intersecting the plot perimeter were excluded but included as neighbouring trees for other focal individuals (see Table A3.1 for sample sizes). We captured competition from all trees ("symmetric competition", Figure 3.2a), from taller trees only ("asymmetric competition", Figure 3.2b), and genus-specific competition from all trees ("genus-level symmetric competition", Figure 3.2c) and from taller trees only ("genus-level asymmetric competition", Figure 3.2d). Symmetric competition was calculated as the sum of all crown projected area within the circular neighbourhood, divided by the area of the neighbourhood circle (crown area index, CAI, Figure 3.2a). Asymmetric competition was calculated using only the canopy projected area of the taller individuals (height > 90 % focal tree height) within each neighbourhood (Figure 3.2b). Similar thresholds to define asymmetric competition have been applied in other studies (e.g. Coomes et al., 2014). Genus-specific symmetric and asymmetric competition are calculated as CAI for each genus within the neighbourhood, with heterogeneric competition from trees of the opposite genus and congeneric from trees of the same genus as

the target tree (Figure 3.2c and d). Distributions of all neighbourhood metrics can be found in the Appendix (Figure A3.3).

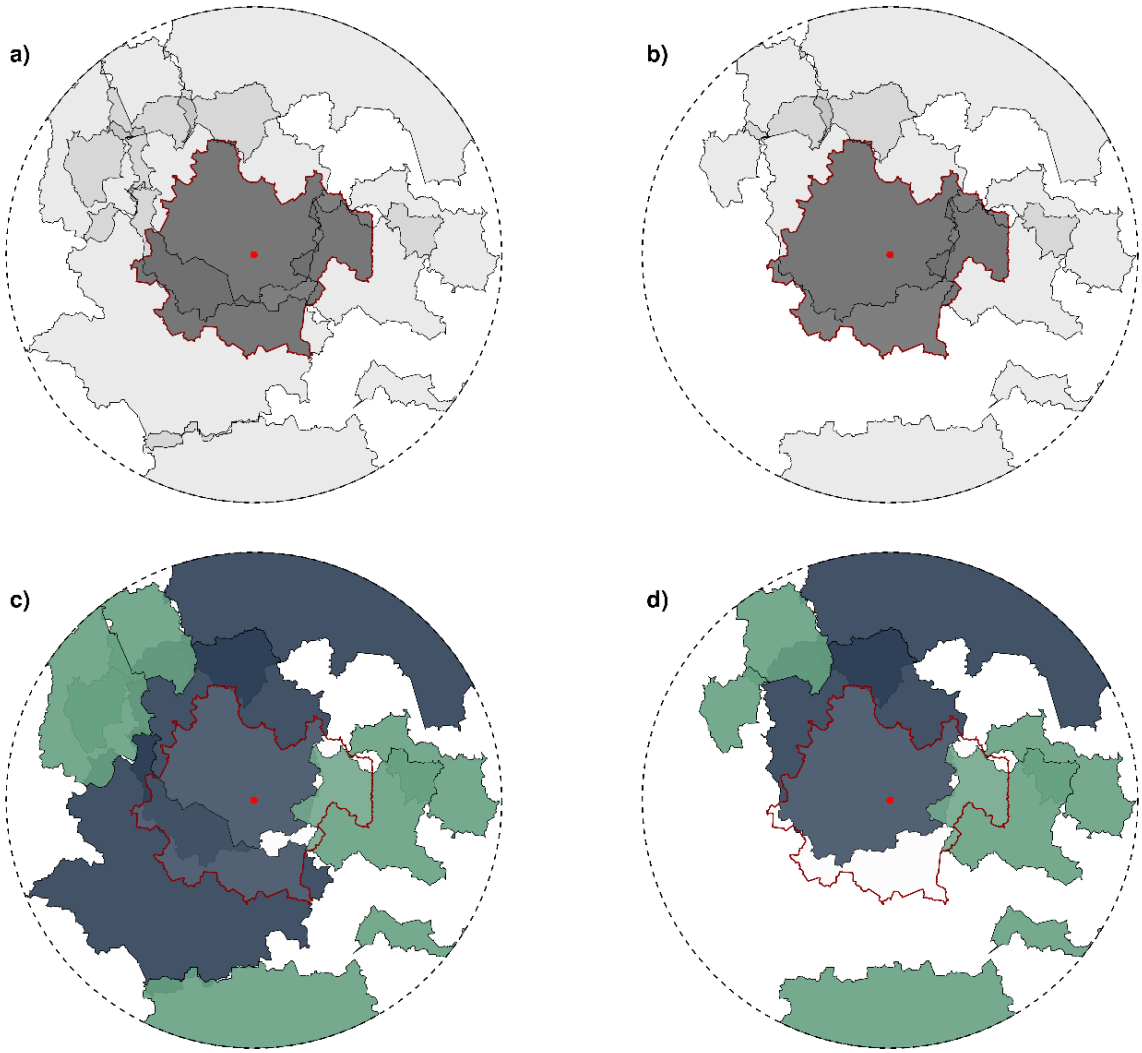

Figure 3.2 Example TLS-derived neighbourhood competition metrics. Nadir view of a *Q. faginea* tree crown from Alto Tajo, Spain, showing; a) asymmetric, b) symmetric, c) symmetric congeneric and heterogeneric and d) asymmetric congeneric and heterogeneric neighbourhood competition metrics of the tree. Dashed circles represent the neighbourhood (defined as twice focal trees' maximum crown diameter). Red dots show the focal crown centroid and neighbourhood centre, and red line the focal crown edge. a) and b), The focal crown is shown in dark grey and neighbouring trees in light grey. c) and d), The focal tree crown is shown in outline only, surrounded by pines (here, heterogeneric) in blue and oaks (here, congeneric) in green.

3.2.6 Statistical estimation of scaling exponents and competitive effects

We fit height–crown metric relationships and tested the importance of neighbourhood competition using log-transformed data using linear mixed models (LMM) within the lme4 package in R (Bates et al., 2015). We fit models separately for each species, and we separated multi-stemmed individuals (present for oak species only) and performed separate analyses on them as they are likely to show distinct scaling properties to single-stemmed individuals of the same species. Only the exponents will be presented for multi-stems. We tested models of increasing complexity (described below), comparing at each step to find the best model for each species using the Akaike Information Criterion (AIC; see Tables S2 and S3 for full AIC model comparison).

For each species (or multistem group) s, we first determined whether height-crown scaling for individual i varies between plots (j), by testing the inclusion of an intercept only random plot effect:

$$\log(CM_i) = a_s + b_s \log H_i + c_s \, Site_i \quad (3.1)$$

$$\log(CM_i) = a_s + b_s \log H_i + c_s \, Site_i + Plot_{s,j} \quad (3.2)$$

where H_i is the height of the stem, $Site_i$ a blocking factor to account for variability between sites, a_s, b_s and c_s are parameters to be fit, CM represents each of our six crown metrics and $Plot_{s,j}$ is the random plot effect, (all parameters are species/multi-stem group specific).

Next, we determined which mode of neighbourhood competition metric (NM: either symmetric or asymmetric) was most important for each crown metric, by adding each in turn to the chosen model from the previous step (either Equation 3.1 or 3.2):

$$\log(CM_i) = a_s + b_s \log H_i + c_s \, Site_i + d_s \, NM_i \quad (3.3)$$

$$\log(CM_i) = a_s + b_s \log H_i + c_s \, Site_i + d_s \, NM_i + Plot_{s,j} \quad (3.4)$$

where NM_i is either asymmetric or symmetric neighbourhood competition, without (Equation 3.3) or with (Equation 3.4) a random plot effect (a_s, b_s, c_s and d_s are parameters to be fit, $Site_i$ a blocking factor to account for variability between sites and $Plot_{s,j}$ a random plot effect). Lastly, if the best model included either symmetric or asymmetric competition, we tested further models that split the selected competition type into two genus-specific components (separate congeneric and heterogeneric competition, either asymmetric or symmetric depending on the previous step):

$$\log(CM_i) = a_s + b_s \log H_i + c_s Site_i + d_s CON_i + e_s HET_i \quad (3.5)$$

$$\log(CM_i) = a_s + b_s \log H_i + c_s Site_i + d_s CON_i + e_s HET_i + Plot_{s,j} \quad (3.6)$$

where CON_i and HET_i are congeneric and heterogeneric asymmetric or symmetric competition, a_s, b_s, c_s, d_s and e_s are species-specific parameters to be fit, $Site_i$ a blocking factor to account for variability between sites and $Plot_{s,j}$ is the random plot effect. We also tested whether the magnitude of the random effect is statistically different across two groups (mono genus and mixed genus) at the plot scale.

We also fit scaling exponent results using Standardized Major Axis (SMA) using the R package smatr (Warton et al., 2012). SMA is often used for allometric scaling when there is no clear relationship between two variables and the objective is to simply estimate the intercept and slope of the line (Smith, 2009), but is less flexible than LMMs as random effects (e.g. plot effect) cannot be included. Results were consistent across methods, with the exception of crown relative depth where although both methods showed a negative relationship, the slope for SMA was steeper than for LMM results suggesting a weak relationship and lack of robustness (Warton et al., 2006; Table 3.1, S3.4 and S3.5).

3.3 Results

3.3.1 Competitive and plot effects were evident for all species

Model comparison identified competitive effects to be important for most metrics and species (Table 3.1). Scaling within multi-stemmed trees was highly variable, with large error bars on estimates of the exponent, and for some metrics multi-stems showed substantial deviation from their single-stemmed individuals of the same species. These groups also had lower sample sizes (Table A3.1); therefore, we present results for multi-stem scaling exponents but not their competitive effects. Crown depth was the only metric to show insensitivity to competition, except *P. nigra*, with tree height the only selected predictor and crown relative depth the only metric where plot effects were not in the final model, but this was for the pines only. All other metrics selected for models including a random plot effect, that accounted for variability between plots not captured in other explanatory variables. The random plot effect variation was consistently higher for the pines than for oaks, with *P. sylvestris* showing the strongest variability across plots for all metrics (see Table 3.1). Our results also highlight how misrepresentations of tree morphology and competition can arise from traditional ground data (see Figures 2.10 and 2.13) by overlooking the complex shapes, spatial configurations and plasticity that trees adopt to fill space as well as their clustering (see Figure 2.20).

Table 3.1 Model selection results showing the strongest neighbourhood competition metric drivers of height-crown scaling variation. AIC comparison of LMM model results of single-stems only, comparing candidate models including asymmetric, symmetric, and heterogeneric/congeneric neighbourhood metrics as explanatory variables (Equations 3.1-3.6). Species are ordered according to their shade tolerance. Results where either Equations 3.1 or 3.2 were selected are not displayed in the table. Estimates for the coefficient (c and d in Equations 3.1-3.6) of the most important competitive metrics are shown for each variable and species (single-stemmed individuals). Delta AIC results for all models are available within the Appendix (Table A3.2).

Crown Metric	Term[1]	Coefficient[2]	95% CI	Random Effect (SD)
log(Crown Volume)				
P. sylvestris	Asymmetric Competition	-0.64***	(-0.44,-0.77)	0.87
P. nigra	Asymmetric Competition	-0.65***	(-0.58,-0.71)	0.36
Q. faginea	Symmetric Congeneric	-0.46***	(-0.34,-0.56)	0.33
"	Symmetric Heterogeneric	-0.19	(0.11,-0.4)	0.33
Q. ilex	Symmetric Competition	-0.67***	(-0.44,-0.8)	0.32
log(Crown Surface Area)				
P. sylvestris	Asymmetric Competition	-0.56***	(-0.39,-0.68)	0.97
P. nigra	Asymmetric Competition	-0.58***	(-0.5,-0.65)	0.35
Q. faginea	Symmetric Congeneric	-0.34***	(-0.23,-0.44)	0.27
"	Symmetric Heterogeneric	-0.13	(0.12,-0.32)	0.27
Q. ilex	Symmetric Competition	-0.42**	(-0.14,-0.6)	0.24
log(Crown Projected Area)				
P. sylvestris	Asymmetric Competition	-0.54***	(-0.37,-0.67)	0.56
P. nigra	Asymmetric Competition	-0.59***	(-0.51,-0.65)	0.31
Q. faginea	Symmetric Congeneric	-0.33***	(-0.21,-0.44)	0.33
"	Symmetric Heterogeneric	-0.08	(0.19,-0.3)	0.33
Q. ilex	Symmetric Competition	-0.43**	(-0.12,-0.63)	0.26
log(Crown Radius)				
P. sylvestris	Asymmetric Competition	-0.32***	(-0.2,-0.41)	0.24
P. nigra	Asymmetric Competition	-0.36***	(-0.3,-0.41)	0.15
Q. faginea	Symmetric Congeneric	-0.18***	(-0.1,-0.24)	0.14
"	Symmetric Heterogeneric	-0.04	(0.1,-0.16)	0.14
Q. ilex	Symmetric Competition	-0.22*	(-0.03,-0.37)	0.13
log(Crown Depth)				
P. nigra	Symmetric Competition	-0.15**	(-0.04,-0.25)	0.14
log(Crown Relative Depth)				
P. sylvestris	Asymmetric Competition	-0.36***	(-0.18,-0.49)	-
P. nigra	Asymmetric Competition	-0.15**	(-0.03,-0.25)	-
Q. faginea	Symmetric Congeneric	-0.2***	(-0.11,-0.27)	0.17
"	Symmetric Heterogeneric	-0.03	(0.13,-0.17)	0.17

[1] AIC ≤ 2

[2] *** $P \leq 0.001$, ** $P \leq 0.01$, * $P \leq 0.05$

3.3.2 Crown scaling exponents were below MST prediction for most species and metrics

We compared scaling exponents (b in Equations 3.1-3.6) for the best fit model for each species and metric (Table 3.1) with those predicted by MST. We found that height-crown scaling relationships were highly variable between species, and within a species multi-stemmed individual showed higher variation than single stemmed equivalents (Figure 3.3). Most, but not all, height-crown scaling relationships were at or lower than MST predictions, supporting our hypothesis (**H1**). Our results were also supported by SMA analyses (Table A3.3) and evidenced inter-specifically (Table A3.4). Crown volume scaling exponents for all species were significantly smaller than predicted by MST (Figure 3.3a), despite our models including both competitive and plot effects. Crown surface area exponent estimates overlapped MST predictions for *P. sylvestris* and *Q. ilex* but were lower for *P. nigra* and *Q. faginea* (Figure 3.3b). For exponents estimated from the 2D hull, most are significantly below those predicted by MST, although *Q. ilex* and *P. sylvestris* nearer of the four species (Figure 3.3c and 3d). Inter-genus differences in scaling exponents were particularly striking for crown depth and relative depth (Figure 3.3e and 3.3f), with this difference in relative depth even more pronounced using the SMA approach (see Table A3.3). *P. sylvestris* had higher exponents for all metrics than *P. nigra*, and *Q. faginea* had lower than *Q. ilex* for all but crown depth scaling. *P. nigra* and *Q. faginea* had exponents closer to one another than to species of the same genus and lower for all but depth and relative depth, while both oaks had exponents that never overlapped for all metrics. For the diameter-height scaling conducted on a subset of the data, we found pines to scale at MST and therefore, elastic similarity, and both oaks below MST.

Crown depth scaled non-linearly with height for three out of four species, in contrast to MST predictions. Oaks and pines showed distinct crown scaling with height in the opposite direction to our second hypothesis (**H2)**; both oak species had deeper crowns for a given height than MST predictions, and both pine species had shallower (Figure 3.3e). MST predicts no relationship between relative depth and tree height but here we find not only height dependence, but differences between genera, with oaks showing smaller and pines larger relative crown depths, with increasing height (Figure 3.3f).

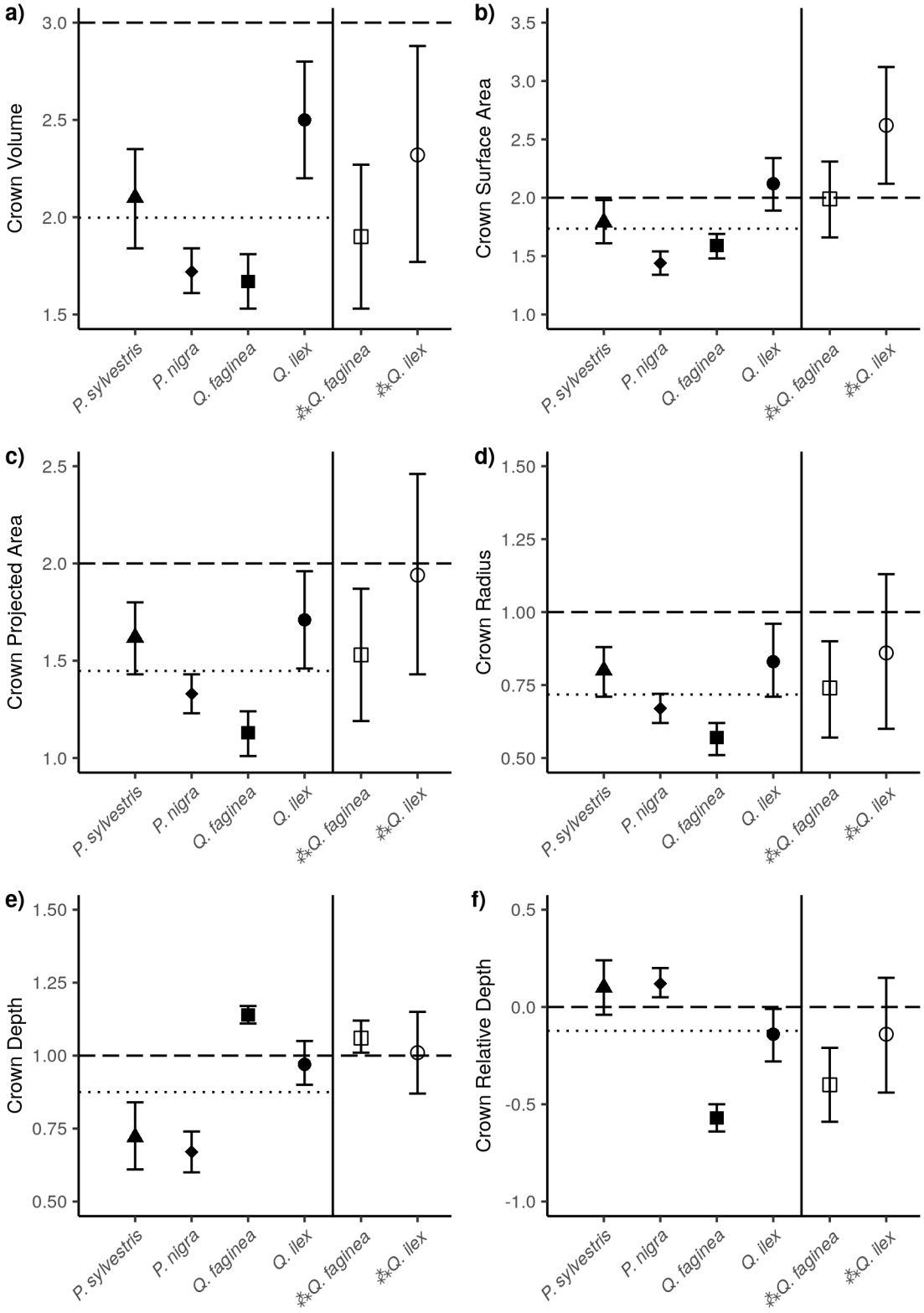

Figure 3.3 LMM-derived exponents of height-crown relationships (b in Equations 3.1-3.6) from the best model for each species, selected using AIC (Table 3.1). Error bars represent 95% confidence intervals. Exponents are shown for all species' single stem data, with multi-stem individuals' relationships were fit separately (oak species only), separated by the solid vertical black line. Species are ordered according to shade tolerance (Niinemets & Valladares, 2006; Puglielli et al., 2021), increasing left to right. MST predictions are shown by the horizontal dashed line whilst the dotted is the average of the four single-stem exponents (single-stem data only, left of solid black line).

3.3.3 Shade tolerance explained inter-specific differences in sensitivity to competition type

Using model comparison (Table 3.1) we found that, across all crown metric scaling relationships, competition negatively affected crown size and changed crown shape. The most important competitive effects were asymmetric for *P. sylvestris* and *P. nigra* and symmetric for *Q. faginea* and *Q. ilex*, in support of our hypothesis that shade tolerance determines the most important competitive effects (**H3**), since these pines are less shade tolerant than the oaks. *P. nigra* was the only species to show crown depth sensitivity to competition, with decreasing depth with increasing symmetric competition, which is notably in contrast to the sensitivity to asymmetric competition for its other metrics. Relative depth was negatively affected by competition for all species except *Q. ilex*, with crowns narrower relative to height with increasing competition and the effects asymmetric for *P. sylvestris* and *P. nigra* and symmetric for *Q. ilex*. Symmetric competition rather than asymmetric was most important in positively effecting both pines and *Q. ilex* tree height, whereas asymmetric neighbours had negative effects on *Q. faginea* height. All but *Q. faginea* selected for models rejected models that split neighbourhood metrics into genus-level. Even when selected, heterogeneric effects were negligible, with confidence intervals consistently spanning zero, whilst congeneric effects were consistently negative. Across data, most heterogeneric neighbourhood values were very low (see distributions in Figure A3.3). Post-hoc analyses on the random effect showed limited evidence of plot-level diversity effects; only two metrics (crown surface area and depth) of two species (*P. nigra* and *Q. faginea)* had statistically significant differences ($p < .05$) between mono genus and mixed genus plots.

3.4 Discussion

3.4.1 Crown metrics scaled below MST predictions

Almost all species' crown metrics were smaller for a given height than predicted by MST (Figure 3.2). These results agree with findings using simple ground-based measurements from regional forest inventory data (Lines et al., 2012; Olson et al., 2018), and provides further evidence for the role of external factors in determining complex crown morphology, and the power of TLS to reveal these. These findings were consistent whether species were considered separately or together (Table 3.1 and S3.3). In addition, the significance of plot effects of many species suggests additional abiotic drivers (e.g. exposure, aspect,

topographic wetness index) not captured by our analyses (Jucker et al., 2018; Muscarella et al., 2020). We found little evidence that our plot effect is capturing residual genus diversity affects, with statistical differences in its magnitude across mono and mixed genus plots only significant for two species (*P. nigra* and *Q. faginea*) and two metrics (crown surface area and crown depth). Nutrient richness has also likely impacts on tree allometry (e.g. Urban et al ., 2013) but this information was not available across our sites but a strong protocol was deployed to minimise these differences (Baeten et al., 2013). In this water limited ecosystem, individuals may increase crown size at a slower rate due to higher allocation to belowground than aboveground organs (Ledo et al., 2018), and due to the need for crowns to function within a safer hydraulic margin, necessitating reduced hydraulic path lengths (Poorter et al., 2012; Smith et al., 2014). Negative relationships between crown dimensions and precipitation have also been found across continents (Panzou et al., 2021).

Despite the fact that all species' volumes scaled below MST predictions, several one and two-dimensional metrics scaled at or above MST, demonstrating the value of three-dimensional data to provide a robust test of crown morphological theoretical predictions. For example, in this study, *Q. faginea* scaled above MST for crown depth but below for crown projected area, radius and volume. Pretzsch & Dieler, (2012) also found different crown metric scaling exponents to be above and below MST within the same species. All species had lower crown radius scaling exponents than MST, with water limitation one possible explanation (Lines et al., 2012; Dai et al., 2009). Narrower crowns could also be caused by higher wind exposure in taller trees (Loehle, 2016), which can be evident even when under hydraulic stress (Niez et al., 2019), but there is also evidence of larger crowns in areas of increasing wind speed (Panzou et al., 2021). Crown radius to height scaling is a core assumption for scaling from individual canopy and stand level space filling predictions in MST (West et al. 2009). However, our results highlight that lateral extension of tree crowns is reduced by both asymmetric and symmetric competition, and even when this was accounted for, exponents fell below MST. Given that trees respond to reduced water availability through reductions in height, and therefore path length (Olson et al., 2018), increased hydraulic safety may emerge through reduced lateral path length (Smith, 2014). In fact, trees under stress often shed terminal branches (Rood et al., 2000; McDowell et al., 2008), with remaining branches shorter in path length (Olson et al., 2018), lowering the risk of embolism. Within

homogenously structured stands, crown abrasion through wind sway is also likely to spatially restrict lateral expansion (Meng et al., 2006). The multi-stemmed individuals had scaling relationships with much higher variation (Figure 3.3), highlighting the need for separate allometric approaches for re-sprouting multi-stemmed trees (Matula et al., 2015).

We found high variability in crown volume scaling between species but known drought tolerances mostly fail to explain these differences. *Q. ilex* had the highest volume and projected area scaling exponents, suggesting its extensive root systems and drought tolerance may relieve hydraulic constraints on crown expansion (David et al., 2007; Forner, Valladares, & Aranda, 2018). However, the next largest exponents were *P. sylvestris*, which is at its southernmost part of its range and its physiological limits (Castro et al., 2004), as well as being the least drought tolerant species in our study, with rooting mostly confined to shallow soil layers (Irvine et al., 1998). In this dataset, many *P. sylvestris* stems are in riparian sites in Cuellar, affording greater access to water reserves (McDowell et al., 2019) and allowing crowns to expand without risking hydraulic failure (Dawson, 1996). Trees at this site were also able to extend more in height for a given DBH (see Table A3.5), suggesting greater availability of water is alleviating limits to height posed by hydraulics (Ryan and Yoder, 1997). This still fails to explain the relatively wider CIs and higher SD in plot effects for this species (Figure 3.1 and Table 3.1), and mostly higher scaling exponents compared to *P. nigra*, because site was included as a blocking factor within each model. Although *P. sylvestris* is the less drought tolerant of the two (Niinemets & Valladares, 2006; Grossiord et al., 2015), height-diameter allometry is thought to have been driven by distinct historical and climate constraints (Vizcaíno-Palomar et al., 2016) and offer a possible explanation to this divergent pattern. The differences between scaling exponents for oaks, with *Q. faginea* generally lower than *Q. ilex* (Figure 3.3), may reflect differences in these species' responses to water limitation. For example, studies have found reduced bud development (Montserrat-Martí et al., 2009) and basal-area growth (Granda et al., 2013) in *Q. faginea* compared to *Q. ilex* with increasing drought. The height-DBH exponent was identical between the two species (see Figure A3.2) with both showing a shorter stature compared to both pines, providing greater safety from embolism (Fajardo et al., 2019). Despite *Q. faginea* having deep rooting and capacity to maintain open stomata during drought (Cochard et al., 1996), it is more sensitive to edaphic

conditions (Alonso-Forn et al., 2020). In addition, *Q. ilex* remains more photosynthetically active during summer months (Montserrat-Martí et al., 2009) with greater radial root expansion (Alday et al., 2020) and more fine roots than *Q. faginea* (Coll et al., 2012).

In this study we found minimal difference between *Q. faginea* and *P. nigra* for crown volume scaling. However, for a similar volume-height scaling exponent, *P. nigra* crowns have smaller crown depth but larger radius and therefore high relative depth, whereas the opposite was true for *Q. faginea.* The shape adopted by *Q. faginea* is presumed to be the more hydraulically efficient form (Smith et al., 2014) but also associated with higher self-shading (Pearcy et al., 2005) which may limit its emergence to shade tolerant species, as evidenced by *Q. faginea*. Shade tolerance may also explain the difference in surface area scaling between both *P. nigra* and *Q. faginea*, with a larger value reflecting a higher degree of penetrating cavities, indicative of more foliage in the interior of the crown (Osawa, 1995). *Q. faginea* may have greater drought tolerance than *P. nigra* (Forner, Valladares, & Aranda, 2018) but some evidence suggests the latter is potentially more competitive in the long run (Forner, Valladares, Bonal, et al., 2018) and has deep roots enabling similar deep-water exploitation (Peñuelas & Filella, 2003).

3.4.2 Sensitivity to competition type is driven by shade tolerance

Species' shade tolerance was a key determinant of whether asymmetric or symmetric competition was more important. Both pines' crown metrics were consistently negatively affected by asymmetric competition, suggesting shading by neighbours is an important determinant of crown morphology. Others have highlighted the significance of light limitation in driving pine dynamics (Bravo-Oviedo et al., 2006; Martin-Benito et al., 2011), and our findings align with findings of smaller crown projected area (Thorpe et al., 2010; Lines et al., 2012; Dieler & Pretzsch, 2013) and crown radius (del Río et al., 2019), but contrast (Harja et al., 2012), who found minimal sensitivity in volume or lateral extent to light availability. The observed effect of asymmetric competition on crown morphology suggests a greater investment in height growth than branching with apical dominance, which is typical of shade intolerant conifer species (Poorter et al., 2012; Valladares & Niinemets, 2008; Carnicer et al., 2013), and aggravated in dense stands (Henry & Aarssen, 1999). In fact, analysis of

height-DBH allometry found symmetric rather than asymmetric competition, which was predominant for all other metrics, to drive height extension (see Table A3.5) and therefore vertically confront neighbours in attempt to overtop (Gruntman et al., 2017). The shift in allocation away from crown expansion when prioritising height not only improves mechanical stability but also reduces hydraulic embolism risk, since large crowns necessitate a large stem xylem cross-sectional area (Shinozaki et al., 1964), which is often compromised with height extension (MacFarlane & Kane, 2017). Although stability against wind may drive crown morphology (Loehle, 2016), the proximity of trees in more competitive neighbourhoods lessens tree sway (Brüchert & Gardiner, 2006), reducing buckling risk.

The consistent negative effect of symmetric competition on oak crown metrics suggests that below-ground factors may be more important in determining crown morphology for oaks than for pines, in line with expectations based on shade-tolerance (Coates et al., 2009). Although both oaks had similar height-DBH exponents, they showed distinct impacts of competition on height, with *Q. faginea* shorter with increasing asymmetric competition and *Q. ilex* showing the opposite response (see Table A3.5). Jucker et al., (2014) found pines to be shorter and oaks taller when mixed with the opposite genus at the plot scale, but we found no such effects at the neighbourhood scale. Errors in height measurements using traditional techniques may be more sensitive to stand structure and species than those from TLS (Wang et al., 2019).

Q. ilex root systems are dimorphic with the dependence on deeper roots increasing during summer (Cubera & Moreno, 2007; Moreno & Cubera, 2008; Joffre & Rambal, 1993; Barbeta et al., 2015). Morán-López et al. (2016) and Forner et al. (2020) both found positive hydraulic response in *Q. ilex* with increasing fragmentation, suggesting that crown size (volume) is mediated by the ability of its extensive root system to exploit inter-tree space for water. Defoliation during drought in this species also suggests that deep roots don't always equate to insensitivity to water limitation (Corcuera et al., 2004) with topography one possible factor that could restrict access (Fan et al., 2017). Sensitivity to symmetric competition by *Q. faginea* is likely associated with it functioning near threshold tolerance in this landscape (Forner et al., 2014) and its

dependence on a reliable water supply (Castro-Díez et al., 1997), evidenced by defoliation events during drought (Corcuera et al., 2004).

3.4.3 Neighbourhood genus diversity effects on crown morphology

For most species, models selected for total competitive effects, with separate congeneric and heterogeneric effects only important for *Q. faginea*. Neighbourhood genus diversity had consistent effects on *Q. faginea*, by reducing crown size and changing crown shape, whereas all other species selected for models containing only total competitive effects for all crown metrics. Post-hoc tests showed little evidence for genus diversity effects at a plot level; genus diversity was only important for two metrics (crown surface area and crown depth) for two species; *Q. faginea* and *P. nigra*. Our results for both pine species are in agreement with other studies which found the same species to be primarily sensitive to total competition over mixing effects (Condés et al., 2020). The consistent negative effects of congenerics on *Q. faginea* highlight that, for this species, competition is most intense among neighbourhoods containing the same genus, in agreement with findings at the species level (Kunstler et al., 2016) and suggesting resource partitioning (Tilman, 1982; Uriarte et al., 2004; Gómez-Aparicio et al., 2011). This may also suggest a positive effect of shallow-rooted heterogenerics such as *P. sylvestris* within its neighbourhood, as is observed in our study sites (Grossiord et al., 2015). *Q. ilex*, which in contrast to *Q. faginea* was sensitive to total competition, is not found with *P. sylvestris* within its neighbourhood in our study sites but is found with *P. nigra* which is able to grow deep roots and therefore compete belowground (Punuelas and Filella, 2004; Grossiord et al., 2015). When neighboured by more shallow rooted species such as *P. halepensis*, there is evidence that *Q. ilex* grows deeper roots, increasing spatial complementarity in water extraction (Sardans et al., 2004; del Castillo et al., 2016). Without these trait differences, *Q. ilex* may be confined to shallower depths, where competition for water is greatest (Craine & Dybzinski, 2013).

Although our study did not identify positive heterogeneric effects at the neighbourhood scale, post hoc analyses on the plot effect showed that for two metrics and two species, plot-level genus diversity may alter crown plasticity. In contrast to our findings, Jucker et al. (2014) found consistent positive plot diversity effects

on pine and oak crown volume. This may be due to the difference in how volume is estimated by ground methods that rely on two-dimensional measures (radius and depth) versus using our 3D point clouds. However, we found no evidence of a plot genus diversity effect on measures of crown lateral extent or volume for any of our study species. Within water-limited forest communities, interactions are dynamic and depend on many abiotic factors and can easily shift from positive to negative (Holmgren et al., 1997) making the identification of clear drivers using a single field campaign difficult.

3.4.4 Shade not drought tolerance determines crown depth

We found that shade tolerant species had deeper crowns than shade intolerant species, in agreement with Poorter et al. (2012) and Ackerly, (1999) who propose that leaves and branches are abscised once they become a net carbon drain. Shade and drought tolerance rankings are the same for our study species, meaning that we found no evidence that drought intolerant species had deeper crowns to self-shade and reduce radiation stress (as hypothesised by Pearcy et al., 2005 and Domingo et al., 2019), and indeed we found no effect of neighbourhood competition - which would increase shading and therefore reduce radiation stress - on depth for most species. The more drought sensitive pines had shallower crowns for a given height and the shade tolerant oaks deeper, with the former below and the latter at or above MST scaling predictions. *Q. ilex* was the only species to scale isometrically with tree height, as predicted by MST, whereas *Q. faginea* had crown depth–height scaling exponent greater than one. Confidence intervals for exponents were narrow, and plot-plot variability low, for all species. This suggests that height is a strong predictor of crown depth, in agreement with a global analysis (Shenkin et al., 2020). That study found an exponent of 2/3, which is close to our result for pines but much lower than that of our oaks. Both oaks' scaling exponents are higher than findings in savannah ecosystems, and pines higher than those in light-limited forests (Panzou et al., 2021). Our findings also align with a recent TLS study in the tropics where crown depth was shallower for light-demanding and deeper for shade tolerant species (Martin-Ducup et al., 2020). Higher shade tolerance in both oaks facilitates the maintenance of lower branches and therefore more leaf layers with net carbon gain (Niinemets, 2010), whereas both light-demanding pines are likely to abscise lower branches to avoid a negative carbon balance (Aiba & Nakashizuka, 2009; Poorter et al., 2012). This pattern may also emerge due to denser wood being

more resistant to damage and disease (Loehle, 1988). Shade tolerant species are likely more able to retain, or even increase in the case of *Q. faginea,* crown depth with height, resulting in crowns having many vertical leaf layers (Niinemets, 2010), which may be beneficial in moderating drought (Domingo et al. 2019) but in direct contradiction to (Horn, 1971). Crown depth was the least systematically variable crown metric across our study site (Table 3.1), being the only metric to select for models excluding plot as a random effect (Table A3.2). Competitive effects on crown depth were absent for most species (except *P. nigra*), in contrast to other studies that have found a response to local light availability (Harja et al., 2012; Poorter et al., 2012).

3.4.5 New, high-resolution crown and competition metrics from TLS

The capacity of TLS to capture the full irregularity of tree crown structure means the potential not only for better depictions of crown morphology within existing frameworks, but also to represent three-dimensional shading effects within neighbourhoods in full. This study demonstrates how we can use TLS to accurately characterise crown interactions and avoid geometric assumptions, which likely overstate competition for light (Krůček et al., 2019; Figure 2.20b). A movement towards more refined light illumination indices (e.g. Canham et al., 2004; Rüger and Condit, 2012) underpinned by highly accurate representations of crown morphology and positioning (Metz et al., 2013) and leaf/wood separated point clouds (Vicari et al., 2019), will lead to more comprehensive analyses of tree to tree interactions informed by explicitly represented shading effects. Novel analyses working with full three-dimensional tree canopy interactions will provide new insights into tree-tree interactions above and belowground.

3.5 Conclusions

This study has demonstrated that a wide range of TLS-derived crown metrics scaled below theoretical predictions and were negatively affected by aboveground competition. We found that other factors than optimisation principles were important in determining crown morphology: asymmetric competition was important for pine species and symmetric competition was for oaks. These findings agree with known shade tolerances, with pines showing higher sensitivity to shading and oaks able to tolerate sub-canopy conditions and therefore mostly sensitive to belowground competition. In contrast to other work in these forests, our

novel TLS neighbourhood analyses showed little evidence of the effect of local scale genus diversity on crown morphology, though post-hoc analyses, showed that genus diversity might be influential at the plot scale. We have demonstrated the capacity of TLS to capture two- and three-dimensional crown properties, and to characterise, high-resolution neighbourhood competition metrics not available using traditional techniques. These have allowed us to not only test a prominent ecological scaling theory's assumptions and predictions along with competitive interactions in wholly new ways, but also highlight the further potential of these three-dimensional data to understand forest ecological processes.

Chapter 4

Structural plasticity and light capture in Mediterranean Forests

Abstract

Tree plasticity is a key driver of forest dynamics, determining the competitiveness of an individual, and therefore its capacity to adapt morphologically with a forest community. Tree plasticity emerges as a response to changing environmental conditions but is limited along trade-off axes where trees need to compete for resources such as light but also minimise risk by maintaining mechanical and hydraulic safety. Tree size can also inflict biophysical limits on tree crown plasticity but its disentanglement from the effects of light availability has limited detailed examination. Altogether, the sum of all the variety in shapes, size and arrangement arising from plasticity is thought to drive positive biodiversity-productivity relationships but exact mechanisms are still poorly understood due to abstract representations of plasticity and light interception.

In this study, we calculate high resolution three-dimensional crown metrics from Terrestrial Laser Scanning data for *Pinus. sylvestris*, *P. nigra*, *Quercus. faginea* and *Q. ilex* trees from a water-limited forest community in central Spain to provide a comprehensive analysis of tree plasticity, its structural trade-offs and relationship with light capture. We demonstrate new TLS methods that for the first time, produce spatially explicit metrics of tree light capture and its uniformity and interpret results of three-dimensional crown plasticity metrics along a gradient of light availability. We also apply these novel structural and light indices to the plot scale to explore diversity crown packing relationships and overall light interception in a forest stand.

Inter-specific differences were evident between species and genera for most crown plasticity metrics with shade tolerance and leaf-habit explaining some of these differences. Pine's exhibit stronger trade-offs between crown size and plasticity, highlighting biomechanical differences and, alongside *Q. faginea* a strong response in vertical elongation to low light. Only the oaks displaced to increase light capture uniformity, but all species

increased light capture through lateral extension. Finally, we find that diversity leads to higher complexity, not higher volume filling and to an increased amount of shaded foliage.

4.1 Introduction

The capacity of an individual tree to efficiently arrange photosynthetically active foliage within its crown is a crucial determinant of not only its own light capture (Valladares & Niinemets, 2008), but also of that experienced by neighbouring trees, and therefore represents a fundamental component of forest dynamics (Pacala et al., 1996). The principal reason a tree grows a trunk is to overtop neighbouring plants when competing for light (Purves & Pacala, 2008), and even in forests where competition for water is important (such as the Mediterranean), competition for light plays an important role in determining the dynamics of a forest stand (Zavala & Bravo de la Parra, 2005; Kunstler et al., 2016). At the plot level, the sum of the size, shape and arrangement of individual tree crowns has been shown to be tightly linked to productivity (Williams et al., 2017), habitat space for biodiversity(Coops et al., 2016), and microclimate (Zellweger et al., 2019).

Plasticity refers to the ability of an organism to develop and mould its morphology to enhance fitness within its immediate environmental context, for example, tree crowns mould and spatially arrange their crowns in order to enhance light capture (Purves et al., 2007). Within forest ecology, morphological plasticity is evident across scales, from the leaf level (Williams et al., 2020), through to the whole crown (Jucker et al., 2015), and is an important influence on tree survival, given their sessile nature; according to optimal partitioning theory (Bloom et al., 1985), trees will dynamically allocate biomass to improve acquisition of the most limiting resource to growth. Structural plasticity can manifest itself in several ways to ensure sufficient acquisition of light and survival within a community (Gruntman et al., 2017; Novoplansky, 2009); with vertical elongation promoting competitive dominance, shade tolerance and leaf arrangement enabling persistence in the understorey, and lateral extension/displacement reducing competition. The relative contribution of each type of plasticity to the overall tree performance may be linked to inter-specific differences in shade tolerance (Henry & Aarssen, 2001) and apical control where the growth in the terminal shoot is prioritised over lateral growth (Brown et al., 1967).

A single tree crown is subject to an array of biotic and abiotic forces that characterise its shape over long periods of time, leading to trade-offs in growth and allocation that enhance survival under a particular set of environmental conditions (Niklas, 1994; Verbeeck et al., 2019). Tree height extension can be arrested by early crown expansion (Fransson et al., 2021), whilst lateral extension may be reduced by mechanical abrasion (Pretzsch, 2019), hydraulic limitation (Lines et al., 2012; Jacobs et al., 2021), and wood density (Loehle, 2016). Although it is clear that mechanical and hydraulic factors constrain allometry, the relative trade-offs in expressing morphological plasticity on crown vigour (for example size) are less clear. Whether shade tolerant species simply persist in the understorey (Givnish, 1988) or also express structural plasticity to seek higher light exposure (Valladares & Niinemets, 2008) is still debated, but both are thought to play important roles in crown packing theories (Jucker et al., 2015; Williams et al., 2017). The ability of trees to reposition crowns to reduce competition varies by species (Longuetaud et al., 2013) but recent work suggests structural convergence may occur across light availability and shade tolerance (MacFarlane & Kane, 2017; Martin-Ducup et al., 2020).

Tree size also enforces biophysical constraints on growth (Mencuccini et al., 2007) but its disentanglement from the effects of light is difficult, but necessary, to understanding shifting allocation through ontogeny (Metcalf et al., 2009; Dolezal et al., 2021). Fortunately, the advent of new technologies are not only enabling the quantification of foliage arrangement and density (Seidel, 2018; Martin-Ducup et al., 2018), but also of a tree's light environment in a spatially explicit manner, enabling a more comprehensive evaluation of the interplay between plasticity and light capture (Rüger et al., 2011). Novel insights into crown plasticity are also emerging within the literature (Kunz et al., 2019; Martin-Ducup et al., 2020), but their evaluation within the context of light interception are limited by the use of simple characterisations of light availability. Determining the light captured by an individual tree is a complex problem, with diurnal sun angles (Pierik & de Wit, 2014), canopy gaps (Ishii & Higashi, 1997), and the effect of even partial shading on crown growth (Schoonmaker et al., 2014) making accurate quantification difficult. The determination of intra- and inter-specific differences in crown structure along light and size gradients is an important step towards understanding how trees interact and compete for space.

The cumulative sum of plasticity expressed by individual trees in response to one another in three-dimensional space characterises overall structure and crown packing at the community scale, providing the link between individual and community structure and dynamics. Species' variation and complementarity in resource-use is thought to be a principial mechanism behind positive diversity-productivity relationships in forests (Hooper et al., 2005), increasing the space filled by tree crowns (Guillemot et al., 2020). Whilst no single measure of tree or crown plasticity exists, several metrics have been used to explore its properties. For example, both conventional ground-based measurements (Jucker et al., 2015; Williams et al., 2017), and more novel detailed branching analyses (Kunz et al., 2019; Guillemot et al., 2020) have found positive diversity effects on crown size and shape. The latter have shown greater allocation to stem and branch growth in mixed and diverse plots, especially in morphologically flexible species. However, relying on traditional ground measurements to understand fine-scale crown structure typically relies on using 2D measurements to fit 3D geometrical primitives, therefore heavily abstracting a tree's structural complexity. Novel remote sensing such as terrestrial laser scanning (TLS) offers the opportunity to directly measure complexity, but to date this technology has not been used to analyse stem and crown plasticity and their relationship with light capture.

This study makes use of highly accurate TLS measurements from Spanish forests (Owen *et al.* 2021, Chapters 2 and 3) to understand tree plasticity and light interception and analyses the relationship between plasticity and light capture at the individual tree and whole plot scale. Specifically, we address the following questions: **Q1)** Do different species exhibit different plasticity characteristics, and are these explained by shade tolerance? **Q2)** How does tree size affect crown plasticity? **Q3**) What are the relative effects of plasticity on light capture and overall crown size, and **Q4)** Are crown packing, complexity, and light capture higher in mixed plots than mono-genus plots? To address these questions, we calculated metrics of stem and crown plasticity, crown and plot filling, and crown light capture. We analyse structural plasticity using vertical elongation, stem, and crown displacement. We use network analyses to derive tree path fraction (Malhi et al., 2018), a holistic but highly representative measure of a trees shape and hydraulic proficiency (Smith et al., 2014). We use box dimension to characterise complexity and space filling both within a single tree crown and within a plot (Seidel, 2018). Finally, we demonstrate how TLS data can be used for novel characterisation of

the full light environment in a spatially explicit manner, by calculating both tree light capture and uniformity (the latter representing partial shading; (Schoonmaker et al., 2014).

4.2 Methods

4.2.1 Definitions of plasticity, space filling and light capture

In this chapter we use TLS data to calculate individual tree plasticity, space filling and light capture using a set of structural metrics that capture individual stem and crown structural variation, fill and complexity (**Stem$^{Disp^{\circ}}$**, **Crown$^{Disp^{\circ}}$**, **Stem^{Elon}**, **Crown^{PaFrac}**, **Box$^{\beta}$** and **Box$^{\alpha}$**), and whole-plot space filling (**Plot^{CrPa}**, **Plot$_{Box}^{\alpha}$**). Here we give conceptual explanations of each, with details in proceeding sections.

We quantified individual tree stem and crown *displacement angle* (**Stem$^{Disp^{\circ}}$** and **Crown$^{Disp^{\circ}}$**) as the zenith angle between the stem base and crown base and stem base to crown centroid, showing displacement of each component independent of tree size. We quantified stem elongation (**Stem^{Elon}**, calculated as tree height - **Stem^{Height}**, *m* - divided by stem diameter, **Stem^{DBH}**, cm) and used network analyses to quantify the *path fraction* for each tree crown (**Crown^{PaFrac}**), where values nearer 0 are indicative of a pole-like object and values closer to one, more umbrella shaped and more efficient at intercepting light (Malhi et al., 2019). Crown volume (**Crown^{Vol}**), tree height and DBH were calculated as described in Chapters 2 and 3. We quantified the internal filling and complexity of a tree crown and the whole plot in three-dimensional space using the two *box dimension* coefficients (Seidel, 2018; Guzmán et al., 2020). The individual tree beta coefficient (**Box$^{\beta}$**) is conventionally a measure of size (Mandelbrot, 1977) but is also indicative of the overall complexity of a tree's crown (Dorji et al., 2019), while the individual tree alpha coefficient (**Box$^{\alpha}$**) represents space-filling (Seidel et al., 2019b), and was also calculated at the plot level (**Plot$_{Box}^{\alpha}$**). Box dimension coefficients are calculated by performing a linear regression on the number of boxes of progressively smaller size (both log-transformed) required to fill the space occupied by the tree crown (or plot). The larger the crown, the more boxes will be required to cover its points (resulting in high **Box$^{\beta}$**), and the more complex and volume-filling crowns will require increasingly more boxes as the resolution of the boxes increases (steeper regression slope, high Box$^{\alpha}$). The main coefficient, **Box$^{\alpha}$**, represents filling from 1D (i.e., a line), through to 2D (a plane) and finally 3D (a volume). Finally, we quantified plot-scale crown packing (**Plot^{CrPa}**) following a standard approach used in ground-based ecology, namely the occupied volume by tree crowns divided by the available canopy space (Jucker et al., 2015).

To calculate light capture we used openly available ray tracing software (Bechtold & Höfle, 2020) and developed new indices to calculate two metrics of individual light capture. The role of these indices is to establish a trees' relative exposure to light as a whole, its uniformity along its vertical column, and to determine the extent at which individuals maintain shaded foliage. As a measure of overall *exposure*, light fraction (**Crown^{LiFrac}**) was calculated as the average light capture of a crown's foliage divided by the maximum available (the 99th percentile of irradiance across entire plot), and crown light uniformity (**Crown^{LiUni}**) as the proportion of the crown that receives direct light. Evidence suggests that trees potentially respond differently to partial than full shading (Schoonmaker et al., 2014) so the use of **Crown^{LiUni}** complements **Crown^{LiFrac}**, as they represent different components of light interception. We also calculated **Plot^{LiFrac}** using the same method as for an individual tree (**Crown^{LiFrac}**) but instead applied to the whole plot point cloud. Finally, as in Chapter 3, we used shade tolerance rankings from Valladares & Niinemets, (2008) with the exception of *Q. faginea* which we ranked between *P. nigra* and *Q. ilex* (Jucker et al., 2014).

4.2.2 Field site and study design

This chapter uses the same TLS dataset as the previous chapters. 38 Mediterranean pine/oak 30 x 30 m forest plots were sampled across two areas of central Spain in July 2018 (Figure 2.2): 34 in Alto Tajo Natural Park, in Guadalajara province (40.9°N, 1.9°W), and four in Cuellar in Segovia province (41°N, 4°W). Plots in Alto Tajo (Baeten et al., 2013) form part of the wider FUNDIV project network, are situated at 960-1400 m a.s.l and dominated by two pine (*Pinus sylvestris* and *Pinus nigra*) and two oak (*Quercus faginea* and *Quercus ilex*) species. *P. sylvestris* is the most shade intolerant species, followed by *P. nigra, Q. faginea,* and *Q. ilex*. In total, there were 172 *P. sylvestris,* 338 *P. nigra,* 579 (including 132 multi stem) *Q. faginea* and 173 including (47 multi-stem) *Q. ilex*. The area is characterised by rugged topography and Mediterranean climate (mean annual temperature = 10.2°C; mean annual precipitation = 499 mm year^{-1}). Plots in Cuellar (Madrigal-González et al., 2017) are situated at 841 m a.s.l., and are dominated by *P. pinaster,* with *P. sylvestris* in riparian zones. The terrain is flat and climate Mediterranean (mean annual temperature = 11.9°C; mean annual precipitation = 430 mm year^{-1}).

4.2.3 TLS data collection and initial processing

We scanned plots using a Leica HDS6200 scanner, using a square grid system of 16 scans spaced at 10 m, (Wilkes et al., 2017). We used a scanner resolution set to 3.1 mm and spherical targets to enable scans to be combined to create whole plot point clouds. Scans were co-registered using Leica's propriety Cyclone software, and xyz coordinate data were exported. Using tools from the Point Cloud Library (PCL), we cut plot clouds with a 7.5m horizontal buffer to the plot boundary, filtered using height-dependent statistical filtering to minimise information loss in the upper areas of the canopy where returns were less dense, and downsampled to 2.5 cm. Trees were automatically identified and segmented from the whole-plot cloud using the treeseg package (Burt et al., 2019), followed by manual refinement to ensure all canopy trees were identified and represented correctly (Calders et al., 2016). Individual tree point clouds were processed to separate leaf and wood material using the TLSeparation python library (Vicari et al., 2019). Stem maps recorded in the field, created using a 10 m grid within our plot, were used to determine species of each tree in each point cloud. Multi-stem trees were identified automatically as stems that bifurcated below 1.3 m, and results were visually verified and corrected where necessary (see Chapter 2 for more details).

4.2.4 Calculation of individual tree plasticity

We computed metrics of $Stem^{Elon}$, $Stem^{Disp^{\circ}}$, $Crown^{Disp^{\circ}}$ and $Crown^{PaFrac}$ for each target tree based on the separated leaf and wood clouds. As in chapter 3, to calculate the necessary crown metrics we first removed the lowest (by vertical height) 3% of points of the leaf cloud, to avoid errors due to inaccurate classification, returns from re-sprouts or otherwise spurious foliage – in particular this avoids inter-specific biases in estimating crown metrics due to pines often having multiple dead lower branches (Schoonmaker et al., 2014). The crown base location was extracted using both leaf and wood clouds; the bottom of the leaf cloud was calculated as the minimum value on the z-axis, which was then used to extract three 0.25 m slices from the wood cloud. Each slice underwent stability analysis where the standard deviation along both x and y axes was determined – this was to minimise the effect of branching in determining the stem centroid. The stem top/crown base was then calculated as the mean of all coordinates within the slice exhibiting the lowest variability. Stem displacement ($Stem^{Disp^{\circ}}$) was calculated as the angle between the stem base (centroid of the lowest 10 cm of the stem) and the crown base. Crown displacement ($Crown^{Disp^{\circ}}$) was calculated as the angle

between the crown base and the mean of all leaf points weighted by path length to ensure the true directionality. Stem elongation ($Stem^{Elon}$) was calculated as $Stem^{Height}/Stem^{DBH}$. The path fraction ($Crown^{PaFrac}$), defined as the mean of all path lengths to each leaf point divided by the maximum path length, was determined for each tree by skeletonising the tree's entire point cloud into a network using graph theory, with each leaf point assigned the shortest distance following the tree's branching network to the stem base. This was done using open-source python software within the "pc2graph" library (available at https://github.com/mattbv/pc2graph), see Figure 4.1a).

To calculate both box dimension coefficients (Box^{β} and Box^{α}), we first removed the main tree stem by filtering all points below the crown base coordinate to remove the effect of the one-dimensional tree bole in the calculation. We then voxelated each tree crown – i.e., covered the three-dimensional point cloud with cubic volumetric pixels (voxels) – across a range of different voxel resolutions. For each tree we set the largest voxel as the smallest single voxel that covered the whole tree crown and iterated down in 25 steps to the smallest voxel size (the resolution of the cloud; here 0.025 m), counting the number of boxes required to cover all wood and leaf crown points at each step. A standardised major axis regression line (Warton et al., 2006) was fit between the log of the inverse of the voxel size ($\ln(1/r)$) and the log of the number of voxels needed ($\ln(N_r)$) for each tree individually. The box alpha dimension (Box^{α}) was calculated as the slope of the SMA regression line, and the box beta as the intercept (Box^{β}). Voxelisation was implemented using the 'rTLS' package (Guzmán et al., 2020) and SMA using the 'smatr' package (Warton et al., 2012), both in R. Examples of all individual plasticity metrics for six contrasting trees may be seen in Figure 4.2.

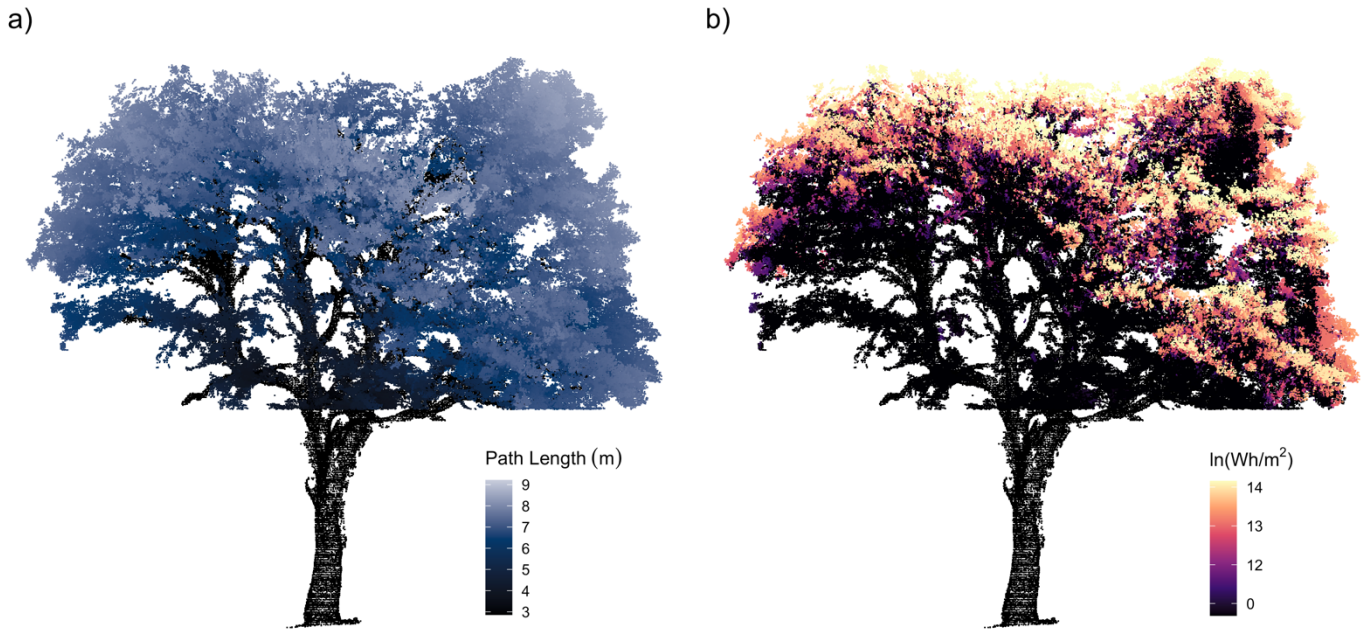

Figure 4.1 An open growth *Q. ilex* tree in Alto Tajo National Park, Spain. a) Leaf points are coloured by path length (dark blue to light blue). b) Leaf points are coloured by irradiance (black to yellow) which has been log transformed for visual purposes. The units are Watt hours per m^2 summed over the entire simulation (see section 2.4 for further details). Black points in both figures are the wood cloud.

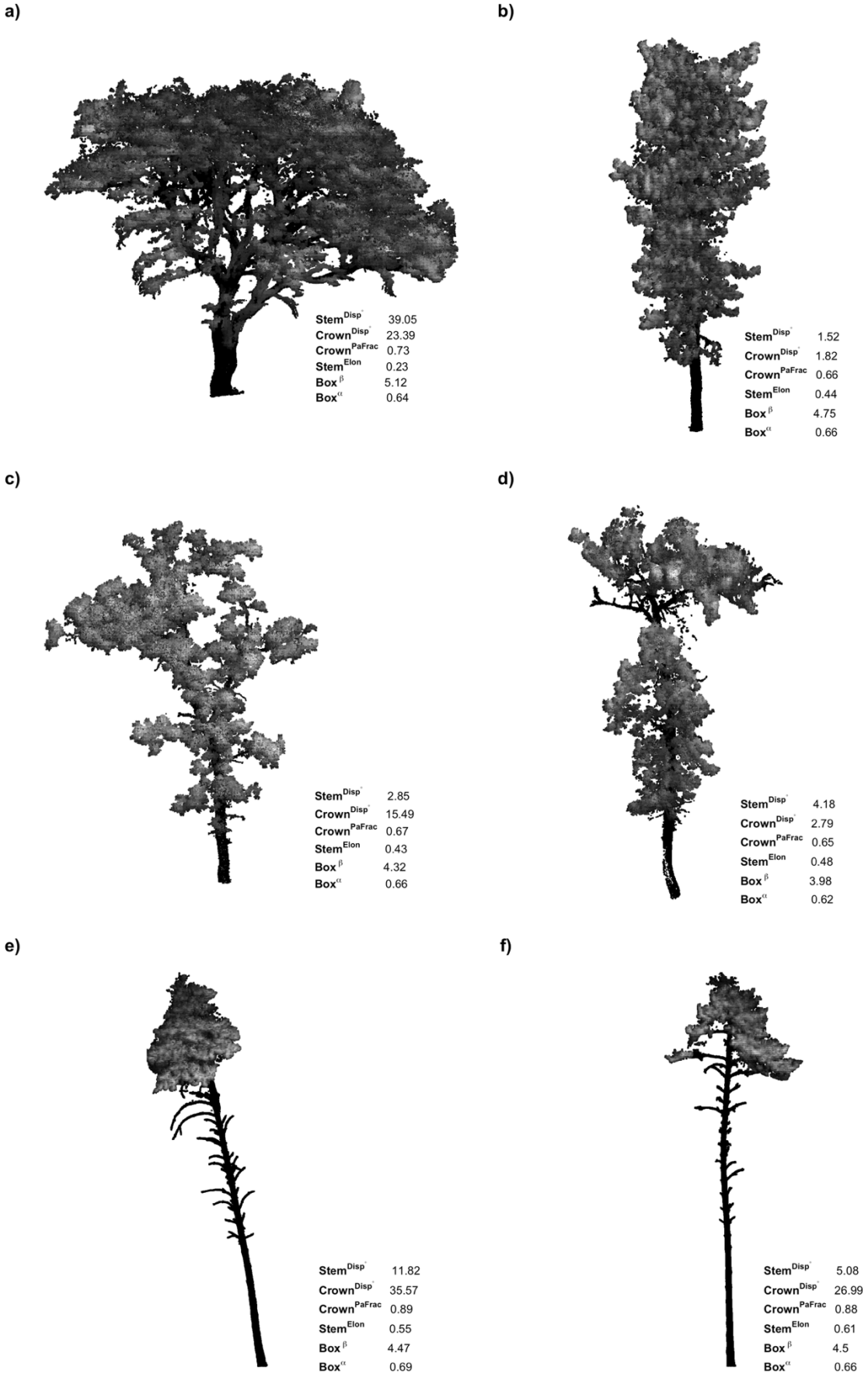

Figure 4.2 Examples of contrasting individual tree structural plasticity metrics for a selection of contrasting trees located in Alto Tajo, Spain where a) *Q faginea* b) *P. sylvestris* c) *Q. faginea* d) *Q. faginea* e) *P. sylvestris* f) *P. sylvestris*/

4.2.5 Calculation of light interception

We characterised the irradiance received for each tree crown using the openly available C++ library ray tracing algorithm 'vostok' (Bechtold & Höfle, 2020). This algorithm simulates the diurnal movement of the sun across the sky, firing rays into a three-dimensional point cloud which are either intercepted by a point, miss all points or are shaded by a neighbouring point. As input, we combined 0.025 m-resolution point clouds for all trees within a plot into one plot cloud, retaining individual tree ID information for each point. The whole-plot cloud was used to create the shading cloud, which is a voxelised cloud at the same resolution acting as the shading component for the algorithm (no transmittance is simulated). In order to establish whether a given point will intercept an incoming ray at any given angle or not, surface normals are needed. This was calculated for each point using an estimate of expected number of neighbours within a given volume (here 0.25 m), which is the cube of the point spacing (see Chapter 2 section 2.6.5 for a wider discussion). We applied the vostok algorithm to calculate irradiance for the summer of 2018 (April to October) at 30-minute increments within a single day and at monthly increments (i.e., one day for each month), to account for diurnal and monthly variability in sun angles, choosing a spatial resolution (0.025 m) that was computationally viable. Parameters used to derive sun angle were automatically extracted from a database (http://rredc.nrel.gov/solar/codesandalgorithms/solpos/). The output for each point of each tree was the summed irradiance intercepted (watt hours per m^2). A visual depiction of the summed irradiance for an individual tree in Figure 4.1.b), and an example of an entire plot can be seen in Figure 4.3.

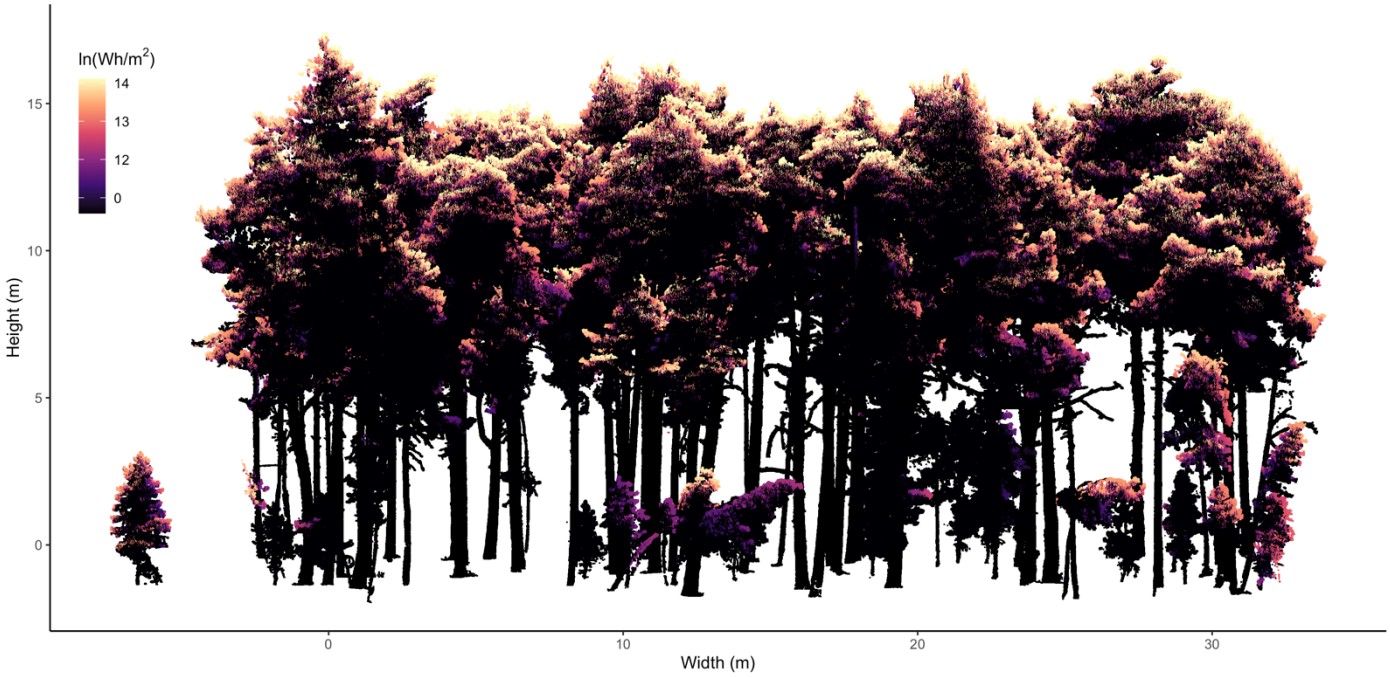

Figure 4.3 Example output from the Vostok ray tracing algorithm of an example plot containing *Pinus sylvestris* in Alto Tajo National Park, Spain. Points are coloured according to irradiance (black to yellow) on a log scale with 0 meaning completely shaded. Black points are the wood cloud.

4.2.6 Individual tree light capture

To compare light capture between trees we calculated two metrics for each tree, characterising mean light capture relative to the maximum possible light capture within the plot, $Crown^{LiFrac}$, and light capture homogeneity across a trees vertical crown axis, $Crown^{LiUni}$. We calculated $Crown^{LiFrac}$ as the mean of all the leaf points' summed irradiance divided by the plot maximum summed irradiance, representing the average light capture of a crown relative to that available (comparable to path fraction). $Crown^{LiUni}$ was calculated by slicing the crown horizontally from top to bottom and calculating the ratio of slices that intercepted direct light to the total number of slices. Ten slices were extracted in total with a minimum size of 0.25 m, along the z axis. If a tree contained fewer than 10 slices of 0.25 m, than the number of slices was adjusted by splitting the tree crown into 0.25 m slices. Slices were classified as intercepting direct light if the 75th percentile was different to 0, i.e., no direct sun light received.

4.2.7 Quantifying canopy packing and complexity at the plot scale

In order to quantify space filling within each plot, we calculated crown packing ($Plot^{CrPa}$) as the amount of space filled by the concave hulls of all trees' crowns (wood and leaf above the crown base; section 2.3) divided by the total available volume for each plot (where the vertical extent was calculated by subtracting the maximum $Stem^{Height}$ from the lowest branch height), following the ground-based approach in Jucker et al., (2015). Using the same approach as for individual trees, we calculated plot complexity with the box dimension approach, to determine $Plot_{Box}^{\alpha}$. To do this, all tree crowns (leaf and wood above the crown base; section 2.3) were combined into one point cloud, with the XY coordinates clipped to the plot boundary and the box dimension calculated as before but with the smallest possible box size set to 0.25 m (of the order a cluster of leaves). To examine the role of different stand structures across the plot network we calculated crown area index ($Plot^{CAI}$, the ratio of total crown projected area to plot area), again, clipped to the plot boundary.

4.2.8 Quantifying plot-scale light capture

To compare light capture between mixed and mono-genus forest communities we calculated one metric for each plot that characterises the mean light capture relative to the maximum possible light available. Here, plot light fraction ($Plot^{LiFrac}$) was calculated using the same method as for an individual tree (see section 2.5) but instead applied to the whole plot point cloud (clipped to within 5 metres of the plot boundary to remove any edge effects arising from missing trees on the plot edge that would otherwise be casting shade).

4.2.9 Statistical analyses

To explore inter-specific differences in plasticity characteristics (**Q1**), we compared mean individual tree plasticity metrics for the four species using non-parametric Wilcoxon tests in the statistical software R. To determine the effect of tree size (height see chapter 3) on crown plasticity (**Q2**), we fit mixed effects models using the lme4 package in R, for each species *s*:

$$TP_i = a_s + b_s\, Stem^{Height}{}_i + Site_i + Plot_{s,j} \quad (4.1)$$

where TP is each of our six tree plasticity metrics, $Stem^{Height}_i$ is the height of the stem, $Site_i$ a blocking factor to account for variability between sites (see Chapter 3), $Plot_{s,j}$ is the random plot effect, and a_s and b_s are parameters to be fit (all parameters are for single-stem trees only). We quantified relationships between crown metrics (CM_i) $Crown^{Vol}$, $Crown^{LiFrac}$ and $Crown^{LiUni}$ and four tree plasticity metrics (**Q3**):

$$CM_i = a_s + b_s\, Stem^{Height}_i + c_s\, Stem^{Elon} + d_s\, Crown^{PaFrac} + e_s\, Stem^{Disp^\circ} + f_s\, Crown^{Disp^\circ} + Site_i + Plot_{s,j} \qquad (4.2)$$

Where $Stem^{Height}$ a covariate controlling for tree size, $Stem^{Elon}$, $Crown^{PaFrac}$, $Stem^{Disp^\circ}$ and $Crown^{Disp^\circ}$ predictor variables, $Site_i$ a blocking factor to account for variability between sites, $Plot_{s,j}$ is the random plot effect, a_s, b_s, c_s, d_s, e_s and f_s are parameters to be fit. To assess the role of diversity in determining plot scale crown packing and structural complexity (**Q4**), ANCOVA tests were performed using a binary genus plot diversity factor (monoculture/diverse plot, following classifications within Baeten et al., 2013) and $Plot^{CAI}$ as a continuous covariate that accounts for different stand structure between plots. ANCOVA tests were also used to determine differences in light environment between mono-genus and mixed-genus plots to determine whether mixed plots intercept more light or maintain greater proportions of shaded foliage.

4.3 Results

4.3.1 Inter-specific differences in stem and crown plasticity

There were statistically significant differences in all crown plasticity metrics between different species and genera (Figure 4.4). Species' mean $Crown^{PaFrac}$ and $Stem^{Elon}$ ranked with shade tolerance (Figure 4.4a and 4.4b), with progressively decreasing values from *P. sylvestris* to *Q. ilex*. Pines had statistically significantly higher path fractions than the oaks ($P < 0.01$), and *P. sylvestris* statistically higher than *P. nigra* and *Q. ilex* higher than *Q. faginea* (Figure 4.4a), suggesting pines extend horizontally but shorten their crowns vertically to intercept more light. Similarly, pines had significantly more elongated stems than oaks ($P < 0.01$), and *Q. faginea* was more elongated than *Q. ilex* (Figure 4.4b). All species were statistically significantly different for both angular displacement metrics ($Stem^{Disp^\circ}$ and $Crown^{Disp^\circ}$), with *Q. ilex* showing the highest displacement

(Figure 4.4c and 4.4d). Box^{β} statisically significantly different for all species (Figure 4.4e), whereas Box^{α} was significantly different between pines and oaks, and between both oaks, but not both pines (Figure 4.4f).

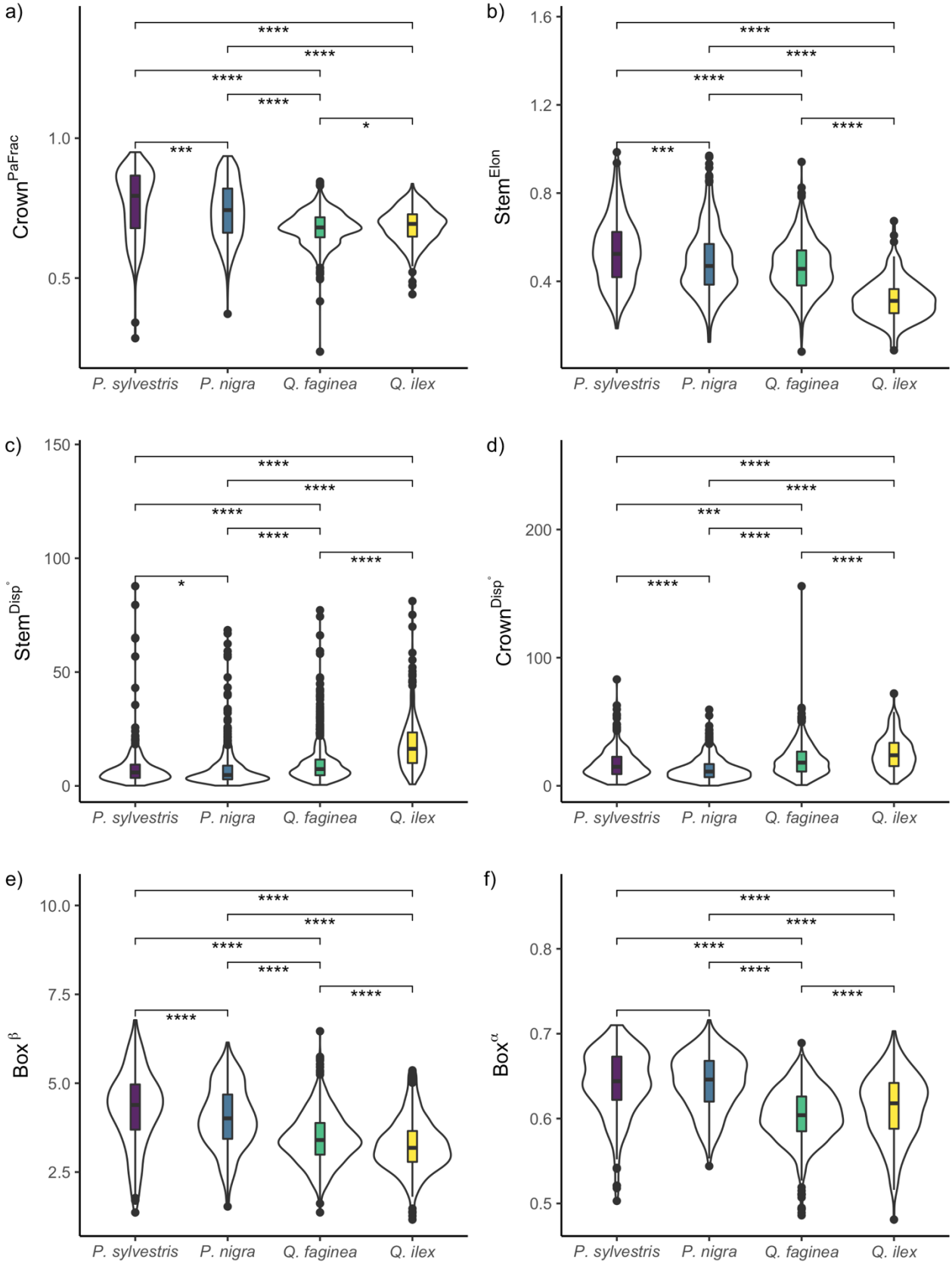

Figure 4.4 Violin plots of all crown plasticity metrics where Crown^{PaFrac} is the average path fraction of the crown, Stem^{Elon} is the stem elongation - an indicator of prioritised height extension, Stem$^{Disp°}$ and Crown$^{Disp°}$ are the angles of stem and crown displacement respectively in degrees, Box$^{\square}$ is a box dimension measure of crown size and Box$^{\square}$ of complexity and space-filling (see details in section 2.4). Species are ordered according to their shade tolerance, with the least shade tolerant on the left (Valladares and Niinemets, 2007). See section 2.1 for details. (* = 0.05, ** = 0.01, *** = 0.001, **** = 0.0001)

4.3.2 Significant effects of height on crown plasticity

We tested whether tree size affected plasticity using linear mixed-effects models, controlling for plot and site. We found that taller pine trees had higher $Crown^{PaFrac}$, but this was not the case for oaks (Figure 4.5a.). Taller oak trees had lower $Crown^{Disp^{\circ}}$, but higher values for *P. nigra,* and there was no relationship for *P. sylvestris* (Figure 4.5b), whereas all species had declining $Stem^{Disp^{\circ}}$ with height. Taller trees had higher values of both box dimensions (Box^{β} and Box^{α}) for all species, with *Q. ilex* having the steepest slopes for both metrics, and differences in slope between the oaks greater than between the pines (Figure 4.5e and 4.5f).

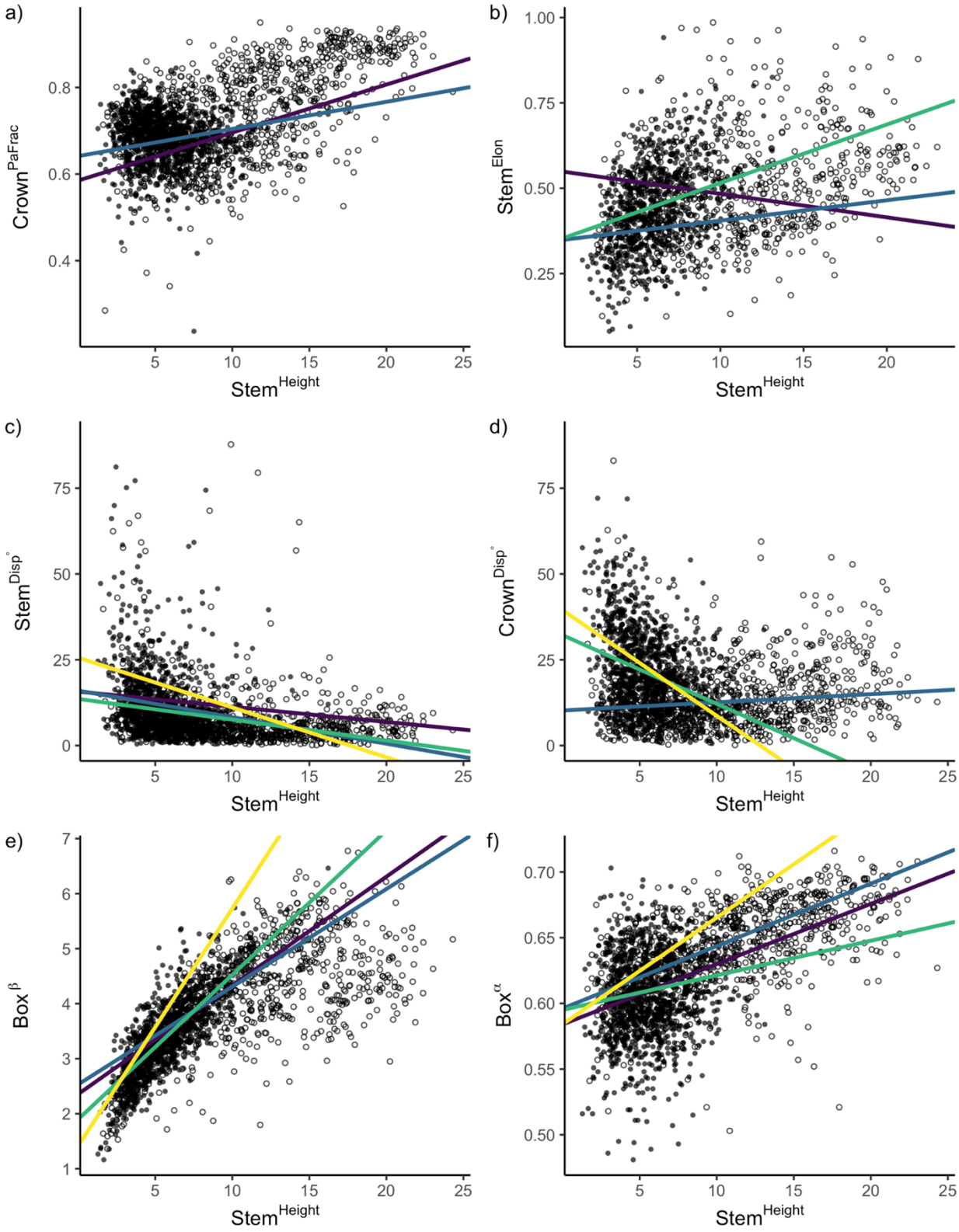

Figure 4.5 Scatter plot of height vs. crown plasticity for all trees (equation 1). $Crown^{PaFrac}$ is the average path fraction of the crown, $Stem^{Elon}$ is the stem elongation - an indicator of prioritised height extension, $Stem^{Disp°}$ and $Crown^{Disp°}$ are the angles of stem and crown displacement respectively, Box^{β} is a box dimension measure of crown size and Box^{α} a of complexity and space-filling (see details in section 2.4). Oak data points are closed circles and pines open circles. Statistically significant model fits are show by coloured lines: *P. sylvestris* is in purple, *P. nigra* in blue, *Q. faginea* green, and Q. *ilex* is in yellow.

4.3.3 Contrasting effects of plasticity on crown size and light capture

We tested the effect of tree plasticity on crown size ($Crown^{Vol}$) and both light capture indices ($Crown^{LiFrac}$ and $Crown^{LiUni}$), whilst accounting for size effects in the model by including $Stem^{Height}$ as an independent variable – see equation 4.2 (Table 1). Increased $Stem^{Elon}$ significantly reduced in crown size in all but *Q. ilex*, which showed low overall $Stem^{Elon}$ (Figure 4.4), with the largest negative effect for the most elongated species, *P. sylvestris*. Higher path fraction values were negatively associated with crown size in both pines, whereas the effect was significantly positive for *Q. faginea,* and non-significant for *Q. ilex*, suggesting oaks retain or increase $Crown^{Vol}$ as they extend, whereas pines may either lose $Crown^{Vol}$ or small pine $Crown^{Vol}$ values may necessitate higher $Crown^{PaFrac}$. The oaks showed positive significant relationships between $Crown^{Vol}$ and $Stem^{Disp°}$, with a stronger effect for *Q. ilex* than *Q. faginea*. There were no significant relationships between $Crown^{Disp°}$and $Crown^{Vol}$.

The oaks showed statistically significant positive relationships between displacement and $Crown^{LiUni}$, but $Crown^{LiFrac}$ had no such relationships, and all were non-significant for pines. We found that $Stem^{Disp°}$ increased $Crown^{LiUni}$ for *Q. faginea*, whereas $Crown^{Disp°}$ increased $Crown^{LiUni}$ for *Q. ilex*. $Crown^{PaFrac}$ was the only plasticity metric to be positively related to $Crown^{LiFrac}$ for all species, and its effect on $Crown^{LiUni}$ was significantly positive for all but *P. sylvestris*, suggesting that increasing $Crown^{PaFrac}$ is an effective means to increase both overall light capture and its vertical uniformity. $Stem^{Elon}$ had significantly negative effects on $Crown^{LiFrac}$ for both *P. nigra* and *Q. ilex,* and on and $Crown^{LiUni}$ for both *P. nigra* and *Q. faginea*.

Table 4.1 Table showing coefficients from Equation (2) with $Crown^{Vol}$, $Crown^{LiFrac}$ and $Crown^{LiUni}$ as response variables for each species and the four tree plasticity metrics ($Stem^{Elon}$, $Crown^{PaFrac}$, $Stem^{Disp°}$ and $Crown^{Disp°}$) as predictor variables. $Crown^{Vol}$ is the crown volume, and $Crown^{LiFrac}$ and $Crown^{LiUni}$ represent crown light capture fraction and uniformity. Four plasticity metrics were chosen as explanatory variables; $Crown^{PaFrac}$ as a measure of crown shape, $Stem^{Elon}$ an indicator of height extension, and $Stem^{Disp°}$ and $Crown^{Disp°}$ are stem and crown displacement angle, respectively. Statistically significant coefficients are highlighted in bold and with asterix symbols.

Species	**$Stem^{Elon}$**	**$Crown^{PaFrac}$**	**$Stem^{Disp°}$**	**$Crown^{Disp°}$**
Crown Volume				
P. sylvestris	**-0.45*** [-0.55,-0.35]**	**-0.4*** [-0.55,-0.25]**	0.01 [-0.09,0.1]	0.08 [-0.02,0.18]
P. nigra	**-0.3*** [-0.35,-0.25]**	**-0.27*** [-0.34,-0.21]**	0.02 [-0.03,0.06]	-0.03 [-0.07,0.01]
Q. faginea	**-0.22*** [-0.26,-0.18]**	**0.06** [0.02,0.1]**	**0.05* [0.01,0.09]**	0.03 [-0.01,0.08]
Q. ilex	-0.08 [-0.18,0.02]	0 [-0.1,0.09]	**0.16** [0.06,0.25]**	0.09 [-0.01,0.19]
Light Fraction				
P. sylvestris	-0.14 [-0.29,0.02]	**0.36** [0.12,0.6]**	-0.02 [-0.16,0.11]	-0.02 [-0.15,0.12]
P. nigra	**-0.36*** [-0.47,-0.25]**	**0.37*** [0.23,0.51]**	0 [-0.1,0.09]	0.02 [-0.07,0.11]
Q. faginea	-0.06 [-0.14,0.02]	**0.2*** [0.13,0.27]**	0.06 [-0.01,0.13]	0.02 [-0.06,0.1]
Q. ilex	**-0.19* [-0.34,-0.04]**	**0.26*** [0.12,0.41]**	-0.02 [-0.17,0.12]	0.07 [-0.08,0.22]
Light Uniformity				
P. sylvestris	-0.13 [-0.27,0.02]	0.12 [-0.12,0.35]	-0.04 [-0.17,0.09]	0.12 [-0.01,0.25]
P. nigra	**-0.39*** [-0.5,-0.29]**	**0.18** [0.05,0.31]**	0.06 [-0.03,0.15]	0.08 [0,0.17]
Q. faginea	**-0.14*** [-0.22,-0.07]**	**0.07* [0,0.14]**	**0.08* [0.01,0.15]**	0.05 [-0.03,0.12]
Q. ilex	-0.13 [-0.29,0.02]	**0.16* [0.01,0.32]**	0.07 [-0.09,0.22]	**0.26** [0.1,0.42]**

*** $P \leq 0.001$, ** $P \leq 0.01$, * $P \leq 0.05$

4.3.4 Higher crown complexity but not packing in mixed plots

Contrary to previous work at this site, we found that plot crown packing ($Plot^{CrPa}$) was not statistically significantly different between mixed and monoculture plots (Figure 4.7a), Plot complexity ($Plot_{Box}^{\alpha}$) was significantly higher in mixed-genus than mono-genus plots ($P < 0.05$) suggesting that mixed plots have higher complexity but no more efficient in packing canopy space than mon-genus (Figure 4.7b). $Plot^{LiFrac}$ was higher in monoculture than mixed plots, suggesting a greater presence of shaded foliage in mixed-genus plots (Figure 4.7c).

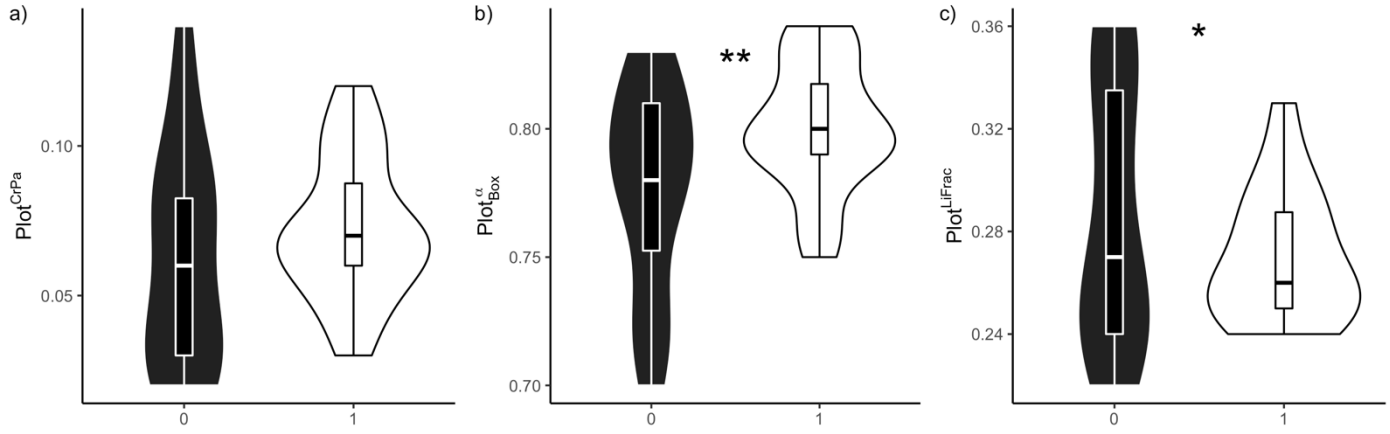

Figure 4.7 Violin plots of Plot-level crown packing ($Plot^{CrPa}$), the ratio of cumulative crown volume ($Crown^{Vol}$) to available plot volume and complexity ($Plot_{Box}^{\alpha}$), the box dimension representing the complexity of the plot. Both metrics are compared between mono-genus (black) and mixed-genus (white) using ANCOVA analyses, controlling for plot density using $Plot^{CAI}$, with significance annotated where applicable ($P < 0.05$).

4.4 Discussion

Across all plasticity metrics there is evidence of differences between and within each genus, and individual species, in line with the agreement with previous work that plasticity differs among species (Valladares & Niinemets, 2008). Our study assessed plasticity across a range of shade tolerance, included varying leaf types (evergreen and deciduous) and two genera of trees (pines and oaks). We found evidence contrary to the common belief that shade tolerance is negatively associated with plasticity (Valladares & Niinemets, 2008), and highlight how plasticity metrics that reflect different forms of structural response to competition (Gruntman et al., 2017) can unveil inter-specific differences in plasticity and its relation to light capture.

4.4.1 Inter-specific differences in crown plasticity

Across all plasticity metrics, pines were significantly different from oaks but differences between the two oaks was more pronounced than between the two pines (Figure 4.4). Differences between pine and oak plasticity were most evident for $Crown^{PaFrac}$ and Box^{α} (Figure 4.4), suggesting that pines may better optimise the spatial arrangement of foliage to maximize light capture and avoid negative carbon balance (Niinemets, 2010). $Crown^{PaFrac}$ was however more variable within the pines than oaks (Figure 4.4), and other studies have found that pines can maintain foliage at depth and close to the stem (Osunkoya et al., 2007). Chapter 3 highlighted a tight exponential relationship between height and crown depth in both pines, with crowns proportionally shorter with height, which may explain the variability in $Crown^{PaFrac}$ found here.

Inter-specific differences in $Stem^{Elon}$ were evident across all species, except between *P. nigra* and *Q. faginea*, with the strongest different between *Q. ilex* and all others (Figure 4.4). Higher $Stem^{Elon}$ in both pines agrees with work finding that light-demanding species afford greater risk by growing slender, biomechanically weaker trees in order to position their crown in direct light (Poorter et al., 2005), gambling on future benefits rather than current light capture (King, 1990; Sterck et al., 2001). Lower wood density has been found to be highly efficient in height extension whilst retaining mechanical safety (Anten & Schieving, 2010), leading to extension prioritised over light interception (Poorter et al., 2003). *Q. faginea* showed $Stem^{Elon}$ averages closer to both pines than to *Q. ilex*, despite its proclaimed status as a shade tolerant species (Jucker et al., 2014). *Q. faginea* is the only deciduous species in this study, at its most productive during spring when water is more

readily available (Montserrat-Martí et al., 2009), potentially necessitating the placement of foliage into high light to maximize carbon assimilation within a narrow window (Baldocchi et al., 2010). *Q. ilex* was comparatively much less elongated, selecting a more conservative strategy that attributes more growth towards enhancing current light capture (Valladares et al., 2012), reflecting its lower productivity than *Q. faginea* (Castro-Díez et al., 1997). Although $Stem^{Elon}$ has exposed interesting inter-specific differences that align well with shade tolerance (Niinemets & Valladares, 2006), and such as those also found in tropical forests (Martin-Ducup et al., 2020), trees are likely to cease height extension to match the surrounding canopy (Nagashima & Hikosaka, 2012) and begin to express a different growth investment strategy matching the new light environment (Sterck, 1999). Therefore, $Stem^{Elon}$ likely reflects both current investment towards light and historical light availability as it can take several years for a species to morphologically adapt to changing light conditions.

The lesser elongation response of *Q. ilex* contrasted with its greater capacity to displace horizontally compared to other species in this study. Both $Stem^{Disp^{\circ}}$ and $Crown^{Disp^{\circ}}$ were higher on average and more variable (Figure 4.4). This may be due to *Q. ilex* prioritising light capture and productivity early in its life-cycle (Escudero et al., 2017), with lasting consequences on the location of its crown relative to its stem. Across both $Stem^{Disp^{\circ}}$ and $Crown^{Disp^{\circ}}$, statistical differences were evident that show trade-offs between extending vertically and horizontally (Figure 4.4). Given the significance of path length in water limited environments (Olson et al., 2018; Fajardo et al., 2020), any incremental increase laterally through displacement adds to the hydraulic pathway but proportionally less to absolute height, whilst also imparting greater mechanical strain on the supporting stem (Anten & Schieving, 2010). Whereas most species allocated biomass to vertical elongation, *Q. ilex* allocated more to displacement, which may facilitate shade avoidance and reduce competition for light (Gruntman et al., 2017), an effect that may be intensified on slopes through optimised sun incidence angles through the canopy (Ishii & Higashi, 1997).

The box dimension metrics (Box^{β} and Box^{α}) are increasingly being used to understand tree complexity and filling along an inter-dimensional axis (Seidel, 2018; Seidel et al., 2019a; Guzmán et al., 2020). Here we

applied these metrics to compliment measures of external crown form with one that reflects the internal structure of a tree crown, condensing many aspects of tree morphology into two metrics (Dorji et al., 2019). Box^{α} was statistically indistinguishable between the two pines, reflecting similar branching and foliage arrangements that result from similar life histories (Givnish, 1988). In general, gymnosperms accumulate more foliage than angiosperms (Duursma & Falster, 2016), while oaks are able to regulate leaf area to match water availability (Baldocchi et al., 2010), both of which likely contribute to lower Box^{α} values of oaks compared to pines. The evergreen leaves of *Q. ilex* may drive its higher Box^{α} than the deciduous *Q. faginea*, because its leaf habit enables leaves to accumulate over time (Niinemets, 2010). We found significant relationships between $Stem^{Height}$ and Box^{β} , in contrast to other work finding weak relationships with $Stem^{DBH}$ and height, and stronger relationships with crown width and crown volume (Dorji et al., 2019) .

4.4.2 Significant effects of size on tree plasticity

Increasing in size is fundamental to overtopping neighbouring trees and acquire the resources necessary to enhance survival but it also creates biophysical constraints on tree growth (Mencuccini et al., 2007), and allocation changes throughout ontogeny (Dolezal et al., 2021). Our finding of higher $Crown^{PaFrac}$ in taller pines but not oaks suggests a more efficient foliage arrangement in larger pines, which may facilitate increased light capture and minimise self-shading (Niinemets, 2010). In fact, larger trees often have a greater fraction of woody biomass (Givnish, 1988), allocating less to foliage and more towards respiring roots, stems and branches (Niinemets, 2006; Poorter et al., 2012; Valladares et al., 2016; Poorter et al., 2019), so imposing greater demands on light acquisition in order to maintain the greater proportion of non-photosynthetic biomass (Givnish, 1988). The significant and positive relationships between $Stem^{Height}$ and both Box^{β} and Box^{α} , may facilitate greater light capture (Niinemets, 2010) across all species, through greater complexity and space-filling in larger trees. Within the oaks, this trend is not accompanied with increasing path fraction as is the case with the pines, suggesting oaks increase complexity but retain relatively lower path fraction values when growing in height, potentially reflecting shade tolerance differences where deep, shaded leaves are retained (Poorter et al., 2012). The lack of a significant relationship between height and $Crown^{PaFrac}$ in oaks suggests a more efficient foliage arrangement isn't necessary in younger trees, as proposed by Niinemets et al., (2005). Both oaks were more displaced when smaller in stature than larger, with the decline with height greater in

$Crown^{Disp^{\circ}}$ than $Stem^{Disp^{\circ}}$, signifying how oaks develop more symmetrical foliage arrangements when taller but retain overall structural displacement. Early $Stem^{Disp^{\circ}}$ is likely to leave a lasting effect and remain through ontogeny, whereas $Crown^{Disp^{\circ}}$ may be reduced through expansion of new branches into available space once the canopy has been breached (Martin-Ducup et al., 2020). Oaks not only have more efficient means to extend laterally (Anten & Schieving, 2010), but also lower risk of embolism given their comparatively smaller stature (Fajardo et al., 2019).

4.4.3 Contrasting trade-offs between plasticity and crown size

All species that expressed elongation as a strategy to compete for light did so at the detriment to overall crown volume. *P. sylvestris*, *P. nigra* and *Q. faginea* all had significantly negative effects of $Stem^{Elon}$ on $Crown^{Vol}$, even after accounting for tree size and plot effects, providing further evidence that trees allocating resources to stem extension are unable to also invest in leaf construction (Valladares et al., 2016) as it becomes rapidly unsustainable (Henry & Aarssen, 1997). It is also plausible that elongated trees that are heavily competing for light are also suffering from greater crown abrasion due to closer proximity, reducing lateral expansion (Pretzsch, 2019). The added hydraulic strain posed by growing taller may further aggravate drought impacts, and therefore constrain crowns to a small compact form (e.g. Jacobs et al., 2021). Both displacement metrics had no effects on the pines, but $Crown^{Disp^{\circ}}$ was positively linked with $Crown^{Vol}$ for both oaks, which may be due to biomechanical differences that enable oaks to expand in size whilst remaining stable despite the increased displacement in centre of mass (Moulia et al., 2006; Alméras & Fournier, 2009). *Q. faginea* and *Q. ilex* were the only two species to show significantly positive or non-significant effects of $Crown^{PaFrac}$ on $Crown^{Vol}$ whereas both pines had significantly negative effects. This suggests that, as oaks expand their $Crown^{Vol}$, little to no change in efficiency in foliage display (higher $Crown^{PaFrac}$) are necessary, whereas small pine crowns require high $Crown^{PaFrac}$ to maximise carbon gain due to lower shade tolerance (Niinemets, 2010; Niinemets et al., 2005). As pines compete for light, resources are allocated to $Stem^{Elon}$ at the expense to $Crown^{Vol}$, affording a less stable structure associated with high risk to escape low light (Valladares et al., 2012) and therefore unable to support a large crown (Loehle, 2016). A paralleled increase in $Crown^{PaFrac}$ with height could also indicate increases light requirements due to the increased proportion of biomass to foliage

(Givnish, 1988), necessitating a structure that maximises direct light interception. The added hydraulic stress of growing taller (Fajardo et al., 2019) also means growing a smaller crown lessens total evaporative demand and therefore water requirements (Dawson, 1996). In contrast, both oaks are able to expand in crown volume irrespective of displacement and afford minimal to no changes in the display of foliage ($Crown^{PaFrac}$).

4.4.4 Plasticity mediated light capture

All species, irrespective of shade tolerance, showed significant relationships between structural plasticity and light interception. As expected, $Stem^{Elon}$ was negatively correlated with both $Crown^{LiFrac}$ and $Crown^{LiUni}$, a pattern that held even with the most shade tolerant species in the dataset (*Q. ilex*). This suggests that, even for trees species that are well adapted to survive in low light (Valladares et al., 2012), shading can still induce vertical stretching to improve light capture. Competition for light is temporally dynamic, so current structural plasticity may reflect past light conditions or light-capture strategies. For example, *Q. ilex* has been found to seek high light and risk photoinhibition in early life-stages but shift to a more conservative, self-shaded structure through development (Escudero et al., 2017). Furthermore, theory postulates that surrounding canopy structure can impose optimal understory heights resulting from the interaction between incident angles and canopy gaps (Ishii & Higashi, 1997), leading to height extension to a point, followed by height maintenance (Fransson et al., 2021).

$Crown^{PaFrac}$ had the most consistent effect on light capture across all species, increasing both $Crown^{LiFrac}$ and $Crown^{LiUni}$ (Table 1). Others have found crowns to expand once they breach the canopy, a processed termed the 'liberation effect' (Martin-Ducup et al., 2020), but this is the first study to explicitly find evidence supporting its effect for enhancing light capture. The lack of response in $Crown^{PaFrac}$ to height in the oaks (Figure 4.5a) could reflect the preservation of low stature and therefore higher hydraulic safety (Fajardo et al., 2019) and in turn the formulation a canopy that is both efficient in transporting water and intercepting light (Bentley et al., 2013; Smith et al., 2014; Malhi et al., 2018). $Crown^{PaFrac}$ had an even larger positive effect on pine $Crown^{LiFrac}$, presumably due to high competition and proximity to neighbouring trees (Pretzsch, 2019) creating a steep light extinction gradient (Kükenbrink et al., 2021). Only the oak species showed any significant effects of displacement on light capture, with *Q. faginea* increasing $Crown^{LiUni}$ through $Stem^{Disp^{\circ}}$

and *Q. ilex* through $Crown^{Disp}$, likely indicative of shade avoidance as an important response (Gruntman et al., 2017). Across all species we found no evidence to studies suggesting that trees in low light exhibit monolayered (high $Crown^{PaFrac}$) canopies (Horn, 1971; Givnish, 1988), in fact we find the opposite, in agreement with others (Martin-Ducup et al., 2020). The effect of increasing $Crown^{PaFrac}$ on $Crown^{LiFrac}$ was comparatively less with the oaks than pines, which together with oaks on average having lower $Crown^{PaFrac}$ suggests that shade tolerant species partially exposed to high light can maintain more leaf layers leading to extended crowns (Niinemets, 2010), in agreement with height-crown depth scaling exponents in Chapter 3.

A tree's light environment changes throughout ontogeny and our analyses give new insight into structural adaptation for acquiring light, but more work is needed to fully understand this process. Our dataset contains only a small number of completely shaded individuals, and future work should include more sub-canopy stems to understand how structure adapts throughout ontogeny, including the independent effects of size and light (Rüger et al., 2011) across a broader spectrum of size and light. Furthermore, deeper insights into light capture also requires an understanding of foliage clustering and arrangement, both now attainable with TLS (Béland & Baldocchi, 2020), to tackle questions around potential benefits of self-shading, especially in water limited environments (Pearcy et al., 2005). Lastly, our light interception metrics only account for direct light, ignoring radiation transmission and sun flecks that enable light to penetrate deeper into the tree crown (Way & Pearcy, 2012), with potentially large benefits to overall carbon capture (Uemura et al., 2006).

4.4.5 Crown complexity, not overall volume-packing or light capture, is higher in mixed genus plots

The cumulation of all inter-specific variability in tree structure and plasticity is thought to be the principal driver behind observed positive diversity-productivity relationships in forests (Ishii et al., 2004; Sapijanskas et al., 2014). We first tested whether our TLS-derived measures of volume show the same patterns that emerged using traditional ground based measurements (Jucker et al., 2015), that is that, diverse plots are more efficient at filling available canopy volume. We split our plot network into mono and mixed-genus and found no statistical evidence that $Plot^{CrPa}$ is higher when mixed genus species are mixed together. Chapter 2 highlighted the extent to which $Crown^{Vol}$ can be overstated when fitting geometrical primitives to simple one

and two-dimensional measurements, which likely explains the difference in findings here. Despite the difference in conclusions based on volume filling, new box dimension analyses (Guzmán et al., 2020) revealed statistically significant higher complexity ($Plot_{Box}^{\alpha}$) in mixed-genus plots, meaning whilst occupied space is not higher, the overall complexity in growth forms is greater in our mixed genus plots. Complexity has recently been identified as a strong indicator of productivity, outperforming conventional structural metrics and diversity measures (Gough et al., 2019), and TLS offers substantial opportunity to reveal these relationships across varying forest types. Other TLS analyses have found higher complexity in mixed-species forests (Walter et al., 2021), with greater investment towards lateral branch extension (Kunz et al., 2019), but the presence of shade tolerant species and therefore shaded foliage in the understorey is less well understood (Morin et al., 2011).

Given the water limitation of these forests, tolerance of both drought and shade is unusual (Valladares et al., 2007) but there is growing evidence in the benefits of shade to tree prosperity, depending on an individual's shade tolerance (Kothari et al., 2021). The presence of shaded foliage is however hard to measure due to complex interactions between canopy and diurnal sun angles (Pierik & de Wit, 2014) making it difficult to draw conclusions around the presence and persistence of shaded foliage. Therefore, there remains no consensus on whether plasticity and added complexity leads to greater light capture, or whether the stratification of foliage through varying shade tolerance the importance factor (Sapijanskas et al., 2014; Williams et al., 2017). Fotis & Curtis, (2017) argue that the light environment is less variable in complex canopies due to higher porosity, whilst others highlight the prominent role of increased filling of shaded foliage (Juchheim et al., 2017) and max height (Morin et al., 2011). Our novel plot scale light interception metric $Plot^{LiFrac}$ showed significantly lower overall light interception in mixed than mon-genus plots, emphasising the importance of shade tolerance and multi-layered foliage structures efficiently utilising resources (Ishii et al., 2004). These results also align with the idea that functional dissimilarity. (i.e., shade tolerance) rather than phylogenetic distance (diversity) is an important driver of positive diversity effects (Toïgo et al., 2018).

4.5 Conclusion

To our knowledge, this study is the first to demonstrate how TLS can not only accurately quantify tree crown plasticity and configuration in three-dimensional space but also to embed new light-tracing algorithms to understand light-mediated tree crown structure and its variability at the individual level. Previous analyses have relied on coarse abstractions of competition for light and interception, and our work has demonstrated how factors such as tree size can now be interpreted independent of light capture to understand the role of size in determining growth strategies in trees. New individual tree metrics can be scaled to the whole plot, providing a more detailed understanding of diversity mediated plot crown packing and the role of both plasticity and shade tolerance that challenges past work. Tree growth and architecture is subject to multiple trade-offs (Verbeeck et al., 2019) and a tree must do many things well (Niklas, 1994) which ultimately means structures often deviate from highly optimised transport networks in a context dependent manner, as evidenced here. Future work should therefore build upon these new analysis techniques, incorporating topographical and climatic information and their interaction with tree structure in order to comprehensively assess the role of environmental context in determining tree form.

Chapter 5

5 Conclusions

5.1 Chapter summary

This thesis first presented a comprehensive overview of the challenges of the application of terrestrial laser scanning to structurally complex Mediterranean forests. In **chapter 2**, the steps taken from data collection through to the computation of novel light interception indices were described, with an emphasis on the complexities that arose from applying existing techniques developed in tall tropical rainforests and simple plantations to dry forests that have a completely different structure. This chapter presents not only opportunities from TLS but also challenges that had to be overcome through the modification of off-the-shelf software and discusses methodological development to derive information ecologically meaningful information. The chapter finishes by showcasing our approach to calculating a set of ecological metrics derived from TLS. The application of TLS to water-limited forests was not simple, with existing approaches mostly adapted and parameterised to function in either plantation forests with a simple structure or tall, highly stratified tropical forests with large trees. Furthermore, the substantial processing chain from data collection through to the eventual extraction of metrics highlighted the vast amount of work involved in using these data in ecology, meaning the value of the information extracted from these data must be high to justify the work necessary to extract it.

A significant issue that was encountered arose from trees within these ecosystems, often stunted, with low bifurcation points and therefore crowns low to the ground, are multi-stemmed, and surrounded by an abundant shrub layer, obstructing the visibility of stems. This issue arose in two places; firstly, within the initial stage of segmentation where tree stems are identified to subsequently build trees and secondly, when tree diameter at breast height (DBH) and no. of stems (multi-stems) needed to be extracted. Given the small vertical space along a stem to find a clear set of points on which to fit a stem cylinder, an approach was needed that could retain the original procedures to cylinder fitting but at a finer scale. This study highlights two necessary steps to finding and extracting stem metrics in these ecosystems. To begin with, stability cannot be found across an

entire cross-section because stems here are highly sinuous, twisting and turning close to the ground, therefore stability needs to be found within additional cross-sections. Next, most TLS data is downsampled to aid computation and ensure an even spacing between points along a tree's axis, but recollection of higher-resolution data at each tree stem not only creates more space to fit cylinders but also enables the inclusion of smaller trees and identification of numerous resprouts. Given that most TLS is downsampled to not only reduce computational demand but also to homogenise the resolution of a point cloud along its vertical axis and therefore reduce spatial bias, this part of the study demonstrated the additional benefit of going back to the original high resolution point cloud when working with highly complex tree stems such as those in Mediterranean forests. The added resolution at this height meant that more space was available along a stem section to find cylindrical stability in not only locating tree stems but also in extracting important metrics such as DBH and classifying trees as single or multi-stems.

Comparisons between TLS estimates, and simulated ground measurements demonstrated how traditional measures overestimate crown morphological features with the effect larger at higher dimensions (i.e., volume). When considered alongside the lack of data on the spatial location of a tree crown, it is evident that traditional approaches are likely to misrepresent crown interactions, calling into question what is meant by a 'crown' measurement. Similarly, our analyses found that crown radius measurements taken along the perimeter of a crown, incorporating the irregularity of crown shape, can produce accurate measures of crown area, but that the commonly used measurement of averaged maximum radius and its perpendicular can result in overestimation. There are also clear advantages to be made from quantifying three-dimensional light capture from TLS data, and indices presented in chapter 2 including spatially statistics such as hot spot analyses are exciting opportunities to understand fine scale relationships between structure and light capture.

While chapter 2 provided the methodological base for the application of TLS to address ecological questions, chapters 3 and 4 sought to answer fundamental questions in forest ecology from the perspective of new three-dimensional data. In **chapter 3**, more precise measures of crown morphology and height were used to test metabolic scaling theory, a prominent and provocative theory within forest ecology. To ascertain whether

competition from larger trees, crowding or a specific species affects scaling, this chapter reinterprets traditional approaches to calculating competition to develop neighbourhood metrics from TLS that are more accurate and representative of tree-tree interactions aboveground. The results are discussed within the context of both competition for light and water, prominent features of Mediterranean forests. Competition negatively affected all crown metrics except crown depth, and asymmetric competition was the strongest driver of pine crown morphology, but oaks were more sensitive to symmetric competition. Effects of neighbourhood species ID was not important for most species, but *Q. faginea* showed sensitivity to neighbourhoods containing species of the same genus. Across all species and most crown dimensions, height-crown scaling exponents were below those predicted by MST, potentially driven by water-limitation in this ecosystem. In height-depth scaling large differences were evident between the two genera, with pines considerably shallower and oaks deeper with height, in contrast to theoretical predictions.

Chapter 4 also builds on the foundations laid in chapter 2 by demonstrating the capacity of TLS data to quantify a tree's morphological adaptability (structural plasticity), and how this varies across four major tree species in the Spanish Mediterranean. This chapter also presents metrics of tree light capture derived from new spatially explicit measures of light interception by foliage in a tree crown. Inter-species differences in plasticity were assessed and interpreted in the context of allocational trade-offs and relationships to light capture at the individual scale, while at the community scale, the impacts of diversity on structure and light capture were determined. Taken together, the new measures of plasticity and light interception provided insights into diversity-induced tree crown space filling, complexity and light capture at the plot scale that have not been possible before, and which call into question prior understanding of the relationship between diversity and crown packing.

Inter-specific differences in tree structural plasticity were evident between species and genera with shade tolerance an important factor explaining some of these differences. Both pines and *Q. faginea* had higher stem elongation values on average than *Q. ilex* but stem displacement was higher in *Q. ilex* compared to all other species. Crown path fraction and crown complexity was also significantly higher in pines than oaks, with the

former significantly correlated to tree height in both pines, but not in either oak species, suggesting a more efficient canopy structure is necessary with increasing size in the less shade tolerant species. Crown complexity increased with size for all species, but crown displacement had a steep declining relationship with height for both oaks, potentially pointed to a greater mechanical capacity in oaks symmetrically filling canopy space once the canopy has been breached. Of all the structural plasticity metrics, crown path fraction consistently increased light capture for all species, although the effect was stronger in the pines. As expected, the negative response of stem elongation to increasing light interception aligned with species shade tolerance, with the most shade tolerant *Q. ilex* showing no significant relationship and *P. sylvestris* the highest sensitivity. However, oaks did show significant relationships between stem displacement (*Q. faginea*) or crown displacement (*Q. ilex*) and uniformity in light interception. This chapter finishes by presenting novel insights into diversity-structure relationships at the plot scale, namely that complexity, not crown volume packing, is higher in mixed species plots and that overall light capture is lower, suggesting a greater presence of shaded foliage in mixed species plots.

5.3 Future work

5.3.1 Methodological development across instruments and ecosystems

For TLS to contribute widely to forest ecology it will need to be embraced by an array of users with varying budgets, scales of interest and repeatability in procedures that remain consistent across time. There is no doubt TLS presents an exciting new way to measure trees and explicitly determine structure-function relationships at scale as highlighted in this thesis but methodological development is necessary that facilitates the transition from traditional measurement techniques to three-dimensional data acquisition with laser scanners. To date, TLS data acquisition and processing is not only highly time-consuming but also complicated by current methodological approaches relying upon high fidelity point clouds, which when not met, often mean manual intervention is required, adding even more time and effort. Existing tools are bespoke and often tailored to the ecosystem type that it was developed within, limiting transferability to different forest types where even simple field measures such as DBH can be difficult to derive (chapter 2; Liu et al., 2018). There is optimism towards implementing TLS into forest inventory (Abegg et al., 2017; Bauwens et al., 2016; Maas et al., 2008; Moskal

and Zheng, 2012) but given the scale, time and remoteness of inventory sites, many are leaning more towards mobile laser scanning systems that are light, cheaper and quicker (Bauwens et al., 2016; Bienert et al., 2018; Donager et al., 2021; Gollob et al., 2020). Although occlusion is undoubtedly higher with mobile lightweight systems (Morsdorf et al., 2018) and a hinderance to extracting metrics (Abegg et al., 2017; Wang et al., 2019), mobile systems have shown some promise in particular contexts in extracting attributes such as DBH, stem density and height but have struggled to resolve a trees entire branching structure (Bienert et al., 2018).

A major obstacle will be in formulating easy to use automated procedures from scan acquisition through to metrics that are applicable across different forest species compositions and structure and that meet the needs of forest inventory where reliability, applicability and scalability are all important considerations. Fundamental steps such as automated tree segmentation are still in their infancy and problematic with mid-range instruments in complex forest structures, as shown in this thesis (chapter 2), let alone with lower powered mobile scanners, necessitating further development (e.g., Donager et al., 2021). Expectations also need to be grounded, with prospects in measuring attributes such as leaf area index (LAI) at scale within inventory optimistic (Liang et al., 2014), especially given that single scans from more powerful instruments still considerably underestimate LAI (Yun et al., 2019). The temporal component of forest inventory is of considerable value to understanding forest dynamics (Purves and Pacala, 2008) and future measurements should prioritise maintaining consistency between old approaches to measurement and newer ones arising from TLS. Here, development should ensure TLS can consistently measure existing tree attributes within inventory alongside newer developments that provide novel insights into tree form and function. The backwards compatibility of TLS-based tree measurements with inventory datasets will be crucial to understanding long-term trees in forest structure and productivity in a changing climate.

5.3.2 Consensus on ecological metrics

Given the considerable amount of information that may be derived from TLS data, and the choices that must be made to generate metrics, there is a clear need within the forest ecology community for consensus on data collection, open-source methods and, most importantly, the establishment of a framework of metrics that have

independent and ecological meaningful underpinnings. Our and other analyses using TLS have highlighted conceptual inconsistencies in measuring trees due to the ability to characterise certain attributes, for example crown volume, in various ways from 3D data (Zhu et al., 2021). An abundance of TLS-derived ecological forest metrics have emerged across the literature in recent years, with researchers striving to produce and present more effective and better representations of tree crown attributes (e.g. (Dorji et al., 2019; Ehbrecht et al., 2017; Liu et al., 2018; Martin-Ducup et al., 2018; Martin-Ducup et al., 2020; Seidel et al., 2019b; Stovall et al., 2021; van der Zee et al., 2021; Walter et al., 2021)) and, to a lesser extent, competition metrics (e.g. (Krůček et al., 2019; Kunz et al., 2019; Metz et al., 2013; Olivier et al., 2016)). An agreed framework would help the field move forward – and analogies for this kind of consensus exist; for example, the essential biodiversity variables framework which was created as a conceptual framework that synthesised data streams into an amalgamation of measures that capture biodiversity and its function from satellite data (Jetz et al., 2016; Pettorelli et al., 2016; Skidmore et al., 2015). Verbeeck et al., (2019) have proposed the 'plant structural spectrum' condensing many axes of crown structural variation into a few descriptive axes, but only tropical and temperate species were considered, while it also lacks discussion on the methodological standardisation in measuring these 'spectra' across instruments and forest type. Nonetheless it highlights the scope and necessity in constructing a conceptual framework to move forward in applying TLS to forest ecology.

Within ecology, TLS will be most powerful when used as a tool in conjunction with theoretical understanding of the fundamental processes that govern tree structure, and when it can add value to existing long-term but simpler datasets such as national forest inventories (Purves and Pacala, 2008). TLS can point towards the most effective measurement methods to calculate crown attributes from the ground, provide error margins and improve allometric relationships of crown dimensions to size within theoretical frameworks (Taubert et al., 2015; West et al., 2009, Chapter 2), and forest process models which include crown plasticity (Purves et al., 2007), where the scaling of crown radius, depth and volume are important parameters. New representations of crown volume, such as 'green volume', voxel versus hull based extraction and metrics derived through fractal analysis to understand size (Dorji et al., 2019) are all attempting to observe the same thing, but from different perspectives. It is paramount that new development is additional and complimentary to existing

metrics to avoid scenarios where inter-comparisons of results and studies becomes difficult. At the same time, TLS presents a novel opportunity to measure trees at scale, in ways never before possible (Disney, 2019). Theoretical understandings of plant hydraulics for example has prompted the calculation of metrics such as path fraction which makes use of network analyses on 3D point clouds to derive a holistic measure of hydraulic and light interception efficiency (Malhi et al., 2018; Smith et al., 2014, Chapter 2, Figure 2.19) that would not be possible with traditional ground measurements. And other abiotic drivers of tree shape can be examined too; for example, theoretical understanding of biomechanics combined with accurate, TLS derived 3D models of tree architecture are substantially improving our understanding of tree sway in the wind and what factors make a tree vulnerable to wind throw (Huang et al., 2020; Jackson et al., 2021, 2020). Terrestrial laser scanning is an opportunity to look at tree structure in wholly new ways and as such, there is a need to develop consistent methods informed by an ecological underpinning which, where possible, retains interpretability with historical data.

5.3.3 Casting new light on tree-tree interactions

This thesis highlights the ability of TLS to provide a completely new and comprehensive perspective on tree-tree interactions that are fundamental to understanding forest ecosystem functions (Trogisch et al., 2021). While the approach derived in chapter 2 provided a detailed measure of a trees' local neighbourhood, by accurately representing crown positioning, irregularity, and size (see Figure 2.20a), it stills depends on some form of distance-based threshold to determine the zone of influence and a height threshold that split taller trees and therefore competition for light, and all trees, that represents competition for water. The idea is that aboveground, larger individuals acquire a disproportionately greater amount of light, and therefore asymmetric competition is termed, whereas belowground competition is thought to be proportional to size, and termed symmetric (Weiner, 1990). The problem is that thresholding neighbouring trees purely based on height thresholds to characterise asymmetric competition for light is unlikely to accurately characterise the degree of shading induced on an individual tree given the complex nature of light/canopy interactions (Braghiere et al., 2020; Pierik and de Wit, 2014). In any particular neighbourhood, increased complexity and variability in height structure may enable more light to penetrate to greater depths (Fotis and Curtis, 2017),

making the selection of an arbitrary height threshold increasingly difficult. One solution that functions within the limits of inventory type data is crown overlap, posed by Zambrano et al., (2019) as an effective means to provide an effective, distance-independent way to characterise asymmetric competition when using inventory type data. Crown overlap can be calculated using TLS, but within our data, crown overlap values were very low, suggesting this approach may not be enough to understand competitive interactions. In addition, we found crowns are highly plastic to avoid neighbours and fill canopy space (Figure 2.20a). Competition for light is prominent but lateral shading, which is known to invoke a strong structural response in trees regardless (Schoonmaker et al., 2014), may be at least as important as overtopping. Shading characterised as presence of taller trees has however proven effective in many studies, including this thesis where distinct patterns emerged between shade intolerant and tolerant species. Here, competition belowground is likely an important driver but characterisation based on aboveground structure is not reliable. Indeed, for a long time, below ground competition has been considered symmetric (Craine and Dybzinski, 2013; Weiner, 1990; Weiner et al., 1997) but some argue that large trees have larger roots and therefore better access to resources, suggesting an asymmetric component (Frank et al., 2010; Rajaniemi, 2003; Rasmussen et al., 2019). While some have found shading by larger neighbouring trees can ameliorate abiotic stress (McIntire and Fajardo, 2014), others suggest positive effects of shading depend on the recipients shade tolerance (Kothari et al., 2021). Positive effects of shading on trees where trees are exposed to abiotic stress is plausible given the manner in which plants open and close stomata in a dynamic manner in response to light intensity to avoid water stress (Devireddy et al., 2018). There is also evidence of trees arranging foliage in a way that maximises photosynthesis at certain times of the day, avoiding excessively high midday light intensities (Ventre-Lespiaucq et al., 2018). When a canopy is shaded by neighbouring trees however, these patterns in arrangement were completely opposite, with crowns optimised to harness light at midday peak (Charbonnier et al., 2013). In all, evidence suggests that light-structure relationships can vary considerably between species and environmental context and likely necessitate more comprehensive representations of light interception to develop our understanding further.

To truly understand the exact competitive mechanisms that concepts of asymmetric competition represent there is a clear need for improved characterisations of light and shading at the individual scale. Not only will

this enable ecologists to analyse the independent effect of larger trees on smaller ones from shading, but in separating competition for light from other sources, will allow better inference in the strength of belowground competition. Previous attempts using light interception models within forest dynamic models (Canham et al., 1999), highlighted the importance of belowground competition by accounting for shading effects from neighbouring trees explicitly (Coates et al., 2009) but these approaches have depended on coarse abstraction of crown shape, size and spacing, completely disregarding plasticity. For example, Sapijanskas et al., (2014), used the same light simulation framework, representing tree crowns as cylinders, a geometric primitive found in this thesis to overstate crown volume by around 4 times that of TLS estimates (chapter 2, Figure 2.13). Ray tracing techniques combined with highly accurate 3D point clouds of individual and neighbouring trees presents an exciting opportunity in forest ecology to, for the first time, quantify competition for light in a spatially explicit manner (Bittner et al., 2012). Future work should use these new data to not only gain a deeper, more comprehensive understanding of belowground competition for water and nutrients (Craine and Dybzinski, 2013) but also in tracing back to existing inventory measurements and conduct comparative analyses to understand how best to represent light capture within the limits of inventory measurement. There are of course legacy effects of competition where current patterns and interactions are a result of interactions over long periods of time, necessitating temporal studies and/or the inclusion of independent variables that reflect past competitive conditions (Pommerening and Sánchez Meador, 2018). Through explicit 3D quantification of light capture, TLS can potentially provide novel insights into light mediated structure and identify structural characteristics that are telling of past conditions.

5.3.4 New understanding of light - structure relationships

The principal function of building a canopy is to optimise light capture for photosynthesis and shade neighbouring trees that are competing for the same resource (Valladares and Niinemets, 2007). Leaves are the photosynthetic machinery of a canopy and their arrangement in three-dimensional space can affect the light conditions experienced by trees below (Kükenbrink et al., 2021) but also used to mediate the amount of light received within an individual canopy itself (Pearcy et al., 2005). The effective representation of leaves and their collective arrangement into a canopy within radiative transfer models is of fundamental importance to

their accuracy (Côté et al., 2009) and therefore in deriving fundamental forest functions such as photosynthesis (Vilfan et al., 2019). In fact, TLS combined with field spectroscopy has been used to produce a virtual forest that has visually realistic images of canopies from above and below (Calders et al., 2018) with important ramifications for deriving robust metrics from satellites (Disney, 2019; Jetz et al., 2016). TLS is therefore highly valuable for determining the radiation regime within a forest. Here key characteristics such as vertical light extinction (Kükenbrink et al., 2021) and the ratio of shaded to sunlit foliage which is fundamental to understanding canopy-level photosynthesis (Chen et al., 2012) can be explicitly measured. Within forest ecology there is potential to analyse tree structure-light-capture relationships at scales relevant to an individual tree, where for example, foliage traits and therefore productivity, vary strongly across tree crowns depending on radiation levels (Williams et al., 2020). The heterogeneity in light across a tree is known to be important at the metre scale (Valladares and Guzmán, 2006). However, to date most field studies have been confined to point measurements of light (Kothari et al., 2021; Williams et al., 2020) with low sample sizes due to the laborious work, with many developments restricted to theoretical (Duursma et al., 2010) or modelling studies where crown structure is represented abstractly only (Canham et al., 2004; Sapijanskas et al., 2014).

Here, Chapter 3 analysed how crown morphology scales with size, but there remain unanswered questions about changes in foliar properties, including leaf area and density. There is evidence to suggest that as trees increase in size foliage becomes proportionally less (Coomes et al., 2012), spread across a crowns periphery (Zeide and Pfeifer, 1991) to avoid self-shading and homogenise productivity (Duursma et al., 2010), but this is untested with direct TLS measurements. Likewise, chapter 4 presented novel insights into how trees structurally respond to competition through different means to improve light capture but didn't account for shifts in arrangement and orientation of foliage (Hagemeier and Leuschner, 2019). It is plausible that trees in the understorey organize foliage in a more planar and sparse way that maximises light capture (Valladares and Niinemets, 2007) or that canopy trees shield lower leaves from midday radiation (Hagemeier and Leuschner, 2019; Pearcy et al., 2005; Valladares et al., 2005) but general metrics of displacement, filling and branch networks don't explicitly characterise these features. TLS is now beginning to shed new light on foliage

characteristics including leaf angle (Stovall et al., 2021; Vicari et al., 2019), distribution (Martin-Ducup et al., 2018), fractal space filling (Seidel et al., 2019b) and clustering (Béland and Baldocchi, 2020), but there remain many opportunities to test ecological theory and concepts with these data.

5.3.5 Enhanced characterisation of abiotic effects on structure

The results of this thesis have been interpreted comprehensively within the context of abiotic factors, more specifically water limitation, but future work should look to explicitly account for these factors more directly through the combined use of TLS and ALS in characterising high resolution topographical variables. High topographical heterogeneity leads to variable wind exposure (Coomes et al., 2018), accessibility to deep water (Fan et al., 2017) and highly variable radiation regimes affecting water availability, for example, greater exposure on south-facing steep slopes (Schwartz et al., 2019) and relief from excessive radiation through shading (Greiser et al., 2020). The availability of deep water to trees is crucial to predicting effects of aridity on productivity (Nadal-Sala et al., 2021), particularly in ecosystems such as Spanish Mediterranean where groundwater is an important resource to trees (Barbeta and Peñuelas, 2017) but hard to measure directly. While measures of wind exposure can be effectively described based on topographic position and surrounding vegetation structure (Brüchert and Gardiner, 2006) and direct terrain effects on tree structure (Ishii and Higashi, 1997) through simple extractions of slope and aspect. To build upon results presented in chapters 3 and 4, analyses should aim to incorporate abiotic variables known to affect tree structure and tree-tree interactions through readily available means, such as proxies derived from topographical variables.

The interplay between tree function and topography has gained more attention in recent years, with some advocating for increased research within the ‘critical zone’, which is the interface between vegetation and fresh unaltered bedrock (Dawson et al., 2020) and subsurface hydrological processes (McLaughlin et al., 2020). The availability of national ALS data in countries such as Spain means high resolution digital terrain models can be derived and subsequently used to derive effect proxies of hydraulic (Chitra-Tarak et al., 2018), nutrient (Jucker et al., 2018) and wind conditions (Mikita and Klimánek, 2010; Ruel et al., 2002), which are all abiotic factors known to affect tree structure (Jacobs et al., 2021; Loehle, 2016; Urban et al., 2013). In dry

environments, hydraulic refugia that emerge within certain topographical settings could be quantified (McLaughlin et al., 2017) adding further abiotic context to the interplay between drought, individual structure and competition effects on tree function and mortality (Mcdowell et al., 2008; McLaughlin et al., 2017; Olson et al., 2018; Ruiz-Benito et al., 2013). A more complete depiction of a trees immediate environment will also help disentangle the continuing debate around positive and negative interactions between trees for belowground resources (Fichtner et al., 2020; Grossiord, 2019; Grossiord et al., 2014; Jourdan et al., 2020; Jucker et al., 2014; Wright et al., 2014).

ALS aside, TLS has the potential to characterise very localised topography where the fine scale slopes, undulations, and shape (concave or convex) of the immediate terrain surrounding a tree effects on resource availability. Tauc et al., (2020) found pits provided micro-refugia against drought due to higher water retention, Franklin and Buckley, (2019 and Kern et al., (2019) found fine scale topography affects tree recruitment and survival, while Valtera and Schaetzl, (2017) found higher nutrient retention in pits available to neighbouring trees (Valtera and Schaetzl, 2017). The combination of ALS and TLS has the potential to characterise topography at multiple scales and derive variables that reflect hydraulic, wind and nutrient variability in space with data that is normally removed in the early stages of LiDAR processing applied to forest ecology. These datasets will enable a deeper understanding of the results presented in chapters 3 and 4, where plot-plot variation held within the random effect in the mixed effects models could explained more directly or disentangled through post-hoc analyses. These data will refine approaches taken aiming to disentangle the relative contributions of abiotic factors (e.g., water, wind slope) in shaping tree form and function amongst the interactive complexity of tree-tree competition for resources (Craine and Dybzinski, 2013).

References

AAkerblom, M., Raumonen, P., Mäkipää, R., Kaasalainen, M., 2017. Automatic tree species recognition with quantitative structure models. Remote Sens. Environ. 191, 1–12.

Abegg, M., Kükenbrink, D., Zell, J., Schaepman, M.E., Morsdorf, F., 2017. Terrestrial Laser Scanning for Forest Inventories—Tree Diameter Distribution and Scanner Location Impact on Occlusion. Forests 8, 184.

Ackerly, D., 1999. Self-shading, carbon gain and leaf dynamics: a test of alternative optimality models. Oecologia, 119(3), pp.300-310.

Aiba, M. & Nakashizuka, T. (2009) Architectural differences associated with adult stature and wood density in 30 temperate tree species. Functional Ecology. 23 (2), 265–273.

Alday, J.G., Camarero, J.J., Revilla, J. & Resco de Dios, V. (2020) Similar diurnal, seasonal and annual rhythms in radial root expansion across two coexisting Mediterranean oak species. Tree Physiology. 40 (7), 956–968.

Alméras, T. & Fournier, M. (2009) Biomechanical design and long-term stability of trees: Morphological and wood traits involved in the balance between weight increase and the gravitropic reaction. Journal of Theoretical Biology. 256 (3), 370–381.

Alonso-Forn, D., Peguero-Pina, J.J., Ferrio, J.P., Mencuccini, M., Mendoza-Herrer, Ó., Sancho-Knapik, D. & Gil-Pelegrín, E. (2020) Contrasting functional strategies following severe drought in two Mediterranean oaks with different leaf habit: Quercus faginea and Quercus ilex subsp. rotundifolia. Tree Physiology.

Ameztegui, A., Coll, L., Benavides, R., Valladares, F. & Paquette, A. (2012) Understory light predictions in mixed conifer mountain forests: Role of aspect-induced variation in crown geometry and openness. Forest Ecology and Management. 27652–61.

Anest, A., Charles-Dominique, T., Maurin, O., Millan, M., Edelin, C., Tomlinson, K.W., 2021. Evolving the structure: climatic and developmental constraints on the evolution of plant architecture. A case study in Euphorbia. New Phytologist.

Annighöfer, P., Ameztegui, A., Ammer, C., Balandier, P., Bartsch, N., Bolte, A., Coll, L., Collet, C., Ewald, J., Frischbier, N., Gebereyesus, T., Haase, J., Hamm, T., Hirschfelder, B., Huth, F., Kändler, G., Kahl, A., Kawaletz, H., Kuehne, C., Lacointe, A., Lin, N., Löf, M., Malagoli, P., Marquier, A., Müller, S., Promberger, S., Provendier, D., Röhle, H., Sathornkich, J., Schall, P., Scherer-Lorenzen, M., Schröder, J., Seele, C., Weidig, J., Wirth, C., Wolf, H., Wollmerstädt, J., Mund, M., 2016. Species-specific and generic biomass equations for seedlings and saplings of European tree species. European Journal of Forest Research 2, 313–329.

Anten, N.P.R. & Schieving, F. (2010) The Role of Wood Mass Density and Mechanical Constraints in the Economy of Tree Architecture. The American Naturalist. 175 (2), 250–260.

Atkins, J.W., Fahey, R.T., Hardiman, B.S., Gough, C.M., 2018. Forest Canopy Structural Complexity and Light Absorption Relationships at the Subcontinental Scale. Journal of Geophysical Research: Biogeosciences 123, 1387–1405.

Aubry-Kientz, M., Dutrieux, R., Ferraz, A., Saatchi, S., Hamraz, H., Williams, J., Coomes, D., Piboule, A., Vincent, G., 2019. A Comparative Assessment of the Performance of Individual Tree Crowns Delineation Algorithms from ALS Data in Tropical Forests. Remote Sensing 11, 1086.

Bae, S., Levick, S.R., Heidrich, L., Magdon, P., Leutner, B.F., Wöllauer, S., Serebryanyk, A., Nauss, T., Krzystek, P., Gossner, M.M., Schall, P., Heibl, C., Bässler, C., Doerfler, I., Schulze, E.-D., Krah, F.-S., Culmsee, H., Jung, K., Heurich, M., Fischer, M., Seibold, S., Thorn, S., Gerlach, T., Hothorn, T., Weisser, W.W., Müller, J., 2019. Radar vision in the mapping of forest biodiversity from space. Nature Communications 10, 1–10.

Baeten, L., Verheyen, K., Wirth, C., Bruelheide, H., Bussotti, F., Finér, L., Jaroszewicz, B., Selvi, F., Valladares, F., Allan, E., Ampoorter, E., Auge, H., Avăcăriei, D., Barbaro, L., Bărnoaiea, I., Bastias, C.C., Bauhus, J., Beinhoff, C., Benavides, R., et al. (2013) A novel comparative research platform designed to determine the functional significance of tree species diversity in European forests. Perspectives in Plant Ecology, Evolution and Systematics. 15 (5), 281–291.

Baldocchi, D.D., Ma, S., Rambal, S., Misson, L., Ourcival, J.-M., Limousin, J.-M., Pereira, J. & Papale, D. (2010) On the differential advantages of evergreenness and deciduousness in mediterranean oak woodlands: a flux perspective. Ecological Applications. 20 (6), 1583–1597.

Bär, A., Michaletz, S.T., Mayr, S., 2019. Fire effects on tree physiology. New Phytologist 223, 1728–1741.

Barbeito, I., Dassot, M., Bayer, D., Collet, C., Drössler, L., Löf, M., del Rio, M., Ruiz-Peinado, R., Forrester, D.I., Bravo-Oviedo, A., Pretzsch, H., 2017. Terrestrial laser scanning reveals differences in crown structure of Fagus sylvatica in mixed vs. pure European forests. For. Ecol. Manag. 405, 381–390.

Barbeta, A., Mejía-Chang, M., Ogaya, R., Voltas, J., Dawson, T.E. & Peñuelas, J. (2015) The combined effects of a long-term experimental drought and an extreme drought on the use of plant-water sources in a Mediterranean forest. Global Change Biology. 21 (3), 1213–1225.

Barbeta, A., Peñuelas, J., 2017. Relative contribution of groundwater to plant transpiration estimated with stable isotopes. Scientific Reports 7, 10580.

Bates, D., Mächler, M., Bolker, B. & Walker, S. (2015) Fitting Linear Mixed-Effects Models Using lme4. Journal of Statistical Software. 67 (1), 1–48.

Bauwens, S., Bartholomeus, H., Calders, K., Lejeune, P., 2016. Forest inventory with terrestrial LiDAR: A comparison of static and hand-held mobile laser scanning. Forests 7, 127.

Bauwens, S., Bartholomeus, H., Calders, K., Lejeune, P., 2016. Forest inventory with terrestrial LiDAR: A comparison of static and hand-held mobile laser scanning. Forests 7, 127.

Bechtold, S. & Höfle, B. (2020) VOSTOK - The Voxel Octree Solar Toolkit.

Bejan, A., Lorente, S., Lee, J., 2008. Unifying constructal theory of tree roots, canopies and forests. Journal of Theoretical Biology 254, 529–540.

Béland, M. & Baldocchi, D. (2020) Is foliage clumping an outcome of resource limitations within forests? Agricultural and Forest Meteorology. 295108185.

Béland, M., Baldocchi, D., 2020. Is foliage clumping an outcome of resource limitations within forests? Agricultural and Forest Meteorology 295, 108185.

Bell, D.L., Galloway, L.F., 2007. Plasticity to neighbour shade: fitness consequences and allometry. Funct. Ecol. 21, 1146–1153.

Bella, I.E. (1971) A New Competition Model for Individual Trees. Forest Science. 17 (3), 364–372.

Benavides, R., Carvalho, B., Matesanz, S., Bastias, C.C., Cavers, S., Escudero, A., Fonti, P., Martínez-Sancho, E., Valladares, F., 2021. Phenotypes of Pinus sylvestris are more coordinated under local harsher conditions across Europe. Journal of Ecology.

Benoit Mandelbrot, 1977. The Fractal Geometry of Nature.

Bentley, L.P., Stegen, J.C., Savage, V.M., Smith, D.D., von Allmen, E.I., Sperry, J.S., Reich, P.B., Enquist, B.J., 2013. An empirical assessment of tree branching networks and implications for plant allometric scaling models. Ecology Letters 16, 1069–1078.

Berger, U. & Hildenbrandt, H. (2003) The strength of competition among individual trees and the biomass-density trajectories of the cohort. 8.

Bienert, A., Georgi, L., Kunz, M., Maas, H.-G., Von Oheimb, G., 2018. Comparison and Combination of Mobile and Terrestrial Laser Scanning for Natural Forest Inventories. Forests 9, 395.

Bienert, A., Georgi, L., Kunz, M., Maas, H.-G., Von Oheimb, G., 2018. Comparison and Combination of Mobile and Terrestrial Laser Scanning for Natural Forest Inventories. Forests 9, 395.

Biging, G.S. & Dobbertin, M. (1992) A Comparison of Distance-Dependent Competition Measures for Height and Basal Area Growth of Individual Conifer Trees. Forest Science. 38 (3), 695–720.

Biging, G.S., Dobbertin, M., 1992. A Comparison of Distance-Dependent Competition Measures for Height and Basal Area Growth of Individual Conifer Trees. For. Sci. 38, 695–720.

Bittner, S., Gayler, S., Biernath, C., Winkler, J.B., Seifert, S., Pretzsch, H., Priesack, E., 2012. Evaluation of a ray-tracing canopy light model based on terrestrial laser scans. Canadian Journal of Remote Sensing 38, 619–628.

Blanchard, E., Birnbaum, P., Ibanez, T., Boutreux, T., Antin, C., Ploton, P., Vincent, G., Pouteau, R., Vandrot, H., Hequet, V., Barbier, N., Droissart, V., Sonké, B., Texier, N., Kamdem, N.G., Zebaze, D., Libalah, M., Couteron, P., 2016. Contrasted allometries between stem diameter, crown area, and tree height in five tropical biogeographic areas. Trees 30, 1953–1968.

Bloom, A.J., Chapin, F.S. & Mooney, H.A. (1985) Resource Limitation in Plants-An Economic Analogy. Annual Review of Ecology and Systematics. 16 (1), 363–392.

Bohlman, S., Pacala, S., 2012. A forest structure model that determines crown layers and partitions growth and mortality rates for landscape-scale applications of tropical forests. J. Ecol. 100, 508–518.

Bohn, F.J., Huth, A., 2017. The importance of forest structure to biodiversity–productivity relationships. Royal Society Open Science 4, 160521.

Bonnesoeur, V., Constant, T., Moulia, B., Fournier, M., 2016. Forest trees filter chronic wind-signals to acclimate to high winds. New Phytologist 210, 850–860.

Bourdier, T., Cordonnier, T., Kunstler, G., Piedallu, C., Lagarrigues, G. & Courbaud, B. (2016) Tree Size Inequality Reduces Forest Productivity: An Analysis Combining Inventory Data for Ten European Species and a Light Competition Model. PLOS ONE. 11 (3), e0151852.

Braghiere, R.K., Quaife, T., Black, E., Ryu, Y., Chen, Q., De Kauwe, M.G., Baldocchi, D., 2020. Influence of sun zenith angle on canopy clumping and the resulting impacts on photosynthesis. Agricultural and Forest Meteorology 291, 108065.

Braghiere, R.K., Wang, Y., Doughty, R., Sousa, D., Magney, T., Widlowski, J.-L., Longo, M., Bloom, A.A., Worden, J., Gentine, P., Frankenberg, C., 2021. Accounting for canopy structure improves hyperspectral radiative transfer and sun-induced chlorophyll fluorescence representations in a new generation Earth System model. Remote Sens. Environ. 261, 112497.

Brandt, M., Tucker, C.J., Kariryaa, A., Rasmussen, K., Abel, C., Small, J., Chave, J., Rasmussen, L.V., Hiernaux, P., Diouf, A.A., Kergoat, L., Mertz, O., Igel, C., Gieseke, F., Schöning, J., Li, S., Melocik, K., Meyer, J., Sinno, S., Romero, E., Glennie, E., Montagu, A., Dendoncker, M., Fensholt, R., 2020. An unexpectedly large count of trees in the West African Sahara and Sahel. Nature 587, 78–82.

Bravo-Oviedo, A., Sterba, H., del Río, M. & Bravo, F. (2006) Competition-induced mortality for Mediterranean Pinus pinaster Ait. and P. sylvestris L. Forest Ecology and Management. 222 (1), 88–98.

Bravo-Oviedo, A., Sterba, H., del Río, M., Bravo, F., 2006. Competition-induced mortality for Mediterranean Pinus pinaster Ait. and P. sylvestris L. Forest Ecology and Management 222, 88–98.

Breidenbach, J., Koch, B., Kändler, G., Kleusberg, A., 2008. Quantifying the influence of slope, aspect, crown shape and stem density on the estimation of tree height at plot level using lidar and InSAR data. International Journal of Remote Sensing 29, 1511–1536.

Brodribb, T.J., Powers, J., Cochard, H., Choat, B., 2020. Hanging by a thread? Forests and drought. Science 368, 261–266.

Brown, C.L., McAlpine, R.G. & Kormanik, P.P. (1967) Apical Dominance and Form in Woody Plants: A Reappraisal. American Journal of Botany. 54 (2), 153–162.

Brüchert, F. & Gardiner, B. (2006) The effect of wind exposure on the tree aerial architecture and biomechanics of Sitka spruce (Picea sitchensis, Pinaceae). American Journal of Botany. 93 (10), 1512–1521.

Bruggisser, M., Dorigo, W., Dostálová, A., Hollaus, M., Navacchi, C., Schlaffer, S., Pfeifer, N., 2021. Potential of Sentinel-1 C-Band Time Series to Derive Structural Parameters of Temperate Deciduous Forests. Remote Sensing 13, 798.

Burt, A., Calders, K., Cuni-Sanchez, A., Gómez-Dans, J., Lewis, P., Lewis, S.L., Malhi, Y., Phillips, O.L., Disney, M., 2020. Assessment of bias in pan-tropical biomass predictions. Front. For. Glob. CHANGE 3.

Burt, A., Disney, M. & Calders, K. (2019) Extracting individual trees from lidar point clouds using treeseg. Methods in Ecology and Evolution. 10 (3), 438–445.

Calders, K., Adams, J., Armston, J., Bartholomeus, H., Bauwens, S., Bentley, L.P., Chave, J., Danson, F.M., Demol, M., Disney, M., Gaulton, R., Krishna Moorthy, S.M., Levick, S.R., Saarinen, N., Schaaf, C., Stovall, A., Terryn, L., Wilkes, P., Verbeeck, H., 2020. Terrestrial laser scanning in forest ecology: Expanding the horizon. Remote Sens. Environ. 251, 112102.

Calders, K., Burt, A., Origo, N., Disney, M.I., Nightingale, J., Raumonen, P., Lewis, P.E., 2016. Large-Area Virtual Forests Fromterrestrial Laser Scanning Data 1765–1767.

Calders, K., Newnham, G., Burt, A., Murphy, S., Raumonen, P., Herold, M., Culvenor, D., Avitabile, V., Disney, M., Armston, J. & Kaasalainen, M. (2015) Nondestructive estimates of above-ground biomass using terrestrial laser scanning. Methods in Ecology and Evolution. 6 (2), 198–208.

Calders, K., Origo, N., Burt, A., Disney, M., Nightingale, J., Raumonen, P., Åkerblom, M., Malhi, Y., Lewis, P., 2018. Realistic Forest Stand Reconstruction from Terrestrial LiDAR for Radiative Transfer Modelling. Remote Sensing 10, 933.

Calders, K., Origo, N., Disney, M., Nightingale, J., Woodgate, W., Armston, J. & Lewis, P. (2018) Variability and bias in active and passive ground-based measurements of effective plant, wood and leaf area index. Agricultural and Forest Meteorology. 252231–240.

Camarero, J.J., Gazol, A., Sangüesa-Barreda, G., Oliva, J., Vicente-Serrano, S.M., 2015. To die or not to die: Early warnings of tree dieback in response to a severe drought. Journal of Ecology 103, 44–57.

Canham, C.D., Coates, K.D., Bartemucci, P., Quaglia, S., 1999. Measurement and modeling of spatially explicit variation in light transmission through interior cedar-hemlock forests of British Columbia. Canadian Journal of Forest Research.

Canham, C.D., LePage, P.T. & Coates, K.D. (2004) A neighborhood analysis of canopy tree competition: effects of shading versus crowding. Canadian Journal of Forest Research. 34 (4), 778–787.

Carnicer, J., Barbeta, A., Sperlich, D., Coll, M. & Peñuelas, J. (2013) Contrasting trait syndromes in angiosperms and conifers are associated with different responses of tree growth to temperature on a large scale. Frontiers in Plant Science. 4.

Carnicer, J., Coll, M., Ninyerola, M., Pons, X., Sanchez, G., Penuelas, J., 2011. Widespread crown condition decline, food web disruption, and amplified tree mortality with increased climate change-type drought. Proceedings of the National Academy of Sciences 108, 1474–1478.

Carrière, S.D., Ruffault, J., Cakpo, C.B., Olioso, A., Doussan, C., Simioni, G., Chalikakis, K., Patris, N., Davi, H., MartinSt-Paul, N.K., 2020. Intra-specific variability in deep water extraction between trees growing on a Mediterranean karst. Journal of Hydrology 590, 125428.

Carvalhais, N., Forkel, M., Khomik, M., Bellarby, J., Jung, M., Migliavacca, M., Mu, M., Saatchi, S., Santoro, M., Thurner, M., Weber, U., Ahrens, B., Beer, C., Cescatti, A., Randerson, J.T., Reichstein, M., 2014. Global covariation of carbon turnover times with climate in terrestrial ecosystems. Nature 514, 213–217.

Castro-Díez, P., Villar-Salvador, P., Pérez-Rontomé, C., Maestro-Martínez, M. & Montserrat-Martí, G. (1997) Leaf morphology and leaf chemical composition in three Quercus (Fagaceae) species along a rainfall gradient in NE Spain. Trees. 11 (3), 127–134.
Castro-Díez, P., Villar-Salvador, P., Pérez-Rontomé, C., Maestro-Martínez, M. & Montserrat-Martí, G. (1997) Leaf morphology and leaf chemical composition in three Quercus (Fagaceae) species along a rainfall gradient in NE Spain. Trees. 11 (3), 127–134.
Castro, J., Zamora, R., Hódar, J.A. & Gómez, J.M. (2004) Seedling establishment of a boreal tree species (Pinus sylvestris) at its southernmost distribution limit: consequences of being in a marginal Mediterranean habitat. Journal of Ecology. 92 (2), 266–277.

Cattaneo, N., Schneider, R., Bravo, F., Bravo-Oviedo, A., 2020. Inter-specific competition of tree congeners induces changes in crown architecture in Mediterranean pine mixtures. For. Ecol. Manag. 476, 118471.

Charbonnier, F., le Maire, G., Dreyer, E., Casanoves, F., Christina, M., Dauzat, J., Eitel, J.U.H., Vaast, P., Vierling, L.A., Roupsard, O., 2013. Competition for light in heterogeneous canopies: Application of MAESTRA to a coffee (Coffea arabica L.) agroforestry system. Agricultural and Forest Meteorology 181, 152–169.

Chen, J.M., Mo, G., Pisek, J., Liu, J., Deng, F., Ishizawa, M., Chan, D., 2012. Effects of foliage clumping on the estimation of global terrestrial gross primary productivity. Global Biogeochemical Cycles 26.

Chen, Y., Wright, S.J., Muller-Landau, H.C., Hubbell, S.P., Wang, Y., Yu, S., 2016. Positive effects of neighborhood complementarity on tree growth in a Neotropical forest. Ecology 97, 776–785.

Chitra-Tarak, R., Xu, C., Aguilar, S., Anderson-Teixeira, K.J., Chambers, J., Detto, M., Faybishenko, B., Fisher, R.A., Knox, R.G., Koven, C.D., Kueppers, L.M., Kunert, N., Kupers, S.J., McDowell, N.G., Newman, B.D., Paton, S.R., Pérez, R., Ruiz, L., Sack, L., Warren, J.M., Wolfe, B.T., Wright, C., Wright, S.J., Zailaa, J., McMahon, S.M., 2021. Hydraulically-vulnerable trees survive on deep-water access during droughts in a tropical forest. New Phytologist.

Chitra-Tarak, R., Ruiz, L., Dattaraja, H.S., Kumar, M.S.M., Riotte, J., Suresh, H.S., McMahon, S.M., Sukumar, R., 2018. The roots of the drought: Hydrology and water uptake strategies mediate forest-wide demographic response to precipitation. Journal of Ecology 106, 1495–1507.

Christidis, N., Jones, G.S., Stott, P.A., 2015. Dramatically increasing chance of extremely hot summers since the 2003 European heatwave. Nature Climate Change 5, 46–50.

Cloud Compare, 2021. Available at - https://www.danielgm.net/cc/

Coates, K.D., Canham, C.D. & LePage, P.T. 2009. Above- versus below-ground competitive effects and responses of a guild of temperate tree species. Journal of Ecology. 97 (1), 118–130.

Cochard, H., Bréda, N. & Granier, A. 1996. Whole tree hydraulic conductance and water loss regulation in Quercus during drought: evidence for stomatal control of embolism? Annales des Sciences Forestières. 53 (2–3), 197–206.

Coll, L., Camarero, J.J. & Aragón, J.M.D. 2012. Fine root seasonal dynamics, plasticity, and mycorrhization in 2 coexisting Mediterranean oaks with contrasting aboveground phenology. Écoscience. 19 (3), 238–245.

Condés, S., Aguirre, A. & del Río, M. 2020. Crown plasticity of five pine species in response to competition along an aridity gradient. Forest Ecology and Management. 473118302.

Coomes, D.A. (2006) Challenges to the generality of WBE theory. Trends in Ecology & Evolution. 21 (11), 593–596.

Coomes, D.A., Allen, R.B., 2007. Effects of size, competition and altitude on tree growth. J. Ecol. 95, 1084–1097.

Coomes, D.A., Allen, R.B., 2009. Testing the Metabolic Scaling Theory of tree growth. Journal of Ecology 97, 1369–1373.

Coomes, D.A., Flores, O., Holdaway, R., Jucker, T., Lines, E.R. and Vanderwel, M.C., 2014. Wood production response to climate change will depend critically on forest composition and structure. Global change biology, 20 (12).

Coomes, D.A., Holdaway, R.J., Kobe, R.K., Lines, E.R., Allen, R.B., 2012. A general integrative framework for modelling woody biomass production and carbon sequestration rates in forests. Journal of Ecology 100, 42–64.

Coomes, D.A., Šafka, D., Shepherd, J., Dalponte, M., Holdaway, R., 2018. Airborne laser scanning of natural forests in New Zealand reveals the influences of wind on forest carbon. Forest Ecosystems 5, 1–14.

Coops, N.C., Hilker, T., Wulder, M.A., St-Onge, B., Newnham, G., Siggins, A., Trofymow, J.A., 2007. Estimating canopy structure of Douglas-fir forest stands from discrete-return LiDAR. Trees - Structure and Function 21, 295–310.

Coops, N.C., Tompaski, P., Nijland, W., Rickbeil, G.J.M., Nielsen, S.E., Bater, C.W. & Stadt, J.J. 2016. A forest structure habitat index based on airborne laser scanning data. Ecological Indicators. 67346–357.

Corcuera, L., Camarero, J.J. & Gil-Pelegrín, E. 2004. Effects of a severe drought on Quercus ilex radial growth and xylem anatomy. Trees - Structure and Function. 18 (1), 83–92.

Costanza, R., de Groot, R., Sutton, P., van der Ploeg, S., Anderson, S.J., Kubiszewski, I., Farber, S., Turner, R.K., 2014. Changes in the global value of ecosystem services. Global Environmental Change 26, 152–158.

Côté, J.-F., Widlowski, J.-L., Fournier, R.A., Verstraete, M.M., 2009. The structural and radiative consistency of three-dimensional tree reconstructions from terrestrial lidar. Remote Sensing of Environment 113, 1067–1081.

Coutand, C., Dupraz, C., Jaouen, G., Ploquin, S., Adam, B., 2008. Mechanical Stimuli Regulate the Allocation of Biomass in Trees: Demonstration with Young Prunus avium Trees. Annals of Botany 101, 1421–1432.

Craine, J.M. & Dybzinski, R. 2013. Mechanisms of plant competition for nutrients, water and light. Functional Ecology. 27 (4), 833–840.

Crowther, T.W., Glick, H.B., Covey, K.R., Bettigole, C., Maynard, D.S., Thomas, S.M., Smith, J.R., Hintler, G., Duguid, M.C., Amatulli, G., Tuanmu, M.N., Jetz, W., Salas, C., Stam, C., Piotto, D., Tavani, R., Green, S., Bruce, G., Williams, S.J., Wiser, S.K., Huber, M.O., Hengeveld, G.M., Nabuurs, G.J., Tikhonova, E., Borchardt, P., Li, C.F., Powrie, L.W., Fischer, M., Hemp, A., Homeier, J., Cho, P., Vibrans, A.C., Umunay,

P.M., Piao, S.L., Rowe, C.W., Ashton, M.S., Crane, P.R., Bradford, M.A., 2015. Mapping tree density at a global scale. Nature 525, 201–205.

Cubera, E. & Moreno, G. 2007. Effect of single Quercus ilex trees upon spatial and seasonal changes in soil water content in dehesas of central western Spain. Annals of Forest Science. 64 (3), 355–364.

Cui, L., Jiao, Z., Zhao, K., Sun, M., Dong, Y., Yin, S., Li, Y., Chang, Y., Guo, J., Xie, R., Zhu, Z., Li, S., 2020. Retrieval of Vertical Foliage Profile and Leaf Area Index Using Transmitted Energy Information Derived from ICESat GLAS Data. Remote Sensing 12, 2457.

Curtis, P.G., Slay, C.M., Harris, N.L., Tyukavina, A., Hansen, M.C., 2018. Classifying drivers of global forest loss. Science 361, 1108–1111.

Dai, A., 2013. Increasing drought under global warming in observations and models. Nature Climate Change 3, 52–58.

Dai, X., Jia, X., Zhang, W., Bai, Y., Zhang, J., Wang, Y. & Wang, G. 2009. Plant height–crown radius and canopy coverage–density relationships determine above-ground biomass–density relationship in stressful environments. Biology Letters. 5 (4), 571–573.

Danson, F.M., Hetherington, D., Morsdorf, F., Koetz, B., Allgower, B., 2007. Forest Canopy Gap Fraction From Terrestrial Laser Scanning. IEEE Geosci. Remote Sens. Lett. 4, 157–160.

Dassot, M., Constant, T., Fournier, M., 2011. The use of terrestrial LiDAR technology in forest science: Application fields, benefits and challenges. Ann. For. Sci. 68, 959–974.

David, T.S., Henriques, M.O., Kurz-Besson, C., Nunes, J., Valente, F., Vaz, M., Pereira, J.S., Siegwolf, R., Chaves, M.M., Gazarini, L.C. & David, J.S. (2007) Water-use strategies in two co-occurring Mediterranean evergreen oaks: Surviving the summer drought. Tree Physiology. 27 (6), 793–803.

Davies, A.B., Asner, G.P., 2014. Advances in animal ecology from 3D-LiDAR ecosystem mapping. Trends in Ecology and Evolution 29, 681–691.

Dawson, T.E. 1996. Determining water use by trees and forests from isotopic, energy balance and transpiration analyses: the roles of tree size and hydraulic lift. Tree Physiology. 16 (1–2), 263–272.

Dawson, T.E., Hahm, W.J., Crutchfield-Peters, K., 2020. Digging deeper: what the critical zone perspective adds to the study of plant ecophysiology. New Phytologist 226, 666–671.

del Castillo, J., Comas, C., Voltas, J. & Ferrio, J.P. 2016. Dynamics of competition over water in a mixed oak-pine Mediterranean forest: Spatio-temporal and physiological components. Forest Ecology and Management. 382214–224.

del Río, M., Bravo-Oviedo, A., Ruiz-Peinado, R. & Condés, S. 2019. Tree allometry variation in response to intra- and inter-specific competitions. Trees. 33 (1), 121–138.

Devireddy, A.R., Zandalinas, S.I., Gómez-Cadenas, A., Blumwald, E., Mittler, R., 2018. Coordinating the overall stomatal response of plants: Rapid leaf-to-leaf communication during light stress. Sci. Signal. 11.

Dieler, J. & Pretzsch, H. 2013. Morphological plasticity of European beech (Fagus sylvatica L.) in pure and mixed-species stands. Forest Ecology and Management. 29597–108.

Disney, M. 2019. Terrestrial LiDAR: a three-dimensional revolution in how we look at trees. New Phytologist. 222 (4), 1736–1741.

Disney, M., Burt, A., Wilkes, P., Armston, J., Duncanson, L., 2020. New 3D measurements of large redwood trees for biomass and structure. Sci. Rep. 10, 16721.

Disney, M.I., Boni Vicari, M., Burt, A., Calders, K., Lewis, S.L., Raumonen, P., Wilkes, P., 2018. Weighing trees with lasers: advances, challenges and opportunities. Interface Focus 8, 20170048. https://doi.org/10.1098/rsfs.2017.0048

Dolezal, J., Jandova, V., Macek, M. & Liancourt, P. 2021. Contrasting biomass allocation responses across ontogeny and stress gradients reveal plant adaptations to drought and cold. Functional Ecology. 35 (1), 32–42.

Domingo, J., Zavala, M.A. & Madrigal-González, J. 2019. Thinning enhances stool resistance to an extreme drought in a Mediterranean Quercus ilex L. coppice: insights for adaptation. New Forests.

Donager, J.J., Sánchez Meador, A.J., Blackburn, R.C., 2021. Adjudicating Perspectives on Forest Structure: How Do Airborne, Terrestrial, and Mobile Lidar-Derived Estimates Compare? Remote Sensing 13, 2297.

Dorji, Y., Annighöfer, P., Ammer, C. & Seidel, D. 2019. Response of Beech (Fagus sylvatica L.) Trees to Competition—New Insights from Using Fractal Analysis. Remote Sensing. 11 (22), 2656.

Duarte, M.M., Moral, R. de A., Guillemot, J., Zuim, C.I.F., Potvin, C., Bonat, W.H., Stape, J.L., Brancalion, P.H.S., 2021. High tree diversity enhances light interception in tropical forests. Journal of Ecology.

Dubayah, R., Blair, J.B., Goetz, S., Fatoyinbo, L., Hansen, M., Healey, S., Hofton, M., Hurtt, G., Kellner, J., Luthcke, S., Armston, J., Tang, H., Duncanson, L., Hancock, S., Jantz, P., Marselis, S., Patterson, P.L., Qi, W., Silva, C., 2020. The Global Ecosystem Dynamics Investigation: High-resolution laser ranging of the Earth's forests and topography. Science of Remote Sensing 1, 100002.

Duchemin, L., Eloy, C., Badel, E., Moulia, B., 2018. Tree crowns grow into self-similar shapes controlled by gravity and light sensing. Journal of The Royal Society Interface 15, 20170976.

Duncanson, L., Dubayah, R., 2018. Monitoring individual tree-based change with airborne lidar. Ecology and Evolution 8, 5079–5089.

Duncanson, L., Neuenschwander, A., Hancock, S., Thomas, N., Fatoyinbo, T., Simard, M., Silva, C.A., Armston, J., Luthcke, S.B., Hofton, M., Kellner, J.R., Dubayah, R., 2020. Biomass estimation from simulated GEDI, ICESat-2 and NISAR across environmental gradients in Sonoma County, California. Remote Sensing of Environment 242, 111779.

Duursma, R.A. & Falster, D.S. 2016. Leaf mass per area, not total leaf area, drives differences in above-ground biomass distribution among woody plant functional types. New Phytologist. 212 (2), 368–376.

Duursma, R.A., Makela, A., 2007. Summary models for light interception and light-use efficiency of non-homogeneous canopies. Tree Physiol. 27, 859–870.

Duursma, R.A., Mäkelä, A., Reid, D.E.B., Jokela, E.J., Porté, A.J., Roberts, S.D., 2010. Self-shading affects allometric scaling in trees. Functional Ecology 24, 723–730.

Ehbrecht, M., Schall, P., Ammer, C., Seidel, D., 2017. Quantifying stand structural complexity and its relationship with forest management, tree species diversity and microclimate. Agricultural and Forest Meteorology 242, 1–9.

Eichhorn, M.P., Ryding, J., Smith, M.J., Gill, R.M.A., Siriwardena, G.M., Fuller, R.J., 2017. Effects of deer on woodland structure revealed through terrestrial laser scanning. J. Appl. Ecol. 54, 1615–1626.

Enquist, B.J. (2002) Universal scaling in tree and vascular plant allometry: toward a general quantitative theory linking plant form and function from cells to ecosystems. Tree Physiology. 22 (15–16), 1045–1064.

Enquist, B.J., West, G.B. & Brown, J.H. (2009) Extensions and evaluations of a general quantitative theory of forest structure and dynamics. Proceedings of the National Academy of Sciences. 106 (17), 7046–7051.

Escudero, A., del Río, T., Sánchez-Zulueta, P. & Mediavilla, S. 2017. Ontogenetic changes in crown architecture and leaf arrangement: effects on light capture efficiency in three tree species differing in leaf longevity. Ecological Research. 32 (4), 595–602.

Estornell, J., Velázquez-Martí, B., Fernández-Sarría, A., Martí, J., 2018. Lidar methods for measurement of trees in urban forests. J. Appl. Remote Sens. 12, 046009.

Fajardo, A., Martínez-Pérez, C., Cervantes-Alcayde, M.A. & Olson, M.E. 2020. Stem length, not climate, controls vessel diameter in two trees species across a sharp precipitation gradient. New Phytologist. 225 (6), 2347–2355.

Fajardo, A., McIntire, E.J. and Olson, M.E., 2019. When short stature is an asset in trees. Trends in ecology & evolution, 34(3), pp.193-199.

Falkowski, M.J., Evans, J.S., Martinuzzi, S., Gessler, P.E., Hudak, A.T., 2009. Characterizing forest succession with lidar data: An evaluation for the Inland Northwest, USA. Remote Sensing of Environment 113, 946–956.

Falster, D.S., Westoby, M., 2003. Leaf size and angle vary widely across species: what consequences for light interception? New Phytologist 158, 509–525.

Fan, Y., Miguez-Macho, G., Jobbágy, E.G., Jackson, R.B., Otero-Casal, C., 2017. Hydrologic regulation of plant rooting depth. Proc Natl Acad Sci USA 114, 10572–10577.

Fang, H., Baret, F., Plummer, S., Schaepman-Strub, G., 2019. An Overview of Global Leaf Area Index (LAI): Methods, Products, Validation, and Applications. Reviews of Geophysics 57, 739–799.

Fei, S., Morin, R.S., Oswalt, C.M., Liebhold, A.M., 2019. Biomass losses resulting from insect and disease invasions in US forests. PNAS 116, 17371–17376.

Fichtner, A., Schnabel, F., Bruelheide, H., Kunz, M., Mausolf, K., Schuldt, A., Härdtle, W., Oheimb, G. von, 2020. Neighbourhood diversity mitigates drought impacts on tree growth. Journal of Ecology 108, 865–875.

Field, C.B., Behrenfeld, M.J., Randerson, J.T., Falkowski, P., 1998. Primary Production of the Biosphere: Integrating Terrestrial and Oceanic Components. Science 281, 237–240.

Fischer, F.J., Maréchaux, I. & Chave, J. 2019. Improving plant allometry by fusing forest models and remote sensing. New Phytologist. 223 (3), 1159–1165.

Fisher, R.A., Koven, C.D., Anderegg, W.R.L., Christoffersen, B.O., Dietze, M.C., Farrior, C.E., Holm, J.A., Hurtt, G.C., Knox, R.G., Lawrence, P.J., Lichstein, J.W., Longo, M., Matheny, A.M., Medvigy, D., Muller-Landau, H.C., Powell, T.L., Serbin, S.P., Sato, H., Shuman, J.K., Smith, B., Trugman, A.T., Viskari, T., Verbeeck, H., Weng, E., Xu, C., Xu, X., Zhang, T., Moorcroft, P.R., 2018. Vegetation demographics in Earth System Models: A review of progress and priorities. Global Change Biology 24, 35–54.

Fleck, S., Mölder, I., Jacob, M., Gebauer, T., Jungkunst, H.F., Leuschner, C., 2011. Comparison of conventional eight-point crown projections with LIDAR-based virtual crown projections in a temperate old-growth forest. Ann. For. Sci. 7, 1173–1185.

Forner, A., Aranda, I., Granier, A. & Valladares, F. 2014. Differential impact of the most extreme drought event over the last half century on growth and sap flow in two coexisting Mediterranean trees. Plant Ecology. 215 (7), 703–719.

Forner, A., Aranda, I., Granier, A., Valladares, F., 2014. Differential impact of the most extreme drought event over the last half century on growth and sap flow in two coexisting Mediterranean trees. Plant Ecology 215, 703–719.

Forner, A., Morán-López, T., Flores-Rentería, D., Aranda, I. & Valladares, F. 2020. Fragmentation reduces severe drought impacts on tree functioning in holm oak forests. Environmental and Experimental Botany. 104001.

Forner, A., Valladares, F. & Aranda, I. 2018. Mediterranean trees coping with severe drought: Avoidance might not be safe. Environmental and Experimental Botany. 155529–540.

Forner, A., Valladares, F., Bonal, D., Granier, A., Grossiord, C. & Aranda, I. 2018. Extreme droughts affecting Mediterranean tree species' growth and water-use efficiency: the importance of timing. Tree Physiology.

Forrester, D.I., Benneter, A., Bouriaud, O. & Bauhus, J. 2017. Diversity and competition influence tree allometric relationships – developing functions for mixed-species forests. Journal of Ecology. 105 (3), 761–774.

Fotis, A.T. & Curtis, P.S. 2017. Effects of structural complexity on within-canopy light environments and leaf traits in a northern mixed deciduous forest. Tree Physiology. 37 (10), 1426–1435.

Fotis, A.T., Morin, T.H., Fahey, R.T., Hardiman, B.S., Bohrer, G., Curtis, P.S., 2018. Forest structure in space and time: Biotic and abiotic determinants of canopy complexity and their effects on net primary productivity. Agricultural and Forest Meteorology 250–251, 181–191.

Frank, D.A., Pontes, A.W., Maine, E.M., Caruana, J., Raina, R., Raina, S., Fridley, J.D., 2010. Grassland root communities: species distributions and how they are linked to aboveground abundance. Ecology 91, 3201–3209.

Franklin, J., Buckley, D., 2019. Influence of Microtopography and Soil Treatments on Tree Establishment on a Reclaimed Quarry. Forests 10, 597.

Fransson, P., Brännström, Å. & Franklin, O. 2021. A tree's quest for light—optimal height and diameter growth under a shading canopy. Tree Physiology. 41 (1), 1–11.

Fraver, S., D'Amato, A.W., Bradford, J.B., Jonsson, B.G., Jönsson, M. & Esseen, P.-A. 2014. Tree growth and competition in an old-growth Picea abies forest of boreal Sweden: influence of tree spatial patterning. Journal of Vegetation Science. 25 (2), 374–385.

Freckleton, R.P., Watkinson, A.R., 2001. Asymmetric competition between plant species. Funct. Ecol. 15, 615–623.

Fridley, J.D. 2012. Extended leaf phenology and the autumn niche in deciduous forest invasions. Nature. 485 (7398), 359–362.

Fry, D.L., Stephens, S.L., Collins, B.M., North, M.P., Franco-Vizcaíno, E., Gill, S.J., 2014. Contrasting spatial patterns in active-fire and fire-suppressed mediterranean climate old-growth mixed conifer forests. PLoS ONE 9.

Gamfeldt, L., Snäll, T., Bagchi, R., Jonsson, M., Gustafsson, L., Kjellander, P., Ruiz-Jaen, M.C., Fröberg, M., Stendahl, J., Philipson, C.D., Mikusiński, G., Andersson, E., Westerlund, B., Andrén, H., Moberg, F., Moen, J., Bengtsson, J., 2013. Higher levels of multiple ecosystem services are found in forests with more tree species. Nat Commun 4, 1340.

Garrigues, S., Lacaze, R., Baret, F., Morisette, J.T., Weiss, M., Nickeson, J.E., Fernandes, R., Plummer, S., Shabanov, N.V., Myneni, R.B., Knyazikhin, Y., Yang, W., 2008. Validation and intercomparison of global Leaf Area Index products derived from remote sensing data. Journal of Geophysical Research: Biogeosciences 113.

Gauthier, S., Bernier, P., Kuuluvainen, T., Shvidenko, A.Z., Schepaschenko, D.G., 2015. Boreal forest health and global change. Science 349, 819–822.

Gea-Izquierdo, G., Aranda, I., Cañellas, I., Dorado-Liñán, I., Olano, J.M., Martin-Benito, D., 2020. Contrasting species decline but high sensitivity to increasing water stress on a mixed pine–oak ecotone. Journal of Ecology.

Getis, A., Ord, J.K., 1991. The Analysis of Spatial Association by Use of Distance Statistics. Geogr. Anal. 24, 189–206.

Getis, A., Ord, J.K., 2010. The Analysis of Spatial Association by Use of Distance Statistics, in: Anselin, L., Rey, S.J. (Eds.), Perspectives on Spatial Data Analysis, Advances in Spatial Science. Springer, Berlin, Heidelberg, pp. 127–145.

Gill, S.J., Biging, G.S., Murphy, E.C., 2000. Modeling conifer tree crown radius and estimating canopy cover. For. Ecol. Manag. 126, 405–416.

Givnish, T. 1988. Adaptation to Sun and Shade: a Whole-Plant Perspective. Functional Plant Biology. 15 (2), 63.

Gollob, C., Ritter, T., Nothdurft, A., 2020. Forest Inventory with Long Range and High-Speed Personal Laser Scanning (PLS) and Simultaneous Localization and Mapping (SLAM) Technology. Remote Sensing 12, 1509.

Gombin, J., Vaidyanathan, R., Agafonkin, V., 2020. concaveman: A Very Fast 2D Concave Hull Algorithm.

Gómez-Aparicio, L., García-Valdés, R., Ruíz-Benito, P., Zavala, M.A., 2011. Disentangling the relative importance of climate, size and competition on tree growth in Iberian forests: implications for forest management under global change. Glob. Change Biol. 17, 2400–2414.

Gómez, C., White, J.C., Wulder, M.A., Alejandro, P., 2014. Historical forest biomass dynamics modelled with Landsat spectral trajectories. ISPRS Journal of Photogrammetry and Remote Sensing 93, 14–28.

Gough, C.M., Atkins, J.W., Fahey, R.T., Hardiman, B.S., 2019. High rates of primary production in structurally complex forests. Ecology 100, e02864.

Gough, C.M., Atkins, J.W., Fahey, R.T., Hardiman, B.S., LaRue, E.A., 2020. Community and structural constraints on the complexity of eastern North American forests. Global Ecology and Biogeography 29, 2107–2118.

Granda, E., Camarero, J.J., Gimeno, T.E., Martínez-Fernández, J. & Valladares, F. (2013) Intensity and timing of warming and drought differentially affect growth patterns of co-occurring Mediterranean tree species. European Journal of Forest Research. 132 (3), 469–480.

Greiser, C., Ehrlén, J., Meineri, E., Hylander, K., 2020. Hiding from the climate: Characterizing microrefugia for boreal forest understory species. Global Change Biology 26, 471–483.

Groover, A., 2016. Gravitropisms and reaction woods of forest trees – evolution, functions and mechanisms. New Phytologist 211, 790–802.

Grossiord, C., 2019. Having the right neighbors: how tree species diversity modulates drought impacts on forests. New Phytologist 0.

Grossiord, C., Forner, A., Gessler, A., Granier, A., Pollastrini, M., Valladares, F. & Bonal, D. 2015. Influence of species interactions on transpiration of Mediterranean tree species during a summer drought. European Journal of Forest Research. 134 (2), 365–376.

Grossiord, C., Granier, A., Gessler, A., Jucker, T. & Bonal, D. 2014. Does Drought Influence the Relationship Between Biodiversity and Ecosystem Functioning in Boreal Forests? Ecosystems. 17 (3), 394–404.

Grossiord, C., Granier, A., Gessler, A., Jucker, T., Bonal, D., 2014. Does Drought Influence the Relationship Between Biodiversity and Ecosystem Functioning in Boreal Forests? Ecosystems 17, 394–404.

Grossiord, C., Granier, A., Ratcliffe, S., Bouriaud, O., Bruelheide, H., Checko, E., Forrester, D.I., Dawud, S.M., Finer, L., Pollastrini, M., Scherer-Lorenzen, M., Valladares, F., Bonal, D., Gessler, A., 2014. Tree diversity does not always improve resistance of forest ecosystems to drought. Proceedings of the National Academy of Sciences 111, 14812–14815.

Grote, R., 2003. Estimation of crown radii and crown projection area from stem size and tree position. Ann. For. Sci. 60, 393–402.

Grote, R., Kraus, D., Weis, W., Ettl, R. & Göttlein, A. (2020) Dynamic coupling of allometric ratios to a process-based forest growth model for estimating the impacts of stand density changes. Forestry: An International Journal of Forest Research.

Gruntman, M., Groß, D., Májeková, M., Tielbörger, K., 2017. Decision-making in plants under competition. Nat. Commun. 8, 2235.

Gschwantner, T., Schadauer, K., Vidal, C., Lanz, A., Tomppo, E., di Cosmo, L., Robert, N., Englert Duursma, D., Lawrence, M., 2009. Common tree definitions for National Forest Inventories in Europe.

Guillemot, J., Kunz, M., Schnabel, F., Fichtner, A., Madsen, C.P., Gebauer, T., Härdtle, W., Oheimb, G. von, Potvin, C., 2020. Neighbourhood-mediated shifts in tree biomass allocation drive overyielding in tropical species mixtures. New Phytol. 228, 1256–1268.

Guiot, J., Cramer, W., 2016. Climate change: The 2015 Paris Agreement thresholds and Mediterranean basin ecosystems. Science 354, 465–468.

Guzmán, J.Q.A., Sharp, I., Alencastro, F., Sánchez-Azofeifa, G.A., 2020. On the relationship of fractal geometry and tree–stand metrics on point clouds derived from terrestrial laser scanning. Methods Ecol. Evol. 11, 1309–1318.

Hackenberg, J., Spiecker, H., Calders, K., Disney, M., Raumonen, P., 2015. SimpleTree - An efficient open source tool to build tree models from TLS clouds. Forests 6, 4245–4294.

Hagemeier, M., Leuschner, C., 2019. Functional Crown Architecture of Five Temperate Broadleaf Tree Species: Vertical Gradients in Leaf Morphology, Leaf Angle, and Leaf Area Density. Forests 10, 265.

Hale, S.E., Gardiner, B.A., Wellpott, A., Nicoll, B.C., Achim, A., 2012. Wind loading of trees: Influence of tree size and competition. European Journal of Forest Research 131, 203–217.

Halle, F., Oldeman, R.A.A., Tomlinson, P.B., 1978. Tropical Trees and Forests: An Architectural Analysis. Springer-Verlag, Berlin Heidelberg.

Halupka, K., Garnavi, R., Moore, S., 2019. Deep Semantic Instance Segmentation of Tree-Like Structures Using Synthetic Data, in: 2019 IEEE Winter Conference on Applications of Computer Vision (WACV). Presented at the 2019 IEEE Winter Conference on Applications of Computer Vision (WACV), IEEE, Waikoloa Village, HI, USA, pp. 1713–1722.

Hancock, S., Anderson, K., Disney, M., Gaston, K.J., 2017. Measurement of fine-spatial-resolution 3D vegetation structure with airborne waveform lidar: Calibration and validation with voxelised terrestrial lidar. Remote Sensing of Environment 188, 37–50.

Hansen, M.C., Potapov, P.V., Moore, R., Hancher, M., Turubanova, S.A., Tyukavina, A., Thau, D., Stehman, S.V., Goetz, S.J., Loveland, T.R., Kommareddy, A., Egorov, A., Chini, L., Justice, C.O., Townshend, J.R.G., 2013. High-resolution global maps of 21st-century forest cover change. Science 342, 850–853.

Harja, D., Vincent, G., Mulia, R. & van Noordwijk, M. 2012. Tree shape plasticity in relation to crown exposure. Trees. 26 (4), 1275–1285.

Harja, D., Vincent, G., Mulia, R., van Noordwijk, M., 2012. Tree shape plasticity in relation to crown exposure. Trees 26, 1275–1285.

Harris, N.L., Goldman, E., Gabris, C., Nordling, J., Minnemeyer, S., Ansari, S., Lippmann, M., Bennett, L., Raad, M., Hansen, M., Potapov, P., 2017. Using spatial statistics to identify emerging hot spots of forest loss. Environ. Res. Lett. 12, 024012.

Hastings, J.H., Ollinger, S.V., Ouimette, A.P., Sanders-DeMott, R., Palace, M.W., Ducey, M.J., Sullivan, F.B., Basler, D., Orwig, D.A., 2020. Tree Species Traits Determine the Success of LiDAR-Based Crown Mapping in a Mixed Temperate Forest. Remote Sensing 12, 309.

Hecht, R., Meinel, G., Buchroithner, M.F., 2008. Estimation of Urban Green Volume Based on Single-Pulse LiDAR Data. IEEE Trans. Geosci. Remote Sens. 46, 3832–3840.

Heinzel, J., Huber, M.O., 2018. Constrained spectral clustering of individual trees in dense forest using terrestrial laser scanning data. Remote Sens. 10.

Henry, H. a. L., Aarssen, L.W., 1999. The interpretation of stem diameter–height allometry in trees: biomechanical constraints, neighbour effects, or biased regressions? Ecology Letters 2, 89–97.

Henry, H.A.L. & Aarssen, L.W. 1997. On the Relationship between Shade Tolerance and Shade Avoidance Strategies in Woodland Plants. Oikos. 80 (3), 575–582.

Henry, H.A.L. & Aarssen, L.W. 2001. Inter- and intraspecific relationships between shade tolerance and shade avoidance in temperate trees. Oikos. 93 (3), 477–487.

Hess, C., Härdtle, W., Kunz, M., Fichtner, A., von Oheimb, G., 2018. A high-resolution approach for the spatiotemporal analysis of forest canopy space using terrestrial laser scanning data. Ecol. Evol. 8, 6800–6811.

Honda, H., 1971. Description of the form of trees by the parameters of the tree-like body: Effects of the branching angle and the branch length on the shape of the tree-like body. J. Theor. Biol. 31, 331–338.

Hooper, D.U., Chapin, F.S., Ewel, J.J., Hector, A., Inchausti, P., Lavorel, S., Lawton, J.H., Lodge, D.M., Loreau, M., Naeem, S., Schmid, B., Setälä, H., Symstad, A.J., Vandermeer, J. & Wardle, D.A. (2005) Effects of Biodiversity on Ecosystem Functioning: A Consensus of Current Knowledge. Ecological Monographs. 75 (1), 3–35.

Hopkinson, C., Chasmer, L., 2009. Testing LiDAR models of fractional cover across multiple forest ecozones. Remote Sensing of Environment 113, 275–288.

Horn, H.S., 1971. The Adaptive Geometry of Trees. Princeton University Press.

Houghton, R.A., Hall, F., Goetz, S.J., 2009. Importance of biomass in the global carbon cycle. J. Geophys. Res. Biogeosciences 114.

Huang, X., Ziniti, B., Torbick, N., Ducey, M.J., 2018. Assessment of Forest above Ground Biomass Estimation Using Multi-Temporal C-band Sentinel-1 and Polarimetric L-band PALSAR-2 Data. Remote Sensing 10, 1424.

Huang, Z., Huang, X., Fan, J., Eichhorn, M.P., An, F., Chen, B., Cao, L., Zhu, Z., Yun, T., 2020. Retrieval of Aerodynamic Parameters in Rubber Tree Forests Based on the Computer Simulation Technique and Terrestrial Laser Scanning Data. Remote Sensing 12, 1318.

Hynynen, J., Ojansuu, R., 2011. Impact of plot size on individual-tree competition measures for growth and yield simulators. Canadian Journal of Forest Research.

Hyyppä, J., Hyyppä, H., Inkinen, M., Engdahl, M., Linko, S., Zhu, Y.H., 2000. Accuracy comparison of various remote sensing data sources in the retrieval of forest stand attributes. Forest Ecology and Management 128, 109–120.

Irvine, J., Perks, M.P., Magnani, F. & Grace, J. (1998) The response of Pinus sylvestris to drought: stomatal control of transpiration and hydraulic conductance. Tree Physiology. 18 (6), 393–402.

Isbell, F., Craven, D., Connolly, J., Loreau, M., Schmid, B., Beierkuhnlein, C., Bezemer, T.M., Bonin, C., Bruelheide, H., De Luca, E., Ebeling, A., Griffin, J.N., Guo, Q., Hautier, Y., Hector, A., Jentsch, A., Kreyling, J., Lanta, V., Manning, P., Meyer, S.T., Mori, A.S., Naeem, S., Niklaus, P.A., Polley, H.W., Reich, P.B., Roscher, C., Seabloom, E.W., Smith, M.D., Thakur, M.P., Tilman, D., Tracy, B.F., Van Der Putten, W.H., Van Ruijven, J., Weigelt, A., Weisser, W.W., Wilsey, B., Eisenhauer, N., 2015. Biodiversity increases the resistance of ecosystem productivity to climate extremes. Nature 526, 574–577.

Ishii, H.T., Tanabe, S. & Hiura, T. 2004. Exploring the Relationships Among Canopy Structure, Stand Productivity, and Biodiversity of Temperate Forest Ecosystems. Forest Science. 50 (3), 342–355.

Ishii, R. & Higashi, M. 1997. Tree coexistence on a slope: an adaptive significance of trunk inclination. Proceedings of the Royal Society of London. Series B: Biological Sciences. 264 (1378), 133–139.

Jackson, T.D., Sethi, S., Dellwik, E., Angelou, N., Bunce, A., van Emmerik, T., Duperat, M., Ruel, J.-C., Wellpott, A., Van Bloem, S., Achim, A., Kane, B., Ciruzzi, D.M., Loheide II, S.P., James, K., Burcham, D., Moore, J., Schindler, D., Kolbe, S., Wiegmann, K., Rudnicki, M., Lieffers, V.J., Selker, J., Gougherty, A.V., Newson, T., Koeser, A., Miesbauer, J., Samelson, R., Wagner, J., Coomes, D., Gardiner, B., 2020. The motion of trees in the wind: a data synthesis. Biogeosciences Discussions 1–21.

Jackson, T.D., Shenkin, A.F., Majalap, N., Jami, J.B., Sailim, A.B., Reynolds, G., Coomes, D.A., Chandler, C.J., Boyd, D.S., Burt, A., Wilkes, P., Disney, M., Malhi, Y., 2021. The mechanical stability of the world's tallest broadleaf trees. Biotropica 53, 110–120.

Jacobs, M., Rais, A., Pretzsch, H., 2021. How drought stress becomes visible upon detecting tree shape using terrestrial laser scanning (TLS). For. Ecol. Manag. 489, 118975.

Jetz, W., Cavender-Bares, J., Pavlick, R., Schimel, D., Davis, F.W., Asner, G.P., Guralnick, R., Kattge, J., Latimer, A.M., Moorcroft, P., Schaepman, M.E., Schildhauer, M.P., Schneider, F.D., Schrodt, F., Stahl, U., Ustin, S.L., 2016. Monitoring plant functional diversity from space. Nature Plants 2, 16024.

Joffre, R. & Rambal, S. (1993) How Tree Cover Influences the Water Balance of Mediterranean Rangelands. Ecology. 74 (2), 570–582.

Joshi, N., Mitchard, E.T.A., Brolly, M., Schumacher, J., Fernández-Landa, A., Johannsen, V.K., Marchamalo, M., Fensholt, R., 2017. Understanding "saturation" of radar signals over forests. Scientific Reports 7, 3505.

Jourdan, M., Kunstler, G., Morin, X., 2020. How neighbourhood interactions control the temporal stability and resilience to drought of trees in mountain forests. Journal of Ecology 108, 666–677.

Juchheim, J., Ammer, C., Schall, P., Seidel, D., 2017. Canopy space filling rather than conventional measures of structural diversity explains productivity of beech stands. Forest Ecology and Management 395, 19–26.

Jucker, T., Bongalov, B., Burslem, D.F., Nilus, R., Dalponte, M., Lewis, S.L., Phillips, O.L., Qie, L. and Coomes, D.A., 2018. Topography shapes the structure, composition and function of tropical forest landscapes. Ecology letters, 21(7), pp.989-1000.

Jucker, T., Bongalov, B., Burslem, D.F.R.P., Nilus, R., Dalponte, M., Lewis, S.L., Phillips, O.L., Qie, L., Coomes, D.A., 2018. Topography shapes the structure, composition and function of tropical forest landscapes. Ecology Letters.

Jucker, T., Bouriaud, O. & Coomes, D.A. 2015. Crown plasticity enables trees to optimize canopy packing in mixed-species forests. Functional Ecology. 29 (8), 1078–1086.

Jucker, T., Bouriaud, O., Avacaritei, D., Dănilă, I., Duduman, G., Valladares, F., Coomes, D.A., 2014. Competition for light and water play contrasting roles in driving diversity-productivity relationships in Iberian forests. Journal of Ecology 102, 1202–1213.

Jucker, T., Caspersen, J., Chave, J., Antin, C., Barbier, N., Bongers, F., Dalponte, M., van Ewijk, K.Y., Forrester, D.I., Haeni, M., Higgins, S.I., Holdaway, R.J., Iida, Y., Lorimer, C., Marshall, P.L., Momo, S., Moncrieff, G.R., Ploton, P., Poorter, L., Rahman, K.A., Schlund, M., Sonké, B., Sterck, F.J., Trugman, A.T., Usoltsev, V.A., Vanderwel, M.C., Waldner, P., Wedeux, B.M.M., Wirth, C., Wöll, H., Woods, M., Xiang, W., Zimmermann, N.E., Coomes, D.A., 2017. Allometric equations for integrating remote sensing imagery into forest monitoring programmes. Global Change Biology 23, 177–190.

Jump, A.S., Ruiz-Benito, P., Greenwood, S., Allen, C.D., Kitzberger, T., Fensham, R., Martínez-Vilalta, J., Lloret, F., 2017. Structural overshoot of tree growth with climate variability and the global spectrum of drought-induced forest dieback. Global Change Biology 23, 3742–3757.

Jung, S.-E., Kwak, D.-A., Park, T., Lee, W.-K., Yoo, S., 2011. Estimating Crown Variables of Individual Trees Using Airborne and Terrestrial Laser Scanners. Remote Sens. 3, 2346–2363.

Jupp, D.L., Parkin, D.A., Poropat, G.V., Lovell, J.L., 2007. Lidar system and method. US7187452B2.

Kaasalainen, S., Holopainen, M., Karjalainen, M., Vastaranta, M., Kankare, V., Karila, K., Osmanoglu, B., 2015. Combining lidar and synthetic aperture radar data to estimate forest biomass: Status and prospects. Forests 6, 252–270.

Kaasalainen, S., Krooks, A., Liski, J., Raumonen, P., Kaartinen, H., Kaasalainen, M., Puttonen, E., Anttila, K., Mäkipää, R., 2014. Change Detection of Tree Biomass with Terrestrial Laser Scanning and Quantitative Structure Modelling. Remote Sens. 6, 3906–3922.

Kane, V.R., Lutz, J.A., Alina Cansler, C., Povak, N.A., Churchill, D.J., Smith, D.F., Kane, J.T., North, M.P., 2015. Water balance and topography predict fire and forest structure patterns. Forest Ecology and Management 338, 1–13.

Keddy, P.A., 2017. Plant ecology. Cambridge University Press.

Keeley, J.E., Bond, W.J., Bradstock, R.A., Pausas, J.G., Rundel, P.W., 2011. Fire in Mediterranean Ecosystems: Ecology, Evolution and Management. Cambridge University Press.

Kern, C.C., Schwarzmann, J., Kabrick, J., Gerndt, K., Boyden, S., Stanovick, J.S., 2019. Mounds facilitate regeneration of light-seeded and browse-sensitive tree species after moderate-severity wind disturbance. Forest Ecology and Management 437, 139–147.

Khoury, S., Coomes, D.A., 2020. Resilience of Spanish forests to recent droughts and climate change. Global Change Biology 26, 7079–7098.

King, D.A. (1990) The Adaptive Significance of Tree Height. The American Naturalist. 135 (6), 809–828.

Kobe, R.K., Pacala, S.W., Silander, J.A. & Canham, C.D. (1995) Juvenile Tree Survivorship as a Component of Shade Tolerance. Ecological Applications. 5 (2), 517–532.

Koçillari, L., Olson, M.E., Suweis, S., Rocha, R.P., Lovison, A., Cardin, F., Dawson, T.E., Echeverría, A., Fajardo, A., Lechthaler, S., Martínez-Pérez, C., Marcati, C.R., Chung, K.-F., Rosell, J.A., Segovia-Rivas, A., Williams, C.B., Petrone-Mendoza, E., Rinaldo, A., Anfodillo, T., Banavar, J.R., Maritan, A., 2021. The Widened Pipe Model of plant hydraulic evolution. Proc. Natl. Acad. Sci. 118.

Korhonen, L., Vauhkonen, J., Virolainen, A., Hovi, A., Korpela, I., 2013. Estimation of tree crown volume from airborne lidar data using computational geometry. International Journal of Remote Sensing 34, 7236–7248.

Kothari, S., Montgomery, R.A., Cavender-Bares, J., 2021. Physiological responses to light explain competition and facilitation in a tree diversity experiment. Journal of Ecology 109, 2000–2018.

Krůček, M., Trochta, J., Cibulka, M., Král, K., 2019. Beyond the cones: How crown shape plasticity alters aboveground competition for space and light—Evidence from terrestrial laser scanning. Agricultural and Forest Meteorology 264, 188–199.

Kükenbrink, D., Schneider, F.D., Schmid, B., Gastellu-Etchegorry, J.-P., Schaepman, M.E., Morsdorf, F., 2021. Modelling of three-dimensional, diurnal light extinction in two contrasting forests. Agric. For. Meteorol. 296, 108230.

Kunstler, G., Falster, D., Coomes, D.A., Hui, F., Kooyman, R.M., Laughlin, D.C., Poorter, L., Vanderwel, M., Vieilledent, G., Wright, S.J., Aiba, M., Baraloto, C., Caspersen, J., Cornelissen, J.H.C., Gourlet-Fleury, S., Hanewinkel, M., Herault, B., Kattge, J., Kurokawa, H., Onoda, Y., Peñuelas, J., Poorter, H., Uriarte, M., Richardson, S., Ruiz-Benito, P., Sun, I.F., St\a ahl, G., Swenson, N.G., Thompson, J., Westerlund, B., Wirth, C., Zavala, M.A., Zeng, H., Zimmerman, J.K., Zimmermann, N.E., Westoby, M., 2016. Plant functional traits have globally consistent effects on competition. Nature 529, 204–207.

Kunstler, G., Lavergne, S., Courbaud, B., Thuiller, W., Vieilledent, G., Zimmermann, N.E., Kattge, J., Coomes, D.A., 2012. Competitive interactions between forest trees are driven by species' trait hierarchy, not phylogenetic or functional similarity: implications for forest community assembly. Ecol. Lett. 15, 831–840.

Kunz, M., Fichtner, A., Härdtle, W., Raumonen, P., Bruelheide, H. & Oheimb, G. von 2019. Neighbour species richness and local structural variability modulate aboveground allocation patterns and crown morphology of individual trees. Ecology Letters. 0 (0).

Lafarge, T. & Pateiro-Lopez, B. 2017. alphashape3d: Implementation of the 3D Alpha-Shape for the Reconstruction of 3D Sets from a Point Cloud.

Lau, A., Martius, C., Bartholomeus, H., Shenkin, A., Jackson, T., Malhi, Y., Herold, M. & Bentley, L.P. 2019. Estimating architecture-based metabolic scaling exponents of tropical trees using terrestrial LiDAR and 3D modelling. Forest Ecology and Management. 439132–145.

Le Toan, T., Quegan, S., Davidson, M.W.J., Balzter, H., Paillou, P., Papathanassiou, K., Plummer, S., Rocca, F., Saatchi, S., Shugart, H., Ulander, L., 2011. The BIOMASS mission: Mapping global forest biomass to better understand the terrestrial carbon cycle. Remote Sensing of Environment 115, 2850–2860.

Lecigne, B., Delagrange, S., Messier, C., 2018. Exploring trees in three dimensions: VoxR, a novel voxel-based R package dedicated to analysing the complex arrangement of tree crowns. Ann. Bot. 121, 589–601.

Ledo, A., Paul, K.I., Burslem, D.F.R.P., Ewel, J.J., Barton, C., Battaglia, M., Brooksbank, K., Carter, J., Eid, T.H., England, J.R., Fitzgerald, A., Jonson, J., Mencuccini, M., Montagu, K.D., Montero, G., Mugasha, W.A., Pinkard, E., Roxburgh, S., Ryan, C.M., et al. 2018 Tree size and climatic water deficit control root to shoot ratio in individual trees globally. New Phytologist. 217 (1), 8–11.

Lee, A.C., Lucas, R.M., 2007. A LiDAR-derived canopy density model for tree stem and crown mapping in Australian forests. Remote Sensing of Environment 111, 493–518.

Lee, H., Slatton, K.C., Roth, B.E., Cropper, W.P., 2010. Adaptive clustering of airborne LiDAR data to segment individual tree crowns in managed pine forests. International Journal of Remote Sensing 31, 117–139.

Lefsky, M.A., Harding, D.J., Keller, M., Cohen, W.B., Carabajal, C.C., Del Bom Espirito-Santo, F., Hunter, M.O., de Oliveira, R., 2005. Estimates of forest canopy height and aboveground biomass using ICESat. Geophysical Research Letters 32, 1–4.

Li, Y., Guo, Q., Su, Y., Tao, S., Zhao, K., Xu, G., 2017. Retrieving the gap fraction, element clumping index, and leaf area index of individual trees using single-scan data from a terrestrial laser scanner. ISPRS J. Photogramm. Remote Sens. 130, 308–316.

Liang, X., Hyyppä, J., Kaartinen, H., Lehtomäki, M., Pyörälä, J., Pfeifer, N., Holopainen, M., Brolly, G., Francesco, P., Hackenberg, J., Huang, H., Jo, H.W., Katoh, M., Liu, L., Mokroš, M., Morel, J., Olofsson, K., Poveda-Lopez, J., Trochta, J., Wang, D., Wang, J., Xi, Z., Yang, B., Zheng, G., Kankare, V., Luoma, V., Yu, X., Chen, L., Vastaranta, M., Saarinen, N., Wang, Y., 2018. International benchmarking of terrestrial laser scanning approaches for forest inventories. ISPRS J. Photogramm. Remote Sens. 144, 137–179.

Liang, X., Kankare, V., Hyyppä, J., Wang, Y., Kukko, A., Haggrén, H., Yu, X., Kaartinen, H., Jaakkola, A., Guan, F., Holopainen, M. & Vastaranta, M. 2016. Terrestrial laser scanning in forest inventories. ISPRS Journal of Photogrammetry and Remote Sensing. 11563–77.

Liang, X., Kukko, A., Kaartinen, H., Hyyppä, J., Yu, X., Jaakkola, A., Wang, Y., 2014. Possibilities of a Personal Laser Scanning System for Forest Mapping and Ecosystem Services. Sensors 14, 1228–1248.

Liang, X., Litkey, P., Hyyppä, J., Kaartinen, H., Vastaranta, M., Holopainen, M., 2012. Automatic stem mapping using single-scan terrestrial laser scanning. IEEE Trans. Geosci. Remote Sens. 50, 661–670.

Lin, Y., Berger, U., Grimm, V., Huth, F., Weiner, J., 2013. Plant Interactions Alter the Predictions of Metabolic Scaling Theory. PLoS ONE 8, e57612.

Lindberg, E., Olofsson, K., Holmgren, J., Olsson, H. akan, 2012. Estimation of 3D vegetation structure from waveform and discrete return airborne laser scanning data. Remote Sensing of Environment 118, 151–161.

Lindh, M., Falster, D.S., Zhang, L., Dieckmann, U., Brännström, Å., 2018. Latitudinal effects on crown shape evolution. Ecol. Evol. 8, 8149–8158.

Lines, E.R., Zavala, M.A., Purves, D.W., Coomes, D.A., 2012. Predictable changes in aboveground allometry of trees along gradients of temperature, aridity and competition. Glob. Ecol. Biogeogr. 21, 1017–1028.

Liu, G., Wang, J., Dong, P., Chen, Y., Liu, Z., 2018. Estimating individual tree height and diameter at breast height (DBH) from terrestrial laser scanning (TLS) data at plot level. Forests 8, 398.

Liu, L., Pang, Y., Li, Z., Si, L., Liao, S., 2017. Combining Airborne and Terrestrial Laser Scanning Technologies to Measure Forest Understorey Volume. Forests 8, 111.

Liu, Y.Y., Van Dijk, A.I.J.M., De Jeu, R.A.M., Canadell, J.G., McCabe, M.F., Evans, J.P., Wang, G., 2015. Recent reversal in loss of global terrestrial biomass. Nature Climate Change 5, 470–474.

Loehle, C. (1988) Tree life history strategies: the role of defenses. Canadian Journal of Forest Research.

Loehle, C., 2016. Biomechanical constraints on tree architecture. Trees - Structure and Function 30, 2061–2070.

Longuetaud, F., Piboule, A., Wernsdörfer, H. & Collet, C. 2013. Crown plasticity reduces inter-tree competition in a mixed broadleaved forest. European Journal of Forest Research. 132 (4), 621–634.

Lorimer, C.G., 1983. Tests of age-independent competition indices for individual trees in natural hardwood stands. For. Ecol. Manag. 6, 343–360.

Loubota Panzou, G.J., Fayolle, A., Jucker, T., Phillips, O.L., Bohlman, S., Banin, L.F., Lewis, S.L., Affum-Baffoe, K., Alves, L.F., Antin, C. and Arets, E., 2021. Pantropical variability in tree crown allometry. Global Ecology and Biogeography, 30(2), pp.459-475.

Luyssaert, S., Schulze, E.D., Börner, A., Knohl, A., Hessenmöller, D., Law, B.E., Ciais, P., Grace, J., 2008. Old-growth forests as global carbon sinks. Nature 455, 213–215.

Maas, H.-G., Bienert, A., Scheller, S., Keane, E., 2008. Automatic forest inventory parameter determination from terrestrial laser scanner data. International Journal of Remote Sensing 29, 1579–1593.

MacFarlane, D.W. & Kane, B. 2017. Neighbour effects on tree architecture: functional trade-offs balancing crown competitiveness with wind resistance. Functional Ecology. 31 (8), 1624–1636.

Madrigal-González, J., Herrero, A., Ruiz-Benito, P. & Zavala, M.A. 2017. Resilience to drought in a dry forest: Insights from demographic rates. Forest Ecology and Management. 389167–175.

Malhi, Y., Jackson, T., Patrick Bentley, L., Lau, A., Shenkin, A., Herold, M., Calders, K., Bartholomeus, H., Disney, M.I., 2018. New perspectives on the ecology of tree structure and tree communities through terrestrial laser scanning. Interface Focus 8, 20170052.

Martin-Benito, D., Kint, V., del Río, M., Muys, B. & Cañellas, I. 2011. Growth responses of West-Mediterranean Pinus nigra to climate change are modulated by competition and productivity: Past trends and future perspectives. Forest Ecology and Management. 262 (6), 1030–1040.

Martin-Ducup, O., Schneider, R. & Fournier, R.A. 2018. Analyzing the Vertical Distribution of Crown Material in Mixed Stand Composed of Two Temperate Tree Species. Forests. 9 (11), 673.

Martin-Ducup, O., Ploton, P., Barbier, N., Takoudjou, S.M., Mofack, G.I., Kamdem, N.G., Fourcaud, T., Sonké, B., Couteron, P., Pélissier, R., 2020. Terrestrial laser scanning reveals convergence of tree architecture with increasingly dominant crown canopy position. Functional Ecology.

Mascaro, J., Detto, M., Asner, G.P., Muller-Landau, H.C., 2011. Evaluating uncertainty in mapping forest carbon with airborne LiDAR. Remote Sensing of Environment 115, 3770–3774.

Matula, R., Damborská, L., Nečasová, M., Geršl, M. & Šrámek, M. (2015) Measuring Biomass and Carbon Stock in Resprouting Woody Plants. PLOS ONE. 10 (2).

McDowell, N., Pockman, W.T., Allen, C.D., Breshears, D.D., Cobb, N., Kolb, T., Plaut, J., Sperry, J., West, A., Williams, D.G. and Yepez, E.A., 2008. Mechanisms of plant survival and mortality during drought: why do some plants survive while others succumb to drought?.New phytologist, 178(4), pp.719-739.

McDowell, N.G., Allen, C.D., 2015. Darcy's law predicts widespread forest mortality under climate warming. Nature Climate Change 5, 669–672.

McDowell, N.G., Allen, C.D., Anderson-Teixeira, K., Aukema, B.H., Bond-Lamberty, B., Chini, L., Clark, J.S., Dietze, M., Grossiord, C., Hanbury-Brown, A., Hurtt, G.C., Jackson, R.B., Johnson, D.J., Kueppers, L., Lichstein, J.W., Ogle, K., Poulter, B., Pugh, T.A.M., Seidl, R., Turner, M.G., Uriarte, M., Walker, A.P., Xu, C., 2020. Pervasive shifts in forest dynamics in a changing world. Science 368.

McDowell, N.G., Grossiord, C., Adams, H.D., Pinzón-Navarro, S., Mackay, D.S., Breshears, D.D., Allen, C.D., Borrego, I., Dickman, L.T., Collins, A., Gaylord, M., McBranch, N., Pockman, W.T., Vilagrosa, A., Aukema, B., Goodsman, D. & Xu, C. (2019) Mechanisms of a coniferous woodland persistence under drought and heat. Environmental Research Letters. 14 (4), 045014.

McIntire, E.J.B., Fajardo, A., 2014. Facilitation as a ubiquitous driver of biodiversity. New Phytologist 201, 403–416.

McLaughlin, B.C., Ackerly, D.D., Klos, P.Z., Natali, J., Dawson, T.E., Thompson, S.E., 2017. Hydrologic refugia, plants, and climate change. Global Change Biology 23, 2941–2961.

McLaughlin, B.C., Blakey, R., Weitz, A.P., Feng, X., Brown, B.J., Ackerly, D.D., Dawson, T.E., Thompson, S.E., 2020. Weather underground: Subsurface hydrologic processes mediate tree vulnerability to extreme climatic drought. Global Change Biology 26, 3091–3107.

McMahon, T.A., Kronauer, R.E., 1976. Tree structures: Deducing the principle of mechanical design. Journal of Theoretical Biology 59, 443–466.

McMullan, M., Rafiqi, M., Kaithakottil, G., Clavijo, B.J., Bilham, L., Orton, E., Percival-Alwyn, L., Ward, B.J., Edwards, A., Saunders, D.G.O., Garcia Accinelli, G., Wright, J., Verweij, W., Koutsovoulos, G., Yoshida, K., Hosoya, T., Williamson, L., Jennings, P., Ioos, R., Husson, C., Hietala, A.M., Vivian-Smith, A., Solheim, H., MaClean, D., Fosker, C., Hall, N., Brown, J.K.M., Swarbreck, D., Blaxter, M., Downie, J.A., Clark, M.D., 2018. The ash dieback invasion of Europe was founded by two genetically divergent individuals. Nat Ecol Evol 2, 1000–1008.

Mediavilla, S., Martín, I., Babiano, J., Escudero, A., 2019. Foliar plasticity related to gradients of heat and drought stress across crown orientations in three Mediterranean Quercus species. PLOS ONE 14, e0224462.

Meigs, G.W., Morrissey, R.C., Bače, R., Chaskovskyy, O., Čada, V., Després, T., Donato, D.C., Janda, P., Lábusová, J., Seedre, M., Mikoláš, M., Nagel, T.A., Schurman, J.S., Synek, M., Teodosiu, M., Trotsiuk, V., Vítková, L., Svoboda, M., 2017. More ways than one: Mixed-severity disturbance regimes foster structural complexity via multiple developmental pathways. Forest Ecology and Management 406, 410–426.

Mencuccini, M., Hölttä, T., Petit, G. & Magnani, F. (2007) Sanio's laws revisited. Size-dependent changes in the xylem architecture of trees. Ecology Letters. 10 (11), 1084–1093.

Meng, S.X., Lieffers, V.J., Huang, S., 2007. Modeling crown volume of lodgepole pine based upon the uniform stress theory. For. Ecol. Manag. 251, 174–181.

Meng, S.X., Rudnicki, M., Lieffers, V.J., Reid, D.E. and Silins, U., 2006. Preventing crown collisions increases the crown cover and leaf area of maturing lodgepole pine. Journal of Ecology, 94(3), pp.681-686.

Messier, C., Parent, S. & Bergeron, Y. (1998) Effects of overstory and understory vegetation on the understory light environment in mixed boreal forests. Journal of Vegetation Science. 9 (4), 511–520.

Metcalf, C.J.E., Horvitz, C.C., Tuljapurkar, S. & Clark, D.A. 2009. A time to grow and a time to die: a new way to analyze the dynamics of size, light, age, and death of tropical trees. Ecology. 90 (10), 2766–2778.

Mette, T., Papathanassiou, K., Hajnsek, I., 2004. Biomass estimation from polarimetric SAR interferometry over heterogeneous forest terrain. Igarss 1, 511–514.

Metz, J.Ô., Seidel, D., Schall, P., Scheffer, D., Schulze, E.-D.D., Ammer, C., 2013. Crown modeling by terrestrial laser scanning as an approach to assess the effect of aboveground intra- and interspecific competition on tree growth. Forest Ecology and Management 310, 275–288.

Mikita, T., Klimánek, M., 2010. Topographic Exposure and its Practical Applications. Journal of Landscape Ecology 3, 42–51

Miller, B.D., Carter, K.R., Reed, S.C., Wood, T.E., Cavaleri, M.A., 2021. Only sun-lit leaves of the uppermost canopy exceed both air temperature and photosynthetic thermal optima in a wet tropical forest. Agricultural and Forest Meteorology 301–302, 108347.

Minamino, R., Tateno, M., 2014. Tree branching: Leonardo da Vinci's Rule versus biomechanical models. PLoS ONE 9, e9353.

Mitchard, E.T.A., Saatchi, S.S., Lewis, S.L., Feldpausch, T.R., Woodhouse, I.H., Sonké, B., Rowland, C., Meir, P., 2011. Measuring biomass changes due to woody encroachment and deforestation/degradation in a forest-savanna boundary region of central Africa using multi-temporal L-band radar backscatter. Remote Sensing of Environment 115, 2861–2873.

Mitchard, E.T.A., Saatchi, S.S., White, L.J.T., Abernethy, K.A., Jeffery, K.J., Lewis, S.L., Collins, M., Lefsky, M.A., Leal, M.E., Woodhouse, I.H., Meir, P., 2012. Mapping tropical forest biomass with radar and spaceborne LiDAR in Lopé National Park, Gabon: Overcoming problems of high biomass and persistent cloud. Biogeosciences 9, 179–191.

Molina, C.M., Galiana-Martín, L., 2016. Fire scenarios in Spain: A territorial approach to proactive fire management in the context of global change. Forests 7.

Montserrat-Martí, G., Camarero, J.J., Palacio, S., Pérez-Rontomé, C., Milla, R., Albuixech, J. & Maestro, M. (2009) Summer-drought constrains the phenology and growth of two coexisting Mediterranean oaks with contrasting leaf habit: implications for their persistence and reproduction. Trees. 23 (4), 787–799.

Morán-López, T., Forner, A., Flores-Rentería, D., Díaz, M. & Valladares, F. 2016. Some positive effects of the fragmentation of holm oak forests: Attenuation of water stress and enhancement of acorn production. Forest Ecology and Management. 37022–30.

Moreno, G. & Cubera, E. 2008. Impact of stand density on water status and leaf gas exchange in Quercus ilex. Forest Ecology and Management. 254 (1), 74–84.

Moreno, J., Oechel, W.C., 2012. Global Change and Mediterranean-Type Ecosystems. Springer Science & Business Media.

Mori, A.S., Dee, L.E., Gonzalez, A., Ohashi, H., Cowles, J., Wright, A.J., Loreau, M., Hautier, Y., Newbold, T., Reich, P.B., Matsui, T., Takeuchi, W., Okada, K., Seidl, R., Isbell, F., 2021. Biodiversity–productivity relationships are key to nature-based climate solutions. Nat. Clim. Chang. 11, 543–550.

Morin, X., Fahse, L., Scherer-Lorenzen, M. & Bugmann, H. 2011 Tree species richness promotes productivity in temperate forests through strong complementarity between species. Ecology Letters. 14 (12), 1211–1219.

Moritz, M.A., Batllori, E., Bradstock, R.A., Gill, A.M., Handmer, J., Hessburg, P.F., Leonard, J., McCaffrey, S., Odion, D.C., Schoennagel, T., Syphard, A.D., 2014. Learning to coexist with wildfire. Nature 515, 58–66.

Morsdorf, F., Kükenbrink, D., Schneider, F.D., Abegg, M., Schaepman, M.E., 2018. Close-range laser scanning in forests: towards physically based semantics across scales. Interface Focus 8, 20170046.

Morsdorf, F., Meier, E., Kötz, B., Itten, K.I., Dobbertin, M., Allgöwer, B., 2004. LIDAR-based geometric reconstruction of boreal type forest stands at single tree level for forest and wildland fire management. Remote Sensing of Environment 92, 353–362.

Moskal, L.M., Zheng, G., 2012. Retrieving Forest Inventory Variables with Terrestrial Laser Scanning (TLS) in Urban Heterogeneous Forest. Remote Sens. 4, 1–20.

Moulia, B., Coutand, C. & Lenne, C. 2006. Posture control and skeletal mechanical acclimation in terrestrial plants: implications for mechanical modeling of plant architecture. American Journal of Botany. 93 (10), 1477–1489.

Muller-Landau, H.C., Condit, R.S., Chave, J., Thomas, S.C., Bohlman, S.A., Bunyavejchewin, S., Davies, S., Foster, R., Gunatilleke, S., Gunatilleke, N., Harms, K.E., Hart, T., Hubbell, S.P., Itoh, A., Kassim, A.R., LaFrankie, J.V., Lee, H.S., Losos, E., Makana, J.R., Ohkubo, T., Sukumar, R., Sun, I.F., Nur Supardi, M.N., Tan, S., Thompson, J., Valencia, R., Muñoz, G.V., Wills, C., Yamakura, T., Chuyong, G., Dattaraja, H.S., Esufali, S., Hall, P., Hernandez, C., Kenfack, D., Kiratiprayoon, S., Suresh, H.S., Thomas, D., Vallejo, M.I., Ashton, P., 2006. Testing metabolic ecology theory for allometric scaling of tree size, growth and mortality in tropical forests. Ecology Letters 9, 575–588.

Murray, J., Blackburn, G.A., Whyatt, J.D., Edwards, C., 2018. Using fractal analysis of crown images to measure the structural condition of trees. Forestry: An International Journal of Forest Research 91, 480–491.

Muscarella, R., Kolyaie, S., Morton, D.C., Zimmerman, J.K. and Uriarte, M., 2020. Effects of topography on tropical forest structure depend on climate context. Journal of Ecology, 108(1), pp.145-159.

Myers, N., Mittermeier, R.A., Mittermeier, C.G., da Fonseca, G.A.B., Kent, J., 2000. Biodiversity hotspots for conservation priorities. Nature 403, 853–858.

Nadal-Sala, D., Medlyn, B.E., Ruehr, N.K., Barton, C.V.M., Ellsworth, D.S., Gracia, C., Tissue, D.T., Tjoelker, M.G., Sabaté, S., 2021. Increasing aridity will not offset CO2 fertilization in fast-growing eucalypts with access to deep soil water. Global Change Biology 27, 2970–2990.

Nagashima, H., Hikosaka, K., 2012. Not only light quality but also mechanical stimuli are involved in height convergence in crowded Chenopodium album stands. New Phytol. 195, 803–811.

Newnham, G., Armston, J., Muir, J., 2012. Evaluation of Terrestrial Laser Scanners for Measuring Vegetation Structure.

Nicoll, B.C., Connolly, T., Gardiner, B.A., 2019. Changes in Spruce Growth and Biomass Allocation Following Thinning and Guying Treatments. Forests 10, 253.

Nie, S., Wang, C., Zeng, H., Xi, X., Li, G., 2017. Above-ground biomass estimation using airborne discrete-return and full-waveform LiDAR data in a coniferous forest. Ecological Indicators 78, 221–228.

Niez, B., Dlouha, J., Moulia, B., Badel, E., 2019. Water-stressed or not, the mechanical acclimation is a priority requirement for trees. Trees 33, 279–291.

Niinemets, Ü. 2006. The controversy over traits conferring shade-tolerance in trees: ontogenetic changes revisited. Journal of Ecology. 94 (2), 464–470.

Niinemets, Ü. 2010. A review of light interception in plant stands from leaf to canopy in different plant functional types and in species with varying shade tolerance. Ecological Research. 25 (4), 693–714.

Niinemets, Ü. & Valladares, F. 2006. Tolerance to Shade, Drought, and Waterlogging of Temperate Northern Hemisphere Trees and Shrubs. Ecological Monographs. 76 (4), 521–547.

Niinemets, Ü., Sparrow, A. & Cescatti, A. 2005. Light capture efficiency decreases with increasing tree age and size in the southern hemisphere gymnosperm Agathis australis. Trees. 19177–190.

Niinemets, Ü., Valladares, F., 2006. Tolerance to Shade, Drought, and Waterlogging of Temperate Northern Hemisphere Trees and Shrubs. Ecological Monographs 76, 521–547.

Niklas, K.J., 1994. Morphological evolution through complex domains of fitness. PNAS 91, 6772–6779.

Nolan, R.H., Gauthey, A., Losso, A., Medlyn, B.E., Smith, R., Chhajed, S.S., Fuller, K., Song, M., Li, X., Beaumont, L.J., Boer, M.M., Wright, I.J., Choat, B., 2021. Hydraulic failure and tree size linked with canopy die-back in eucalypt forest during extreme drought. New Phytologist 230, 1354–1365.

Novoplansky, A., 2009. Picking battles wisely: plant behaviour under competition. Plant Cell Environ. 32, 726–741.

Ogaya, R., Peñuelas, J., 2007. Tree growth, mortality, and above-ground biomass accumulation in a holm oak forest under a five-year experimental field drought. Plant Ecology 189, 291–299.

Ogaya, R., Peñuelas, J., 2021. Climate Change Effects in a Mediterranean Forest Following 21 Consecutive Years of Experimental Drought. Forests 12, 306.

Olivier, M.D., Robert, S., Fournier, R.A., 2016. Response of sugar maple (Acer saccharum, Marsh.) tree crown structure to competition in pure versus mixed stands. For. Ecol. Manag. 374, 20–32.

Olson, M.E., Anfodillo, T., Gleason, S.M., McCulloh, K.A., 2021. Tip-to-base xylem conduit widening as an adaptation: causes, consequences, and empirical priorities. New Phytologist 229, 1877–1893.

Olson, M.E., Soriano, D., Rosell, J.A., Anfodillo, T., Donoghue, M.J., Edwards, E.J., León-Gómez, C., Dawson, T., Martínez, J.J.C., Castorena, M., Echeverría, A., Espinosa, C.I., Fajardo, A., Gazol, A., Isnard, S., Lima, R.S., Marcati, C.R., Méndez-Alonzo, R., 2018. Plant height and hydraulic vulnerability to drought and cold. Proceedings of the National Academy of Sciences 115, 7551–7556.

Orwig, D.A., Boucher, P., Paynter, I., Saenz, E., Li, Z., Schaaf, C., 2018. The potential to characterize ecological data with terrestrial laser scanning in Harvard Forest, MA. Interface Focus 8, 20170044.

Osawa, A. (1995) Inverse relationship of crown fractal dimension to self-thinning exponent of tree populations: a hypothesis. Canadian Journal of Forest Research. 25 (10), 1608–1617.

Osunkoya, O.O., Omar-Ali, K., Amit, N., Dayan, J., Daud, D.S. & Sheng, T.K. (2007) Comparative height–crown allometry and mechanical design in 22 tree species of Kuala Belalong rainforest, Brunei, Borneo. American Journal of Botany. 94 (12), 1951–1962.

Owen, H.J.F., Flynn, W.R.M., Lines, E.R., 2021. Competitive drivers of interspecific deviations of crown morphology from theoretical predictions measured with Terrestrial Laser Scanning. J. Ecol.

Ozanne, C.H.P., Anhuf, D., Boulter, S.L., Keller, H., Kitching, R.L., Körner, C., Meinzer, F.C., Mitchell, A.W., Nakashizuka, T., Silva Dias, P.L., Stork, N.E., Wright, S.J., Yoshimura, M., 2003. Biodiversity meets the atmosphere: A global view of forest canopies. Science 301, 183–186.

Pacala, S.W., Canham, C.D., Saponara, J., Silander, J.A., Kobe, R.K., Ribbens, E., 1996. Forest models defined by field measurements: estimation, error analysis and dynamics. Ecol. Monogr. 66, 1–43.

Panzou, G.J.L., Fayolle, A., Jucker, T., Phillips, O.L., Bohlman, S., Banin, L.F., Lewis, S.L., Affum-Baffoe, K., Alves, L.F., Antin, C., Arets, E., Arroyo, L., Baker, T.R., Barbier, N., Beeckman, H., Berger, U., Bocko, Y.E., Bongers, F., Bowers, S., Brade, T., Brondizio, E.S., Chantrain, A., Chave, J., Compaore, H., Coomes, D., Diallo, A., Dias, A.S., Dimobe, K., Djagbletey, G.D., Domingues, T., Doucet, J.-L., Drouet, T., Forni, E., Godlee, J.L., Goodman, R.C., Gourlet-Fleury, S., Hien, F., Iida, Y., Ilondea, B.A., Muledi, J.I., Jacques, P., Kuyah, S., López-Portillo, J., Loumeto, J.J., Marimon-Junior, B.H., Marimon, B.S., Mensah, S., Mitchard, E.T.A., Moncrieff, G.R., Narayanan, A., O'Brien, S.T., Ouedraogo, K., Palace, M.W., Pelissier, R., Ploton, P., Poorter, L., Ryan, C.M., Saiz, G., Santos, K. dos, Schlund, M., Sellan, G., Sonke, B., Sterck, F., Thibaut, Q., Hoef, Y.V., Veenendaal, E., Vovides, A.G., Xu, Y., Yao, T.L., Feldpausch, T.R., 2021. Pantropical variability in tree crown allometry. Global Ecology and Biogeography 30, 459–475.

Parent, S., Messier, C., 1996. A simple and efficient method to estimate microsite light availability under a forest canopy. Can. J. For. Res. 26, 151–154.

Pausas, J.G., Keeley, J.E., 2009. A Burning Story: The Role of Fire in the History of Life. BioScience 59, 593–601.

Pearcy, R.W., Muraoka, H. & Valladares, F. 2005. Crown architecture in sun and shade environments: Assessing function and trade-offs with a three-dimensional simulation model. New Phytologist. 166 (3), 791–800.

Peduzzi, A., Wynne, R.H., Thomas, V.A., Nelson, R.F., Reis, J.J., Sanford, M., 2012. Combined use of airborne lidar and DBInSAR data to estimate LAI in temperate mixed forests. Remote Sensing 4, 1758–1780.

Peeters, A., Zude, M., Käthner, J., Ünlü, M., Kanber, R., Hetzroni, A., Gebbers, R., Ben-Gal, A., 2015. Getis–Ord's hot- and cold-spot statistics as a basis for multivariate spatial clustering of orchard tree data. Comput. Electron. Agric. 111, 140–150.

Peñuelas, J. & Filella, I. 2003. Deuterium labelling of roots provides evidence of deep water access and hydraulic lift by Pinus nigra in a Mediterranean forest of NE Spain. Environmental and Experimental Botany. 49 (3), 201–208.

Pettorelli, N., Wegmann, M., Skidmore, A., Mücher, S., Dawson, T.P., Fernandez, M., Lucas, R., Schaepman, M.E., Wang, T., O'Connor, B., Jongman, R.H.G., Kempeneers, P., Sonnenschein, R., Leidner, A.K., Böhm, M., He, K.S., Nagendra, H., Dubois, G., Fatoyinbo, T., Hansen, M.C., Paganini, M., Klerk, H.M. de, Asner, G.P., Kerr, J.T., Estes, A.B., Schmeller, D.S., Heiden, U., Rocchini, D., Pereira, H.M., Turak, E., Fernandez, N., Lausch, A., Cho, M.A., Alcaraz-Segura, D., McGeoch, M.A., Turner, W., Mueller, A., St-Louis, V., Penner, J., Vihervaara, P., Belward, A., Reyers, B., Geller, G.N., 2016. Framing the concept of satellite remote sensing essential biodiversity variables: challenges and future directions. Remote Sensing in Ecology and Conservation 2, 122–131.

Pierik, R., de Wit, M., 2014. Shade avoidance: phytochrome signalling and other aboveground neighbour detection cues. Journal of Experimental Botany 65, 2815–2824.

Pitts, D.E., Badhwar, G.D., Reyna, E., 1987. Estimation of biophysical properties of forest canopies using C-band microwave data. Advances in Space Research 7, 89–95.

Point Cloud Library, 2021. Available at - https://github.com/PointCloudLibrary/pcl

Pommerening, A., Sánchez Meador, A.J., 2018. Tamm review: Tree interactions between myth and reality. Forest Ecology and Management 424, 164–176.

Poorter, H., Jagodzinski, A.M., Ruiz-Peinado, R., Kuyah, S., Luo, Y., Oleksyn, J., Usoltsev, V.A., Buckley, T.N., Reich, P.B. & Sack, L. 2015. How does biomass distribution change with size and differ among species? An analysis for 1200 plant species from five continents. New Phytologist. 208 (3), 736–749.

Poorter, H., Niinemets, Ü., Ntagkas, N., Siebenkäs, A., Mäenpää, M., Matsubara, S. & Pons, T. 2019. A meta-analysis of plant responses to light intensity for 70 traits ranging from molecules to whole plant performance. New Phytologist. 223 (3), 1073–1105.

Poorter, L., Bongers, F., Sterck, F.J., Wöll, H., 2003. Architecture of 53 Rain Forest Tree Species Differing in Adult Stature and Shade Tolerance. Ecology 84, 602–608.

Poorter, L., Lianes, E., Moreno-de las Heras, M. & Zavala, M.A. 2012. Architecture of Iberian canopy tree species in relation to wood density, shade tolerance and climate. Plant Ecology. 213 (5), 707–722.

Popescu, S.C., Wynne, R.H., Nelson, R.F., 2003. Measuring individual tree crown diameter with lidar and assessing its influence on estimating forest volume and biomass. Can. J. Remote Sens. 29, 564–577.

Popescu, S.C., Zhao, K., Neuenschwander, A., Lin, C., 2011. Satellite lidar vs. small footprint airborne lidar: Comparing the accuracy of aboveground biomass estimates and forest structure metrics at footprint level. Remote Sensing of Environment 115, 2786–2797.

Potapov, P., Li, X., Hernandez-Serna, A., Tyukavina, A., Hansen, M.C., Kommareddy, A., Pickens, A., Turubanova, S., Tang, H., Silva, C.E., Armston, J., Dubayah, R., Blair, J.B., Hofton, M., 2021. Mapping global forest canopy height through integration of GEDI and Landsat data. Remote Sensing of Environment 253, 112165.

Potvin, C. & Dutilleul, P. 2009. Neighborhood effects and size-asymmetric competition in a tree plantation varying in diversity. Ecology. 90 (2), 321–327.

Pretzsch, H. 2019. The Effect of Tree Crown Allometry on Community Dynamics in Mixed-Species Stands versus Monocultures. A Review and Perspectives for Modeling and Silvicultural Regulation. Forests. 10 (9), 810.

Pretzsch, H. & Dieler, J. 2012. Evidence of variant intra- and interspecific scaling of tree crown structure and relevance for allometric theory. Oecologia. 169 (3), 637–649.

Pretzsch, H., Schütze, G., 2005. Crown Allometry and Growing Space Efficiency of Norway Spruce (Picea abies [L.] Karst.) and European Beech (Fagus sylvatica L.) in Pure and Mixed Stands. Plant Biol. 7, 628–639.

Pretzsch, H.P., Biber, P.B., 2010. Size-symmetric versus size-asymmetric competition and growth partitioning among trees in forest stands along an ecological gradient in central Europe. Can. J. For. Res.

Preuksakarn, C., 2012. Reconstructing plant architecture from 3D laser scanner data (phdthesis). Université Montpellier II - Sciences et Techniques du Languedoc.

Price, C.A., Weitz, J.S., Savage, V.M., Stegen, J., Clarke, A., Coomes, D.A., Dodds, P.S., Etienne, R.S., Kerkhoff, A.J., McCulloh, K., Niklas, K.J., Olff, H., Swenson, N.G., 2012. Testing the metabolic theory of ecology. Ecology Letters 15, 1465–1474.

Prince, D.R., Fletcher, M.E., Shen, C., Fletcher, T.H., 2014. Application of L-systems to geometrical construction of chamise and juniper shrubs. Ecol. Model. 273, 86–95.

Puglielli, G., Hutchings, M.J. and Laanisto, L., 2021. The triangular space of abiotic stress tolerance in woody species: a unified trade-off model. New Phytologist, 229(3), pp.1354-1362.

Purves, D., Pacala, S., 2008. Predictive models of forest dynamics. Science 320, 1452–1453.

Purves, D.W., Lichstein, J.W., Pacala, S.W., 2007. Crown plasticity and competition for canopy space: A new spatially implicit model parameterized for 250 North American tree species. PLoS ONE 2.

Purves, D.W., Lichstein, J.W., Strigul, N., Pacala, S.W., 2008. Predicting and understanding forest dynamics using a simple tractable model. Proceedings of the National Academy of Sciences 105, 17018–17022.

R Core Team, 2021. R: A Language and Environment for Statistical Computing. R Foundation for Statistical Computing, Vienna, Austria.

Rajaniemi, T.K., 2003. Evidence for size asymmetry of belowground competition. Basic and Applied Ecology 4, 239–247.

Rasmussen, C.R., Weisbach, A.N., Thorup-Kristensen, K., Weiner, J., 2019. Size-asymmetric root competition in deep, nutrient-poor soil. Journal of Plant Ecology 12, 78–88.

Raumonen, P., Casella, E., Calders, K., Murphy, S., \AAkerbloma, M., Kaasalainen, M., 2015. Massive-Scale Tree Modelling From Tls Data. ISPRS Ann. Photogramm. Remote Sens. Spat. Inf. Sci. II-3/W4, 189–196.

Raumonen, P., Kaasalainen, M., \AAkerblom, M., Kaasalainen, S., Kaartinen, H., Vastaranta, M., Holopainen, M., Disney, M., Lewis, P., 2013. Fast Automatic Precision Tree Models from Terrestrial Laser Scanner Data. Remote Sens. 5, 491–520.

Rautiainen, M., Stenberg, P., 2005. Simplified tree crown model using standard forest mensuration data for Scots pine. Agric. For. Meteorol. 128, 123–129.

Reichstein, M., Tenhunen, J.D., Roupsard, O., Ourcival, J., Rambal, S., Miglietta, F., Peressotti, A., Pecchiari, M., Tirone, G., Valentini, R., 2002. Severe drought effects on ecosystem CO2 and H2O fluxes at three Mediterranean evergreen sites: revision of current hypotheses? Global Change Biology 8, 999–1017.

Riaño, D., Valladares, F., Condés, S., Chuvieco, E., 2004. Estimation of leaf area index and covered ground from airborne laser scanner (Lidar) in two contrasting forests. Agricultural and Forest Meteorology 124, 269–275.

Ritter, T., Nothdurft, A., 2018. Automatic Assessment of Crown Projection Area on Single Trees and Stand-Level, Based on Three-Dimensional Point Clouds Derived from Terrestrial Laser-Scanning. Forests 9, 237.

Rodríguez-Veiga, P., Wheeler, J., Louis, V., Tansey, K., Balzter, H., 2017. Quantifying Forest Biomass Carbon Stocks From Space. Curr Forestry Rep 3, 1–18.

Rood, S.B., Patiño, S., Coombs, K. and Tyree, M.T., 2000. Branch sacrifice: cavitation-associated drought adaptation of riparian cottonwoods. Trees, 14(5), pp.248-257.

Roussel, J.-R., Auty, D., Coops, N.C., Tompalski, P., Goodbody, T.R.H., Meador, A.S., Bourdon, J.-F., Boissieu, F. de, Achim, A., 2020. lidR: An R package for analysis of Airborne Laser Scanning (ALS) data. Remote Sens. Environ. 251, 112061.

Ruel, J.-C.J.-C., Mitchell, S.J.S.J., Dornier, M., 2002. A GIS Based Approach to Map Wind Exposure for Windthrow Hazard Rating. Northern Journal of Applied Forestry 19, 183–187.

Rüger, N. & Condit, R. (2012) Testing metabolic theory with models of tree growth that include light competition. Functional Ecology. 26 (3), 759–765.

Rüger, N., Berger, U., Hubbell, S.P., Vieilledent, G. & Condit, R. (2011) Growth Strategies of Tropical Tree Species: Disentangling Light and Size Effects. PLOS ONE. 6 (9), e25330.

Ruiz-Benito, P., Lines, E.R., Gómez-Aparicio, L., Zavala, M.A., Coomes, D.A., 2013. Patterns and Drivers of Tree Mortality in Iberian Forests: Climatic Effects Are Modified by Competition. PLoS ONE 8.

Ruiz-Benito, P., Madrigal-González, J., Ratcliffe, S., Coomes, D.A., Kändler, G., Lehtonen, A., Wirth, C., Zavala, M.A., 2014. Stand Structure and Recent Climate Change Constrain Stand Basal Area Change in European Forests: A Comparison Across Boreal, Temperate, and Mediterranean Biomes. Ecosystems 17, 1439–1454.

Ryan, M.G. and Yoder, B.J., 1997. Hydraulic limits to tree height and tree growth. Bioscience, 47(4), pp.235-242.

Saarinen, N., Calders, K., Kankare, V., Yrttimaa, T., Junttila, S., Luoma, V., Huuskonen, S., Hynynen, J., Verbeeck, H., 2021. Understanding 3D structural complexity of individual Scots pine trees with different management history. Ecol. Evol. 11, 2561–2572.

Santoro, M., Beer, C., Cartus, O., Schmullius, C.C., Shvidenko, A., McCallum, I., Wegmüller, U., Wiesmann, A., 2010. The BIOMASAR algorithm: An approach for retrieval of forest growing stock volume using stacks of multi-temporal SAR data. Proceedings of the Living Planet Symposium CD-ROM.

Sapijanskas, J., Paquette, A., Potvin, C., Kunert, N. and Loreau, M., 2014. Tropical tree diversity enhances light capture through crown plasticity and spatial and temporal niche differences. Ecology, 95(9), pp.2479-2492.

Sardans, J., Rodà, F. & Peñuelas, J. 2004. Phosphorus limitation and competitive capacities of Pinus halepensis and Quercus ilex subsp. rotundifolia on different soils. Plant Ecology. 174 (2), 307.

Savage, J.A., Beecher, S.D., Clerx, L., Gersony, J.T., Knoblauch, J., Losada, J.M., Jensen, K.H., Knoblauch, M., Holbrook, N.M., 2017. Maintenance of carbohydrate transport in tall trees. Nat. Plants 3, 965–972.

Savage, V.M., Bentley, L.P., Enquist, B.J., Sperry, J.S., Smith, D.D., Reich, P.B., von Allmen, E.I., 2010. Hydraulic trade-offs and space filling enable better predictions of vascular structure and function in plants. Proceedings of the National Academy of Sciences 107, 22722–22727.

Schoonmaker, A.L., Lieffers, V.J., Landhäusser, S.M., 2014. Uniform versus asymmetric shading mediates crown recession in conifers. PloS One 9, e104187.

Schraik, D., Hovi, A., Rautiainen, M., 2021. Crown level clumping in Norway spruce from terrestrial laser scanning measurements. Agric. For. Meteorol. 296, 108238.

Schwartz, N.B., Budsock, A.M., Uriarte, M., 2019. Fragmentation, forest structure, and topography modulate impacts of drought in a tropical forest landscape. Ecology 100, e02677.

Seidel, D., 2018. A holistic approach to determine tree structural complexity based on laser scanning data and fractal analysis. Ecol. Evol. 8, 128–134.

Seidel, D., Annighöfer, P., Stiers, M., Zemp, C.D., Burkardt, K., Ehbrecht, M., Willim, K., Kreft, H., Hölscher, D., Ammer, C., 2019a. How a measure of tree structural complexity relates to architectural benefit-to-cost ratio, light availability, and growth of trees. Ecol. Evol. 9, 7134–7142.

Seidel, D., Ehbrecht, M., Dorji, Y., Jambay, J., Ammer, C., Annighöfer, P., 2019b. Identifying architectural characteristics that determine tree structural complexity. Trees 33, 911–919. https://doi.org/10.1007/s00468-019-01827-4

Seidl, R., Thom, D., Kautz, M., Martin-Benito, D., Peltoniemi, M., Vacchiano, G., Wild, J., Ascoli, D., Petr, M., Honkaniemi, J., Lexer, M.J., Trotsiuk, V., Mairota, P., Svoboda, M., Fabrika, M., Nagel, T.A., Reyer, C.P.O., 2017. Forest disturbances under climate change. Nature Climate Change 7, 395–402.

Senf, C., Pflugmacher, D., Heurich, M., Krueger, T., 2017. A Bayesian hierarchical model for estimating spatial and temporal variation in vegetation phenology from Landsat time series. Remote Sensing of Environment 194, 155–160.

Shenkin, A., Bentley, L.P., Oliveras, I., Salinas, N., Adu-Bredu, S., Marimon-Junior, B.H., Marimon, B.S., Peprah, T., Choque, E.L., Trujillo Rodriguez, L., Clemente Arenas, E.R., Adonteng, C., Seidu, J., Passos, F.B., Reis, S.M., Blonder, B., Silman, M., Enquist, B.J., Asner, G.P., Malhi, Y., 2020. The Influence of Ecosystem and Phylogeny on Tropical Tree Crown Size and Shape. Front. For. Glob. Change 3.

Shinozaki, K., Yoda, K., Hozumi, K., Kira, T., 1964. A quantitative analysis of plant form-the pipe model theory: II. Further evidence of the theory and its application in forest ecology. Japanese Journal of Ecology 14, 133–139.

Sievänen, R., Godin, C., DeJong, T.M., Nikinmaa, E., 2014. Functional–structural plant models: a growing paradigm for plant studies. Annals of Botany 114, 599–603.

Silva, C.A., Duncanson, L., Hancock, S., Neuenschwander, A., Thomas, N., Hofton, M., Fatoyinbo, L., Simard, M., Marshak, C.Z., Armston, J., Lutchke, S., Dubayah, R., 2021. Fusing simulated GEDI, ICESat-2 and NISAR data for regional aboveground biomass mapping. Remote Sensing of Environment 253, 112234.

Simard, M., Pinto, N., Fisher, J.B., Baccini, A., 2011. Mapping forest canopy height globally with spaceborne lidar. Journal of Geophysical Research: Biogeosciences 116, 1–12.

Simonson, W., Ruiz-Benito, P., Valladares, F., Coomes, D., 2016. Modelling above-ground carbon dynamics using multi-temporal airborne lidar: Insights from a Mediterranean woodland. Biogeosciences 13, 961–973.

Skidmore, A.K., Pettorelli, N., Coops, N.C., Geller, G.N., Hansen, M., Lucas, R., Mücher, C.A., O'Connor, B., Paganini, M., Pereira, H.M., Schaepman, M.E., Turner, W., Wang, T., Wegmann, M., 2015. Environmental science: Agree on biodiversity metrics to track from space. Nature 523, 403–405.

Smith, D.D., Sperry, J.S., Enquist, B.J., Savage, V.M., McCulloh, K.A., Bentley, L.P., 2014. Deviation from symmetrically self-similar branching in trees predicts altered hydraulics, mechanics, light interception and metabolic scaling. New Phytologist 201, 217–229.

Smith, R.J. (2009) Use and misuse of the reduced major axis for line-fitting. American Journal of Physical Anthropology. 140 (3), 476–486.

Stark, S.C., Leitold, V., Wu, J.L., Hunter, M.O., Castilho, C.V. de, Costa, F.R.C., McMahon, S.M., Parker, G.G., Shimabukuro, M.T., Lefsky, M.A., Keller, M., Alves, L.F., Schietti, J., Shimabukuro, Y.E., Brandão, D.O., Woodcock, T.K., Higuchi, N., Camargo, P.B. de, Oliveira, R.C. de, Saleska, S.R., 2012. Amazon forest carbon dynamics predicted by profiles of canopy leaf area and light environment. Ecology Letters 15, 1406–1414.

Sterck, F.J. (1999) Crown development in tropical rain forest trees in gaps and understorey. Plant Ecology. 143 (1), 89–98.

Sterck, F.J., Bongers, F., Newbery, D.M., 2001. Tree architecture in a Bornean lowland rain forest: intraspecific and interspecific patterns. Plant Ecol. 153, 279–292.

Stoll, P., Weiner, J., 2000. A Neighborhood View of Interactions among Individual Plants, in: Dieckmann, U., Law, R., Metz, J.A.J. (Eds.), The Geometry of Ecological Interactions. Cambridge University Press, pp. 11–27.

Stovall, A.E.L., Masters, B., Fatoyinbo, L., Yang, X., 2021. TLSLeAF: automatic leaf angle estimates from single-scan terrestrial laser scanning. New Phytologist.

Stovall, A.E.L., Shugart, H., Yang, X., 2019. Tree height explains mortality risk during an intense drought. Nat Commun 10, 4385.

Stovall, A.E.L., Shugart, H.H., 2018. Improved Biomass Calibration and Validation With Terrestrial LiDAR: Implications for Future LiDAR and SAR Missions.

Tamasi, E., Stokes, A., Lasserre, B., Danjon, F., Berthier, S., Fourcaud, T., Chiatante, D., 2005. Influence of wind loading on root system development and architecture in oak (Quercus robur L.) seedlings. Trees 19, 374–384.

Tang, H., Dubayah, R., Swatantran, A., Hofton, M., Sheldon, S., Clark, D.B., Blair, B., 2012. Retrieval of vertical LAI profiles over tropical rain forests using waveform lidar at la selva, costa rica. Remote Sensing of Environment 124, 242–250.

Tao, S., Wu, F., Guo, Q., Wang, Y., Li, W., Xue, B., Hu, X., Li, P., Tian, D., Li, C., Yao, H., Li, Y., Xu, G., Fang, J., 2015. Segmenting tree crowns from terrestrial and mobile LiDAR data by exploring ecological theories. ISPRS J. Photogramm. Remote Sens. 110, 66–76.

Taubert, F., Jahn, M.W., Dobner, H.-J., Wiegand, T., Huth, A., 2015. The structure of tropical forests and sphere packings. Proceedings of the National Academy of Sciences 112, 15125–15129.

Tauc, F., Houle, D., Dupuch, A., Doyon, F., Maheu, A., 2020. Microtopographic refugia against drought in temperate forests: Lower water availability but more extensive fine root system in mounds than in pits. Forest Ecology and Management 476, 118439.

Taylor, R.G., Scanlon, B., Döll, P., Rodell, M., van Beek, R., Wada, Y., Longuevergne, L., Leblanc, M., Famiglietti, J.S., Edmunds, M., Konikow, L., Green, T.R., Chen, J., Taniguchi, M., Bierkens, M.F.P., MacDonald, A., Fan, Y., Maxwell, R.M., Yechieli, Y., Gurdak, J.J., Allen, D.M., Shamsudduha, M., Hiscock, K., Yeh, P.J.-F., Holman, I., Treidel, H., 2013. Ground water and climate change. Nature Clim Change 3, 322–329.

Terryn, L., Calders, K., Disney, M., Origo, N., Malhi, Y., Newnham, G., Raumonen, P., Å kerblom, M., Verbeeck, H., 2020. Tree species classification using structural features derived from terrestrial laser scanning. ISPRS J. Photogramm. Remote Sens. 168, 170–181.

Thies, M., Spiecker, H., 2004. Evaluation and future prospects of terrestrial laser scanning for standardized forest inventories, in: Laser-Scanners for Forest and Landscape Assessment.

Thompson, D.W., 1917. On growth and form. On growth and form.

Thorpe, H.C., Astrup, R., Trowbridge, A., Coates, K.D., 2010. Competition and tree crowns: A neighborhood analysis of three boreal tree species. For. Ecol. Manag. 259, 1586–1596.

Tilman, D. (1982) Resource competition and community structure. Princeton university press.

Toïgo, M., Perot, T., Courbaud, B., Castagneyrol, B., Gégout, J.-C., Longuetaud, F., Jactel, H., Vallet, P., 2018. Difference in shade tolerance drives the mixture effect on oak productivity. Journal of Ecology 106, 1073–1082.

Tredennick, A.T., Bentley, L.P., Hanan, N.P., 2013. Allometric Convergence in Savanna Trees and Implications for the Use of Plant Scaling Models in Variable Ecosystems. PLOS ONE 8, e58241.

Trochta, J., Kruček, M., Vrška, T., Kraâl, K., 2017. 3D Forest: An application for descriptions of three-dimensional forest structures using terrestrial LiDAR. PLoS ONE 12, e0176871.

Trogisch, S., Liu, X., Rutten, G., Xue, K., Bauhus, J., Brose, U., Bu, W., Cesarz, S., Chesters, D., Connolly, J., Cui, X., Eisenhauer, N., Guo, L., Haider, S., Härdtle, W., Kunz, M., Liu, L., Ma, Z., Neumann, S., Sang, W., Schuldt, A., Tang, Z., van Dam, N.M., von Oheimb, G., Wang, M.-Q., Wang, S., Weinhold, A., Wirth, C., Wubet, T., Xu, X., Yang, B., Zhang, N., Zhu, C.-D., Ma, K., Wang, Y., Bruelheide, H., 2021. The significance of tree-tree interactions for forest ecosystem functioning. Basic and Applied Ecology.

Trumbore, S., Brando, P. and Hartmann, H., 2015. Forest health and global change. Science, 349(6250), pp.814-818.

Turco, M., Bedia, J., Di Liberto, F., Fiorucci, P., Von Hardenberg, J., Koutsias, N., Llasat, M.C., Xystrakis, F., Provenzale, A., 2016. Decreasing fires in mediterranean Europe. PLoS ONE 11.

Uemura, A., Harayama, H., Koike, N., Ishida, A., 2006. Coordination of crown structure, leaf plasticity and carbon gain within the crowns of three winter-deciduous mature trees. Tree Physiology 26, 633–641.

Urban, J., Holusˇova, K., Mensˇık, L., 2013. Tree allometry of Douglas fir and Norway spruce on a nutrient-poor and a nutrient-rich site 14.

Urban, J., Holušová, K., Menšík, L., Čermák, J. and Kantor, P., 2013. Tree allometry of Douglas fir and Norway spruce on a nutrient-poor and a nutrient-rich site. Trees, 27(1), pp.97-110.

Uriarte, M., Condit, R., Canham, C.D. & Hubbell, S.P. (2004) A spatially explicit model of sapling growth in a tropical forest: does the identity of neighbours matter? Journal of Ecology. 92 (2), 348–360.

Valladares, F. & Niinemets, Ü. 2008. Shade Tolerance, a Key Plant Feature of Complex Nature and Consequences. Annual Review of Ecology, Evolution, and Systematics. 39 (1), 237–257.

Valladares, F., Dobarro, I., Sánchez-Gómez, D., Pearcy, R.W., 2005. Photoinhibition and drought in Mediterranean woody saplings: scaling effects and interactions in sun and shade phenotypes. J Exp Bot 56, 483–494.

Valladares, F., Gianoli, E., Gómez, J.M., 2007. Ecological limits to plant phenotypic plasticity. New Phytol 176, 749–763.

Valladares, F., Guzmán, B., 2006. Canopy structure and spatial heterogeneity of understory light in an abandoned Holm oak woodland. Ann. For. Sci. 63, 749–761.

Valladares, F., Laanisto, L., Niinemets, Ü., Zavala, M.A., 2016. Shedding light on shade: ecological perspectives of understorey plant life. Plant Ecology and Diversity 9, 237–251.

Valladares, F., Niinemets, U., 2007. Crowns: From Design Rules to Light Capture and Performance 50.

Valladares, F., Pearcy, R.W., 2002. Drought can be more critical in the shade than in the sun: a field study of carbon gain and photo-inhibition in a Californian shrub during a dry El Niño year. Plant, Cell & Environment 25, 749–759.

Valladares, F., Saldaña, A., Gianoli, E., 2012. Costs versus risks: Architectural changes with changing light quantity and quality in saplings of temperate rainforest trees of different shade tolerance. Austral Ecol. 37, 35–43.

Valladares, F., Skillman, J.B., Pearcy, R.W., 2002. Convergence in light capture efficiencies among tropical forest understory plants with contrasting crown architectures: a case of morphological compensation. Am. J. Bot. 89, 1275–1284.

Valtera, M., Schaetzl, R.J., 2017. Pit-mound microrelief in forest soils: Review of implications for water retention and hydrologic modelling. Forest Ecology and Management 393, 40–51.

van der Plas, F., Ratcliffe, S., Ruiz-Benito, P., Scherer-Lorenzen, M., Verheyen, K., Wirth, C., Zavala, M.A., Ampoorter, E., Baeten, L., Barbaro, L., Bastias, C.C., Bauhus, J., Benavides, R., Benneter, A., Bonal, D., Bouriaud, O., Bruelheide, H., Bussotti, F., Carnol, M., Castagneyrol, B., Charbonnier, Y., Cornelissen, J.H.C., Dahlgren, J., Checko, E., Coppi, A., Dawud, S.M., Deconchat, M., De Smedt, P., De Wandeler, H., Domisch, T., Finér, L., Fotelli, M., Gessler, A., Granier, A., Grossiord, C., Guyot, V., Haase, J., Hättenschwiler, S., Jactel, H., Jaroszewicz, B., Joly, F.X., Jucker, T., Kambach, S., Kaendler, G., Kattge, J., Koricheva, J., Kunstler, G., Lehtonen, A., Liebergesell, M., Manning, P., Milligan, H., Müller, S., Muys, B., Nguyen, D., Nock, C., Ohse, B., Paquette, A., Peñuelas, J., Pollastrini, M., Radoglou, K., Raulund-Rasmussen, K., Roger, F., Seidl, R., Selvi, F., Stenlid, J., Valladares, F., van Keer, J., Vesterdal, L., Fischer, M., Gamfeldt, L., Allan, E., 2018. Continental mapping of forest ecosystem functions reveals a high but unrealised potential for forest multifunctionality. Ecology Letters 21, 31–42.

van der Zee, J., Lau, A., Shenkin, A., 2021. Understanding crown shyness from a 3D perspective. Annals of Botany.

Ventre-Lespiaucq, A., Flanagan, N.S., Ospina-Calderón, N.H., Delgado, J.A., Escudero, A., 2018. Midday Depression vs. Midday Peak in Diurnal Light Interception: Contrasting Patterns at Crown and Leaf Scales in a Tropical Evergreen Tree. Frontiers in Plant Science 9.

Verbeeck, H., Bauters, M., Jackson, T., Shenkin, A., Disney, M., Calders, K., 2019. Time for a Plant Structural Economics Spectrum. Frontiers in Forests and Global Change 2.

Vicari, M., Disney, M., Wilkes, P., Burt, A., Calders, K., Woodgate, W., 2019. Leaf and wood classification framework for terrestrial LiDAR point clouds. Methods Ecol. Evol. 10, 680–694.

Vicari, M.B., Pisek, J., Disney, M., 2019. New estimates of leaf angle distribution from terrestrial LiDAR: Comparison with measured and modelled estimates from nine broadleaf tree species. Agric. For. Meteorol. 264, 322–333.

Viedma, O., Moity, N., Moreno, J.M., 2015. Changes in landscape fire-hazard during the second half of the 20th century: Agriculture abandonment and the changing role of driving factors. Agriculture, Ecosystems & Environment 207, 126–140.

Vilfan, N., Tol, C. van der, Verhoef, W., 2019. Estimating photosynthetic capacity from leaf reflectance and Chl fluorescence by coupling radiative transfer to a model for photosynthesis. New Phytologist 223, 487–500.

da, Richter, J.P., 1970. The Notebooks of Leonardo Da Vinci. Courier Corporation.

Vizcaíno-Palomar, N., Ibáñez, I., González-Martínez, S.C., Zavala, M.A. and Alía, R., 2016. Adaptation and plasticity in aboveground allometry variation of four pine species along environmental gradients. Ecology and Evolution, 6(21), pp.7561-7573.

Walter, J.A., Stovall, A.E.L., Atkins, J.W., 2021. Vegetation structural complexity and biodiversity in the Great Smoky Mountains. Ecosphere 12, e03390. https://doi.org/10.1002/ecs2.3390

Wang, D., Takoudjou, S.M., Casella, E., 2020. LeWoS: A universal leaf-wood classification method to facilitate the 3D modelling of large tropical trees using terrestrial LiDAR. Methods Ecol. Evol. 11, 376–389.

Wang, Y., Fang, H., 2020. Estimation of LAI with the LiDAR Technology: A Review. Remote Sensing 12, 3457.

Wang, Y., Lehtomäki, M., Liang, X., Pyörälä, J., Kukko, A., Jaakkola, A., Liu, J., Feng, Z., Chen, R. and Hyyppä, J., 2019. Is field-measured tree height as reliable as believed–A comparison study of tree height estimates from field measurement, airborne laser scanning and terrestrial laser scanning in a boreal forest. ISPRS journal of photogrammetry and remote sensing, 147, pp.132-145.

Warton, D.I., Duursma, R.A., Falster, D.S. & Taskinen, S. 2012. smatr 3– an R package for estimation and inference about allometric lines. Methods in Ecology and Evolution. 3 (2), 257–259.

Warton, D.I., Wright, I.J., Falster, D.S. & Westoby, M. 2006. Bivariate line-fitting methods for allometry. Biological Reviews. 81 (2), 259–291.

Watt, P.J., Donoghue, D.N.M., 2005. Measuring forest structure with terrestrial laser scanning. Int. J. Remote Sens. 26, 1437–1446.

Way, D.A., Pearcy, R.W., 2012. Sunflecks in trees and forests: from photosynthetic physiology to global change biology. Tree Physiology 32, 1066–1081.

Weiner, J., 1990. Asymmetric competition in plant populations. Trends in Ecology & Evolution 5, 360–364.

Weiner, J., Wright, D.B., Castro, S., 1997. Symmetry of Below-Ground Competition between Kochia scoparia Individuals. Oikos 79, 85–91.

West, G.B., Brown, J.H. and Enquist, B.J., 1999. A general model for the structure and allometry of plant vascular systems. Nature, 400(6745), pp.664-667.

West, G.B., Brown, J.H., Enquist, B.J., 1997. A general model for the origin of allometric scaling laws in biology. Science 276, 122–126. https://doi.org/10.1126/science.276.5309.122

West, G.B., Enquist, B.J., Brown, J.H., 2009. A general quantitative theory of forest structure and dynamics. PNAS 106, 7040–7045.

Wilkes, P., Lau, A., Disney, M., Calders, K., Burt, A., Gonzalez de Tanago, J., Bartholomeus, H., Brede, B., Herold, M., 2017. Data acquisition considerations for Terrestrial Laser Scanning of forest plots. Remote Sens. Environ. 196, 140–153.

Williams, L.J., Cavender-Bares, J., Paquette, A., Messier, C., Reich, P.B., 2020. Light mediates the relationship between community diversity and trait plasticity in functionally and phylogenetically diverse tree mixtures. Journal of Ecology 108, 1617–1634.

Williams, L.J., Paquette, A., Cavender-Bares, J., Messier, C. & Reich, P.B. 2017. Spatial complementarity in tree crowns explains overyielding in species mixtures. Nature Ecology and Evolution. 1 (4), 0063.

Woodgate, W., Armston, J.D., Disney, M., Jones, S.D., Suarez, L., Hill, M.J., Wilkes, P., Soto-Berelov, M., 2016. Quantifying the impact of woody material on leaf area index estimation from hemispherical photography using 3D canopy simulations. Agric. For. Meteorol. 226–227, 1–12.

Woodhouse, I.H., Mitchard, E.T.A., Brolly, M., Maniatis, D., Ryan, C.M., 2012. Radar backscatter is not a "direct measure" of forest biomass. Nature Climate Change 2, 556–557.

Wright, A., Schnitzer, S.A., Reich, P.B., 2014. Living close to your neighbors: the importance of both competition and facilitation in plant communities. Ecology 95, 2213–2223.

Wright, I.J., Reich, P.B., Westoby, M., Ackerly, D.D., Baruch, Z., Bongers, F., Cavender-Bares, J., Chapin, T., Cornelissen, J.H.C., Diemer, M., Flexas, J., Garnier, E., Groom, P.K., Gulias, J., Hikosaka, K., Lamont, B.B., Lee, T., Lee, W., Lusk, C., Midgley, J.J., Navas, M.-L., Niinemets, Ü., Oleksyn, J., Osada, N., Poorter, H., Poot, P., Prior, L., Pyankov, V.I., Roumet, C., Thomas, S.C., Tjoelker, M.G., Veneklaas, E.J., Villar, R., 2004. The worldwide leaf economics spectrum. Nature 428, 821–827.

Wu, B., Yu, B., Wu, Q., Huang, Y., Chen, Z., Wu, J., 2016. Individual tree crown delineation using localized contour tree method and airborne LiDAR data in coniferous forests. International Journal of Applied Earth Observation and Geoinformation 52, 82–94.

Xi, Z., Hopkinson, C., Chasmer, L., 2018. Filtering Stems and Branches from Terrestrial Laser Scanning Point Clouds Using Deep 3-D Fully Convolutional Networks. Remote Sens. 10, 1215.

Xi, Z., Hopkinson, C., Rood, S.B., Peddle, D.R., 2020. See the forest and the trees: Effective machine and deep learning algorithms for wood filtering and tree species classification from terrestrial laser scanning. ISPRS J. Photogramm. Remote Sens. 168, 1–16.

Xu, Q., Cao, L., Xue, L., Chen, B., An, F., Yun, T., 2019. Extraction of Leaf Biophysical Attributes Based on a Computer Graphic-based Algorithm Using Terrestrial Laser Scanning Data. Remote Sens. 11, 15.

Yi, K., Smith, J.W., Jablonski, A.D., Tatham, E.A., Scanlon, T.M., Lerdau, M.T., Novick, K.A., Yang, X., 2020. High Heterogeneity in Canopy Temperature Among Co-occurring Tree Species in a Temperate Forest. Journal of Geophysical Research: Biogeosciences 125, e2020JG005892.

Yrttimaa, T., Luoma, V., Saarinen, N., Kankare, V., Junttila, S., Holopainen, M., Hyyppä, J., Vastaranta, M., 2020. Structural Changes in Boreal Forests Can Be Quantified Using Terrestrial Laser Scanning. Remote Sensing 12, 2672.

Yu, X., Hyyppä, J., Kaartinen, H., Maltamo, M., 2004. Automatic detection of harvested trees and determination of forest growth using airborne laser scanning. Remote Sensing of Environment 90, 451–462.

Yun, T., Cao, L., An, F., Chen, B., Xue, L., Li, W., Pincebourde, S., Smith, M.J., Eichhorn, M.P., 2019. Simulation of multi-platform LiDAR for assessing total leaf area in tree crowns. Agric. For. Meteorol. 276–277, 107610.

Zambrano, J., Beckman, N.G., Marchand, P., Thompson, J., Uriarte, M., Zimmerman, J.K., Umaña, M.N., Swenson, N.G., 2020. The scale dependency of trait-based tree neighborhood models. J. Veg. Sci. 31, 581–593.

Zambrano, J., Fagan, W.F., Worthy, S.J., Thompson, J., Uriarte, M., Zimmerman, J.K., Umaña, M.N., Swenson, N.G., 2019. Tree crown overlap improves predictions of the functional neighbourhood effects on tree survival and growth. Journal of Ecology 107, 887–900.

Zarnoch, S.J., Bechtold, W.A., Stolte, K.W., 2011. Using crown condition variables as indicators of forest health. Can. J. For. Res.

Zavala, M.A. & Bravo de la Parra, R. 2005. A mechanistic model of tree competition and facilitation for Mediterranean forests: Scaling from leaf physiology to stand dynamics. Ecological Modelling. 188 (1), 76–92.

Zeide, B., 1998. Fractal analysis of foliage distribution in loblolly pine crowns 28, 9.

Zeide, B., Pfeifer, P., 1991. A Method for Estimation of Fractal Dimension of Tree Crowns. for sci 37, 1253–1265.

Zellweger, F., Frenne, P.D., Lenoir, J., Rocchini, D. & Coomes, D. (2019) Advances in Microclimate Ecology Arising from Remote Sensing. Trends in Ecology & Evolution. 34 (4), 327–341.

Zhang, N., Evers, J.B., Anten, N.P.R., Marcelis, L.F.M., 2021. Turning plant interactions upside down: Light signals from below matter. Plant Cell Environ. 44, 1111–1118.

Zhang, Q.-W., Zhu, S.-D., Jansen, S., Cao, K.-F., 2020. Topography strongly affects drought stress and xylem embolism resistance in woody plants from a karst forest in Southwest China. Functional Ecology.

Zhao, D., Borders, B., Wilson, M., Rathbun, S.L., 2006. Modeling neighborhood effects on the growth and survival of individual trees in a natural temperate species-rich forest. Ecol. Model. 196, 90–102.

Zhao, M., Running, S.W., 2010. Drought-induced reduction in global terrestrial net primary production from 2000 through 2009. Science 329, 940–943.

Zhu, Z., Kleinn, C., Nölke, N., 2021. Assessing tree crown volume—a review. For. Int. J. For. Res. 94, 18–35.

Zianis, D., Muukkonen, P., Mäkipää, R., Mencuccini, M., 2005. Biomass and stem volume equations for tree species in Europe. FI.

Zolkos, S.G., Goetz, S.J., Dubayah, R., 2013. A meta-analysis of terrestrial aboveground biomass estimation using lidar remote sensing. Remote Sensing of Environment 128, 289–298.

Appendix

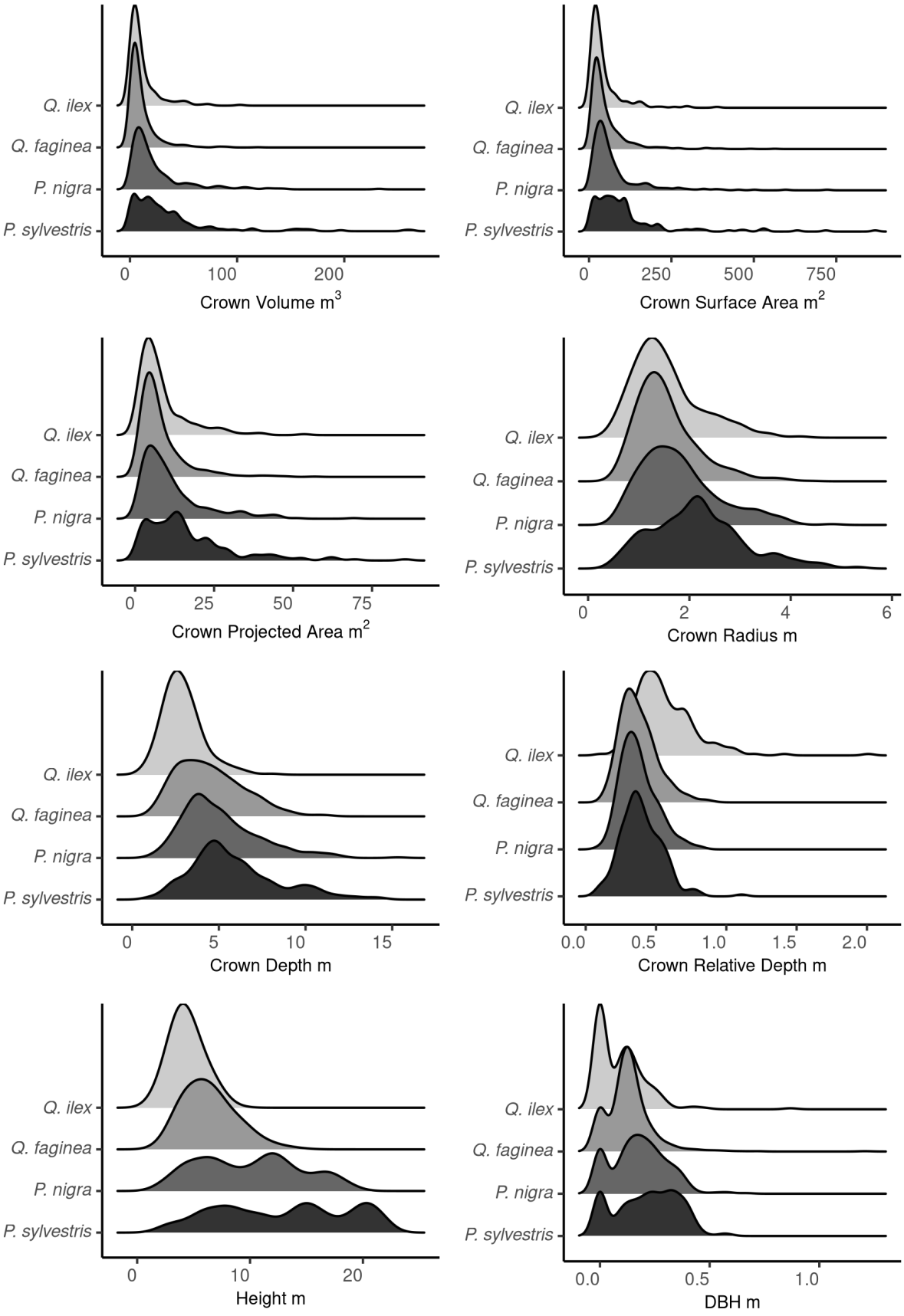

Figure A3.1 The distributions of each crown metric for each species (single-stemmed individuals) with DBH a subset of the data.

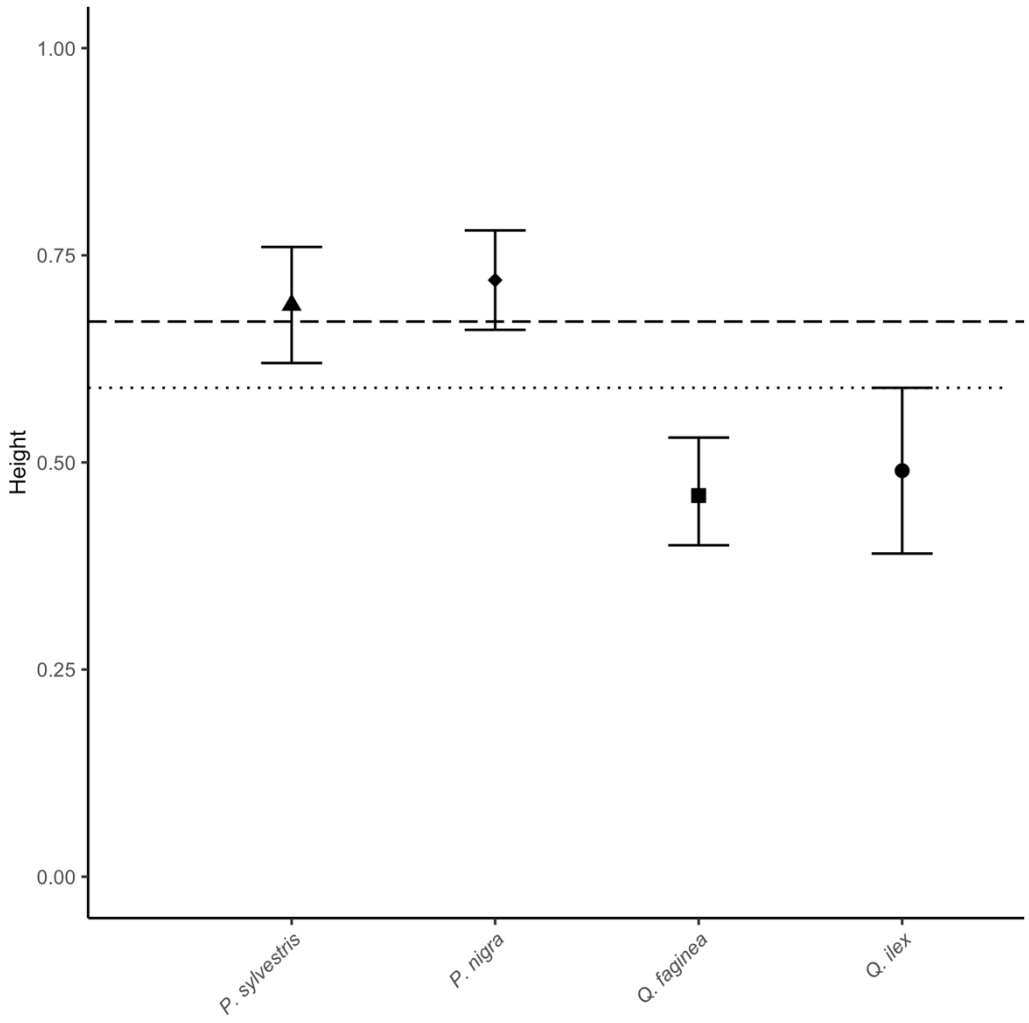

Figure A3.2 LMM-derived exponents of height-DBH relationships (b in Equations 3.1- 3.6) from the best model for each species, for a subset of trees where DBH was extractable, selected using AIC (Table 1). Error bars represent 95% confidence intervals. Species are ordered according to shade tolerance (Niinemets & Valladares, 2006; Puglielli et al., 2020), increasing left to right. MST prediction is shown by the horizontal dashed line whilst the dotted is the average of the four single-stem exponents (single-stem data only).

Table A3.1: Sample sizes for each species. This number represents all trees that had a neighbourhood radius within the plot boundary, and therefore for which we could accurately calculated competition metrics.

Species[1]	N	N_dbh
P. sylvestris	172	139
P. nigra	338	273
Q. faginea	579	462
Q. ilex	173	98
⁂*Q. faginea*	132	0
⁂*Q. ilex*	47	0

[1] ⁂ Multistems

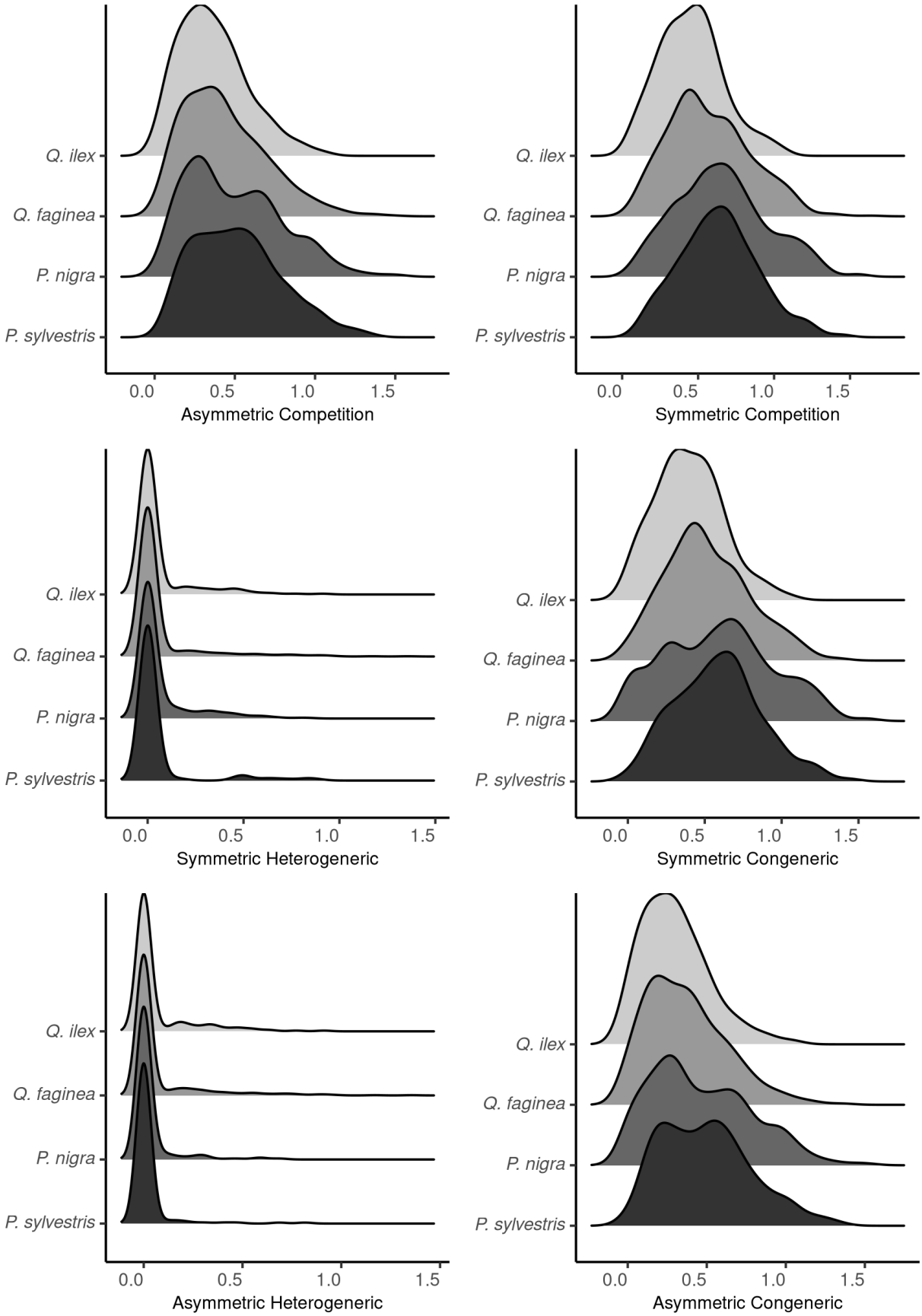

Figure A3.3 The distributions of each neighbourhood competition metric for each species (single-stemmed individuals).

Table A3.2: Model selection results showing the strongest neighbourhood competition metric drivers of height-crown scaling variation. AIC comparison of LMM model results of single-stems only, comparing candidate models including asymmetric, symmetric, and heterogeneric/congeneric neighbourhood metrics as explanatory variables (see Equations 3.1-3.6). Best model and those with delta AIC values <2 are shown in grey for each species and metric. Marginal R^2 (fixed effects only) and conditional R^2 (included random effect) were calculated using the MuMIn package in R (Barton, 2020).

Formula	ΔAIC[1]	Marginal R^2	Conditional R^2	Random Effect (SD)
P. sylvestris - log(Crown Volume)				
log(treeHeight) + Asymmetric Competition + Site + (1 | Plot)	0.00	0.59	0.78	0.87
log(treeHeight) + Asymmetric Congeneric + Asymmetric Heterogeneric + Site + (1 | Plot)	0.84	0.59	0.78	
log(treeHeight) + Site + (1 | Plot)	16.02	0.54	0.76	
P. nigra - log(Crown Volume)				
log(treeHeight) + Asymmetric Competition + (1 | Plot)	0.00	0.75	0.84	0.36
log(treeHeight) + Asymmetric Congeneric + Asymmetric Heterogeneric + (1 | Plot)	2.28	0.75	0.84	
log(treeHeight) + (1 | Plot)	91.63	0.68	0.81	
Q. faginea - log(Crown Volume)				
log(treeHeight) + Symmetric Congeneric + Symmetric Heterogeneric + (1 | Plot)	0.00	0.54	0.64	0.33
log(treeHeight) + Symmetric Competition + (1 | Plot)	3.37	0.52	0.64	
log(treeHeight) + (1 | Plot)	27.80	0.50	0.62	
Q. ilex - log(Crown Volume)				
log(treeHeight) + Symmetric Competition + (1 | Plot)	0.00	0.63	0.69	0.32
log(treeHeight) + Symmetric Congeneric + Symmetric Heterogeneric + (1 | Plot)	2.38	0.63	0.69	
log(treeHeight) + (1 | Plot)	13.55	0.61	0.68	
P. sylvestris - log(Crown Surface Area)				
log(treeHeight) + Asymmetric Competition + Site + (1 | Plot)	0.00	0.57	0.85	0.97
log(treeHeight) + Asymmetric Congeneric + Asymmetric Heterogeneric + Site + (1 | Plot)	1.25	0.57	0.85	
log(treeHeight) + Site + (1 | Plot)	18.96	0.51	0.84	
P. nigra - log(Crown Surface Area)				
log(treeHeight) + Asymmetric Competition + (1 | Plot)	0.00	0.71	0.82	0.35
log(treeHeight) + Asymmetric Congeneric + Asymmetric Heterogeneric + (1 | Plot)	0.39	0.71	0.82	
log(treeHeight) + (1 | Plot)	78.45	0.65	0.80	
Q. faginea - log(Crown Surface Area)				
log(treeHeight) + Symmetric Congeneric + Symmetric Heterogeneric + (1 | Plot)	0.00	0.61	0.71	0.27
log(treeHeight) + Symmetric Competition + (1 | Plot)	1.27	0.60	0.71	
log(treeHeight) + (1 | Plot)	17.75	0.59	0.70	
Q. ilex - log(Crown Surface Area)				
log(treeHeight) + Symmetric Competition + (1 | Plot)	0.00	0.68	0.74	0.24
log(treeHeight) + Symmetric Congeneric + Symmetric Heterogeneric + (1 | Plot)	2.79	0.68	0.74	
log(treeHeight) + (1 | Plot)	3.76	0.68	0.74	
P. sylvestris - log(Crown Projected Area)				
log(treeHeight) + Asymmetric Competition + Site + (1 | Plot)	0.00	0.63	0.79	0.56
log(treeHeight) + Asymmetric Congeneric + Asymmetric Heterogeneric + Site + (1 | Plot)	1.42	0.62	0.79	
log(treeHeight) + Site + (1 | Plot)	17.90	0.56	0.78	
P. nigra - log(Crown Projected Area)				
log(treeHeight) + Asymmetric Competition + (1 | Plot)	0.00	0.70	0.80	0.31
log(treeHeight) + Asymmetric Congeneric + Asymmetric Heterogeneric + (1 | Plot)	1.39	0.70	0.80	
log(treeHeight) + (1 | Plot)	82.00	0.64	0.77	
Q. faginea - log(Crown Projected Area)				
log(treeHeight) + Symmetric Congeneric + Symmetric Heterogeneric + (1 | Plot)	0.00	0.40	0.57	
log(treeHeight) + Symmetric Competition + (1 | Plot)	2.05	0.39	0.57	
log(treeHeight) + (1 | Plot)	14.08	0.38	0.55	
Q. ilex - log(Crown Projected Area)				
log(treeHeight) + Symmetric Competition + (1 | Plot)	0.00	0.53	0.62	0.26
log(treeHeight) + Symmetric Congeneric + Symmetric Heterogeneric + (1 | Plot)	2.73	0.53	0.62	
log(treeHeight) + (1 | Plot)	3.19	0.53	0.61	

P. sylvestris - log(Crown Radius)				
log(treeHeight) + Asymmetric Competition + Site + (1 | Plot)	0.00	0.64	0.80	
log(treeHeight) + Asymmetric Congeneric + Asymmetric Heterogeneric + Site + (1 | Plot)	2.93	0.63	0.80	
log(treeHeight) + Site + (1 | Plot)	17.06	0.57	0.79	
P. nigra - log(Crown Radius)				
log(treeHeight) + Asymmetric Competition + (1 | Plot)	0.00	0.70	0.80	0.15
log(treeHeight) + Asymmetric Congeneric + Asymmetric Heterogeneric + (1 | Plot)	2.65	0.70	0.80	
log(treeHeight) + (1 | Plot)	80.18	0.64	0.78	
Q. faginea - log(Crown Radius)				
log(treeHeight) + Symmetric Congeneric + Symmetric Heterogeneric + (1 | Plot)	0.00	0.41	0.56	0.14
log(treeHeight) + Symmetric Competition + (1 | Plot)	0.36	0.39	0.56	
log(treeHeight) + (1 | Plot)	9.01	0.38	0.54	
Q. ilex - log(Crown Radius)				
log(treeHeight) + Symmetric Competition + (1 | Plot)	0.00	0.52	0.61	0.13
log(treeHeight) + (1 | Plot)	0.42	0.52	0.60	
log(treeHeight) + Symmetric Congeneric + Symmetric Heterogeneric + (1 | Plot)	4.09	0.52	0.61	
P. sylvestris - log(Crown Depth)				
log(treeHeight) + Site + (1 | Plot)	0.00	0.51	0.69	0.28
log(treeHeight) + Symmetric Competition + Site + (1 | Plot)	3.73	0.51	0.70	
log(treeHeight) + Symmetric Congeneric + Symmetric Heterogeneric + Site + (1 | Plot)	7.03	0.51	0.70	
P. nigra - log(Crown Depth)				
log(treeHeight) + Symmetric Competition + (1 | Plot)	0.00	0.54	0.63	
log(treeHeight) + (1 | Plot)	0.77	0.54	0.64	
log(treeHeight) + Symmetric Congeneric + Symmetric Heterogeneric + (1 | Plot)	2.63	0.54	0.62	
Q. faginea - log(Crown Depth)				
log(treeHeight) + (1 | Plot)	0.00	0.92	0.93	0.04
log(treeHeight) + Symmetric Competition + (1 | Plot)	7.26	0.92	0.93	
log(treeHeight) + Symmetric Congeneric + Symmetric Heterogeneric + (1 | Plot)	13.32	0.92	0.93	
Q. ilex - log(Crown Depth)				
log(treeHeight) + (1 | Plot)	0.00	0.81	0.86	0.09
log(treeHeight) + Asymmetric Competition + (1 | Plot)	3.26	0.81	0.85	
log(treeHeight) + Asymmetric Congeneric + Asymmetric Heterogeneric + (1 | Plot)	6.87	0.81	0.85	
P. sylvestris - log(Crown Relative Depth)				
log(treeHeight) + Asymmetric Competition + Site	0.00	0.10	0.10	
log(treeHeight) + Asymmetric Congeneric + Asymmetric Heterogeneric + Site	1.82	0.10	0.10	
log(treeHeight) + Site	11.11	0.03	0.03	
P. nigra - log(Crown Relative Depth)				
log(treeHeight) + Asymmetric Competition	0.00	0.04	0.04	
log(treeHeight) + Asymmetric Congeneric + Asymmetric Heterogeneric	2.00	0.04	0.04	
log(treeHeight)	4.08	0.03	0.03	
Q. faginea - log(Crown Relative Depth)				
log(treeHeight) + Symmetric Congeneric + Symmetric Heterogeneric + (1 | Plot)	0.00	0.35	0.52	0.17
log(treeHeight) + Symmetric Competition + (1 | Plot)	1.10	0.34	0.52	
log(treeHeight) + (1 | Plot)	8.95	0.33	0.50	
Q. ilex - log(Crown Relative Depth)				
log(treeHeight) + (1 | Plot)	0.00	0.03	0.22	
log(treeHeight) + Symmetric Competition + (1 | Plot)	2.02	0.05	0.26	
log(treeHeight) + Symmetric Congeneric + Symmetric Heterogeneric + (1 | Plot)	5.12	0.05	0.27	

[1] Rows sorted in ascending order based on ΔAIC

Table A3.3 Table displaying the scaling exponents and CIs for height-crown metric relationships for each species, fit using SMA (Standardized Major Axis) on log-log data.

Crown Metric	Exponent	95% CI
log(Crown Volume)		
P. sylvestris	2.28	(2.03,2.56)
P. nigra	1.90	(1.77,2.04)
Q. faginea	2.39	(2.26,2.53)
Q. ilex	3.14	(2.84,3.46)
⁂*Q. faginea*	2.65	(2.32,3.02)
⁂*Q. ilex*	3.10	(2.55,3.77)
log(Crown Surface Area)		
P. sylvestris	1.93	(1.71,2.16)
P. nigra	1.67	(1.55,1.8)
Q. faginea	2.13	(2.02,2.24)
Q. ilex	2.59	(2.37,2.83)
⁂*Q. faginea*	2.55	(2.26,2.87)
⁂*Q. ilex*	3.18	(2.69,3.76)
log(Crown Projected Area)		
P. sylvestris	1.71	(1.54,1.91)
P. nigra	1.61	(1.5,1.73)
Q. faginea	1.89	(1.78,2.01)
Q. ilex	2.37	(2.14,2.64)
⁂*Q. faginea*	2.37	(2.07,2.72)
⁂*Q. ilex*	2.69	(2.19,3.31)
log(Crown Radius)		
P. sylvestris	0.84	(0.76,0.93)
P. nigra	0.81	(0.75,0.87)
Q. faginea	0.94	(0.88,1)
Q. ilex	1.18	(1.06,1.31)
⁂*Q. faginea*	1.18	(1.03,1.35)
⁂*Q. ilex*	1.32	(1.08,1.62)
log(Crown Depth)		
P. sylvestris	0.88	(0.78,0.99)
P. nigra	0.80	(0.73,0.87)
Q. faginea	1.19	(1.16,1.22)
Q. ilex	1.07	(1,1.14)
⁂*Q. faginea*	1.11	(1.05,1.17)
⁂*Q. ilex*	1.12	(0.98,1.27)
log(Crown Relative Depth)		
P. sylvestris	0.77	(0.66,0.89)
P. nigra	0.70	(0.63,0.78)
Q. faginea	-0.97	(-1.04,-0.9)
Q. ilex	-0.88	(-1.02,-0.76)
⁂*Q. faginea*	-1.09	(-1.28,-0.92)
⁂*Q. ilex*	-0.98	(-1.32,-0.73)

Table A3.4 Table displaying the scaling exponents and CIs for height-crown metric relationships for all trees together (singe-stems only), fit on log-log data to compare results using SMA (standardized major axis) and LMM (Linear Mixed Effects Models, fit including a random effect).

Crown Metric	Exponent	95% CI	Random Effect (SD)
LMER			
log(Crown Volume)	1.89	(1.8,1.98)	0.64
log(Crown Surface Area)	1.65	(1.58,1.72)	0.56
log(Crown Projected Area)	1.34	(1.27,1.42)	0.42
log(Crown Radius)	0.67	(0.63,0.7)	0.18
log(Crown Depth)	0.88	(0.84,0.91)	0.19
log(Crown Relative Depth)	-0.20	(-0.25,-0.16)	0.16
SMA			
log(Crown Volume)	2.04	(1.97,2.12)	—
log(Crown Surface Area)	1.70	(1.64,1.77)	—
log(Crown Projected Area)	1.55	(1.49,1.61)	—
log(Crown Radius)	0.77	(0.74,0.8)	—
log(Crown Depth)	0.89	(0.86,0.91)	—
log(Crown Relative Depth)	-0.70	(-0.73,-0.66)	—

Table A3.5: Model selection results showing the strongest neighbourhood competition metric drivers of diameter-height scaling variation. AIC comparison of LMM model results of single-stems only, comparing candidate models including asymmetric, symmetric, and heterogeneric/congeneric neighbourhood metrics as explanatory variables (Equations 3.1 – 3.6). Results where either Equations 3.1 or 3.2 were selected are not displayed in the table. Site2 is a blocking factor accounting for variation between *P. sylvestris* trees located across both Cuellar and Alto Tajo. Estimates for the coefficient (c and d in Equations 3.3 - 3.6) of the most important competitive metrics are shown for each variable and species (single-stemmed individuals).

Crown Metric	Term[1]	Coefficient[2]	95% CI	Random Effect (SD)
log(Height)				
P. sylvestris	Symmetric Competition	0.33***	(0.51,0.17)	0.16
"	Site2	0.26*	(0.47,0.04)	0.16
P. nigra	Symmetric Congeneric	0.37***	(0.5,0.24)	0.18
"	Symmetric Heterogeneric	-0.1	(0.16,-0.3)	0.18
Q. faginea	Asymmetric Competition	-0.21***	(-0.14,-0.27)	0.23
Q. ilex	Symmetric Competition	0.31**	(0.61,0.07)	-

[1] AIC ≤ 2

[2] *** $P \leq 0.001$, ** $P \leq 0.01$, * $P \leq 0.05$

Table A3.6 Model selection results showing the strongest neighbourhood competition metric drivers of height-crown scaling variation. AIC comparison of LMM model results of single-stems only, comparing candidate models of both asymmetric and symmetric neighbourhood metrics as explanatory variables (Equations 3.3-3.4). Best model and those with delta AIC <2 are shown in grey for each species and metric.

Formula	ΔAIC[1]
P. sylvestris - log(Crown Volume)	
log(treeHeight) + Asymmetric Competition + Site + (1 | Plot)	0.00
log(treeHeight) + Symmetric Competition + Site + (1 | Plot)	5.21
P. nigra - log(Crown Volume)	
log(treeHeight) + Asymmetric Competition + (1 | Plot)	0.00
log(treeHeight) + Symmetric Competition + (1 | Plot)	25.80
Q. faginea - log(Crown Volume)	
log(treeHeight) + Symmetric Competition + (1 | Plot)	0.00
log(treeHeight) + Asymmetric Competition + (1 | Plot)	14.49
Q. ilex - log(Crown Volume)	
log(treeHeight) + Symmetric Competition + (1 | Plot)	0.00
log(treeHeight) + Asymmetric Competition + (1 | Plot)	4.45
P. sylvestris - log(Crown Surface Area)	
log(treeHeight) + Asymmetric Competition + Site + (1 | Plot)	0.00
log(treeHeight) + Symmetric Competition + Site + (1 | Plot)	7.87
P. nigra - log(Crown Surface Area)	
log(treeHeight) + Asymmetric Competition + (1 | Plot)	0.00
log(treeHeight) + Symmetric Competition + (1 | Plot)	27.93
Q. faginea - log(Crown Surface Area)	
log(treeHeight) + Symmetric Competition + (1 | Plot)	0.00
log(treeHeight) + Asymmetric Competition + (1 | Plot)	10.94
Q. ilex - log(Crown Surface Area)	
log(treeHeight) + Symmetric Competition + (1 | Plot)	0.00
log(treeHeight) + Asymmetric Competition + (1 | Plot)	1.02
P. sylvestris - log(Crown Projected Area)	
log(treeHeight) + Asymmetric Competition + Site + (1 | Plot)	0.00
log(treeHeight) + Symmetric Competition + Site + (1 | Plot)	7.87
P. nigra - log(Crown Projected Area)	
log(treeHeight) + Asymmetric Competition + (1 | Plot)	0.00
log(treeHeight) + Symmetric Competition + (1 | Plot)	30.86
Q. faginea - log(Crown Projected Area)	
log(treeHeight) + Symmetric Competition + (1 | Plot)	0.00
log(treeHeight) + Asymmetric Competition + (1 | Plot)	9.67
Q. ilex - log(Crown Projected Area)	
log(treeHeight) + Symmetric Competition + (1 | Plot)	0.00
log(treeHeight) + Asymmetric Competition + (1 | Plot)	2.55

P. sylvestris - log(Crown Radius)	
log(treeHeight) + Asymmetric Competition + Site + (1 | Plot)	0.00
log(treeHeight) + Symmetric Competition + Site + (1 | Plot)	8.57
P. nigra - log(Crown Radius)	
log(treeHeight) + Asymmetric Competition + (1 | Plot)	0.00
log(treeHeight) + Symmetric Competition + (1 | Plot)	31.11
Q. faginea - log(Crown Radius)	
log(treeHeight) + Symmetric Competition + (1 | Plot)	0.00
log(treeHeight) + Asymmetric Competition + (1 | Plot)	8.80
Q. ilex - log(Crown Radius)	
log(treeHeight) + Symmetric Competition + (1 | Plot)	0.00
log(treeHeight) + Asymmetric Competition + (1 | Plot)	2.10
P. sylvestris - log(Crown Depth)	
log(treeHeight) + Symmetric Competition + Site + (1 | Plot)	0.00
log(treeHeight) + Asymmetric Competition + Site + (1 | Plot)	0.66
P. nigra - log(Crown Depth)	
log(treeHeight) + Symmetric Competition + (1 | Plot)	0.00
log(treeHeight) + Asymmetric Competition + (1 | Plot)	0.43
Q. faginea - log(Crown Depth)	
log(treeHeight) + Symmetric Competition + (1 | Plot)	0.00
log(treeHeight) + Asymmetric Competition + (1 | Plot)	0.44
Q. ilex - log(Crown Depth)	
log(treeHeight) + Asymmetric Competition + (1 | Plot)	0.00
log(treeHeight) + Symmetric Competition + (1 | Plot)	1.42
P. sylvestris - log(Crown Relative Depth)	
log(treeHeight) + Asymmetric Competition + Site	0.00
log(treeHeight) + Symmetric Competition + Site	1.25
P. nigra - log(Crown Relative Depth)	
log(treeHeight) + Asymmetric Competition	0.00
log(treeHeight) + Symmetric Competition	2.44
Q. faginea - log(Crown Relative Depth)	
log(treeHeight) + Symmetric Competition + (1 | Plot)	0.00
log(treeHeight) + Asymmetric Competition + (1 | Plot)	8.63
Q. ilex - log(Crown Relative Depth)	
log(treeHeight) + Symmetric Competition + (1 | Plot)	0.00
log(treeHeight) + Asymmetric Competition + (1 | Plot)	1.90

[1]Rows sorted in ascending order based on ΔAIC